JOURNAL OF THE NIGERIAN SOCIETY OF CHEMICAL ENGINEERS

SPECIAL EDITION FROM THE BI-ANNUAL MINI CONFERENCE AND WORKSHOP ORGANISED BY THE EDUCATION & RESEARCH SECTORAL GROUP (E&R SG) ON THE 27TH – 29TH AUGUST, 2024

RECYCLING OF POLYETHYLENE TEREPHTHALATE (PET) BOTTLES FOR FIBRE PRODUCTION

*Gift-Onyesoh, J. B.[1] and Oji, A.[2]

[1] *Department of Chemical Engineering, World Bank Africa Centre of Excellence, Centre for Oilfield Chemicals Research (ACE-CEFOR), University of Port Harcourt, Choba, Nigeria*
[2] *Centre for Gas, Refining & Petrochemical Engineering, University of Port Harcourt. Nigeria*
**gift-onyesoh.juliet@aceceforuniport.edu.ng, akuma.oji@uniport.edu.ng*

ABSTRACT
Polyethylene terephthalate (PET) is the most favourable material for packaging food and beverages due to its food and drinks safety. However, there are concerns about the negative impact of waste PET bottles disposal on the environment. PET bottles are non-biodegradable. Their lifecycle leans towards ending as waste disposed in a landfill or incinerated. This study aims to construct an extruder for the recycling of waste PET bottles into fibres. The objectives are to define the recycling process and the characteristics of the fibre. The methods used for recycling was extrusion, and the characterization techniques were Brunauer-Emmett-Teller (BET) and Fourier-Transform Infrared Spectroscopy (FT-IR). The BET results show a specific surface area of 13.220m²/g. The FT-IR spectrum shows the presence of functional groups such as alkyl carbonyl and amide. This study concludes that waste PET bottles can be recycled into fibres having adsorptive potential. Further research is recommended to characterize the fibre.
Keywords: Extruder; Fibre; Plastic; Recycle; Waste.

1. INTRODUCTION

Polyethylene terephthalate, commonly abbreviated as PET or PETE, is a thermoplastic polymer widely used for packaging food and beverages (Robertson, 2014; Crawford and Quinn, 2017; Ciobanu et al., 2021). Currently, PET is the most favourable material for food and non-food packaging because it is lightweight, durable, transparent, inert, chemical resistant, stable over wide temperature ranges, and inexpensive compared to other plastic materials such as polyolefins (e.g., polypropylene), which tend to succumb to oxidation or other multilayer and composite materials containing thermoset plastics, which are expensive and more challenging to recycle (Robertson, 2014; Crawford and Quinn, 2017; Sarioğlu and Kaynak, 2018).

The widespread use of PET in packaging food and beverages raises concerns about the impact disposal has on the environment. Incineration and dumping in landfills are the two main ways of disposing of waste plastic materials (Crawford and Quinn, 2017; Zhang et al., 2020; Sadeghi et al., 2021). The incineration of waste plastic materials emits chemicals such as dioxins and furans, which are highly toxic and can cause severe health implications for human beings (Crawford and Quinn, 2017; Sadeghi et al., 2021). Since legislation necessitating the recycling of waste plastic is unenforced in most countries, waste PET bottles are usually disposed of in dumpsites.

PET as a waste occupies a substantial amount of space, which results in ground pollution (Park and Kim, 2014; Sarioğlu and Kaynak, 2018). The global market volume of PET in 2022 amounted to 25.47 million metric tons; it is projected to reach 35.70 million metric tons in 2030 based on the compound annual growth rate of 4.1% forecast between 2023 and 2030 (PET Market Volume Worldwide 2015-2030 | Statista, 2024). These statistics, the non-degradable nature of PET bottles, and the disadvantages associated with incineration and landfilling make waste PET bottle management an environmental issue. Nevertheless, the thermoplastic nature of PET allows for melting by heating and reshaping on cooling, making recycling a viable option for waste management (Park and Kim, 2014).

The non-degradable nature of PET bottles and the disadvantages of landfilling and incineration also make recycling the most desirable option for containing waste PET bottles. Waste PET bottles can be recycled into several products, including fibres. Fibre production from waste PET bottles represents an innovative strategy for waste PET bottle recycling and management. Escamilla-Lara et al. (2023), reported activated carbon, graphene, fullerene, and fibre as adsorbent materials obtained from the total transformation of PET. Park and Kim (2014) reported a 72% of recycled PET conversion into fibre.

Waste PET bottles can be recycled into fibres with adsorptive potential in several ways. According to Crawford and Quinn (2017), as of 2014, over 200 recycling processes have been registered with the United States Food and Drugs Administration and the European Food Safety Authority. Park and Kim (2014) described re-extrusion as the primary and classical method for recycling PET, stating its simplicity and low cost as its advantages.

Extrusion is a polymer processing method for converting thermoplastic polymers in granular or powdered form into a continuous uniform melt re-shapeable into articles of uniform cross-sectional area by driving it through a die (Ebewele, 2000). Waste PET bottles can be recycled into fibre of various shapes and lengths by mechanical extrusion or chemical dissolution

(Ebewele, 2000; Park and Kim, 2014). The mechanical method of recycling PET waste has more advantages than the chemical method. It is comparatively simple and has a minimal negative effect on the environment. It is also low-cost and feedstock flexible as it utilizes readily available materials (Ebewele, 2000).

This study focused on the mechanical method of fibre production from waste PET bottles by extrusion in a constructed single-screw extruder. The objectives are to define the production process and the characteristics of the fibre produced from recycling waste PET as a potential adsorbent for produced water treatment.

2. MATERIALS AND METHODS

This section describes the materials and methods used for recycling the waste PET bottles into fibre and for characterizing the fibre produced.

2.1 Materials

Transparent waste PET bottles initially used for packaging water and or carbonated soft drinks were used in this study. The single rotating cylindrical screw extruder used for the recycling of waste PET bottles into fibre was designed and constructed by the author. A pair of Scissors cut the waste PET bottles into smaller sizes before shredding them in a grinder. Characterization of the fibre sample for the surface area was achieved by Brunauer-Emmett-Teller (BET) method using QUANTACHROME NOVA4200e Made in the USA. Shimadzu Fourier-Transform Infrared Spectrophotometer – FT-IR 8400 S was used with 0.01g kBr anhydrous by mortar agate for functional unit characterization.

2.2 Methods

The conversion of the waste PET bottles into fibre followed the process illustrated in Figure 1. The recycling process started with waste PET bottle collection, sorting, size reduction, washing, drying, and extrusion into the fibre. The methods used to characterize the fibre produced were the Brunauer-Emmett-Teller (BET) method for surface area analysis and Fourier-Transform Infrared Spectrophotometer (FT-IR) for surface chemistry and the functional unit examination.
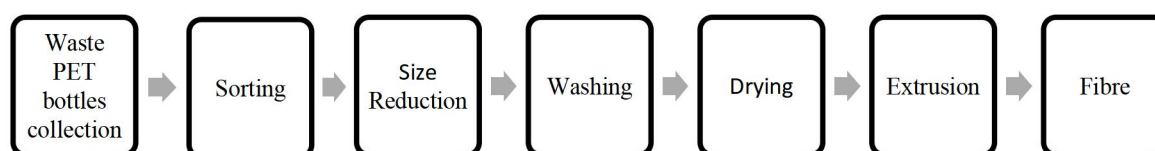
Figure 1. Block flow diagram of the PET extrusion
process

2.2.1 Waste PET bottles collection

The waste PET bottles, initially used for packaging water and or carbonated soft drinks, were collected in a bin from a fast-moving consumer drinks shop.

2.2.2 Sorting

The waste PET bottles were manually sorted to collect only similar transparent bottles with the symbol for recyclable PET bottles illustrated in Figure 2. This sorting process was necessary because, according to Scheirs (1998), *"Even 1% of an incompatible polymer can be sufficient to degrade the properties of an entire batch recyclate."* As mentioned in Lange (2021), in designing for recycling, clear PET bottles should contain $>90\%$ (if possible $>95\%$) of PET; the use of bottle caps and labels should be avoided. Thus, the bottle labels and covers were separated in the sorting process before shredding because they are made of different materials.

Figure 2. Symbol of recyclable PET bottles (Crawford and Quinn, 2017).

2.2.3 Size reduction

Size reduction is an integral part of the PET recycling process. This processing step is necessary for easy transportation and feeding of the waste plastic into the extruder for onward conversion. The waste PET bottles were first cut into larger pieces with scissors and then shredded with a shredder into flakes of particle sizes between 1 mm to $\leq$ 5 mm.

2.2.4 Washing

The PET flakes were washed to rinse off any remaining carbonated drink, dirt, and adhesives from the labels. Adhesives used to stick labels to PET bottles are comprised of rosin acids and esters, which can cause discoloration of the PET (Scheirs, 1998). The washing process was in two stages. The first wash was with warm water at 80 ^{0}C, while the second was with cold water. Though detergent or solvent can be used for washing, no washing agent was applied to avoid leaving behind residues of the washing agent, which tends to catalyze the hydrolysis of PET.

2.2.5 Drying

Another critical step to prevent hydrolytic degradation in the recycling process is drying. Without drying, residual moisture can cause PET to degrade during extrusion (Scheirs, 1998). The washed PET flakes were air-dried naturally in the sun before extrusion by laying them flat on an open surface for some days, during which period they were turned over several times.

2.2.6 Extrusion

The PET flakes were readily recycled into fibre by extrusion in the constructed single-screw extruder. The extruder comprised an AC motor-driven single screw housed within a heated barrel, with provisions for material feed-in through a hopper, melting, mixing, and extrusion. The PET flakes were poured into the hopper, then conveyed by the screw, which is the moving part of the extruder that is inside the barrel, where it is melted and forced out through the tiny holes of the spinneret (die) as continuous filaments of the semi-solid polymer. As the filaments pass through the tiny openings of the spinneret, the liquid polymer is first converted to a rubbery state before solidifying into fibre on cooling. The screw is powered by a 0.25 horsepower (hp) electric motor operating at a frequency of 50Hz. The extruder length-to-diameter (L/D) ratio is 10/1. The three (3) heating bands were set at 240 degrees Celsius (^{0}C), 250^0C, and 260^0C.

2.2.7 Brunauer-Emmett-Teller (BET) method for surface area determination

In preparing the sample for analysis, the sample was weighed into the sample cell, and the filled sample cell bulb was inserted into the heating mantle. The clamp was placed around the mantle to hold the sample cell firm. After which, the sample cell stem is inserted into the sample preparation station. The knurled ring is tightened clockwise to secure the sample cell in the preparation station. After the sample cell was secured in the preparation station, outgassing was initiated by entering the control panel menu on the instrument. The outgassing temperature was set to 250^0C, and the system instructed to start degassing for 3 hours after turning on the heater. When the sample was outgassed for 3 hours, the heating mantle was turned off and cooled. After cooling the heating mantle, the gas station was unloaded, and the sample was removed. The sample cell was then reweighed to determine the weight of the post-out gas sample. The dewar was filled to its internal upper mark with liquid nitrogen to analyze the sample. The sample cell containing the outgassed and weighed sample was placed into the analysis station. All the fields on the start analysis 'Sample' menu were filled and the point selection and tagging on the start Analysis were also completed and used for the BET measurements.

2.2.8 Fourier Transform Infrared Spectrophotometer (FT-IR) method for surface chemistry characterization

The sample was prepared by weighing in 0.01g of the fibre directly on the FT-IR sample holder and homogenized with 0.01g KBr anhydrous. Care was taken to ensure uniform sampling. The mixtures were pressed by vacuum hydraulic at 1.2 psi to obtain a transparent pallet. The scanned samples were passed through infra-red, where the wave detector connected to the computer described the tested sample spectrum. The FT-IR spectrometer is calibrated and set up to measure the infrared absorption of the sample in the spectral area of 600 to 4000 cm-1. The infrared beam was directed through the sample, and the resulting absorption spectrum was recorded. The spectra were collected over a range of wavelengths, and the average of multiple scans was taken to improve the signal-to-noise ratio.

3. RESULTS AND DISCUSSION

This study investigated the recycling of waste PET bottles into fiber by mechanical extrusion process. The results gave insights into the applications of this technique to recycle waste PET bottles and reduce environmental pollution.

3.1 Extruder Design and Construction

The single screw extruder was designed and constructed based on established engineering principles and specifications suitable for plastic recycling. The screw is designed to pick up the PET flakes from beneath the hopper, compress it, mix it, and then transport it as it changes from solid flakes to a viscous melt. The extruder has the following parts: cylindrical screw, hopper, barrel, spinneret, electric motor, heating bands, thermocouple, and temperature controller.

Single Cylindrical Screw Shaft

The cylindrical screw shaft is divided into three zones: feed, compression or transition, and metering. Each of the zones has a distinct channel depth and functions differently. The feed zone, 2.3 diameters long, picks the PET flakes from beneath the hopper and moves them into the heated barrel to initiate the melting. The compression and metering zone, which is 4.7 diameters long, compresses the fed PET flakes, melts, and converts them into a continuous stream of molten material. The air contained in the polymer is removed in the process. The metering zone ensures a uniform flow rate and generates the pressure to force the viscous to melt out of the die.

Hopper

The hopper, through which the PET flakes are fed into the barrel, was designed as a hollow right-inverted rectangular pyramid. The base is 3.5m by 2.3m, the vertex is 0.8m by 1.2m, and the height is 1.78m.

Barrel

The cylindrical barrel, which is designed to house the screw, is made of galvanized steel pipe length 7m.

Die

The die (spinneret) design has several holes of 0.5mm, from where the molten melt exudes and is shaped and cooled into the fibre.

Electric Motor

The 0.25hp three-phase AC electric motor was designed to rotate the screw shaft inside the barrel. It converts electrical energy into mechanical energy through the interaction between the motor's magnetic field and the electric current in the wire. Generating force in the form of torque applied to the motor's shaft. The motor has the following specifications (see Table 1):

Table 1 Specification of the electric motor

Voltage	240 volts
Current	1.6 ampere (A)
Power	0.18 kW
Revolutions per minute (Rpm)	1400
Frequency	50 Hz

Heating Bands

Three circular heating bands made of cast aluminum, which converts electrical current into heat energy, were attached to the barrel to supply the heat required for melting the PET flakes.

Thermocouple

A k-type thermocouple was attached to each of the three heating bands to measure the temperature in the three zones where the heating band was attached.

Temperature Controller

The temperature controller measures and controls temperature readings at the three circular band heaters.

3.2 Extrusion Process

The extruder operating parameters were adjusted to determine the optimal process conditions for recycling waste PET bottles. Parameters such as screw speed, barrel temperature profile, residence time, and feed rate were varied and optimized to achieve consistent melt flow, thorough mixing, and uniform fibre formation. The optimal operating conditions of the constructed extruder are presented in Table 2.

Table 2 Operating parameters of the constructed single screw extruder

Screw speed	20 – 120 rpm
Barrel temperature	Feed zone (200 – 240^{0}C), compression zone (240 – 280^{0}C), metering zone (280 – 300^{0}C).
Residence time	5 – 10 minutes
Feed rate	10 – 50 kg/hr.

3.3 Characterization of recycled PET fibres

The recycled PET fibre was characterized to determine its surface area, surface chemistry, and functional units.

3.3.1 Surface area

Brunauer-Emmett-Teller (BET) method was used to determine the surface area of the fibre by analyzing nitrogen adsorption-desorption isotherms. The BET analysis revealed that the fibers exhibited a specific surface area of 13.220 m²/g. This value indicates the accessible surface area per unit mass of the fibre necessary for adsorption applications. Comparing the research findings with existing literature on similar polymeric fibers, the surface area measured in this study falls within the typical range reported for fibers of similar composition and processing methods. This consistency validates the reliability of the BET method in accurately determining the surface area of polymeric materials, notwithstanding their complex morphology and composition. The surface area has significant implications for potential applications of the fibre. High surface area materials are desirable in separation techniques such as adsorption. The surface area obtained suggests that the fibers could effectively enhance adsorption capacities.

Although the BET method provides valuable insights into the surface area of the fibre, it has limitations. BET method assumes a uniform surface and pore structure, which may not fully capture the complexities of fibrous materials. Thus, future studies could explore other techniques, such as scanning electron microscopy (SEM).

3.3.2 Surface chemistry

Figure 3 shows the FT-IR spectra of the fibre sample produced from recycled waste PET bottles. The FT-IR spectrum of the fibre sample analysed revealed the presence of several characteristic absorption bands corresponding to the different functional groups. The wavenumbers 2924.24 cm⁻¹ and 2851.30 cm⁻¹ peaks are attributed to the asymmetric and symmetric stretching vibrations of the -CH$_2$ groups, indicating the presence of alkyl chains in the polymer structure. Thus, the C-H stretching belongs to the alkyl functional group. The strong peak at wavenumber 1729.63 cm⁻¹ corresponds to the stretching vibration of carbonyl groups (C=O), suggesting the presence of ester or carboxylic acid groups in the polymer. The peak at wavenumber 1550.89 cm⁻¹ reveals N-H bending vibrations, characteristic of amide groups, signifying that the fibre sample may contain polyamide linkages or proteins.
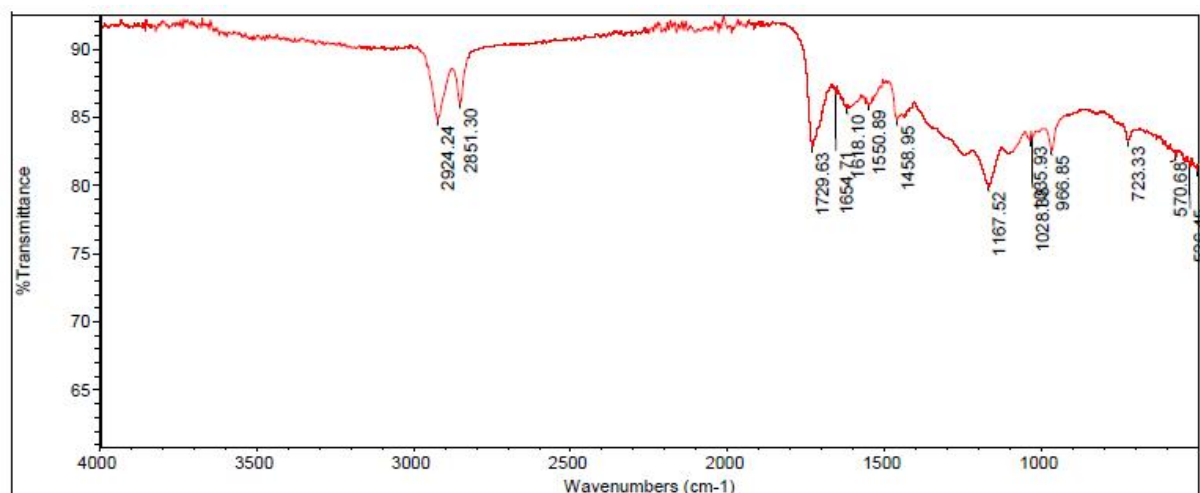
Figure 3. FT-IR spectra of the fibre sample produced from recycled waste PET

The peaks at wavenumbers 1618.10 cm^{-1} and 1458.95 cm^{-1} correspond to the stretching vibrations of the C=C bonds within aromatic rings, indicating the presence of aromatic structures within the polymer matrix. Also identified was C-O-C stretching (Ether Linkage), where the wavenumber peaked at 1167.52 cm^{-1}. This peak is associated with the stretching vibration of C-O-C bonds, typical of ether linkages, suggesting that the polymer contains ether functional groups. The peaks at wavenumbers 835.93 cm^{-1} and 723.33 cm^{-1} are due to C-H bending vibrations. It also confirmed the presence of alkyl groups C-H. Wavenumber 966.85 cm^{-1} peak corresponds to the out-of-plane bending of C-H bonds, commonly found in aromatic compounds. C-O Stretching (Alcohols/Phenols) with wavenumber 1028.13 cm^{-1} peak indicates the presence of hydroxyl groups (O-H) linked to aromatic rings or in alcohol groups.

4. CONCLUSIONS

The thermoplastic nature of polyethylene terephthalate (PET) allows for its effective recycling. Recycling waste PET bottles into fibers is an innovative approach, offering potential applications as adsorbents for produced water treatment. Mechanical recycling of waste PET bottles into fibers is ideal for environmental sustainability and resource conversion for value addition. This research highlights a systematic method for converting waste PET bottles via extrusion into fibers suitable for water treatment applications, emphasizing the importance of effective material handling. Waste recycling involves waste PET collection, sorting, size reduction, washing, drying, and extrusion. The methods by which the fibre sample was characterized were BET analysis for surface area determination and the FT-IR spectrum indicates that the fibre sample from waste PET bottles has complex organic molecules with several functional groups, including alkyl chains, carbonyl, amide, aromatic, and ether groups. The presence of both ester/carboxylic acid and amide groups suggests that the polymer may be a co-polymer or blend containing polyesters and polyamides. Aromatic structure identification points to the likelihood of a rigid, possibly thermally stable polymer backbone. The presence of ether and hydroxyl groups implies potential sites for hydrogen bonding, which could influence the fibre mechanical and chemical properties. Further research into optimizing the fibre properties and exploring its applications is necessary to exploit its technological and commercial potential.

REFERENCES

Ciobanu, C.S., Bulgariu, D., Azamfire, B. and Bulgariu, L. (2021). Obtaining PET-clay Adsorbent Materials and their Use for the Removal of Pb (II) Ions from Aqueous Media. *Bulletin of the Polytechnic Institute of Jassy*, 67 (71): 29-38.

Crawford, C. B. and Quinn, B. (2017). Physiochemical properties and degradation. *Microplastic Pollutants*. 5: 57-100.

Ebewele, R. O. (2000). Polymer science and technology. *Polymer Science and Technology*, 11: 289-299.

Escamilla-Lara, K. A., Lopez-Tellez, J. and Rodriguez, J. A. (2023). Adsorbents obtained from recycled polymeric materials for retention of different pollutants: A review. *Chemosphere*, Vol. 335, September 2023, pp. 139-159

Lange, J. P. (2021). Managing Plastic Waste-Sorting, Recycling, Disposal, and Product Redesign. *ACS Sustainable Chemistry and Engineering*, 9(47), 15722–15738.

Park, S. H. and Kim, S. H. (2014). Poly (ethylene terephthalate) recycling for high value added textiles, *Fashion and Textiles*, Vol. 1, Issue 1, July 2014, pp. 1-17

PET market volume worldwide 2015-2030 | Statista. (2024). https://www.statista.com/statistics/1245264/polyethylene-terephthalate-market-volume-worldwide/

Robertson, G. L. (2014). Food Packaging. *Encyclopedia*

of Agriculture and Food Systems. 232-249

Sadeghi, B., Marfavi, Y., AliAkbari, R., Kowsari, E., Borbor Ajdari, F. and Ramakrishna, S. (2021). Recent Studies on Recycled PET Fibers: Production and Applications: a Review. *Materials Circular Economy*, 3(1).

Sarioğlu, E. and Kaynak, H. K. (2018). PET Bottle Recycling for Sustainable Textiles. *Polyester - Production, Characterization and Innovative Applications*. 2: 1-17.

Scheirs, J. (1998). Polymer recycling: science technology and applications. *Radiation Physics and Chemistry*, Vol. 64, Issue 1, September 1998, pp. 1-616

Zhang, H., Pap, S., Taggart, M. A., Boyd, K. G., James, N. A. and Gibb, S. W. (2020). A review of the potential utilisation of plastic waste as adsorbent for removal of hazardous priority contaminants from aqueous environments. *Environmental Pollution*, Vol. 258, March 2020, pp. 1-12

DRYING OF YELLOW AND RED CASHEW (*ANACARDIUM OCCIDENTALE* L.) APPLE BAGASSE BY A DIRECT NATURAL CONVECTION (PASSIVE MODE) SOLAR DRYER

Oluremi, I. A., Alamu, A. O., Azeez, S. A., Oke, C. O., Aworanti, O. A., Alagbe, S. O., Osuolale F. N. and *Agbede, O. O.

Department of Chemical Engineering, Ladoke Akintola University of Technology, Ogbomoso, Nigeria
*Email of the Corresponding author: ooagbede@lautech.edu.ng

ABSTRACT

A large quantity of cashew apples is usually discarded after the removal of cashew nuts. After the removal of the juices the leftover bagasse can be used as nutritional supplements in consumable products, as source of vitamins, minerals or bioactive substances. Removing cashew moisture content preserves its nutrition and extends shelf life. Solar energy is eco-friendly and can be employed in a solar dryer for the sustainable drying of agricultural produce. Hence, the solar drying of bagasse was investigated using a direct natural convection solar dryer. Juice was extracted from two species by two different methods; the resulting bagasse was then cut into chips and dried in a direct natural convectional solar dryer. All samples dried in the falling rate period with effective moisture diffusivities of $2.86 \times 10^{-10} - 4.75 \times 10^{-10}$ $m^2 s^{-1}$. Hence, renewable solar energy can be explored for the sustainable industrial processing of cashew apple bagasse.

Keywords: Cashew; solar dryer; moisture diffusivity; drying; falling rate period

1. INTRODUCTION

Cashew (*Anacardium Occidentale* L.) fruit belongs to the Anacardiaceae family (Das and Arora, 2017). It is a tropical fruit which originated from Brazil (Rajkumar and Ganesan, 2021) and commercially grown in countries of Central America, Asia and Africa. The cashew fruit is divided into two parts which are cashew nut (the kernel and the true fruit) and the cashew apple (Das and Arora, 2017). The fruit comes in three colours: orange, yellow and bright red. The cashew apple is enlarged peduncle, also called a pseudo fruit or false fruit making up about 90% of the weight of the cashew fruit. Cashew tree is mainly cultivated for the seeds while the cashew apple which is about 9-10 times the weight of the nut is significantly underutilized and considered as a waste product (Zie et al., 2023). For every ton of cashew nuts produced, about 10-15 tons of cashew apples are obtained as a by-product.

Cashew apple can be consumed directly as fresh fruits because of soft peel, juicy pulp, and no seed (Rodríguez et al., 2017). However, it is grossly underutilized because it is highly perishable due to its high moisture content which is between 88 and 90%, the lack of adequate processing technology and its astringency as a result of its high tannin content (Rodríguez et al., 2017; Zie et al., 2023). It is largely used for juice and beverage production, about 65-80% of the juice can be recovered from the fruits depending upon maturity, variety and process of extraction (Walraven and Stark, 2023). The juice has a high nutritional potential and rich in important compounds like vitamins, sugars, amino acids, dietary fibers, minerals, carotenes, and polyphenols,

among other phytonutrients (Reina et al., 2022). It has great antiscorbutic qualities due to its vitamin C content (200 - 300 mg per 100 grams of fresh material). The vitamin C (ascorbic acid) content that has been observed in CA is three to six times higher than that of orange juice and about ten times more than that in pineapple juice. In Nigeria, cashew nuts are usually removed from the fruits and sold while the apples are discarded as byproducts in the fields resulting in huge loss of useful resource, waste disposal problem and environmental pollution (Nwosu et al., 2016).

Cashew apple bagasse or pomace is the by-product of the extraction of juice from cashew apple. It is about 20% of the weight of the apple, so a large quantity of this cashew processing residue is left after juice extraction (Akubor, 2016). This huge residues results in waste disposal and environmental problems. Cashew apple bagasse is rich in macro and micronutrients as well as in bioactive substances. It is a source of dietary fibre, protein, lipids, carbohydrate (including sugars, hemicellulose and cellulose), vitamin C, minerals (zinc, iron, manganese, copper, boron, magnesium, calcium, potassium, sodium and phosphorus), pectin, carotenoids, polyphenols, proanthocyanidin, anthocyanins, flavonoids and Tannins (Zie et al., 2023). The bioactive constituents are natural antioxidants. Cashew apple bagasse can be used as nutritional supplements in animal feeds, cakes, biscuits and pasta, as source of vitamins, minerals or bioactive substances.

As a lignocellulosic biomass, cashew apple bagasse is a potential feedstock for ethanol production via hydrolysis

and fermentation. It can also be converted to other biofuels and bioenergy via thermochemical conversion processes such as combustion, pyrolysis and gasification (Guran, 2018). Biochar, which can be used as soil supplement and biosorbent is also a potential product from cashew bagasse. Cashew apple bagasse, being a byproduct of cashew apple fruit juice extraction, has a high moisture content. This high moisture needs to be removed as soon as possible to avoid microbial growth and reduce biochemical reactions which lead to deterioration (Akubor, 2016)

The energy from the sun is abundant, free and renewable. It can be harnessed for the removal of moisture from agricultural produce and residue. Direct drying in sunlight exposes the material to dust, rodents, insects which can pollute the material undergoing drying. However, solar drying employs solar dryers which are equipment that utilize a drying chamber and the renewable solar energy to dry a material. The solar drying of cashew bagasse/pomace has not been adequately investigated. Hence, this study considered the solar drying of cashew apple bagasse obtained from two varieties of cashew found in Ogbomoso, Nigeria.

2. MATERIALS AND METHODS
2.1. Sample Collection and Preparation
Firm-ripped cashew apple fruits (both yellow and red species shown in Figure 1a and Figure 1b) were plucked from cashew trees and washed with distilled water. Two separate methods were employed to extract juice from each species of cashew apples after washing. First, a set of each species of cleaned fruits was fed into an electric fruit blender and ground at 200 rpm for 2 minutes. The slurry was filtered through a 150 micron filter to separate the juice and the bagasse paste left was pressed between two plates of hydraulic press for 5 minutes. The pressed bagasse was then used in the drying experiments as sample (a) i.e. Red Cashew (a) and Yellow Cashew (a).

A second set of cleaned fruits of each species were directly pressed between two plates of a hydraulic press for 5 minutes; the resulting pressed bagasse was then used in the drying experiment. This is referred to as sample (b) i.e. Red Cashew (b) and Yellow Cashew (b). Images of bagasse obtained by methods "a" and "b" are shown in Figure 1c and Figure 1d, respectively.

(a)

(b)

(c)

(d)

Figure 1: (a) Yellow cashew fruit (b) Red cashew fruit, (c) Bagasse obtained by grinding fruit, filtering and then pressing the paste, and (d) Bagasse obtained by simply pressing out the juice from the cashew apple

2.2. Experimental Procedure for Drying Cashew Apple Bagasse in a Solar Dryer

The cashew bagasse was cut into 4 by 4 mm chips of 2 mm thickness; 10 g of bagasse chips was placed in pre-weighed aluminium drying pans and then placed in a solar dryer. The solar dryer, shown in Figure 2a, was operated as a direct natural convection (passive mode) dryer. The mass of the cashew bagasse in the pan was determined using a digital weighing balance at beginning of the drying process and afterward at 30min until the cashew bagasse chips were totally dried and the mass remain the same. The experiments were carried out in triplicates. Samples of dried cashew apple bagasse are shown in Figure 2b.

(a)   (b)

Figure 2:   (a) Solar dryer (b) Dried cashew apple bagasse

2.3 Determination of Moisture Ratio and Drying Rate

The mass-time data gotten from each set of experiments was changed to moisture content-drying time data. The moisture content of cashew bagasse at time t, X_t (g water, g dry matter^{-1}) is defined as:

$$X_t = \frac{m_t - m_d}{m_d} \qquad (1)$$

where m_t is mass of bagasse chips at time t, m_d is mass (g) of chip when it is completely dry while X_t is the moisture content (g water. g dry matter^{-1}).

The drying rate of cashew apple bagasse chips was estimated by:

$$D_R = \frac{X_{t+dt} - X_t}{dt} \qquad (2)$$

D_R is the drying rate (g water/g dry matter. min), X_{t+dt} is moisture content at time t+dt and dt is the drying interval.

The moisture content can be expressed as dimensionless moisture ratio (M_R):

$$M_R = \frac{X_t - X_e}{X_i - X_e} \qquad (3)$$

For long drying time the moisture ratio can be simplified to:

$$M_R = \frac{X_t}{X_i} \qquad (4)$$

where X_i is the initial moisture content.

2.4 Determination of Effective Moisture Diffusivity

The diffusion from the internal part of the cashew pomace to the surface can be illustrated by Fick's second law of diffusion during the falling rate drying period when internal mass transfer is the controlling mechanism (Agbede et al., 2024). The Fick's law in term of M_R is stated as:

$$\frac{dM_R}{dt} = D_{eff} \frac{d^2 M_R}{dx^2} \qquad (5)$$

Where x is spatial dimension (m) and D_{eff} is the effective moisture diffusivity (m² s^{-1}).

Assuming a one dimensional transport of moisture in an infinite slab, negligible shrinkage, constant initial moisture distribution, negligible external resistant and uniform diffusivity; the mathematical solution of Equation (5) according to (Crank, 1975) is:

$$M_R = \frac{8}{\pi^2} \sum_{i=0}^{\infty} \frac{1}{(2i+1)^2} \exp\left[\frac{-(2i+1)^2 D_{eff} \pi^2 t}{4L^2} \right] \qquad (6)$$

The first term in the sequence expansion of Equation (6) gives a good estimation of the resolution for satisfactorily long drying time (Di Scala and Crapiste, 2008):

$$M_R = \frac{8}{\pi^2} \exp\left[\frac{-D_{eff} \pi^2 t}{4L^2} \right] \qquad (7)$$

where L is the thickness of the slab (m) for one-direction

diffusion and t the time of drying (min). Equation (7) can be written in a linear form as:

$$In\left(M_R\right) = In\left(\frac{8}{\pi^2}\right) - \left(\frac{D_{eff}\pi^2 t}{4L^2}\right) \qquad (8)$$

A graph of $\ln\left(M_R\right)$ versus t produces a straight line with slope from which D_{eff} is estimated:

$$Slope = \frac{D_{eff}\pi^2}{4L^2} \qquad (9)$$

3. RESULTS AND DISCUSSION

3.1. Solar Drying Characteristics

Figure 3a shows the plot of moisture ratio against time while Figure 3b shows the plot of drying rate against drying time for the solar drying of the red and yellow cashew apple bagasse prepared by two different methods "(a)" and "(b)" as previously described in section 2.1.

Figure 3a shows that moisture was progressive removed

from all the four samples until they were completely dry. All the samples were dried within 330 min as shown in Figure 3a and Figure 3b.This implies that the juice extraction (or bagasse production) method did not affect the drying rate of the bagasse. Similarly, the species of cashew did not affect the drying rate, since the same drying time was required to dry samples of both the yellow and red species of cashew bagasse.

The initial drying rates were 0.047 – 0.060 g water/g dry matter min^{-1} as shown in Figure 3b. For all samples of bagasse considered, the drying rate decreased with drying time as shown in Figure 3b. This implies that the drying process for all the cashew bagasse samples generally occurred in the falling rate period and was controlled by the diffusion of moisture from the inside of the bagasse to its surface. Falling drying period has been previously reported for the drying of agricultural produce (Tunde-Akintunde and Ogunlakin, 2011; Agbede et al., 2020).

(a)

(b)
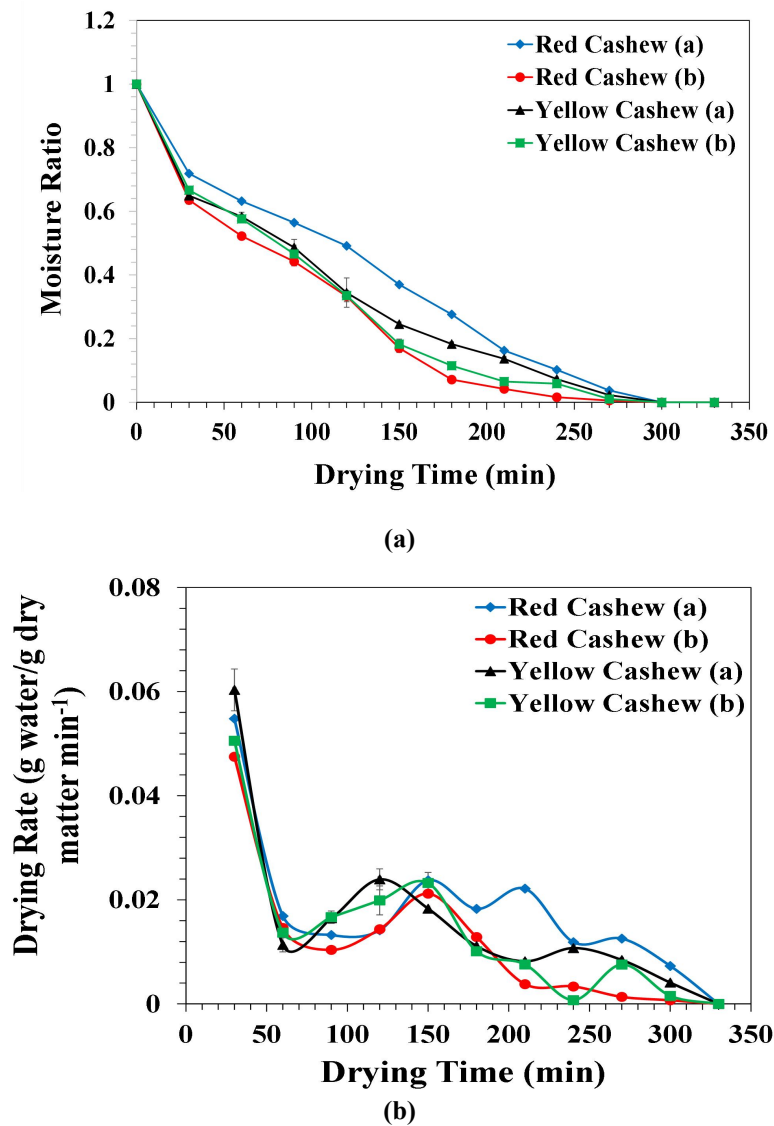
Figure 3: Solar drying of cashew apple bagasse (a) moisture ratio versus drying time (b) drying rate versus drying time

3.2. Effective Moisture Diffusivity

The effective moisture diffusivities for the solar drying of the two species of cashew apple bagasse are shown in Figure 4. The effective moisture diffusivities for the solar drying of the red and yellow cashew apple bagasse obtained by method "a" were 2.86×10^{-10} and 3.33×10^{-10}, respectively while those for the solar drying of red and yellow cashew apple bagasse obtained by method "b" were 4.75×10^{-10} –and 4.20×10^{-10}, respectively. The effective moisture diffusivities for the solar drying of both the red and yellow cashew apple bagasse obtained by the two methods considered in this study are within the range of effective moisture diffusivities of $10^{-12} - 10^{-6}$ m^2 s^{-1} previously reported in the literature for the drying of agricultural produce (Erbay and Icier, 2010).
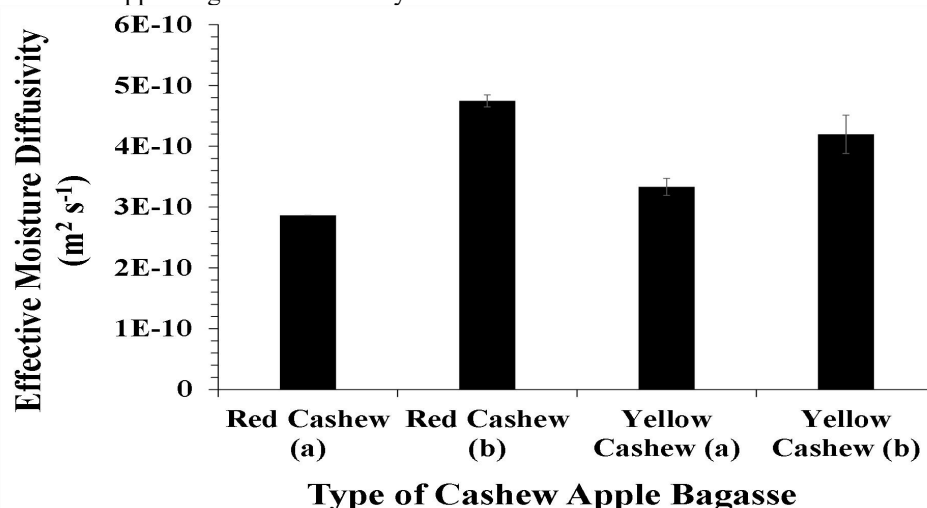
Figure 4: Effective moisture diffusivity for the solar drying of cashew apple bagasse

4. CONCLUSIONS

Cashew apple bagasse obtained from two species of cashew fruits (yellow and red species) by two different juice extraction methods (direct hydraulic pressing and grinding followed by filtering and then pressing) were successfully dried in a solar dryer operated in the passive mode. The juice extraction (or bagasse production) method did not affect the drying rate of the bagasse. Also, the same drying time was required to dry samples of both the yellow and red species of cashew bagasse. The bagasse obtained from both the yellow and red species of cashew apple dried in the falling rate period and was controlled by the diffusion of moisture from the inner part of the bagasse to its surface. The effective moisture diffusivities for the drying of the cashew bagasse were $2.86 \times 10^{-10} - 4.75 \times 10^{-10}$ m^2 s^{-1}. The renewable energy from the sun can be explored for the industrial processing of cashew apple juice extraction residue.

5. ACKNOWLEDGEMENTS

6. REFERENCES

Agbede, O.O., Oke, E.O., Akinfenwa, S.I., Wahab, K.T., Ogundipe, S., Aworanti, O.A., Arinkoola, A.O., Agarry, S.E., Ogunleye, O.O., Osuolale, F.N. and Babatunde, K.A. (2020) Thin layer drying of green microalgae (Chlorella sp.) paste biomass: Drying characteristics, energy requirement and mathematical modeling. *Bioresource Technology Reports*. 11, 100467.

Agbede, O.O., Oyewo, F.A., Aworanti, O.A., Alagbe, S.O., Ogunkunle, O. and Laseinde, O.T. (2024) Convective drying characteristics and moisture transfer properties of Jatropha curcas L. seeds. *Scientific African*, 23, e02122, 1-19.

Akubor, P. (2016). Chemical composition, functional and pasting properties of cashew pomace and wheat flours. *International Journal of Agricultural and Veterinary Science*, 28-37.

Crank, J. (1975). The Mathematical of Diffusion. London. *Oxford University Press.*

Das, I. and Arora, A. (2017) Post-harvest processing technology for cashew apple - A review. *Journal of Food Engineering,* 194, 87-98.

Di Scala, K. and Crapiste, G. (2008) Drying kinetics and quality changes during drying of red pepper. *LWT – Food Science and Technology*, 41 (5):789–795.

Erbay, Z. and Icier, F. (2010) A Review of Thin Layer Drying of Foods: Theory, Modeling, and Experimental Results. *Critical Reviews in Food Science and Nutrition* 50 (5): 441–464.

Guran, S. (2018). Sustainable Waste-to-Energy Technologies: Gasification and Pyrolysis. *Sustainable Food Waste-To-Energy Systems*, 141–158.

Nwosu, C. Adejumo, O.A. and Idoha, W.N. (2016) Cashew Apple Utilization in Nigeria: Challenges and Prospects. *Journal of Stored Products and*

Postharvest Research, 7(2), 29-31.

Rajkumar, H. and Ganesan, N.D. (2021) Effects of freeze-drying process on the production of cashew apple powder: Determination of bioactive compounds and fruit powder properties.*Journal of Food Processing and Preservation*, e15466, 1-10.

Reina, L., Aranguren, D., Forero, L., Tarapuez, L., Sequeda, D and Carazzone, C (2022). Chemical composition and bioactive compounds of cashew (*Anacardium occidentale*) apple juice and bagasse from Colombian varieties. *Heliyon,* 8, e09528, 1-15.

Rodríguez, O., Gomes, W.F., Rodrigues, S. and Fernandes, F.A.N. (2017). Effect of indirect cold plasma treatment on cashew apple juice (*Anacardium occidentale* L.). *LWT– Food Science and Technology*, 84, 457–463.

Tunde-Akintunde, T.Y. and Ogunlakin, G.O. (2011) Influence of drying conditions on the effective moisture diffusivity and energy requirements during the drying of pretreated and untreated pumpkin. *Energy Conversion and Management* 52 (2): 1107–1113.

Walraven, N.V and Stark, A. (2023). From food waste to functional component: Cashew apple pomace. *Critical Reviews in Food Science and Nutrition*, 1-13.

Zie, M., Alabi, T., Karamoko, G. and Blecker, C. (2023) Valorization of cashew apple bagasse in food application: Focus on the use and extraction of nutritional or bioactive compounds. *Food and Humanity* 1, 848 – 863

SLUG FLOW PREDICTION IN PIPELINE-RISER SYSTEMS USING SELECTED MACHINE LEARNING ALGORITHMS

Ehinmowo, Adegboyega Bolu*., Olatunji, Oreoluwa Nifemi and Olaide , Joseph Oluwatobi
Chemical and Petroleum Engineering, University of Lagos
Corresponding Author: aehinmowo@unilag.edu.ng

ABSTRACT
Slug flow is a common flow pattern characterized by the irregular cycle of liquid slugs followed by longer gas bubbles in a pipeline. This can cause significant operational challenges leading to production reduction and sometimes plant shutdown. Proper identification and prediction of slug flow is key to efficient and safe operation of pipelines. In this study, supervised and unsupervised machine learning algorithms were used to predict slug flow. The models were developed and validated using 120 data points from experimental studies of a pipeline-riser system. The results revealed near perfect prediction with genetic algorithm performing best with AUC score of 0.983, followed by the ANN-GA with an AUC score of 0.981, and XGBoost and Extra Trees, both scoring 0.966. The linear models (logistic regression and linear SVC) performed poorly when compared to the performance of other models. The models obtained from this study give insights into the efficiency of machine learning algorithms for slug flow prediction and its potential for applications in the oil and gas industry.
Keywords: Slugging, Multiphase flow, intermittent flow, Genetic Algorithm, ANN

1. INTRODUCTION

Multiphase flow is complex due to the chemical and physical interactions of the phases, as well as differences in flow characteristics, resulting in issues such as corrosion, erosion, and slugging. Flow regimes show the distribution of one phase relative to the others in a multiphase phase system. A major feature of multiphase flow which makes it an extremely challenging problem to understand is the fact that multiphase flow tends to take varying forms. A flow regime map is a common graphical representation of the flow regimes that is organized according to the flow circumstances. Several mapping factors, such as the phase superficial velocities Froude number and change of the phase velocities, are necessary to create a flow regime map and have been employed by various writers (Paglianti et al., 1996; Ouyang and Aziz, 1996; Ouyang and Aziz, 2002). A typical flow regime map for horizontal system is shown in Figure 1. The identified flow regimes in vertical pipes frequently differ from those in horizontal pipelines (Weisman and Kang, 1981). Multiphase flow regimes are significantly affected by phase characteristics and pipe sizes (Spedding et al., 1998). The four basic types of flow regimes in vertical pipelines are bubble flow, slug flow, churn flow, and annular flow (McQuillan and Whalley, 1985). The flow regime map and typical flow patterns for a vertical pipeline are shown in Figure 2.
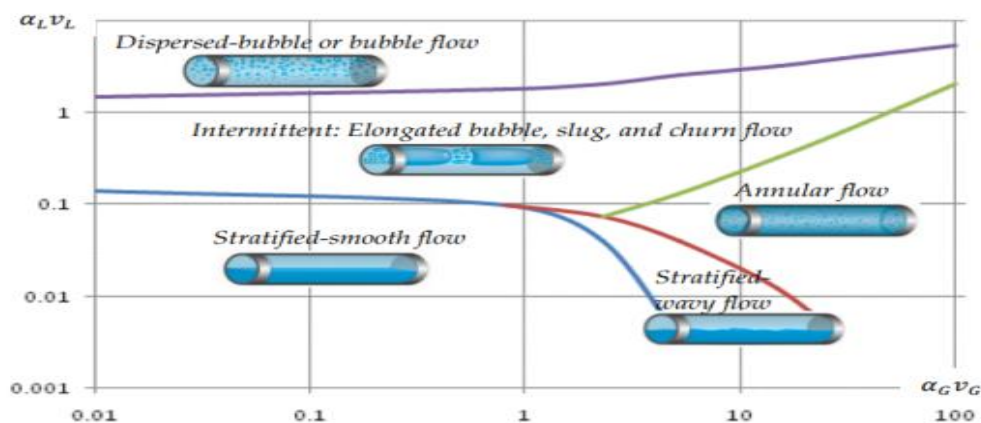
Figure 1: Horizontal pipe steady-state flow regime map. (Ove Bratlad 2010)
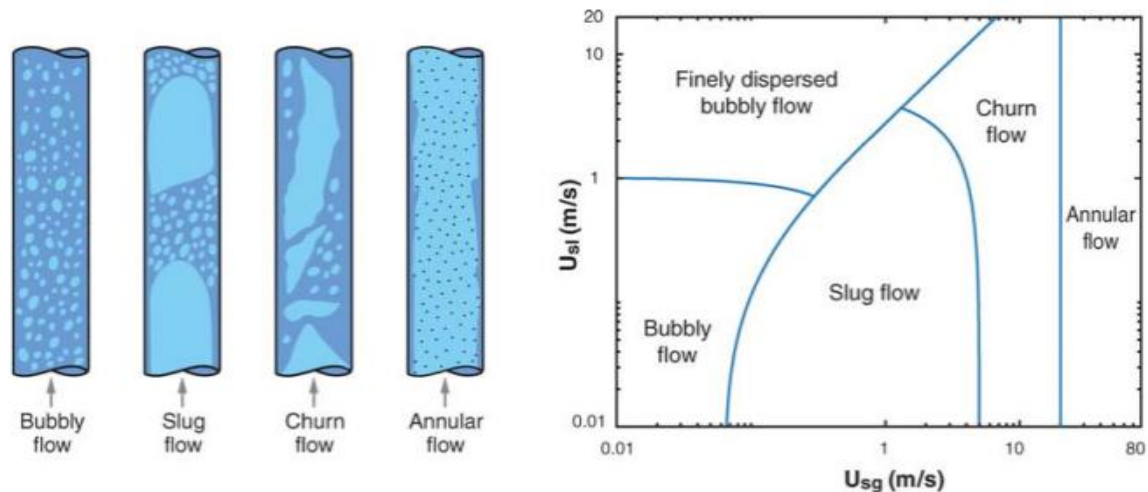
Figure 2: Multiphase flow pattern and flow regime map for vertical pipeline (Ove Bratlad, 2010)

Slug flow is a cyclic flow pattern characterized by pressure fluctuations and the erratic delivery of liquid and gas to processing facilities during oil and gas production and transportation. It shows up as variations in flow and pressure, which can interfere with topside processing facilities and cause harm to the structural integrity of pipeline. These fluctuations can cause separator flooding, a shutdown or reduction in production, erosion, increased corrosion rate, platform trips, and plant shutdown. "The formation of slugs is a complex process that depends on the interaction between fluid properties, pipeline geometry, and operating conditions," Bhagwat and Ghajar (2015). According to Mukherjee and Brill (1985), "slug flow can result in pressure surges that exceed the design limits of the pipeline and cause structural damage or failure." Additionally, the intermittent nature of slug flow can give rise to liquid collection in the pipeline, which can cause corrosion, hydrate development and wax deposition. Maley (1997) investigated slug flow properties in large horizontal pipe diameters. The results indicated that for a particular film Froude number, the liquid holdup increased with the slug viscosity. Zhao et al. (2015) discovered that slug flow occurrence was higher in small diameter pipe when compared with large diameter pipe.

Machine learning prediction of slug flow involves the development of models that can predict the occurrence of slug flow in various pipeline configuration and operating conditions. Several authors have explored machine learning as an efficient tool for slug flow prediction, this is because of their capacity to recognize complex patterns and process large volume of data. Ng et al. (2020) revealed that preprocessed data yielded higher accuracy after carrying out an investigative study to assess the performance of support vector machines (SVM) and artificial neural networks (ANN) on raw and preprocessed data. Alhashem (2019) employed the use of selected supervised machine learning algorithms to predict multiphase flow regimes, Random Forest performed best with an accuracy of 90.8%.

Using experimental data from Ehinmowo (2015), Ehinmowo et al. (2018) used ANN to Predict Riser Base Pressure in a Multiphase Pipeline-Riser System. The results showed near-perfect predictions with a mean square error of 0.00207197 and a regression coefficient of 0.99919.

Chandrasekaran (2018) developed two data models using artificial intelligence techniques for the prediction of liquid hold up and identification of flow patterns in multiphase flow systems. The developed model was built on the experimental results from the Mukherjee correlation for lower operating pressure regimes. Guillen-Rondon et al (2018) used support vector machine to predict flow patterns in multiphase system. The resulting confusion matrices had 99% accuracy. Ebirim et al. (2021) employed random forest to predict liquid hold up and slug flow regime. They conducted an experiment using a 67mm diameter vertical pipe, and after obtaining the parameters for liquid hold-up, void %, structural velocity, slug frequency, length of slug, and film thickness, he applied the machine learning models for prediction. In a similar study, Arteaga-Arteaga et al. (2021) carried out a comprehensive study which showed that Extra Trees (ET) performed well, as high precision was achieved using hyperparameters tuning. The authors used ten machine learning models to predict two-phase flow patterns. The Extra trees model performed best with an accuracy of 98.8%.

Researchers have conducted several studies using data-driven and machine learning approaches to predict the occurrence of slug flow and its characteristics. These models and techniques have aided further understanding of slug flow, its characteristics and it has helped to improve multiphase flow production. However, no author has predicted slug flow occurrence using genetic algorithm. The best performing algorithms will be identified based on the accuracy, ROC AUC score and other selected metrics.

2. **METHODOLOGY**

The aim of this study is to predict slug flow occurrence using machine learning algorithms using data sets

obtained from experiments on slug flow conditions in riser systems. It consists of 120 rows with superficial liquid velocity, superficial gas velocity, and a target that indicates whether the flow is a slug flow.

2.1 Machine Learning Algorithms Deployed in this Study

The algorithms used in this study include logistic regression (LR), linear support vector classifier (Linear SVC), extremely randomized trees (ET), extreme

gradient boosting (XG Boost), genetic algorithm (GA), and a hybrid of artificial neural network with genetic optimization (ANN-GA)

*Logistic Regression (LR)***:** Logistic Regression is a binary classifier that uses a sigmoid function (s-curve) as shown in the diagram below to give an output between 0 and 1.
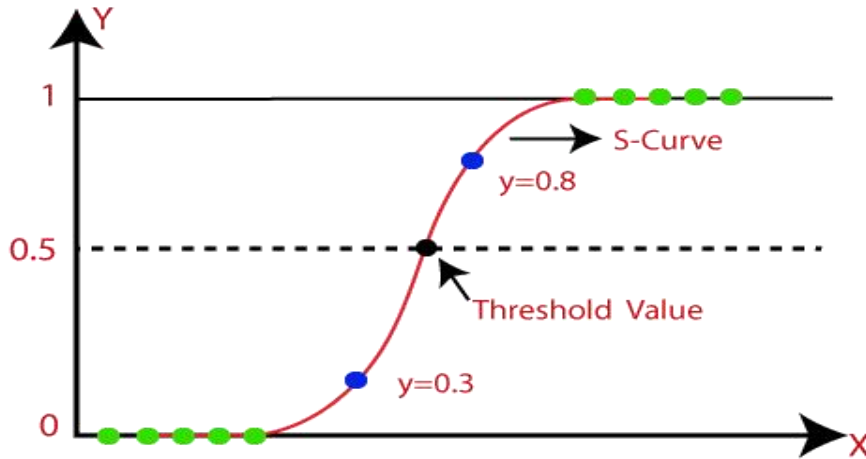
Figure 3: sigmoid function for logistic regression

Linear SVC: Linear SVC is a Support Vector Machine-based linear classifier that draws a straight line to separate data points into two groups and helps classify new data based on their position relative to that line.
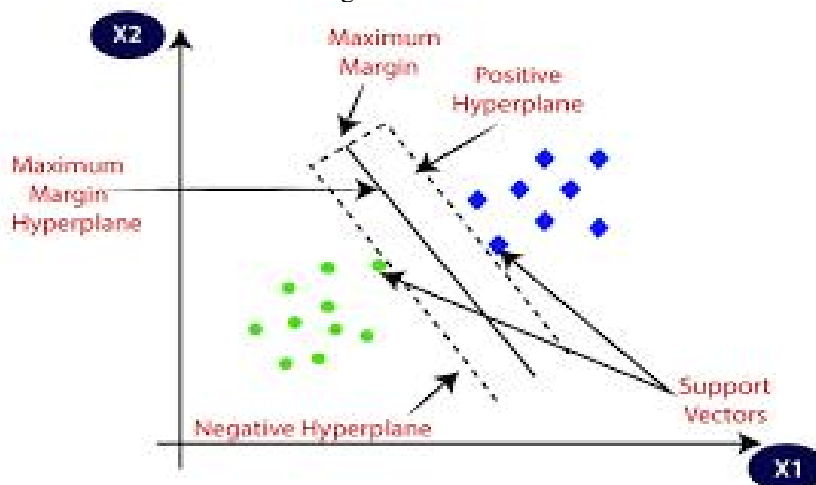
Figure 4: hyperplane for Linear SVC

Extreme Gradient Boosting (XGBoost): This method combines multiple weak decision trees, to create a strong predictive model. This works by gradually adding predictors to an ensemble, with each one correcting its predecessor.
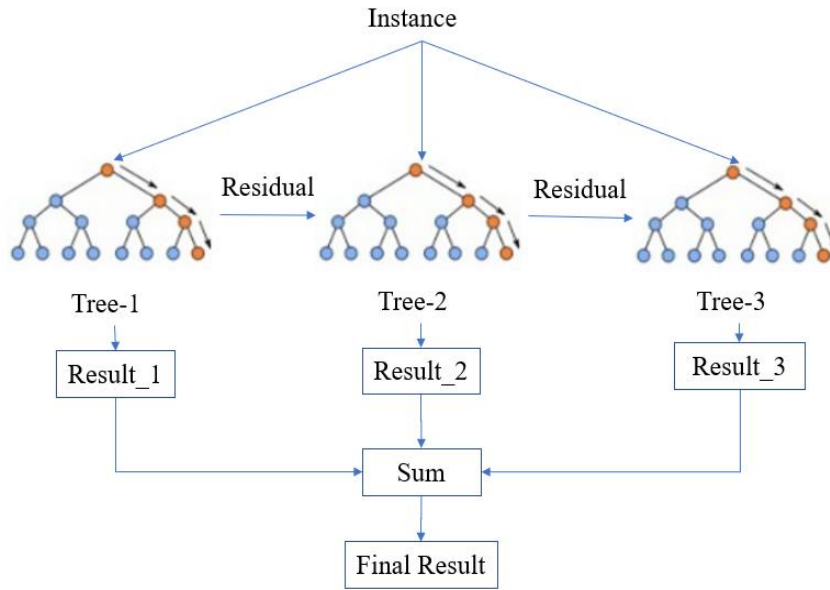
Figure 5: Flowchart for extra trees

Extra-trees (ET): Extremely Randomized Trees is an ensemble learning algorithm like Random Forest but introduces additional randomness during the tree building process. RF choose the best node to split on while ET randomize the node split.
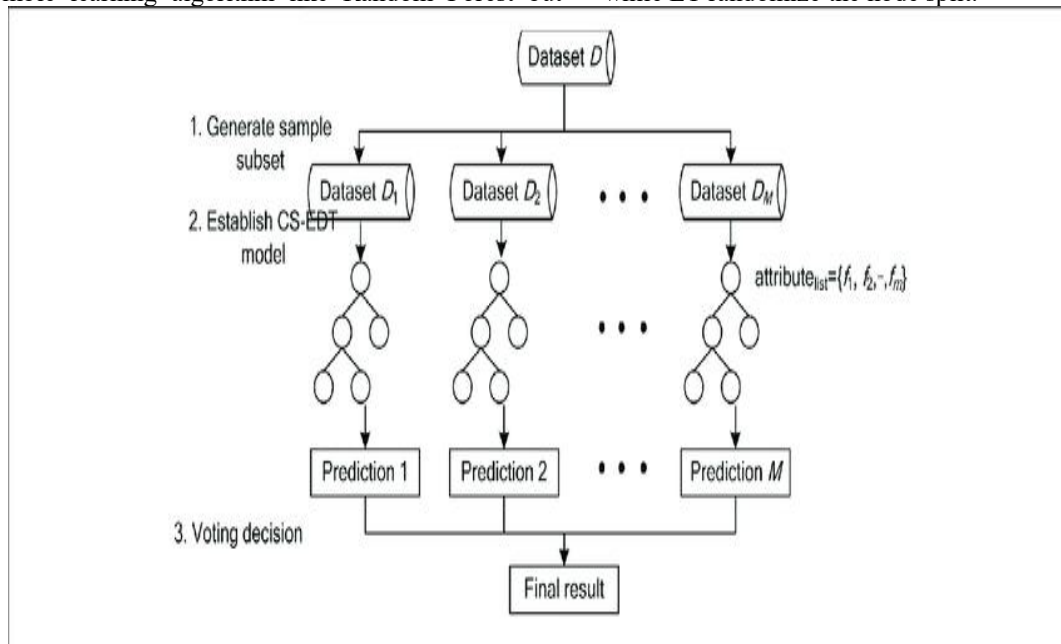
Figure 6: Flowchart for extra trees

ANN-GA: This is a hybrid method that use Artificial Neural Networks as an underlying model for classification and genetic algorithm for optimizing the structure and parameters of the neural network.
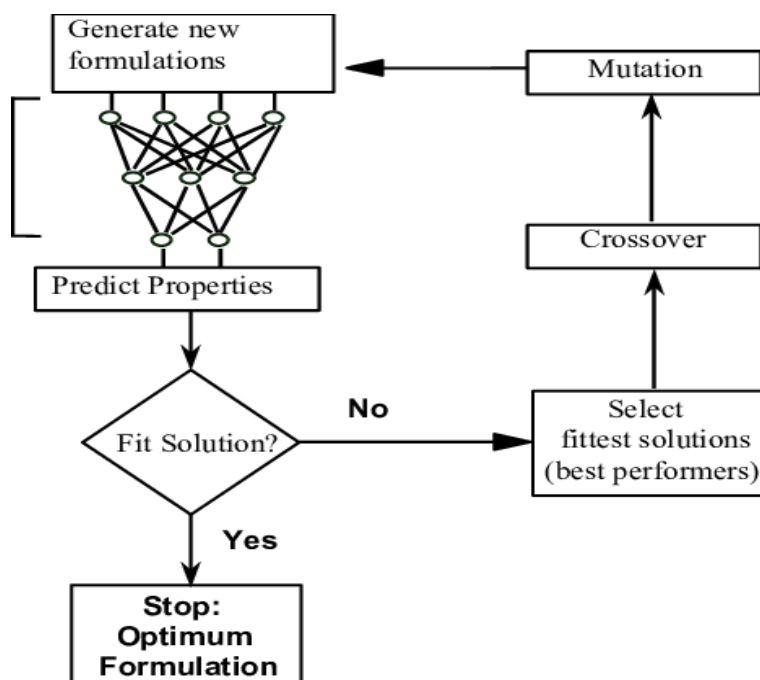
Figure 7: Flowchart for ANN-G*A*

Genetic Algorithm: This is an optimization method which functions by iteratively producing a population of potential solutions, evaluating their fitness, and using genetic operators (selection, crossover, and mutation) to generate new offspring solutions. Figure 8 is a flowchart of Genetic Algorithm.
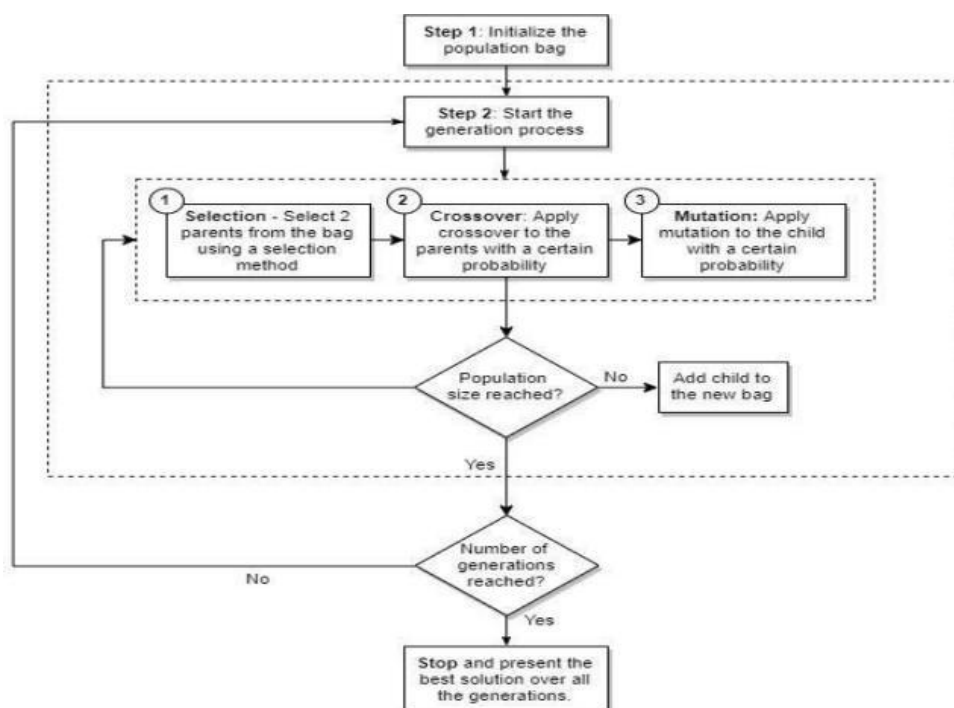
Fig 8: Flowchart of Genetic Algorithm

2.2 Statistical Analysis of Datasets and Metrics for Evaluating Predictions

The data sets used for this study was obtained from experiment on slug flow conditions in pipeline-riser systems. It consists of 120 rows with columns superficial liquid velocity, superficial gas velocity, and

an imbalanced target with ones and zeros. The ones indicate slug flow conditions, while the zeros indicate non-slug flow conditions.

Table 1: Statistical Summary of Experimental data

count	120.000000	120.000000	120.000000
mean	4.771583	0.906900	0.800000
std	3.631485	0.740703	0.401677
min	0.200000	0.030000	0.000000
25%	1.637500	0.250000	1.000000
50%	4.285000	0.740000	1.000000
75%	6.920000	1.480000	1.000000
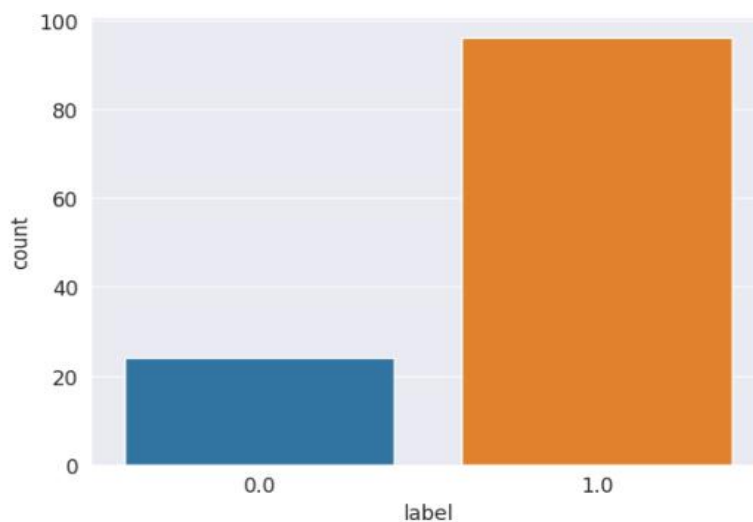
Fig 9: Plot of target distribution where 1 indicates slug conditions and 0 non-slug conditions

2.3 Model Training and Evaluation

The data was grouped based on the target and divided into two subsets, 70% for training and 30% for testing and validation. The train sets were augmented to cater for issues associated with the disproportionate distribution of the target. The data which includes the liquid and gas superficial velocities were loaded after which exploratory data analysis was performed to understand and investigate existing trends. Feature transformation was also done to extract important characteristics needed to train the machine learning model. Finally, the model was trained using the various machine learning techniques listed above and its performance was assessed on a test set to determine its accuracy.

2.4 Metrics for Evaluating Predictions
1. Confusion Matrix.

The confusion matrix gives an informative view of the model's performance, the properly and wrongly predicted classes, as well as the sorts of errors committed.

Table 2: confusioin matrix

	ACTUAL		PREDICTED VALUES
Positive (1)	Negative (0)		
TP	FP		
FN	TN		
Positive (1)	Negative (0)		

2. Accuracy

Accuracy is the percentage of correct predictions generated out of all predictions made.

$$Accuracy = \frac{TP + TN}{TP + TN + FP + FN} \qquad (1)$$

3. Precision

Precision is the quality of a positive prediction made by the model. The higher the precision, the more true positives the model predicts.

$$Precision = \frac{TP}{TP + FP} \qquad (2)$$

4. Recall

This metric assesses the model's ability to detect positive samples.

$$Recall = \frac{TP}{TP + FN} \qquad (3)$$

5. F1-score

Precision and recall must be high for the classifier to obtain a high F1 score. A high F1 score means that the classifier performed well.

$$F_1 score = \frac{2}{\frac{1}{Recall} + \frac{1}{Precision}} \qquad (4)$$

6. Receiver Operating Characteristic Area Under the Curve (ROC AUC)

It quantifies the performance of a model by measuring its ability to distinguish between positive and negative classes across different classification thresholds. It evaluates the performance of the classification models using the ROC curve and AUC values ranging from 0 to 1.
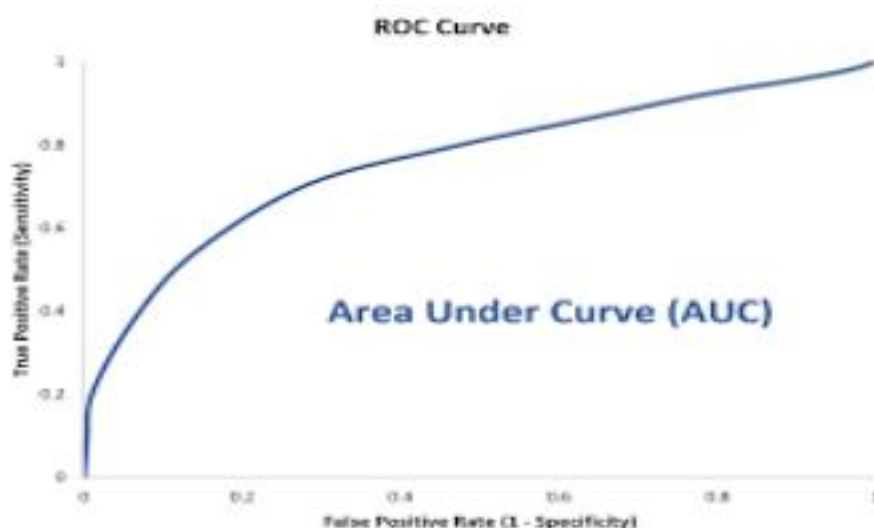
Figure 10: ROC AUC

3. RESULTS AND DISCUSSION

Table 3: Summary of metrics performance of machine learning models

Classifier	Brier loss	Log Loss	Precision	Recall	F1 score	ROC AUC
LOGISTIC REGRESSION	0.211537	0.661282	0.875000	0.725138	0.792453	0.647783
SVC	0.162551	0.479717	0.869565	0.689655	0.769231	0.630542
ETC	0.022833	0.075498	1.000000	0.931034	0.964286	0.965517
XGB	0.042420	0.131836	1.000000	0.931034	0.964286	0.965517
GA	0.015648	0.050045	1.000000	0.965517	0.982456	0.982759
ANN-GA	0.015021	0.061134	1.000000	0.952251	0.980126	0.980563
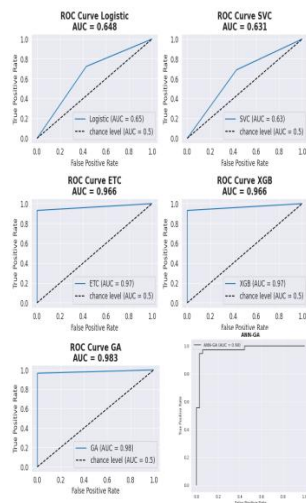
Figure 11: ROC AUC result for ML models

Figure 11 illustrates the ROC AUC for the LR, SVC, ETC, XGB and GA and their respective values. Based on their values, the genetic algorithm performed the best with an AUC score of 0.983, followed by the ANN-GA with an AUC score of 0.981, and XGBoost and Extra Trees, both scoring 0.966. The linear models (logistic regression and linear SVC) performed poorly as compared to others.

In Figure 12, the confusion matrix of various machine learning models is presented. It is observed that the GA model demonstrated the best performance by having only one misclassification, followed by the ANN-GA model which had two misclassifications. The XG Boost and Extra Trees models also showed promising results with two misclassifications each. However, the linear models did not perform as well, with over 10 misclassifications each. This poor performance can be attributed to certain limitations of linear models when dealing with complex data patterns.
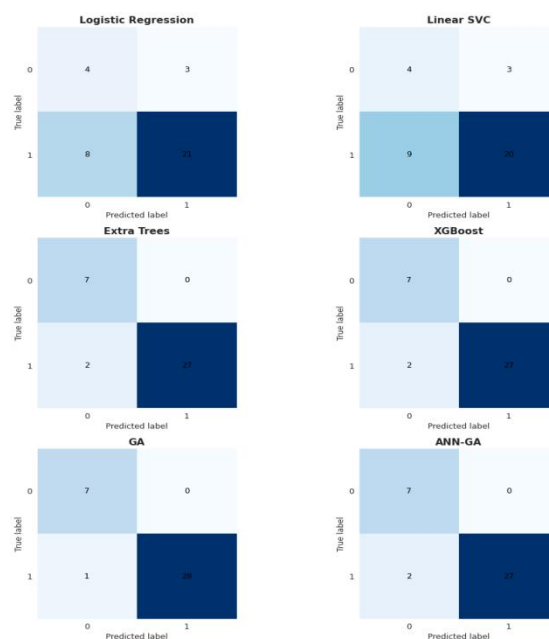
Figure 12: Confusion matrix of the ML models used

The performance metrics of the various classification models tested, including Logistic Regression, Support Vector Classification (SVC), Extra Trees Classifier (ETC), Extreme Gradient Boosting (XGB), and Genetic Algorithm (GA), are summarized in Table 3. The analysis revealed that ETC, XGB, and GA models outperformed the other models in almost all performance metrics, indicating their superior predictive capabilities in identifying slug flow occurrence. However, Logistic Regression and SVC models also showed commendable performance with acceptable precision and recall scores. To determine the best result, the model with the highest ROC AUC and accuracy score was selected.

4. CONCLUSION

This study utilized supervised and unsupervised machine learning algorithms, including logistic regression, linear support vector machine (SVM), extremely randomized trees, extreme gradient boosting (XG boost), genetic algorithm (GA), and a hybrid approach using artificial neural networks (ANN) and genetic algorithm (ANN-GA). The results showed that genetic algorithm performed best, achieving near-perfect prediction with an area under the receiver operating characteristic curve (ROC AUC) score of 0.983. The hybrid ANN-GA model also performed well with an AUC score of 0.981, followed by XGBoost and Extra Trees, both scoring 0.966. The linear models (logistic regression and linear SVM) performed poorly compared to the others.The study highlights the potential of machine learning algorithms for predicting slug flow and their practical applications in the petroleum industry. It also discusses previous research that has used various machine learning techniques, such as decision trees, support vector machines, artificial neural networks, and random forests, for slug flow prediction and multiphase flow analysis.

NOMENCLATURE

XG- extreme gradient
SVC- support vector classifier
ANN- artificial neural networks
GA- genetic algorithm
ROC AUC- receiver operating characteristic area under curve
SVM- support vector machine
ET- extra trees
Vsl- superficial liquid velocity
Vsg- superficial gas velocity
TP- true positive
TN- true negative
FP- false positive
FN- false negative

REFERENCES

Al-safran, E.M., (2003). *An experimental and theoretical investigation of slug flow characteristics in the valley of a Hilly-Terrain pipeline*. The University of Tulsa.

Alhashem, M., (2019), November. Supervised machine learning in predicting multiphase flow regimes in horizontal pipes. In *Abu Dhabi International Petroleum Exhibition and Conference* (p. D021S043R003). SPE.

Arteaga-Arteaga, H.B., Mora-Rubio, A., Florez, F., Murcia-Orjuela, N., Diaz-Ortega, C.E., Orozco-Arias, S., Bravo-Ortíz, M.A., Robinson, M., Guillen-Rondon, P. and Tabares-Soto, R., (2021). Machine learning applications to predict two-phase flow patterns. *PeerJ Computer Science*, 7, p.e798.

Bhagwat, S.M. and Ghajar, A.J., (2015). An Empirical Model to Predict the Transition Between Stratified and Nonstratified Gas–Liquid Two-Phase Flow in Horizontal and Downward Inclined Pipes. *Heat Transfer Engineering*, *36*(18), pp.1485-1494.

Chandrasekaran, S. and Kumar, S., (2018). Flow Pattern and Liquid Holdup Prediction in Multiphase Flow by Machine Learning Approach. *Environmental Science: An Indian Journal Research*, *14*(1), p.173.

Ebirim, F.O., Abdulkadir, M. and Agajo, J., (2021). Development of a random forest model for predicting liquid holdup and slug flow characteristics in vertical two-phase flow using machine learning technique. *International Journal of Pure and Applied Science, 17(9),* ISSN: 1660-5332.

Ehinmowo, A.B., (2015). Stabilising slug flow at large valve opening using an intermittent absorber. Cranfield University, PhD, Oil and Gas Engineering, July 2015.

Ehinmowo, A.B., Bishop, S.A. and Jacob, N.M., (2018). Prediction of Riser Base Pressure in a Multiphase Pipeline-Riser System Using Artificial Neural Networks. *Journal of Engineering Research*, *23*(2), pp.25-34.

Guillén-Rondon, P., Robinson, M.D., Torres, C. and Pereya, E., (2018). Support vector machine application for multiphase flow pattern prediction. *arXiv preprint arXiv:1806.05054*.

Maley, J., (1997). *Slug flow characteristics and corrosion rates in inclined high pressure multiphase flow pipes* (Master's thesis, Ohio University).

McQuillan, K.W. and Whalley, P.B., (1985). Flow patterns in vertical two-phase flow. *International Journal of Multiphase Flow*, *11*(2), pp.161-175.

Mukherjee, H. and Brill, J.P., (1985). Empirical equations to predict flow patterns in two-phase inclined flow. *International journal of multiphase flow*, *11*(3), pp.299-315.

Ng, M.F., Zhao, J., Yan, Q., Conduit, G.J. and Seh, Z.W., (2020). Predicting the state of charge and health of batteries using data-driven machine learning. *Nature Machine Intelligence*, *2*(3), pp.161-170.

Ouyang, L.B. and Aziz, K., (1996). Steady-state gas flow in pipes. *Journal of Petroleum Science and Engineering*, *14*(3-4), pp.137-158.

Ouyang, L.B. and Aziz, K., (2002). A mechanistic model for gas–liquid flow in horizontal wells with radial influx or outflux. *Petroleum science and technology*, *20*(1-2), pp.191-222.

Ove Bratland, (2010). The Flow Assurance Site, Chapter 1.

Paglianti, A., Giona, M. and Soldati, A., (1996). Characterization of subregimes in two-phase slug flow. *International journal of multiphase flow*, *22*(4), pp.783-796.

Spedding, P.L., Woods, G.S., Raghunathan, R.S. and Watterson, J.K., (1998). Vertical two-phase flow. *Chemical Engineering Research and Design*, *5*(76), pp.628-634.

Weisman, J. and Kang, S.Y., (1981). Flow pattern transitions in vertical and upwardly inclined lines. *International Journal of Multiphase Flow*, *7*(3), pp.271-291.

Zhao, Y., Lao, L. and Yeung, H., (2015). Investigation and prediction of slug flow characteristics in highly viscous liquid and gas flows in horizontal pipes. *Chemical Engineering Research and Design*, *102*, pp.124-137.

TECHNO-ECONOMIC FEASIBILITY OF PRODUCING 100,000 METRIC TONNES OF BIODIESEL FROM NEEM OIL VIA TRANSESTERIFICATION

*[1]Fadayini, O., [2]Adeyemo, F., [2]Bello, E.V., [3]Bolaji, O. T., [1]Madu, C., [1]Oso, A.O., [4]Ogbodhu, C. U, K., [5]Obisanya, A. A., [6]Salisu, S. A

[1]Department of Chemical Engineering, Lagos State University of Science and Technology Ikorodu, Lagos, Nigeria.
[2]Chemical & Petroleum Engineering Department, University of Lagos, Akoka, Lagos. Nigeria.
[3] Department of Food Science and Technology, Lagos State University of Science and Technology Ikorodu, Lagos
[4]Department of Chemical Engineering, Delta State University of Science and Technology, Ozoro, Delta, Nigeria
[5]Department of Chemical Engineering, Yaba College of Technology, Lagos, Nigeria
[6]Nigerian National Petroleum Company (NNPC), Abuja, Nigeria
*Corresponding author: fadayini.o@lasustech.edu.ng

ABSTRACT

This research provides a comprehensive techno-economic evaluation of the process design for 1000 metric tonnes per annum biodiesel synthesis from Neem oil implemented on Aspen HYSYS V11.0. The process design includes the removal of oil from Neem seeds, transesterification of the oil to produce biodiesel, and the purification of the biodiesel for assessing the viability and profitability of production for commercial purpose. The outcome reveals the estimated total equipment cost, investment cost, and annual revenue as $592,325.00, $ 31,849,313.94 and $ 95,000,000.00 respectively. This design is highly profitable, with a payback time of 0.34 years, discounted payback period of less than a year with inflation rate up to 50% and positive values of NPV within 5 years of operation. The best optimum condition of methanol to oil ratio (MR) was obtained as 4.5:1 with a yield of 97.49% with validation error of 1.08%.
Keywords: Neem oil; Transesterification; Biodiesel; Process design; Economic analysis.

INTRODUCTION

The biodiesel industry has been rapidly expanding in recent years due to the need to sustain energy matrix demands globally (Igwebuike, 2023; OECD-FAO, 2024). Biodiesel is simply a class of biomass-based biofuels that have garnered much attention as a renewable fuel which is an alternative to fossil fuel like petroleum owing to the impending depletion of fossil fuels and evidential ecological reasons (Costa *et al.,* 2019; Mohan *et al.,* 2023). Asides the environmental challenges posed by the use of fossil fuel, the tendency of fossil fuel as a typical non-renewable energy to run out after a long period of exploration, quantity available as against the teeming population of users either for domestic and industrial use and the increasing hike in price had necessitated the need for alternative source of energy leading to the discovery of vegetable based fuels such as biodiesel (Demirbas and Kara, 2006; Hums *et al*., 2016; Awogbemi *et al.,* 2024).
Biodiesel is made up of fatty-acid methyl esters (FAME) produced from myriads of food stocks like plant oil, animal fats, pyrolysis oil, waste cooking oil (Mohan *et al.,* 2023; Ghosh *et al.,* 2024). A leading example of plant oil for the production of biodiesel is the Neem oil extracted from Neem seed. Neem oil has several advantages as a biodiesel feedstock because of its availability, low cost, and high oil content, Neem plants are scientifically referred to as *Azadirachta indica* with height and girth estimation ranging from 12 to 18 m

and1.8 to 2.4 m respectively (Akbar and Jaka, 2021). Neem seeds are predominantly light to dark brown, bitter to taste making it non-edible, it smells like that of the mixture of peanut and garlic and consists largely of triglycerides (Ravindranath *et al.,* 2011; Ali *et al.,* 2013). The cultivations of Neem plants are reported to be predominant in India, Malaysia, United Arab Emirates and a few others of the South East Asia (Ali *et al.,* 2013). Neem plants are also cultivated and thrive in Nigeria (Banu *et al.,* 2018; Mustapha *et al.,* 2020; Igwebuike, 2023; Suleiman *et al.,* 2023).
Biodiesel portrayed some starling qualities as against fossil fuels (Demribas and Kara, 2006). It is non-toxic, biodegradable, readily available, high heat value, possesses oxygen content in the range of 10 to 11 %, free of sulphur and aromatic compounds; allows for CO_2 reutilization thereby generating low net greenhouse gas (GHG) emissions and can be blend with fossil fuel (Ghosh *et al.,* 2024). The production of biodiesel is viewed in four steps or perspectives namely: (i) direct use or blending approach, (ii) micro emulsions, (iii) thermal cracking means and (iv) transesterification (Chelladurai and Rajamanickam, 2014). Production by transesterification is the most viable and common means (Mohan *et al.,* 2023; Suleiman *et al.,* 2023). The techno-economic analysis is very fundamental to assess and ascertain the feasibility for the production of biodiesel on commercial scale by taking cognizance of the effect of variables associated with biomass availability,

variations in demand, and price fluctuations of raw materials, purchase of process equipment, land for setting layout among others (Akhabue *et al.,* 2020; Nunes and Silva, 2023; Souza *et al.,* 2023).

This article seeks to achieve a feasible route with the use of Aspen Simulation software for the manufacture of biodiesel from Neem seeds; developing a process algorithm, process, and instrumentation drawing for the process flow diagram, to evaluate the cost and economic viability of the process route. Performing in-depth techno-economic analysis is necessary to pique the attention of industry players and encourage them to invest more in biomass-based industries.

2.0 METHODOLOGY

2.1 Process Design

The process design for biodiesel manufacture from Neem oil includes the following steps Neem oil extraction from seed, Neem oil pretreatment, and transesterification, separation of biodiesel and glycerol, biodiesel purification, product storage and distribution of the purified biodiesel.

2.2 Process Simulation Results

The extraction process was simulated using Aspen Hysys. The algorithm and detailed description of the process design is depicted by Figure 1.0 and Figure 2.0 respectively while the equipment design parameters for the simulated process route are presented in Table 1.0.
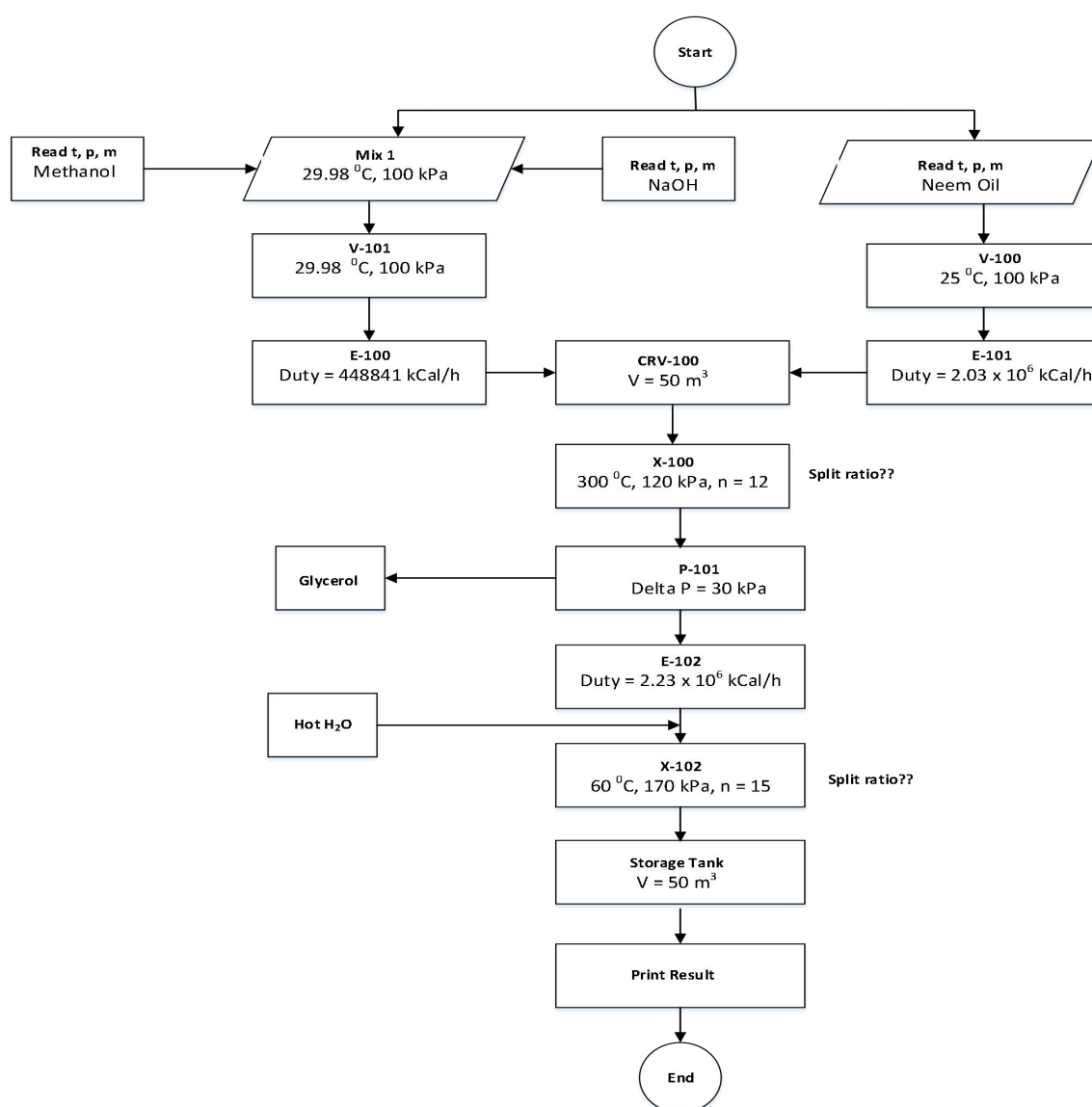
Figure 1.0: Design Algorithm
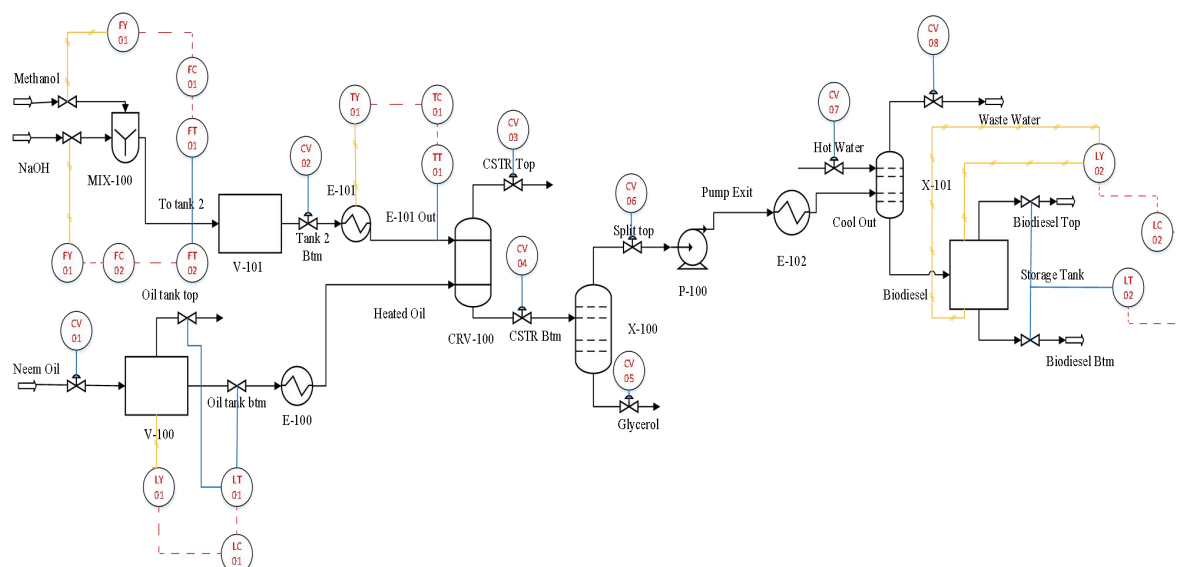
Figure 2.0: Process flow for the synthesis of Biodiesel from Neem oil

Table 1.0: Equipment Design Parameters and Operating Conditions

MIX 100	Temperature (°C)	Pressure (kPa)	
	29.06	100.00	
V101	Temperature (°C)	Pressure (kPa)	Volume (liters)
	29.06	100.00	500
V101	Temperature (°C)	Pressure (kPa)	Volume (liters)
	25.00	100.00	500
E100	Delta T (°C)	Delta P (kPa)	Heat duty (Gcal/hr)
	55	0.00	4620
E101	Delta T (°C)	Delta P (kPa)	Heat duty (Gcal/hr)
	50.094	0.00	9899
Reactor	Temperature (°C)	Pressure (kPa)	Heat duty (Gcal/hr)
	241.3	100	-2.42416
X100	Temperature (°C)	Pressure (bar)	
	300	120	
X101	Temperature (°C)	Pressure (bar)	
	112.1	150	
X101	Temperature (°C)	Pressure (bar)	
	40.00	170	
E102	Outlet temp (°C)	Outlet pressure (kPa)	Heat Duty (Gcal/hr)
	56.53	190	4.61×10^4
	Outlet temp (°C)	Outlet pressure (bar)	
Storage Tank	56.53	190	

Figure 2.0 succinctly illustrates the process flow diagram while Table 1.0 shows the equipment design parameters and operating conditions which are crucial aspects of the manufacturing process of biodiesel from Neem oil. These parameters and conditions such as temperature, and pressure in Aspen HYSYS environment were carefully considered during the design of the equipment and operation of the plant to ensure the safety, efficiency, and quality of the biodiesel production.

3.0 RESULTS AND DISCUSSION
3.1 Process Optimization
Process optimization is an activity carried out to determine the optimal point(s) of any process. A process optimization was conducted by taking the yield of biodiesel at various MeOH/Oil ratios (MR) to study the optimal point. Table 2.0 shows the various values of MeOH/Oil ratios tabulated against the yield of biodiesel.

Table 2.0: Molar ratio optimization plot

MeOH/Oil Ratio	1	2	3	4	5	6	7	8	9	10
% Yield	49.64	49.25	65.03	96.43	95.4	94.29	93.65	93.25	90.63	90.16

Figure 3.0 is the optimization plot. Here, the molar ratios of Methanol: Oil used is between 1– 10, within the Aspen Hysys simulation environment to estimate the yield of the biodiesel. By a molar ratio of 1, means 15.52 kmol/hr of methanol and 15.52 kmol/hr of Neem oil. By a molar ratio of 2, means 31.04 kmol/hr of methanol and 15.52 kmol/hr of Neem oil. The figure reveals that the yield of biodiesel increases within a molar ratio of 1 to 4 and decreases from 4 to 10. The plot shows that the feasible region of the optimum (maximum) yield of biodiesel is between molar ratios of 3.0 to 4.5. The accuracy and reliability of the model, which interprets the plot and experimental results, was rigorously evaluated by calculating the correlation coefficient (R-value). This statistical measure determines the strength and significance of the relationship between the model's predictions and actual experimental data, thereby validating the model's effectiveness in explaining the observed phenomena (Kolakoti et al., 2020; Bello and Olafadehan, 2022).
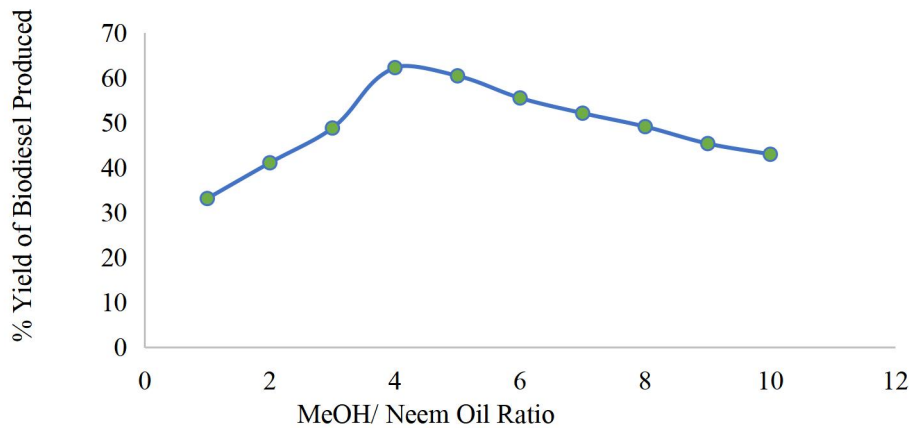
Figure 3.0: Optimization Plot: % Yield of Biodiesel Produced against MeOH / Neem Oil Ratio.

3.1.1   Developing Objective Function

The objective function for the optimization plot is modeled as a quadratic expression with the general equation (1), using mathematical modeling software, Sigma Plot, version 14.0:

$$f = y_o + ax + bx^2 \qquad (1)$$

Owing to the polynomial nature of the experimental results as shown in Figure 3.0, it was modeled as a second-order equation (2) given as:

$$f = -20.995 + 44.865x - 5.993x^2 \qquad (2)$$

where f = yield of biodiesel ; x = molar ratio of methanol to Neem oil; which actually describes the quantity of biodiesel needed to achieve maximum yield of biodiesel from the Neem oil. The ANOVA result reveals that the model could predict the experimental results with a moderately strong correlation coefficient (R^2) value of 0.9905. The model is statistically significant because its p-value is less than 0.05 and it provides a better fit to the data than a null model with no predictors (Bello and Olafadehan, 2022).

3.1.2 Sensitivity Analysis and Optimization

Sensitivity analysis is a method used to identify the effect of variations in the input parameters on the output results of a process (Atadash et al., 2011). In the synthesis of biodiesel from Neem oil, sensitivity analysis was used to evaluate the impact of changes in the volume (m^3/h) of Neem oil used on the quantity of biodiesel (L/h) produced. Table 3.0 is the sensitivity analysis for the synthesis of biodiesel from Neem oil. This shows that increase in flow rate of vegetable oil results to corresponding increase in biodiesel flow rate. Figure 4.0 depicts the sensitivity/response of the Biodiesel manufacturing process to changes in the volumetric flow of the main feedstock used. It clearly illustrates that the higher the rate of feedstock in-flow the higher the rate of product out-flows. The result posits the following: (i) the process system capacity is adequate enough to accommodate such amount of flow rates of Neem oil for large volume of biodiesel production. If the flow rate exceeds the system's capacity, it may not lead to an increase in the production of biodiesel, (ii) the reaction of trans-esterification in the process equipment is effectively being carried at the set conditions or chosen parameters, and (iii) the process

system is operating at sufficient residence time for the completion of the trans-esterification reaction. These aforementioned points translate to the process efficiency

(Filemon and Uriarte, 2010; Atadashi *et al.,* 2011; Hums *et al.,* 2016).

Table 3.0: Sensitivity Analysis

Vol. of Neem Oil (m³/h)	15	16	17	18	19	20	21	22	23	24	25
Vol. of Biodiesel (L/h)	14640	15660	16690	17720	18760	19800	20850	21910	23420	24470	25530
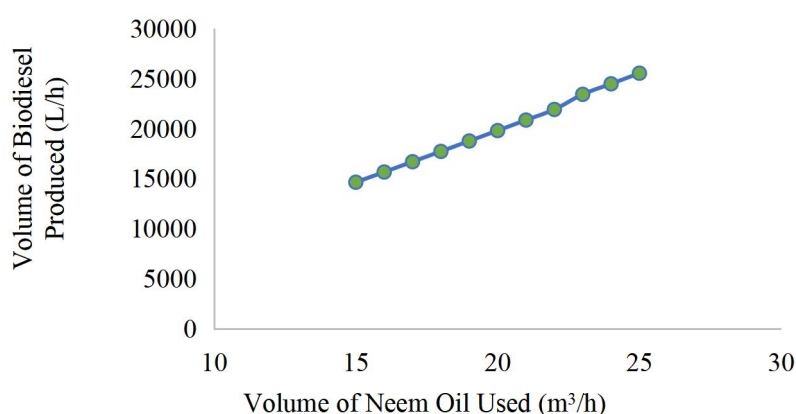
Figure 4.0: Sensitivity Analysis: Vol. of Biodiesel Produced (L/h) against Vol. of Neem Oil used (m³/h).

3.2   MATLAB Optimization

Commercial optimization software*, MATLAB version R2021a* was used for the optimization of the objective function using genetic algorithm. The genetic algorithm credited to Taylor *et al.,* 2018 a meta-heuristic algorithm configured after the biological natural selection process. It is classified as an evolutionary algorithm (Bello and Olafadehan, 2021). The best optimum condition of MR obtained after the complete optimization exercise was found as 4.5:1 resulting to a yield of 97.49 % with validation error of 1.08 %. Hence, the objective of the process optimization is to maximize the biodiesel yield

and quality obtained, while minimizing MeOH/Oil ratio (MR) and waste generated. Optimization is crucial as it maximizes yield and efficiency, reduces costs and environmental impact, and improves process control and sustainability. The optimal process for biodiesel produced from the Neem oil based on the optimization study occurs at a molar ratio (MeOH/Oil) of approximately 5. At this ratio, the biodiesel yield reaches its peak at 96.43%, indicating that the most efficient conversion of Neem oil to biodiesel is achieved with this specific ratio of methanol to oil.

3.3 Economic Evaluation

The economic evaluation of the process design for biodiesel production from Neem oil includes the capital and operating costs of the process, as well as the revenue generated from the sale of biodiesel. Capital costs include the cost of equipment, such as the oil extraction press, transesterification reactor, and centrifuge, as well

as the cost of land, buildings, and utilities. Operating costs include the cost of raw materials, labour, maintenance, and utilities. The revenue generated from the sale of biodiesel depends on the market price of biodiesel and the production capacity of the plant. The profitability of the biodiesel plant depends on the difference between the revenue generated from the sale

of biodiesel and the total capital and operating costs of the plant. Hence, the equipment cost for this process route is done using the Aspen Energy Analyzer of Aspen HYSYS version 8.8. Table 4.0 shows the major equipment cost as estimated on the Aspen Energy Analyzer of Aspen HYSYS version 8.8. As seen above, the major equipment are Pump, Feed mixer, Storage Tank, Separating funnel, Heaters, Cooler, and Tanks. The cost escalation, fixed capital investment was computed employing as suggested by Sinnot and Towler, (2009). The cost escalation and fixed capital investment were calculated as $ 592,325 and $ 592,325.00 respectively. The selling price of 1 tons of biodiesel was

estimated as $ 950. For 100,000 tonnes/year the price will translate to $ 95,000,000.00.

The fixed capital investment was computed using Table A in the appendix to obtain the direct cost (On and Off Sites likewise the indirect cost). Details of the calculations can be found in the supplementary materials. The Net Present Value (NPV), Pay-Back Time (PBT), Discounted Pay-Back Time (DPBT) were employed to access the investment profitability. The estimated discounted payback periods from the second year to the fifth year of operation were found to be 0.5019, 0.5660, 0.6210 and 0.6685 year with inflation rate of 20 %, 30 %, 40 % and 50 % respectively.

Table 4.0: Equipment cost

Equipment name	Pump (P-100)	Feed mixer	Cooler (E-100)	Reactor (CRV-100)	Degummer (X102)	Storage tank	Tank 1 (V-100)	Separating funnel (X-100)	Heater (E-102)	Tank 2 (V-101)	E-101	Total
Cost ($)	4,900	2700	9,900	84,000	8,600	108,800	137,800	8,600	23,100	5,600	14,500	408,500

4.0 CONCLUSION

The research work established the possibility, viability and the potential of Biodiesel production from Neem seeds oil. This has several advantages as a sustainable and renewable source of energy especially in Africa where Neem trees are commonly found. By utilizing a locally sourced, non-edible feedstock such as Neem oil, this approach not only reduces dependency on fossil fuels but also contributes to rural development and job creation. The optimized yield of 97.49% at MeOH/Oil ratios of 4.5:1 with the narrow margin of validation error; the short payback period estimated at 0.34 year; discounted payback period of less than a year for inflation rate of up to 50%, and positive values

of Net Present Value (NPV) within five years of operation depicts high profitability for commercial purpose. The availability, abundance and accessibility of Neem seeds in most African countries stand the chance to compliment the economy of production of biodiesel and reduce the over-dependence on fossil fuel. Furthermore, the use of Neem oil, which is often regarded as a by-product or waste in many regions, adds value to agricultural practices and promotes a circular economy, thereby strengthening the overall economic resilience of biodiesel production through this process. However, future research direction could involve conducting empirical studies to validate the findings, serving as a natural extension or second phase of this investigation.

REFERENCES

Akbar, M and Jaka, S (2021). Techno-economic Analysis for Biomass Supply Chain: A state-of-the-art Review. *Renewable and Sustainable Energy Reviews*, 135,110164–110178. https://doi.org/10.1016/j.rser.2020.110164

Akhabue, C. E., Osa-Benedict, E. O., Oyedoh, E. A., Otoikhian, S. K. (2020). Development of a Bio-Based Bifunctional Catalyst for Simultaneous Esterification and Transesterification of Neem Seed Oil: Modeling and Optimization Studies. *Renewable Energy, 152*, Pp.724–735.

Ali, M. H., Mashud, M., Rubel, M.R. and Ahmad, R.H. (2013). Biodiesel from Neem Oil as an Alternative Fuel for Diesel Engine. *Procedia Engineering*. 56, Pp, 625-630. https://doi.org/10.1016/j.proeng.2013.169

Atadash, I, Aroua, M, Aziz, A and Suleiman, N. (2011). Membrane Biodiesel Production and Refining Technology: A Critical Review. *Renewable and Sustainable Energy Reviews*, 15, Pp.5051-5062. https://doi.org/10.1016/j.rser.2011.07.051

Awogbemi, O, Ojo, A. A. and Adeleye, S. A. (2024). Advancements in the Application of Metal Oxide Nanocatalysts for Sustainable Biodiesel Production. *Discover Applied Sciences*. 6 (250), Pp. 1-31. https://doi.org/10.1007/s42452-024-05920-3

Banu, H .D, Shallangwa, T .B, Joseph, I., Magu, T. O, Hitler, L. and Ahmed, S. (2018). Biodiesel Production from Neem Seed (Azadirachta indica) Oil using Calcium oxide as a Heterogeneous Catalyst. *Journal of Physical Chemistry & Biophysics*, 8 (2), 1000266. https://doi.org/10.4172/2161-0398.1000266

Bello, V. E. and Olafadehan, O. A. (2022). Evaluation of Heterocyclic Aromatic Compound Dye (methylene blue) on Chitosan Adsorbent Sourced from African Snail Shell: Modelling and Optimization Studies. *Journal of Applied Science & Process Engineering*. 9 (2022), Pp. 1054–1090, https://doi.org/10.33736/jaspe.4464.2022

Bello, V. E. and Olafadehan, O.A. (2021). Comparative investigation of RSM and ANN for Multi-Response Modeling and Optimization Studies of Derived

Chitosan from *Archachatina marginata* shell. *Alexandria Engineering Journal*. Pp. 603869-3899. https://doi.org/10.1016/j.aej.2021.02.047

Costa, J. A., Ariza, O. C., & Lima, L. B. (2019). A Study on the Production of Biodiesel from Waste Frying Oil. *Chemical EngineeringTransactions,*74, Pp. 157–162.

Demirbas, A. and Kara, H. (2006). New Options for Conversion of Vegetable Oils to Alternative Fuels. Energy Sources. *Part A: Recovery, Utilization and Environmental Effect*, 619-626

Filemon, A.and Uriarte, J. (2010). Biofuels from Plant Oil. *ASEAN Foundation*, Indonesia, Pp, 124-125.

Ghosh, N., Patra, M. and Halder, G. (2024). Current Advances and Future Outlook of Heterogeneous Catalytic Transesterification towards Biodiesel Production from Waste Cooking Oil. Sustainable Energy and Fuels. *Royal Society of Chemistry*. 8, (I), Pp. 1105-1152. https://doi.org/10.1039/d3se01564e

Hums M, E, Cairncross, R. A and Spatari, S. (2016). Life-Cycle Assessment of Biodiesel Produced from Grease Trap Waste. *Environmental Science & Technology*, 50 (5). Pp. 1-65. https://doi.org/10.1051/e3conf/202344102019

Mustapha, A.O., Bawa, H.A and Ali, K.S.M. (2020). Fuel Properties of Biodiesel from Neem (*Azadirachta*) and Jatropha (*Jatropha curcas*) Seed Oils using Whole-Cell Biocatalysts. *Journal of Chemical Society*. 45 (5), Pp. 929-934.

Nunes. L.J. R and Silva. S. (2023) Optimization of the Residual Biomass Supply Chain: Process Characterization and Cost Analysis, *MDPI, Logistics 2023*, 7, 48. https://doi.org/10.3390/logistics7030048

Organization for Economic Co-operation and Development/ Food and Agriculture Organization (FAO) of the United Nations (OECD-FAO, 2024). Biofuels, in OECD.

STATISTICAL ANALYSIS OF TEMPERATURE AND TIME OPTIMIZATION FOR PRODUCTION OF COW BONE BIOCHAR

Adedosu, H.O.,[1]* Ogunmoroti E.A.[1], and Ayoola P.B.[1].

[1] *Department of Science Laboratory Technology, LAUTECH Ogbomoso.*
Email of corresponding author: hoadedosu@lautech.edu.ng

ABSTRACT

This research optimized the influence of operating temperature and residence time on biochar yield from the waste cow bone based on the Response Surface Methodology experimental design to develop the Cow Bone Biochar (CBB). Cow bones were collected, washed, air-dried, crushed, milled and screened to <1 mm. Residence time (1-5 h) and temperature (300-700 ℃) were varied to produce CBB in a Muffle Furnace. The highest raw yield of 70.8 % was obtained at 337 ℃, and 3.5 h, while the highest washed yield of 66.03 % was obtained at 400 ℃ and 2 h. Models developed for the Raw and washed yields had F-values of 27.08 and 9.68, respectively with R^2 values of 0.9207 and 0.9064. The study indicated that the selected production conditions have a direct effect on the characteristics of the CBB which is very effective as an adsorbent.
Keywords: max. *Biochar; Pyrolysis; Residence time; Response Surface Methodology; Yield.*

1. INTRODUCTION

Pollution levels in the ecosystem are frequently associated with population expansion and anthropogenic activity (Xanthan, 2018). Due to the long-term or even fatal effects that water poisoning has on living things, it is an extremely divisive subject on a global basis (Eshaq *et al*., 2019). Industrial, residential, and agricultural uses account for more than one-third of the world's renewable freshwater resources. Most of these uses contaminate water with a variety of geogenic and synthetic substances, such as pesticides, fertilizers, dyes, fertilizers, radionuclides, and heavy metals (Mashkoor and Nasar, 2020). Therefore, it is not unexpected that water poisoning brought on by a range of human activities has raised concerns about a public health issue on a worldwide basis (Carneiro *et al*., 2020).

The most popular techniques for eliminating pollutants include chemical oxidation, adsorption, flocculation–coagulation, biodegradation, and flocculation (Deng *et al*., 2011). Adsorption technique is one of these techniques that is both attractive and successful for treating wastewater. Bone char (BC) as an adsorbent is made up of about 90% calcium phosphate and 10% carbon (Mohamed *et al*., 2019). BC is a perfect adsorbent for controlling environmental pollution because of its exceptional physicochemical qualities (Abarasi *et al*., 2023). Consequently, using BC made from leftover bones to filter water encourages a circular economy and is a practical way to lessen environmental pollution through waste valorization (Hart and Aliu, 2022). Gasification and pyrolysis are the methods that can be used to produce BC. 90% of the calcium phosphate in the form of hydroxyapatite and 10%

carbon make up most of the generated BC. hence, , BC functions as an adsorbent and has a porous hydroxyapatite structure with carbon dispersed all over the surface (Azeem, 2022). BC is an inorganic material, therefore, it has a high adsorption capacity and can effectively remove other organic and inorganic components or compounds and metallic contaminants from water (Wang *et al*., 2020). The effectiveness of the adsorption process is significantly influenced by the performance of a BC adsorbent, particularly by its porous network structure and surface chemistry. Synthesis circumstances have a significant impact on these physical-chemical characteristics of BC (Hart *et al*., 2022). Through the optimization of bovine bone pyrolysis settings, the BC's metal uptake increased by 143%, from 68.3 to 119.4 mg/g (Abarasi *et al*., 2023).

The two primary processes for producing bone char (BC) are gasification and pyrolysis. While gasification entails partially oxidizing bone biomass at high temperatures (800-1200 ºC) (Biswajit and Sonali, 2021) to produce BC and a gaseous energy carrier (syngas), pyrolysis is the thermal breakdown of discarded bone under the oxygen-limited environment that produces BC residue and bio-oil (250°C–850°C). BC produced by pyrolysis has a range of physiochemical properties that depend on variables such as heat rate, inert medium and flow rate, and residence time (Abarasi *et al*., 2023). The amount of stable biochar in a biochar system depends on the conversion efficiency during pyrolysis, a portion of the raw yield is given off as ash which would rather reduce the expected functionality of biochar (Enders *et al* 2012). Several studies have sought to develop production

models using machine learning tools based on biomass characteristics, such as its proximate and ultimate analyses for product yields (Vlasova, 2021). A previous study reported the highest significant influence of temperature and heating rate for the development of a prediction model based on the biomass' fixed carbon content, reaction temperature, and heating rate using the response surface methodology (Mariyam *et al*., 2023). Therefore, to the best of our knowledge, this study is the first to comprehend the effect of operating temperature and residence time of Cow Bone Biochar (CBB) on production yield and washed yield.

2. MATERIALS AND METHODS

Materials
The raw material used in this research work was cow bone... Distilled water was used throughout the study to carry out all the experiments. The equipment used includes muffle furnace, Electric Oven, (Saisho S 936, temperature 250 ^{O}C), and Digital weighing balance, (DT 502A, MAX 500g, d_ 0.01g).

Material Collection
Discarded Cow bones were purchased from local butchers' shops at Atenda Abattoir Oja Tuntun along Ilorin-Ogbomoso Express Road Ogbomoso. The cow bone was pre-treated to remove the debris of fat and flesh. The pre-treated cow bone was then thoroughly washed with hot distilled water and then air dried. The air-dried bones are oven-dried in an oven at 110 °C for 24 h. The dried bones were crushed, sieved to particle size (<1mm) and stored in dry containers.

Optimization of Biochar Pyrolysis Condition
The production condition of Cow Bone Biochar (CBB) was optimized by varying production temperature and time using Simple Lattice Design (SLD) under a mixture methodology of the Design Expert Software (Version 6.0.8). The ranges used were between 337.87 to 762.13 and 1.38 to 5.00 for temperature and time respectively as presented in Table 1, these temperature and residence time ranges are typically known to be the best for biochar production (Zuhara *et al*., 2022). Twelve experimental runs were generated for the optimization, 40 g of the sieved cow bone was weighed into a pre-weighed crucible as an initial weight for each of the runs and transferred into the furnace. The percentage raw yield was estimated for each run using Equation 1.

$$\% \ yield = \frac{w_3 - w_1}{w_2 - w_1} \ x \ 100 \qquad (1)$$

Where w_1 is the weight of the empty crucible in g, w_2 is the weight of the crucible + the weight of the bone before pyrolysis in g and w_3 is the weight of the crucible + the weight of the bone after pyrolysis in g.

Table 1 Simple Lattice design for optimization of CBB production

Name	Units	Minimum	Maximum
Temperature	^{o}C	400	700
Time	h	2.00	5.00

Estimation of Washed Yield
Evaluation of stable biochar in each of the runs was done by washing with 100 ml distilled water to remove ashes, the washing procedure was repeated till the water in the adsorbent was clear and uncloudy. The washed CBB were air-dried in the laboratory for 24 h and oven-dried at 80 ^{O}C for 1 h. The washed yield was estimated using Equation 2

$$\frac{w_2 - w_1}{w_1} \ x \ 100 \qquad (2)$$

Where w_1 is the weight before washing in g and w_2 is the weight after washing in g.

3.0 Results and Discussion

Responses from experimental data
The response summary statistics for the raw yield and washed are presented in Table 2 the result showed that production temperature and pyrolysis duration influence both raw yield and washed yield. The highest raw yield (70.85) and washed yield (64.25), were at runs 11 (337.87 OC, 3.50 H) and 1 (550 ^{O}C, 3.5 H) respectively. The lowest raw yield (62.63%) and washed yield (57.45 %) were obtained at Run 5 (700 °C, 5 H), and Run 4 (700 °C, 2 H), respectively.

Observation of the response from experimental data established that temperatures greater than 550 ^{o}C with residence time greater than 3.5 H have both lower raw yield and washed yield, CBB produced at lower temperatures with longer residence time also have lower yields, same trend was observed for higher temperature with low residence time. Generally, the raw yield increased with decreased temperature and time but the washed yield did not follow the same trend. CBBs with high raw yield and low washed yield are unsuitable for water treatment because they have lower removal efficiency and the particles get dispersed easily giving the water a characteristic colour.

Table 2. Response from experimental data

Run	Factor 1		Response	
	A: Temperature (°C)	B: Time (H)	Raw Yield (%)	Washed Yield (%)
1	550.00	3.50	65.58	64.75
2	550.00	3.50	66.13	62.58
3	400.00	2.00	70.63	66.03
4	700.00	2.00	63.55	57.45
5	700.00	5.00	62.63	59.6
6	550.00	3.50	65.85	64.25
7	400.00	5.00	65.00	61.05
8	550.00	5.62	65.05	59.63
9	762.13	3.50	63.48	60.38
10	550.00	1.38	70.81	60.63
11	337.87	3.50	70.85	60.2
12	550.00	3.50	65.65	62.23

Design Summary

The software used in this research, Design Expert, 12.0.1.0, recommends a central composite design type for the factorial experimental design. The study type for the response yield, and washed yield was Response Surface, a quadratic design model was selected for the wash yield, while the 2FI model was used for raw yield. No transformation was done on the raw yield and washed yield (Table 3). The minimum values obtained for raw yield, and washed yield were 62.3 % and 57.45 % while the maximum values were 70.85 % and 66.03 % respectively.

Table 3: Design Summary

Response	Name	Units	Minimum	Maximum	Transform	Model
R1	Raw Yield	%	62.63	70.85	None	2FI
R2	Washed Yield	%	57.45	66.03	None	Quadratic

Analysis of Variance (ANOVA) for Optimization of CBB

The ANOVA generated from the software for the raw yield and washed yield presented in Tables 4 and 5 the model F values of 27.08 and 9.68 were obtained for raw yield and washed yield respectively which implies the methods are significant and the model is excellent for predicting the response (percentage char yield and washed yield). Furthermore, the model F-value of 27.08 and 9.68 implies there is only a 0.43% and 0.03% chance that an F-value this large could occur due to noise. The F values and the P values follow the expected trend, higher F values give Lower P values hence, the term with the highest F value had the least P value, which indicates the reliability of the result. P-values less than 0.0500 for all responses indicate model terms are significant. In this case, A, B, and A are significant models for raw yield, A, AB, and B² are significant models for washed yield, while AB, A², and B² are significant model terms for both raw yield and washed yield. Values greater than 0.1000 indicate the model terms are not significant. The lack of fit F-values of 22.32 and 0.52, were obtained for the respective responses, non-significant lack of fit is good as we want the model to fit, however, a significant lack of fit is bad.

Table 4: ANOVA for raw yield

Source	Sum of Squares	Df	Mean Square	F-value	p-value
Model	65.07	3	21.69	27.08	0.0003*
A-Temperature	49.37	1	49.37	61.63	0.0001*
B-Time	10.16	1	10.16	12.68	0.0092*
AB	5.55	1	5.55	6.92	0.0339*
Residual	5.61	7	0.8010		
Lack of Fit	5.42	4	1.36	22.32	0.0144*
Pure Error	0.1823	3	0.0608		
Cor Total	70.68	10			

* Significant at P<0.05, ^ Signiant at 0.05<p<0.1, # Not significant at P<0.1

Table 5: ANOVA for Washed yield

Source	Sum of Squares	Df	Mean Square	F-value	p-value
Model	59.53	5	11.91	9.68	0.0131*
A-TEMPERATURE	24.80	1	24.80	20.17	0.0065*
B-TIME	2.25	1	2.25	1.83	0.2339#
AB	12.71	1	12.71	10.34	0.0236*
A²	0.2724	1	0.2724	0.2216	0.6577#
B²	20.03	1	20.03	16.29	0.0100*
Residual	6.15	5	1.23		
Lack of Fit	1.57	2	0.7861	0.5154	0.6421#
Pure Error	4.58	3	1.53		
Cor Total	65.68	10			

* Significant at P<0.05, ^ Signiant at 0.05<p<0.1, # Not significant at P<0.1

Regression Statistics of Optimization of CBB

Regression statistics of optimization of the production condition of CBB are presented in Table 6. The standard deviation obtained from raw yield and washed yield are 0.8950 and 1.11 respectively. The values of the coefficient of determination $(R)^2$ obtained for raw yield and washed yield, are 0.9207 and 0.9064 respectively. The adjusted R^2 values were 0.8867 and 0.8128 respectively for the two responses. , the difference between the predicted R^2 and adjusted R^2 for each response is less than 0.2, which shows the model can predict the response accurately (Mariyam *et al.*, 2023). The coefficient of Variance CV is the ratio of the standard error of estimate to the mean value of observed responses. The values obtained for the CV for the raw yield, and washed yield are 1.36, and 1.80 respectively. The adequate precision measures the signal-to-noise ratio. Adequate precision having a ratio greater than 4 is desirable because it indicates an adequate signal of the model. The values of Adequate precision for the raw yield and washed yield are 15.7418 and 9.9042 respectively.

Table 6: Fit Summary statistics from production conditions and adsorption of methylene blue by CBB

Properties	Std. Dev	Mean	C.V. %	R²	Adjusted R²	Predicted R²	Adeq Precision
Raw Yield	0.895	65.85	1.36	0.9207	0.8867	0.7146	15.7418
Washed Yield	1.11	61.69	1.8	0.9064	0.8128	0.6181	9.9042

Model Equations for Optimization of Production Conditions and Adsorption of Methylene Blue by CBB

The model equations generated by the software to produce CBB are expressed in Eqns 3 and 4. The equation in terms of coded factor can be used to make predictions about the response for given levels of each factor. The coded equation is useful for identifying the relative impacts of factors by comparing the factor coefficients. The positive and negative coefficients indicate positive and negative influences respectively on independent variables in the selected responses.

$$Raw\ Yield = +66.02 - 2.48A - 1.32B + 1.18AB \quad (3)$$

$$Washed\ Yield = +63.45 - 2.27\ A - 0.5305B + 1.78\ AB - 0.2610\ A^2 - 1.83B \quad (4)$$

Diagnostic Studies on the Response for Raw yield, Washed yield, Removal efficiency and Adsorption capacity of CBB

Considering the positive note of the prediction model from the statistics, the Design Expert Software gave other diagnostic tools based on the experimental data and model for further analysis. The diagnostic tools in this research include the normal plot of residuals, residuals versus predicted and residuals versus the run. The graphs help us understand if there are any outliers in the experimental results. Figures 1 a and b show the normal plot of residuals for the raw yield and washed yield respectively. This plot is used to indicate the normality of the model only with one glance. This graph is the cumulative distribution function (CDF) of errors. For normal errors, the plotted graph must be a straight line, because, in a normal situation, 50 % of errors are less than zero while the other half is greater than zero and no irregular behavior exists. If errors are non-normal the plot may be a curve. Only for definite patterns like an S-shaped curve which indicates that a transformation of the response may provide a better analysis.
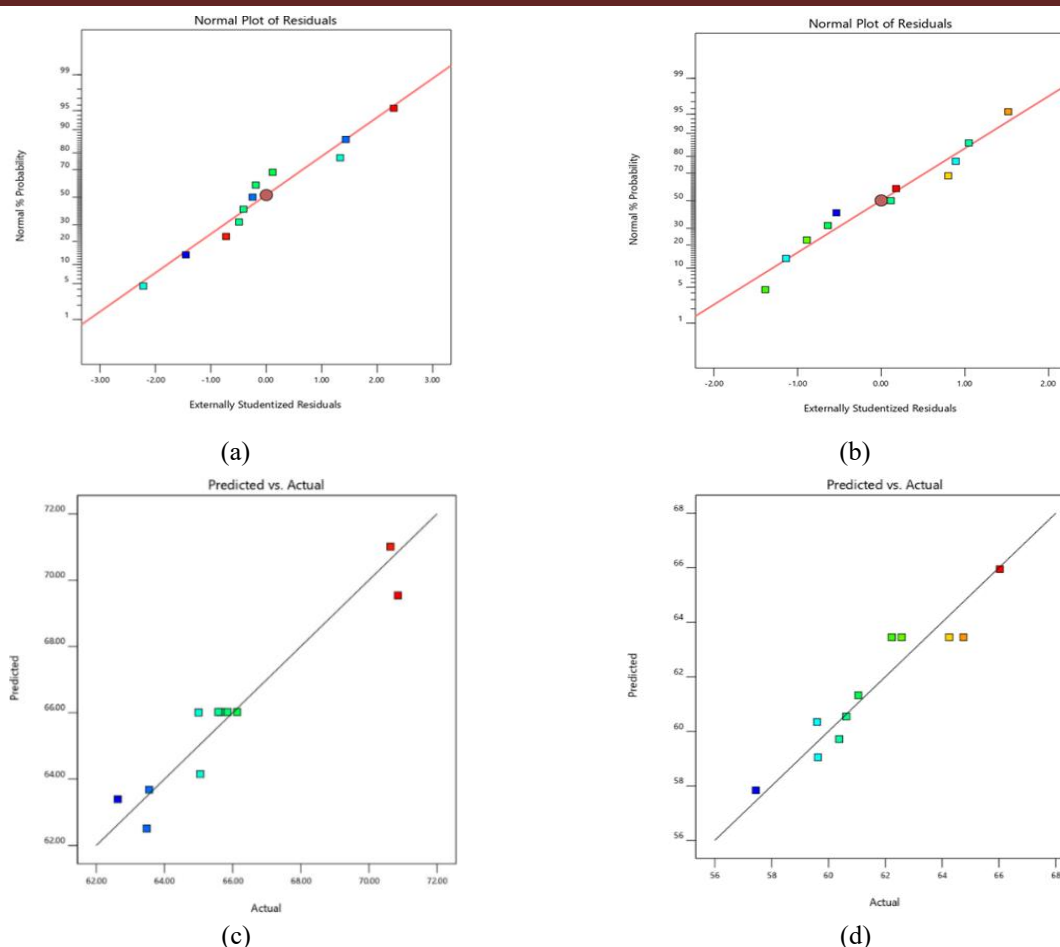
Figure 1: Normal plot of residuals of production optimization of CBB (a) Raw yield (b) washed yield, and plot of Predicted vs Actual for production optimization of CBB (c) Raw yield (d) washed yield

Predicted versus actual plot

Diagnostic analysis of the CBB compares the values obtained from BCC responses with those generated using Design Expert (version 12.0.0). Proximity of the plots determines the R^2 values, closer plots have higher R^2 values while scattered plots have higher R^2 values (Figures 2 a and b). For raw yield, runs 3, 4, 5 and 11 yielded positive residual values while runs 1, 2, 6, 7, 8, and 9 yielded negative residual values. Regarding washed yield runs 2, 4, 5, 7 and 12 had negative values while runs 1, 3, 8, 9 and 10 had positive residual values (Figures 3 a and b). Residual values indicate the proximity of actual values to predicted values, with positive residual values indicating actual values exceeding predictions and negative residual values indicating actual values falling below prediction.
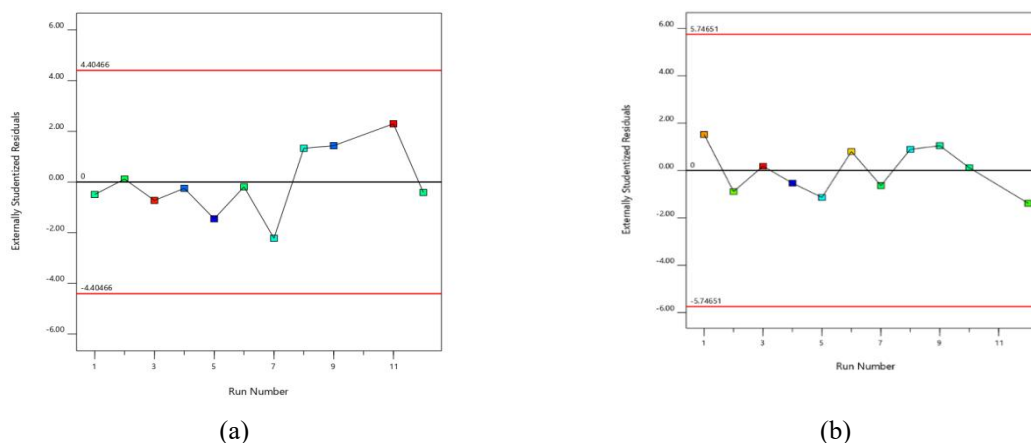
Figure 2. Residual vs run of production optimization of CBB (a) Raw yield (b) washed yield.

Model Graph

The contour and 3-D graphs for raw yields and washed yields are illustrated in Figures 4 and 5 respectively. This explains the impact of production conditions on Biochar. The red zone (hot zone) indicates the point at which the raw yield and washed yield, are pronounced (at maximum) while the blue zone (cold zone) indicates where raw yield, washed yield, removal efficiency and adsorption capacity are minimum. The maximum raw yield and washed yield were observed at distinct points, with the mixture ratio at point A. Notably high raw yield, washed yield, removal efficiency and adsorption capacity were achieved.

Comparison with previous research

Chagtmi *et al*., 2022 varied the production temperature of CBB between 500 and 700 ºC and maintained a residence time of 1 h, maximum yield of 55.6 % was obtained at 500 ºC, as compared to the findings of this study, the maximum raw yield of 70.85 % was obtained at 337.87 ºC and 3.5 h. Maximum wash yield of 66.03 % was however obtained at 400 ºC and residence time of 2 h.

(a)

(b)

(c)

(d)
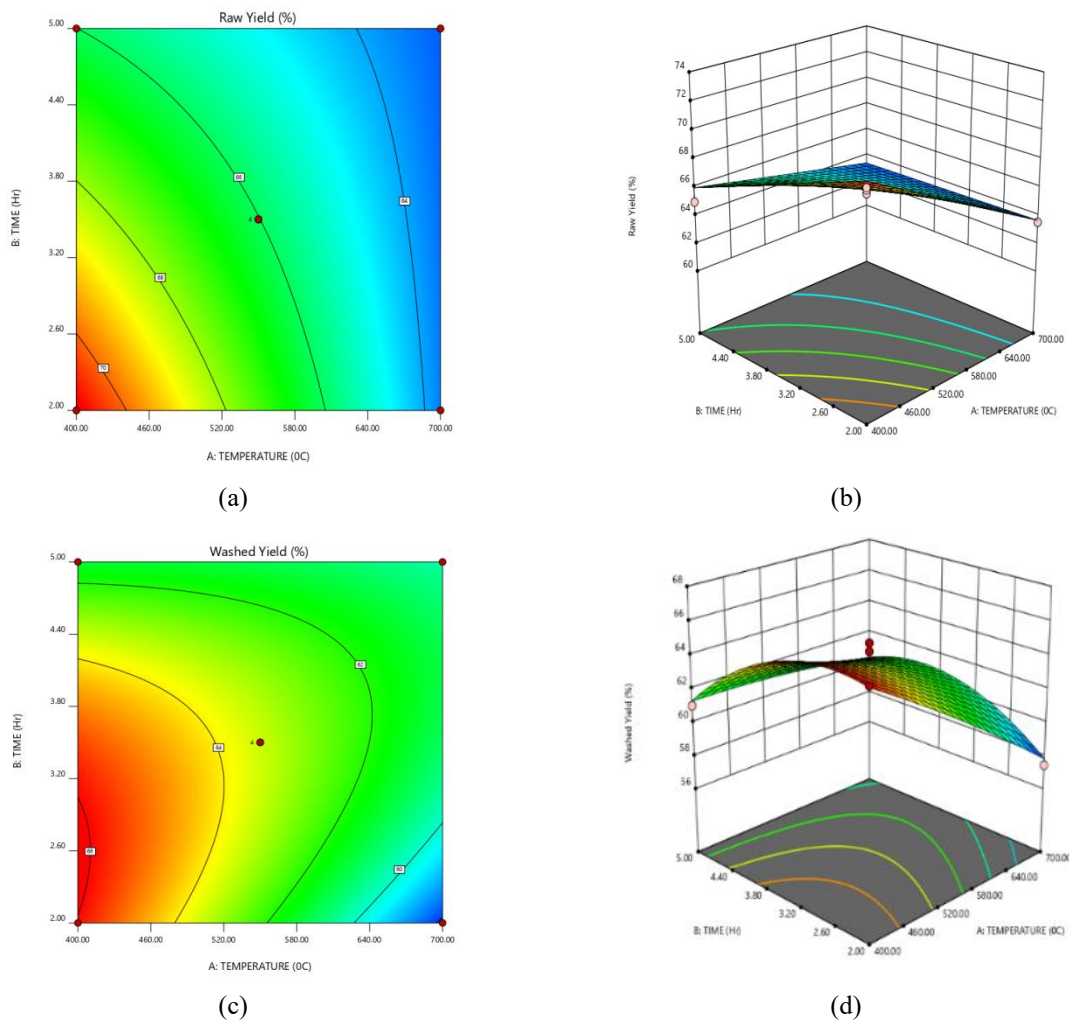
Figure 3: contour and 3D plot of the raw yield of CBB (a) Contour plot (b) 3d plot, and Contour and 3D plot of the washed yield of CBB (c) Contour plot (d) 3d plot

Conclusion

Biochar is an efficient adsorbent for soil regeneration and water treatment; however, its effectiveness depends on the quality of the produced biochar. While the raw yield is an indicator of better product quantity, the quality is assessed by washed yield, especially for water treatment. Cow bones were pyrolysed at different conditions to obtain optimum absolute yield Findings from this research establish that Production conditions have a direct effect on the characteristics of CBB, Biochar raw yield reduces at higher temperatures (> 500 ºC) and longer residence time (> 4 H). Optimum raw yield is at 3.5 H and 337.87 ºC best quality of biochar is however obtained at 400 º C and 2 H residence time.

References

Abarasi, H., Porbeni, D.W., and Omonmhenle, S. (2023). Waste bone char-derived adsorbents : characteristics, adsorption mechanism and model approach. *Environmental Technology Reviews ISSN:* https://doi.org/10.1080/21622515.2023.2197128

Azeem, M. (2022). Removal of potentially toxic elements from contaminated soil and water using bone char compared to plant- and bone-derived biochars: A review. *J. of Hazard Mater.*, *128131*, 427.

Biswajit, S., and Sonali, S. (2021). *Role of Biochar in Water Treatment* (Issue September). https://doi.org/10.1201/9781003138303-11

Carneiro, T., Taketa, R. J., Gomes Neto, J.L., Oliveira, E.V.R., Campos, M.A., de Moraes, C.M.G., da Silva, M.M., Beppu, L.F. and Fraceto, R. (2020). Removal of glyphosate herbicide from water using biopolymer membranes. *J. Environ. Manage*, *5*(56),353–360.

Deng, H., Lu, J., Li, G., Zhang, G., and Wang, X. (2011). Adsorption of methylene blue on adsorbent materials produced from cotton stalk. *Chemical Engineering Journal*, *172*(1),326–334. https://doi.org/10.1016/j.cej.2011.06.013

Eshaq, G., Elmetwally, A., and Bmim, E. (2019). OAc]-Cu2O/g-C3N4 as a multi-function catalyst for sonophotocatalytic degradation of methylene blue. *Ultrason Sonochem*, *53*, 99–109.

Gupta, S., Patel, P., and Mondal, P. (2022). Biofuel production from pine needles via pyrolysis: process parameters modeling and optimization through combined RSM and ANN-based approach. *Fuel*, *122230*, 310.

Hart, A. and Aliu, E. (2022). Materials from eggshells and animal bones and their catalytic applications. In: Minh Doan Pham, editor. Design and applications of hydroxyapatite-based catalysts. *Boschstr Weinheim, Germany*, *12*(69469), 437–479.

Hart, A., Ebiundu, K., and Peretomode, E. (2022). Value-added materials recovered from waste bone biomass: technologies and applications. *RSC Adv.*, *34*(12), 22302– 22330.

Mariyam, S., Alherbawi, M., Pradhan, S., Al, T., and Gordon, A. (2023). Biochar yield prediction using response surface methodology : effect of fixed carbon and pyrolysis operating conditions. *Biomass Conversion and Biorefinery*, *0123456789*. https://doi.org/10.1007/s13399-023-03825-6

Mashkoor, F., and Nasar, A. (2020). Magsorbents: Potential candidates in wastewater treatment technology – A review on the removal of methylene blue dye. *Journal of Magnetism and Magnetic Materials*, *500*(January), 166408. https://doi.org/10.1016/j.jmmm.2020.166408

Mohamed, N., Rashed, A., Abd-Elmenaim, G., and Nada Magdy, F. (2019). *Adsorption of Cd (II) and Pb (II) Using Physically Pretreated*. *2*(4), 347–364.

Vlasova, M. (2021). Application of the biochar in wastewater treatment. *Tampere University Thesis*, *May*.

Wang, M., Liu, Y., and Yao, Y. (2020). Comparative evaluation of bone chars derived from bovine parts: physicochemical properties and copper sorption behavior. *Sci Total Environ.*, *134470*, 700.

Xanthan, I. (2018). Gum/titanium dioxide nanocomposite for photocatalytic degradation of methyl orange dye. *Int. J. Biol. Macromol.*, *2*(121), 1046–1053.

Zuhara, S., Mackey, H., Al-Ansari, T., and McKay, G. (2022). A review of prospects and current scenarios of biomass co-pyrolysis for water treatment. *Biomass Convers Biorefinery*. **14**, 6053–6082 (2024). https://doi.org/10.1007/s13399-022-03011-0

METHODS OF HYDROGEN PRODUCTION AND TWELVE (12) PRINCIPLES OF GREEN CHEMISTRY; A REVIEW OF QUESTION OF GREENNESS

Abdullahi Bello[1]*.,   Ibrahim K. Muritala[2].

[1]*West African Science Service Centre for Climate Change and Adapted Land Use*
[2]*Research & Innovation Department, Afridat Research and Innovation GmbH, Duisburg, Germany.*
*Email: binabdullahi378@gmail.com

ABSTRACT
Hydrogen has been positioned to be a key player in the energy sector. Hydrogen burns as a clean fuel, emitting little or no greenhouse gas, and is readily abundant in renewable forms. However, large percent of the current sources of extracting hydrogen comes from polluting non-renewable fossil fuels. This paper aims to examine some of the hydrogen production methods in accordance with the twelve (12) principles of green chemistry that is design to provide for the design and practice of safe and environmentally friendly chemical processes. these techniques were classified according to the source of their feedstocks, and it was established that biological processes of treating renewable sources of hydrogen offered the most environmentally friendly techniques while noting the large amount of heat required for the techniques that uses fossil fuels as hydrogen sources coupled with the CO_2 emissions at every step of the techniques.
Keywords: Hydrogen; Renewable energy; Green chemistry; Non-renewable; Environment

1. INTRODUCTION

Over the years this climate change have been attributed to the continuous rise in temperature of the earth through global warming, Inter-governmental panel on climate change (IPCC) have been consistent in the update in the rate at which the earth's climate is changing. Many researches have related the abnormal rise in temperature to the greenhouse effect which is influenced by the presence of greenhouse gases, gases like Carbon dioxide (CO_2), Methane (CH_4) and others which makes up the greenhouse gases.

Agricultural practices and other natural processes have been identified to contribute to the emissions of this greenhouse gases (Qian et al., 2023). However, Electricity and heat production are the largest contributors to global emissions. This is followed by transport, manufacturing, construction (largely cement and similar materials), and agriculture (Hannah et al., 2020). Because of the high contribution of Energy generation, there are international efforts and commitment to limit the release of greenhouse gases and one of such is the Paris Agreement which parties are committed to prevent the rise in the earth's temperature beyond 1.5ºC.

The paradigm shift in the production and usage of fossil based fuels to cleaner green renewable energy sources is called 'energy transition'. Energy transition is necessary in order to reduce the utilization of fossil based energy sources and to secure the necessary reduction of hazardous impact to the environment (Sandro et al., 2023). This renewables Energy systems are expected to be very reliable, but renewable energy is inherently intermittent. We explore energy storage as a solution to this problem (Paul et al. 2023.).

Recently, the use of hydrogen as a renewable energy source have further sparked the question about the environmental friendliness of the various methods used in the production of hydrogen, even when the product of its usage is harmless water. Till date about 50% of world's hydrogen supply is through steam reforming, 30% through oil and naphtha reforming, 18% from gasification of coal and 3.9% from electrolysis and 0.1% from other sources (Nnabuife et al., 2023). Part of the reasons of hydrogen posed to be a key player in the long energy transition includes; it's very low Environmental impact factor (EIF), very high Hydrogen content factor (HCF) and very high Greanization factor (GF) in comparison to other forms of fuels (Dincer and Acer, 2014).

$$EIF = \frac{Kg\ CO_2\ product\ of\ combustion}{Kg\ of\ fuel} \quad (1)$$

$$GIF = \frac{EIF_{max} - EIF}{EIF_{max}} \quad (2)$$

$$HCF = \frac{Kg\ of\ H_2\ in\ fuel}{Kg\ of\ fuel} \quad (3)$$

Anita et al., (2017) defined ''green chemistry or Sustainable Chemistry as a term related to the creation of chemical products and processes that reduce or eliminate the use and production of harmful substances'' this off cause includes protection of the environment, lives and properties. Paul and John (1998). highlighted that, green chemistry is guided by twelve principles which are as follows: Waste prevention; atom economy; less hazardous chemical synthesis; Designing safer chemicals; safer solvents and auxiliaries; designing for energy efficiency; use of renewable feedstocks; derivatives reduction; usage of catalyst; design for degradation; real time analysis of pollution prevention; and inherently safer chemistry for accident prevention

Table 1. Twelve principles of Green chemistry with brief explanation

	Explanations
1.Waste prevention	It's better to stop waste than cleaning
2.Atom economy	Maximum incorporation of reactants to the products
3.Less hazardous chemical synthesis	Less hazard means safe work place and environment
4.Design safer chemicals	During design, ensure the chemicals will be less toxic
5.Safer solvents and auxiliaries	Solvents for reactions should be less toxic
6.Energy efficiency	Reaction should happen at room temperature and pressure
7.Using renewable feedstocks	It's better to use resources that are renewable
8. Reducing derivatives	Derivatives should be avoided
9.Catalysis	Employ catalyst instead of ordinary reaction
10.Designing for degradation	Materials should be degradable after lifetime
11. Real time analysis	Monitoring the process for toxicity formation
12.Safer chemistry	Both raw materials and products should be safe chemicals

Studies on high temperature methods of producing hydrogen have been reported by Muritala et al. (2019) as fossil resources (coal, crude oil and natural gas) provide the largest of its annual production globally. China been the largest producer and consumer of hydrogen globally. Exploring a range of hydrogen production methods tailored to the specific resources available in each region is crucial, as this approach ensures the optimization of local assets and capabilities. At the same time, the overarching goal of decarbonization should guide the selection of production techniques that have a minimal environmental footprint. By aligning regional production strategies with sustainability objectives, we can advance toward cleaner hydrogen solutions while addressing both local and global environmental concerns.
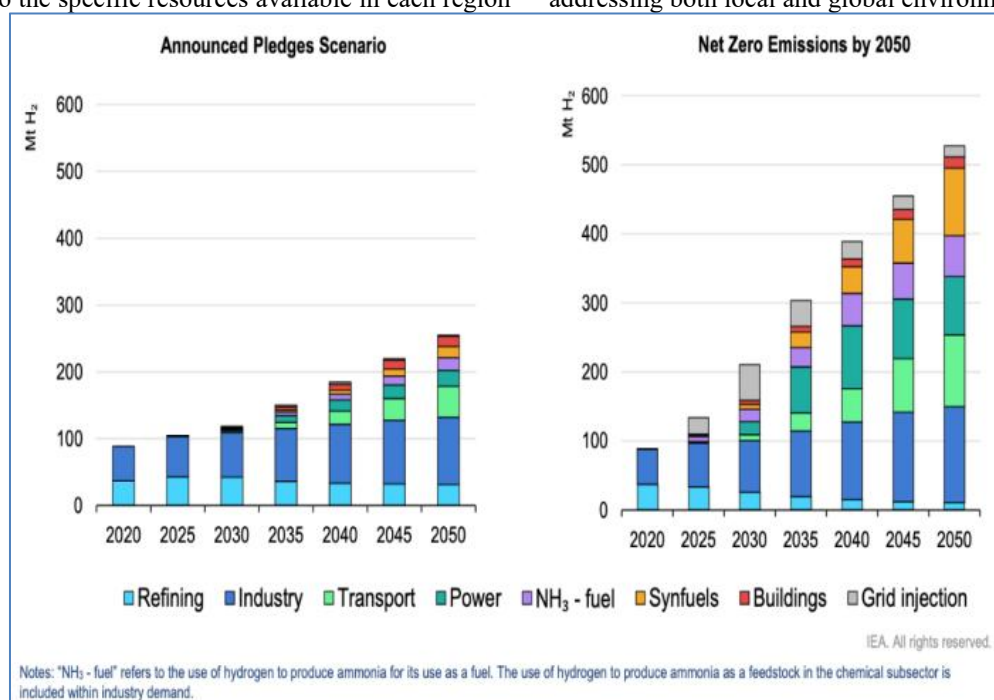
Figure 1: Projected Hydrogen Demand by Sector: Annual Pledges and Net-Zero Emission Scenarios (2020–2050) (Sourced from IEA Report 2021)

To achieve a net-zero emissions scenario by 2050, the International Energy Agency (IEA) estimates that global hydrogen production will need to reach 530 million tonnes as presented in Figure 1. This represents approximately a six-fold increase from current hydrogen production levels. Such a dramatic rise underscores the urgent need to significantly scale up clean hydrogen production and infrastructure. Meeting this target will require substantial advancements in technology, investment in green hydrogen production methods, and a

comprehensive strategy to integrate hydrogen into various sectors of the economy. This expansion is essential not only to meet future energy demands but also to drive progress towards a sustainable and decarbonized global energy system.

This paper we will try to briefly study and analyse the various methods of hydrogen production and how much green such processes are. This is very important especially when there is an accelerated call and awareness for environmental protection and ecological justice. If usage of hydrogen is a strategy aim at curtailing environmental destruction through climate change, then there is need for a systematic evaluation on the greenness of the methods of which hydrogen is produced themselves.

2. MATERIALS AND METHODS

Comparative method of study was chosen for this study and conclusions were derived from the available evidence. Techniques for hydrogen production operates on different principles and concepts, these concepts were used as basis for comparison with the twelve principles of green chemistry. Not all principles were considered in this study, this was done according to the relevance of every principle of green chemistry to the concept and mechanisms of which these techniques operate. Sources of hydrogen were divided into renewable and non-renewable sources, and all these sources were examined in Accordance with twelve (12) principles of green chemistry.

Similar studies have been done by Çelik and Yıldız (2017), this study is necessitated to further push for adherence to the principles of green chemistry when developing techniques for the production of sustainable and clean energy fuels like hydrogen.

3. RESULTS AND DISCUSSIONS

3. 1 Methods of hydrogen production

Although in abundance, hydrogen is hardly found in a free state but in combined state in the form of fossil fuels, biomass, hydrogen sulphide and others. Nnabuife et al., (2023). classified the sources of hydrogen into renewable sources and non-renewable sources. Renewable sources were identified as water and Biomass, while the fossil fuels were identified as the non-renewable sources. However, how the sources are treated for the extraction of hydrogen greatly depends on which method is employed. Hota et al., (2023), identified that The process of water treatment to produce hydrogen is termed "water splitting" and involves Electrolysis, thermolysis and photolysis as provided in figure 2. while Nguyen-Thi et al., (2024) stated that the treatment of biomass involves biological and thermochemical treatments with bio-photolysis, dark fermentation and photo fermentation as biological methods and liquefaction, gasification, pyrolysis and combustion as thermochemical methods of biomass treatment.

Non-renewable sources that involve fossil fuels can either be processed by a reforming process or through pyrolysis. Hydrocarbon reforming methods include steam reforming, partial oxidation and autothermal reforming (Nikolaidis and Poullikkas 2017).

These identified methods are further divided according to the source of energy required for the extraction which include electrical, thermal, biological and hybrid techniques as provided in table 2. And will be compared to the 12 principles of green chemistry that have been itemized in table 1.

Table 2. showing the various hydrogen production techniques.

Energy source	Technique
Electrical	1. Electrolysis 2. Plasma Arc Decomposition
Thermal	1. Thermochemical water splitting 2. Gasification 3. Steam reforming 4. Thermolysis 5. Biomass conversion
Biological	1. Bio-photolysis 2. Dark fermentation 3. Photo fermentation 4. Artificial photosynthesis
Hybrid	1. Photo-electrochemical methods 2. High temperature electrolysis

3.1.0 Renewable sources for hydrogen production

Here we will try to look at how the various renewable sources of hydrogen under some techniques processing produce hydrogen and how well these techniques satisfied the principles of green chemistry.

3.1.1 Thermolysis method of producing hydrogen

This is single step dissociation of water at a very high temperature typically of 2500 K or more, this dissociation result in the production of hydrogen and oxygen as products (Dincer and Acar, 2014).

the reaction step is given as follows:

$$H_2O \xrightarrow{heat} H_2 + \frac{1}{2}O_2 \qquad (4)$$
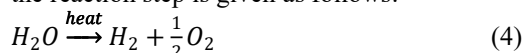
The production process is a single step reaction and only oxygen is the by-product, principle 1 and 2 are obeyed while also obeying principle 7 and 8 respectively due to the fact that the raw material water is readily renewable, and the process lacks derivatives respectively. However, due to the large amount of energy input require for the optimum performance, the process violated principle 6 of energy efficiency.

3.1.2 Thermochemical water splitting process for hydrogen production

Thermochemical water-splitting (TWS) processes are regarded as one of the most environmentally friendly strategies, capable of harnessing high-temperature waste heat from industries, renewable energy, and nuclear power sources to produce clean hydrogen (H_2) on a large scale (Bahram et al., 2023). This process uses high temperature (500 °C to 2000 °C) to drive a series of chemical reactions to produce hydrogen.

Çelik and Yıldız. (2017) positioned that, '' the Most common and well-developed form of thermochemical

cycle is the S-I cycle. Although all chemicals of the S-I cycle system are recyclable, it employs sulphuric acid as a medium. The advantages of this method are as follows: there is no need for an oxygen-hydrogen separation membrane, temperature range is 600 to1200 K which is lower than thermolysis, and electricity input is low, down to zero''.

The first S-I cycle reaction is thermally driven and is given as written below

$$H_2SO_{4(aq)} \xrightarrow{heat\ (300ºC-500ºC)} H_2O_{(g)} + SO_{3(g)} \quad (5)$$
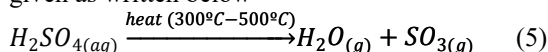
The gaseous products (H_2O and SO_3) are further heated to about 800 °C to 900 °C where SO_3 is decomposed thermally.

$$SO_{3(g)} \xrightarrow{heat\ (800ºC-900ºC)} SO_{2(g)} + \frac{1}{2}O_{2(g)} \quad (6)$$
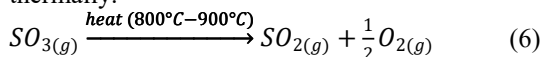
The liberated SO_2 gas at room temperature undergoes and exothermic reaction with Iodine spontaneously.

$$SO_{2(g)} + I_{2(g)} + 2H_2O_{(l)} \rightarrow 2HI_{(g)} + H_2SO_{4(aq)} \quad (7)$$
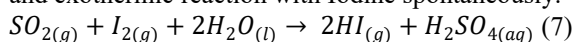
the generated 2HI finally thermally decompose into Hydrogen gas and Iodine at temperatures about 400ºC to 450ºC.

$$2HI_{(g)} \xrightarrow{heat\ (400ºC-450ºC)} H_{2(g)} + I_{2(g)} \quad (8)$$
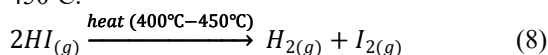
Thermochemical water splitting due to its high temperature heat requirement violates principle 6, has hazardous chemicals with no safe auxiliaries hence violating principle 3 and 5 respectively. Although the process prevents waste through recycling and every atom is accounted for but the process involves derivatives formations therefore, satisfying principle 1 and 2 but violating principle 8. The feedstock is renewable satisfying principle 7 but generally principle 12 is violated as the entire chemistry of the process have proven to be not safe.

3.1.3 Electrolysis approach based on water resources

The process by which electricity interact with chemical species to bring about chemical reaction is regarded as 'electrolysis'. water is split into hydrogen and oxygen in the electrolysis of water, this method of hydrogen production is expected to increase in significance in the coming future (Dincer and Acar, 2014). There are different form of electrolysers from Alkaline electrolysers to proton exchange membrane and solid oxide electrolysers, they all operate on the same principles but only differ with some materials. When the electricity powering the electrolysers come from renewable energy sources like wind, solar and hydropower, such hydrogen is referred to as 'Green hydrogen'

In this study we will consider Alkaline Electrolyser which uses 40% potassium hydroxide (KOH) as electrolyte at an optimal temperature of about 70 ºC-90 °C. the reaction process is provided below.

$$Anode: H_2O_{(l)} \rightarrow \frac{1}{2}O_{2(g)} + 2H^+ + 2e^- \quad (9)$$

$$Cathode: 2H^+ + 2e^- \rightarrow H_{2(g)} \quad (10)$$

$$Overall: H_2O_{(l)} \rightarrow \frac{1}{2}O_{2(g)} + H_{2(g)} \quad (11)$$

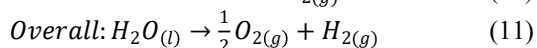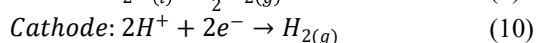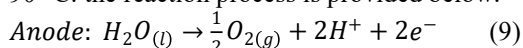KOH is easily recoverable and can be reused, but it poses disposal, handling and storage problem hence the process violates principle 12 and 3 respectively. The

electrodes are made up of heavy metals with uncertain life cycle, hence the process doesn't satisfy principle number 10 of designing for degradable. However, since the raw material is water, it is readily available and renewable, thereby obeying principle 7. Finally, the entire process has only oxygen as the by product, incorporates all the reactant reagent at the product and lacking of derivatives formation, therefore, supports principle 1, 2 and 8 respectively.

3.1.4 Biomass thermochemical conversion method of producing hydrogen

Biomass is considered CO_2 neutral because the amount of CO_2 emitted when processed is equal to the amount absorbed during lifetime photosynthesis. Biomass sources include forest trees, agricultural wastes, municipal wastes and livestock's waste. The general biomass conversion process is provided in the equation below.

The production of tar is one of the problem of this process, as a by-product it causes sludging and slurry, but catalyst can be used to prevent the creation of such (Dincer and Acar, 2014). Due to this, biomass conversion doesn't obey principle 1 of waste prevention and obviously a long step reaction as this isn't devoid of derivative formation, hence violating principle 8. This process of hydrogen production also violate the principle 2 of atom economy and a process as energy demanding as this can't be energy efficient, doesn't obey principle 6. but the process has the advantage of using renewable feedstocks hence principle 7 and employing catalyst principle 9.

3.1.5 Dark fermentation method

This method has been reported to be a promising technique in the production of hydrogen. Dark fermentation is the conversion of biochemical energy stored in organic matter to other forms of energy in the absence of light, this done by Microorganisms such as bacteria and algae can produce hydrogen through biological processes (Rafał et al., 2018). One advantage of this process is that hydrogen can be generated from waste, either agricultural or municipal waste.

Dark fermentation uses renewable feedstock of biomass, uses enzymes as catalyst, takes place at room temperature and degradable materials, hence satisfy principle 7, 9, 6 and 10 respectively. However, drawbacks like organic acid formations, lack of atom economy and formations of derivatives makes the techniques violates principle 1, 2, and 8 respectively.

3.1.6 Photo fermentation method

This technique produces hydrogen without the production of oxygen, it is photonic driven biochemical process of hydrogen production from water (Dincer and Acar, 2014). This process occurred at room temperature in the presence of light sensitive bacteria.

The creation of derivatives by these techniques makes it a violation of principle 8, but the use of renewable feedstock, use of microorganisms in the principle of catalyst, the occurrence at room temperature and the

degradability of the materials makes this process a satisfaction of principle 7, 9, 6 and 10 respectively.

3.1.7 Bio-photolysis method

Agyekum et al., (2022) described the process as '' This is a biological process that employs similar principles that are seen in algae and plants photosynthesis which are adapted for the production of hydrogen gas. Only carbon dioxide reduction occurs in green plants, as there is an absence of the enzyme that catalysed the formation of hydrogen''. this technique employs the decomposition of water to produce hydrogen in the presence of light just as in photosynthesis just that this time it's facilitated by cyanobacteria. This could be done under direct and indirect bio-photolysis. The process can be represented by the equation below;

$$H_2O \xrightarrow{\text{light+bacteria or algea enzyme}} H_{2(g)} + O_{2(g)} \quad (12)$$
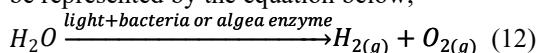
This technique operate at room temperature, with water as the feedstock its renewable and the atoms are accounted for with no waste formation, therefore satisfying principle 6, 7, 1 and 2 respectively. The biological catalysts employed in the process are readily degradable obeying principle 9 and 10 respectively. However, due to the complex biological routes for the formation, this technique violates principle 8.

3.1.8 Artificial photosynthesis method

This technique is based on the concept of imitating the natural process of photosynthesis as indicated in the work of (Meyer, 1989). This technique for the production of hydrogen involves the capture of carbon dioxide on a photo sensitive artificial photo-sensitive pigment where carbon dioxide reacts with water to produce carbohydrate and on which carbohydrates produced is catalysed to produce hydrogen. The overall reaction is the splitting of water using light in presence of some pigments.

This technique is considered environmentally friendly because it satisfies most of the principles like principle 1, 2, 6, 7, and 9. However, the technique's reaction routes create derivatives and materials are not degradable, thereby violating principle 8 and 10 respectively.

3.1.9 High temperature electrolysis method

this method is pictured more efficient than the conventional electrolysis, it involves heating water to steam to about 700 ºC-1000 °C, this technique is carried out in solid oxide electrolysers and the electrical is heated in the process of water heating since most of this electrolysers require higher temperatures for maximum functioning (Dincer, 2012).

$$H_2O \xrightarrow{\text{heat+electricity}} H_{2(g)} + \frac{1}{2}O_{2(g)} \quad (13)$$

Although the temperature requirement for this technique is less than that of thermolysis, the technique still doesn't satisfy principle 6 of energy efficiency, this reaction just like conventional electrolysis prevents waste and account for atoms therefore satisfying principle 1 and 2. This technique also uses renewable feedstock of water, prevents derivatives, and prevents the use of KOH which makes it agree with principle 7, 8 and 5 respectively. Unfortunately, principle 10 cannot be satisfied due to the non-degradable nature of the materials.

3.1.10 Photo electrochemical method

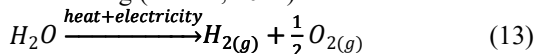This technique employs the electrolysis of water to produce hydrogen using semiconductors photo-electrodes as a single unit mostly as the anode. These photo electrodes as most covered with photo catalyst, during the process light hits the photo catalyst where electrons are generated to yield electrons or oxidation (Zhao et al., 2023).

In this technique the working temperature is at room temperature satisfying principle 6, it accounts for atoms and doesn't create waste, therefore obeying principle 2 and 1 respectively. This technique, further, meets principle 7 of renewable feedstocks, principle 8 of derivative prevention and principle 9 of the use of catalyst. However, it violates principle 10 of materials degradation and 12 that gives room for a safe chemistry.

3.1.11 Non-renewable sources for hydrogen production

in this section several methods of hydrogen production will be checked for adherence to the 12 principle of green chemistry, fossil fuels like oil, coal and gas will form a most feedstocks that will be discussed in the various techniques

3.1.12 Steam reforming of liquid or gaseous fossil

This technique takes place at temperatures about 500 ºC-900 °C at a pressure of 20 atm to 30 atm. It involves the use of gas or liquid fossil fuel to form syngas which is a mixture of hydrogen and carbon monoxide. Using methane or natural gas is currently the cheapest and most popular of producing hydrogen.

The overall reaction equation is summarized as:

$$CH_{4(g)} + H_2O_{(g)} \leftrightarrows CO_{(g)} + H_{2(g)} \quad (14)$$
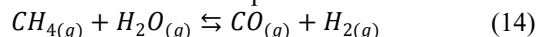
This reaction is an equilibrium reaction and atom economy is not obeyed, the high temperature makes this technique not energy efficient, this further produces waste as carbon monoxide, therefore principle 2, 6 and 1 respectively are not met by this technique. However, principle 7, 8 and 9 are obeyed especially if biogas from biomass is used instead of natural gas to makes the input methane renewable and the reaction is devoid of derivatives with the use of catalyst also.

3.1.13 Gasification method

This technique of hydrogen production involves the heating of solid fuels like coal or biomass at very high temperature and pressure. CO and CO_2 are produced at every step of this technique giving the hydrogen produced from this technique the name black or brown hydrogen.

$$C_{(s)} + H_2O_{(g)} \leftrightarrows CO_{(g)} + H_{2(g)} \quad (15)$$
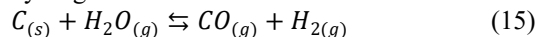
The produced CO is further converted to CO_2 in water-gas shift reaction producing more hydrogen as indicted in equation (18) below.

$$CO_{(s)} + H_2O_{(g)} \leftrightarrows CO_{2(g)} + H_{2(g)} \quad (16)$$
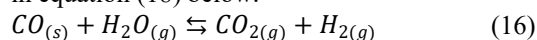
If biomass is chosen as the feedstock, the above technique satisfy principle 7 of usage of renewables but if otherwise violates it but clearly aligned with principle 9 due to the application of catalyst water-gas shift reaction step. CO, CO_2 and H_2 produced in every step of

the reaction making it a complex reaction, but it can be said that derivatives are minimized in the entire technique thereby aligning with principle 8.

The high temperature requirement for this technique violates principle 6 of energy efficiency and also violates both principle 1 and 2.

3.1.14 Plasma arc decomposition method

This technique involves the decomposition of natural gas (Methane) into hydrogen and carbon black (soot) due to the thermal plasma activity. This uses high voltage in the decomposition of natural gas as provided in the equation (19) below.

$$CH_{4(g)} \rightarrow C_{(s)} + 2H_{2(g)} \qquad (17)$$
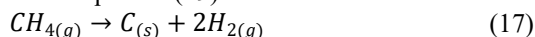
Although the technique satisfies principle 2 of atom economy, the production of carbon soot as waste makes the technique a violation of principle 1. The feedstock of natural gas is not renewable thereby violating principle 7 and the high voltage can be considered as been energy inefficient violating principle 6, although it clearly obeys the 8th principle of not having derivatives.

4. CONCLUSION

The purpose of the study was to analysed well known techniques of hydrogen production and how well they agree with the 12 principles of green chemistry. With the growing concern for environmental concerns and preservation, evaluation of these techniques was important to ascertain their greenness. The cost of producing hydrogen and their efficiencies were not captured in this study, it is worthy to note that most techniques that have water and biomass as feedstocks obeyed principle 7 of usage of renewable raw materials. All techniques that employed the usage of thermal emits carbon dioxide and violates the principle of energy efficiencies, therefore, carbon capture techniques should be incorporated in most of this techniques in other to compliment global efforts of combating climate change through reduction in global greenhouse gas emission.

All biological methods have been proven to be environmentally friendly, although most are at the development stages, electrolysis has proven to be the most environmentally friendly method in comparison to plasma arc decomposition. In times to come hydrogen production methods techniques will be developed and use in accordance with the 12 principles of green chemistry

References

Agyekum, E.B., Nutakor, C., Agwa, A.M., and Kamel S. (2018) A Critical Review of Renewable Hydrogen Production Methods: Factors Affecting Their Scale-Up and Its Role in Future Energy Generation. Membranes 2022, 12, 173. https://doi.org/10.3390/ membranes12020173

Anastas, P. T. and Warner, J. C. (1998). Green Chemistry: Theory and Practice, Oxford University Press: New York, p.30. By permission of Oxford University Press

Anita I., Ana D., Anita M.B., and Stanislava T. (2017) Review of 12 Principles of Green Chemistry in Practice. International Journal of Sustainable and Green Energy. Vol. 6, No. 3, pp. 49-48. doi: 10.11648/j.ijrse.20170603.12

Bahram G., Sohrab Z., Yan Z., Hadis Z. and Ioannis C. (2023). Thermochemical water-splitting structures for hydrogen production: Thermodynamic, economic, and environmental impacts, Energy Conversion and Management, Volume 297, 117599, ISSN 0196-8904, https://doi.org/10.1016/j.enconman.2023.117599.

Çelik, D., and Yıldız, M. (2017). Investigation of hydrogen production methods in accordance with green chemistry principles. International Journal of Hydrogen Energy, 42(36), 23395-23401.

Dincer I. and Acar C. (2014). Review and evaluation of hydrogen production methods for better sustainability, International Journal of Hydrogen Energy, http://dx.doi.org/10.1016/j.ijhydene.2014.12.035

Dincer, I. (2012). Green methods for hydrogen production. International journal of hydrogen energy, 37(2), 1954-1971.

Hannah R., Pablo R. and Max R. (2020) - "Breakdown of carbon dioxide, methane and nitrous oxide emissions by sector" Published online at OurWorldInData.org. Retrieved from: 'https://ourworldindata.org/emissions-by-sector' [Online Resource]

Hota, P., Das, A., and Maiti, D. K. (2023). A short review on generation of green fuel hydrogen through water splitting. International Journal of Hydrogen Energy, 48(2), 523-541.

International Energy Agency (2021) Global Hydrogen Review;https://iea.blob.core.windows.net/assets/5bd46d7b-906a-4429-abda-e9c507a62341/GlobalHydrogenReview2021.pdf

Kheirollahivash, M., Rashidi, F. & Moshrefi, M.M. (2019). Hydrogen Production from Methane Decomposition Using a Mobile and Elongating Arc Plasma Reactor. Plasma Chem Plasma Process 39, 445–459 https://doi.org/10.1007/s11090-018-9950-y

Meyer, T. J. (1989). Chemical approaches to artificial photosynthesis. Accounts of Chemical Research, 22(5), 163-170.

Muritala, I. K., Guban, D., Roeb, M., and Sattler, C. (2020). High temperature production of hydrogen: Assessment of non-renewable resources technologies and emerging trends. international journal of hydrogen energy, 45(49), 26022-26035.

Nguyen-Thi, T. X., Nguyen, P. Q. P., Tran, V. D., Ağbulut, Ü., Nguyen, L. H., Balasubramanian, D., and Pham, N. D. K. (2024). Recent advances in hydrogen production from biomass waste with a focus on pyrolysis and

gasification. *International Journal of Hydrogen Energy*, *54*, 127-160.

Nikolaidis P. and Poullikkas A. (2017). A Comparative Overview of Hydrogen Production Processes. Renew. Sustain. Energy Rev. 67, 597–611. [CrossRef]

Nnabuife S.G., Darko, C.K., Obiako, P.C., Kuang, B., Sun, X. and Jenkins, K.(2023). A Comparative Analysis of Different Hydrogen Production Methods and Their Environmental Impact. Clean Technol. 5, 1344–1380. https://doi.org/ 10.3390/cleantechnol5040067

Orfilla M, Linares M, Molina R, Botas JA, Sanz R & Marugan J. (2016). Perovskite materials for hydrogen production by thermochemical water splitting. Int J Hydrogen Energy ;41:19329e419.

Paul C., Tony R. and Stan Z. (2023). Intermittency and periodicity in net-zero renewable energy systems with storage, Renewable Energy, Volume 212, Pages 299-307, ISSN 0960-1481, https://doi.org/10.1016/j.renene.2023.04.135.

POROUS SILICA-ALGINATE-CHITOSAN SYSTEMS FOR BIOETHANOL PRODUCTION: BIOKINETIC MODELLING AND SIMULATION STUDIES

Abdulmumin[1*], B., Atta[2], H.I., Atta[1], A.Y., Jibril[1], B., Y.

[1]*Department of Chemical Engineering, Faculty of Engineering, Ahmadu Bello University, Zaria, Nigeria*
[2]*Department of Microbiology, Faculty of Life Sciences, Ahmadu Bello University, Zaria, Nigeria*
*Coresponding author contact:
Email: bilal4riid13@gmail.com
Phone: +2348034727601

ABSTRACT

This study investigates the biokinetic modelling and simulation of bioethanol production using porous silica-alginate Saccharomyces cerevisiae capsules. Four models were analysed: Monod, Michaelis-Menten, First Order, and Second Order. The Monod model provided the best fit, with a high coefficient of determination (R^2) of 0.9799 for the G-3 sample. Additionally, three modified Monod models were employed to evaluate bioethanol inhibition, substrate kinetics for cell maintenance, and glucose inhibition. The R^2 values for Monod E, Monod EM, and Monod EMG were 0.9874, 0.9996, and 0.9996, respectively, indicating that bioethanol production is influenced by product inhibition and substrate usage for cell maintenance, while glucose inhibition is negligible. The study concludes that Monod EM model best describes the bioreactions for porous silica-alginate-chitosan bioethanol production, highlighting its potential for heterogeneous bioprocesses.
Keywords: Silica-alginate/chitosan capsules, bioethanol production, yeast encapsulation, biokinetics modelling, Monod model

1.0 INTRODUCTION

The fusion of cell biochemistry and organic-inorganic material engineering is needed to synergistically propel heterogeneous bioethanol production, addressing the pressing need to mitigate the ever-increasing global demand for sustainable energy sources.

Alginate is the most extensively utilized organic polymer for encapsulating microorganisms (Ching et al., 2017; Rathore et al., 2013). To gain a deeper understanding of this system, rigorous studies on biokinetics are essential. Whole-cell bioreaction, whether free or alginate-encapsulated, typically involves several phases. In the lag phase, encapsulated cells adapt to the new environment. During this phase, there is minimal cell growth, and consequently, few bioproducts are formed. This is followed by the exponential growth phase, where the bioreaction rate is highest, with rapid cell growth and increased bioproduct formation. Next is the stationary phase, where the rate of cell growth equals the rate of cell death, leading to a plateau in the number of viable cells and product levels. Finally, the death phase occurs, where the number of dying cells exceeds the number of growing cells, resulting in a decline in the overall cell population. Several models describing bioprocesses have been developed (Lee, 1992). Although deviations from these models are common. Factors responsible for such deviations include substrate or product inhibitions and cell maintenance metabolism (Nosrati-Ghods et al., 2020).

There have been several researches conducted to fit experiment data of Ca-alginate bioethanol production (Birol et al., 1998; Nosrati-Ghods et al., 2020). However, a discernible gap exists in the literature when it comes to silica-alginate/chitosan systems, and to the best of our knowledge, there is a complete absence of research on porous silica-alginate/chitosan, the system that we developed.

Hence, this study aims to study biokinetics modelling and simulation of porous silica-alginate/chitosan systems. Biokinetic behaviours were analysed by deploying four distinct models namely Monod, Michaelis-Menten, First Order, and Second Order. Furthermore, three modified Monod namely Monod E, Monod EM, and Monod EMG models were employed to investigate bioethanol inhibition, substrate kinetics for cell maintenance, and glucose inhibition respectively. Isqnonlin function of MATLAB software was employed for simulation.

2.0 MATERIALS AND METHODS

2.1 Materials

Saccharomyces cerevisiae was MIC23 was procured from the Microbiology Department, ABU Zaria. APTES (3-aminotriethoxysilane) and, chitosan was purchased from Sigma-Aldrich (Germany), other chemicals were purchased from Haddis commercial supplier: calcium chloride (Daejung Chemical and Metal Co., Korea), sodium alginate (MERCK Chemicals Co., Ltd., Germany), Tween 20 (Duksan Pharmaceutical Co., Ltd., Korea), CMC (Carboxymethylcellulose) and D-glucose (VWR Chemicals BDH, England), DNSA reagent (dinitro salicylic acid, sodium potassium tartrate tetrahydrate), YPD (yeast extract, peptone, dextrose) (Merck, Germany), and Potassium dichromate reagent (Jinhuada Chemical Reagent Co., Ltd, Guangzhou, China).

2.2 Methods

2.2.1 Encapsulation of cells of *Saccharomyces cerevisiae* in silica-alginate-chitosan capsules

Encapsulation of cells of *Saccharomyces cerevisiae,* chitosan, alginate, and silica Coating and ethanol production was carried out according to (Ylitervo et al., 2013). The modified silica coating was carried out similarly to the traditional silica procedure, except that a pore-forming agent (glucose) was included in this route. The glucose amount was varied (0.75, 1.5 and 3 g). After coating, the glucose was removed through water extraction by immersing the capsules in a 250 ml beaker at room temperature for 24 hours. The set of capsules was designated as G-0.75, G-1.5, and G-Aerobic fermentation and cell growth measurement. The ethanol and glucose was determined according to (Singh & Singh 2015).

2.2.2 Kinetic studies

Four models were employed to study the kinetics of bioethanol production: Michaelis-Menten, First and Second order, and Monod models as given by equations 1, 2, 3, and 4, respectively. Further biokinetics analysis was also carried out with equations 5, 6, and 7 to account for bioethanol and glucose as well as cell maintenance factors respectively. Equation 8 describes the cell growth. A MATLAB code was writt to fit the glucose consumption data, estimate the kinetics constants, and simulate the models to compare the results with experiment data, the data for free cells were used as the initial guesses as given by (Fogler 2004).

$$\frac{dCs}{dt} = r\max * \frac{Cs}{(Km+Cs)} \tag{1}$$

$$\frac{dCs}{dt} = k1 \cdot Cs \tag{2}$$

$$\frac{dCs}{dt} = k2 \cdot Cs^2 \tag{3}$$

$$\frac{dCs}{dt} = Ysc * u\max * Cc \cdot \frac{Cs}{(Ks+Cs)} \tag{4}$$

$$\frac{dCs}{dt} = Ysc * u\max * \left(1 - \frac{Cp}{CP}\right)^n \cdot Cc \cdot \frac{Cs}{(Ks+Cs)} \tag{5}$$

$$\frac{dCs}{dt} = Ysc * u\max * \left(1 - \frac{Cp}{CP}\right)^n * Cc \cdot \frac{Cs}{\left(Ks+\frac{Cs^2}{KI}+Cs\right)} \tag{6}$$
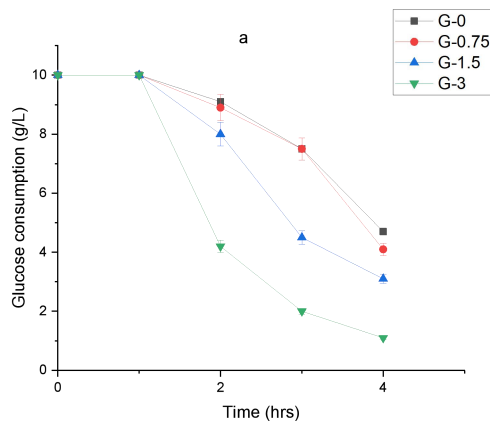
$$\frac{dCs}{dt} = Ysc * u\max * \left(1 - \frac{Cp}{CP}\right)^n * Cc \cdot \frac{Cs}{\left(Ks+\frac{Cs^2}{KI}+Cs\right)} - km \cdot Cs \tag{7}$$

$$\frac{dCc}{dt} = u\max * \left(1 - \frac{Cp}{CP}\right)^n \cdot Cc \cdot \frac{Cs}{(Ks+Cs)} - kd \cdot Cc \tag{8}$$

$$\frac{dCs}{dt} = Ysc * u\max * \left(1 - \frac{Cp}{CP}\right)^n * Cc \cdot \frac{Cs}{(Ks+Cs)} - km \cdot Cs \tag{9}$$

3.0 RESULTS AND DISCUSSION

In this section, the kinetics of glucose consumption and bioethanol production using porous silica-alginate-chitosan encapsulated S. cerevisiae (Figure 1) was presented. The experimental data were modelled using four different biokinetic models (Figure 2). Additionally, three modified Monod models were analysed based on the experimental data (Figure 3). The investigation identified the optimal model to accurately describe the bioreaction (Equation 9).

3.1 Bioethanol production

All four types of capsules were employed for bioethanol production. A clear increase in both bioethanol production and glucose consumption was observed from G-0 to G-0.75, G-1.5, and G-3 (Figure 1). While the traditional reference capsule, G-0, exhibited bioethanol productivity of approximately 2.7 g/L, G-3 achieved an impressive 4.5 g/L, representing a 1.7-fold improvement over the reference sample. The glucose consumption (Figure 1a) and bioethanol production (Figure 1b) revealed interesting insights into the fermentation process. Initially, during the first hours of fermentation, no bioethanol production was observed from any of the capsule samples. This initial lack of production can be attributed to the time required for the cells to adapt to their new environment before metabolic activities commence. However, an approximately linear relationship between glucose consumption and bioethanol production with time was observed from the second through the fourth hour. This linear progression indicates the entry into the second phase of metabolic activity, characterized by high activity (Tse et al., 2021). Within the four hours of bioethanol production, only the G-3 sample has almost converted all the substrate, reaching about 95 conversions.
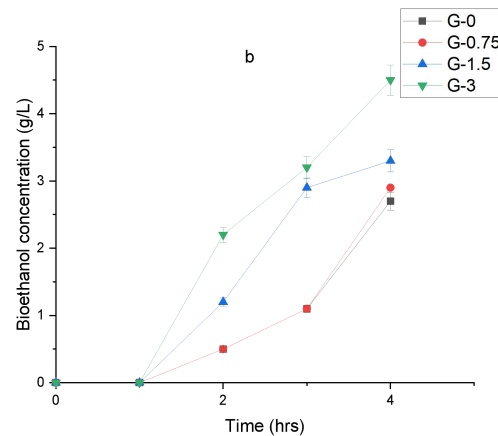
Figure 1: (a) glucose consumption and (b) bioethanol production using porous silica-alginate-chitosan at 30 ºC, 150 rpm, pH 5, 30 capsules and 10 g/L glucose.

3.2 Biokinetic studies

The kinetics of glucose consumption by encapsulated *Saccharomyces cerevisiae* was modelled employing four different biokinetic models—Monod, Michaelis-Menten, first order, and second order (Figure 2). Notably, the Monod model as expected emerged as the most suitable for describing the glucose consumption kinetics for all four capsule samples. The coefficient of determination (R-Square) between the experimental data and the Monod model for G-0 and G-3 stood at an impressive 0.986 and 0.9799 (Table 1), respectively, indicating an almost perfect fit. The Michaelis-Menten (MM) model also demonstrated a strong fit to the experimental data, particularly for G-0 and G-0.75, where the fit exceeded 0.95.

**Table 1: Level of fit (R-Square) of different models**

Sample	First Order R^2	Second Order R^2	Machealis Menten R^2	Monod R^2	Monod E R^2	Monod EM R^2	Monod EMG R^2
G-0	0.7912	0.7297	0.964	: 0.986	0.9990	0.9996	0.9996
G-0.75	0.77	0.7037	0.9728	: 0.9879	0.9982	0.999	0.999
G-1.5	0.8514	0.7687	0.9539	0.9792	0.9892	1.00	1.00
G-3	0.85	0.7401	0.8653	0.9799	0.9874	0.9996	0.9996

However, the MM model struggled to accurately describe the kinetics of glucose consumption for G-3, yielding a fit of 0.87. This discrepancy in the MM model can be attributed to the fact that the model primarily accounts for enzyme kinetics, focusing solely on the enzymes responsible for glucose consumption. In contrast, bioethanol production involves a more intricate interplay of kinetics, including cell growth, maintenance, and death. So, the limitations of the MM model became more apparent with the complex dynamics associated with G-3. Both the First-Order and Second-Order models fell short of providing satisfactory descriptions of substrate consumption kinetics. The First-Order model achieved a fit ranging from 0.77 to 0.85 for the four samples, while the second-order model yielded an even lower

fit, approximately 0.70 to 0.77. The challenges faced by these models in accurately capturing the experimental data underscore the nuanced nature of substrate

To investigate these considerations, experimental data were compared with variations that incorporated these factors. The term (1-Cp/CP)^n, as given by Fogler (2004), was included to represent bioethanol inhibition. Here, CP signifies the concentration beyond which no yeast can survive, so the term accounts for bioethanol concentration inhibition. The overall term becomes negligible when Cp is zero but exerts the highest effect at CP when all yeast cells perish. The values of CP and n for all capsules are provided in Table 3. Upon adding the ethanol inhibition term to the Monod model (Monod E), bioethanol inhibition was observed for the capsules—G-0, G-0.75, G-1.5, and G-3. The level of fit to the experimental data slightly improved with the inclusion of the ethanol inhibition term, with R-square values of 0.990, 0.9982, 0.9892, and 0.9874, respectively. In comparison, the Monod model without the ethanol inhibition term (Monod) exhibited R-square values of 0.986, 0.9978, 0.9792, and 0.9799 for the same capsules. This suggests a subtle influence of ethanol inhibition, aligning with the insights shared by Fogler (2004).

consumption kinetics in this study. In biokinetics, ideally, two behaviours exist (Nosrati-Ghods et al., 2020): exponential phase (first order- at lower substrate concentration), stationary (zero order- at high substrate concentration). Both ideal Monod and MM models incorporate these behaviours: exponential and stationary phases. In comparison, the First-Order model incorporates just one (exponential phase), but the Second-Order incorporates none. Perhaps this informs why the first order is closer to fit the data compared to the second

3.3 Modified Monod Models

In the pursuit of a more comprehensive understanding of the bioethanol production kinetics, factors not accounted for in the ideal Monod equation were explored. Specifically, the impacts of bioethanol ((1-Cp/CP)^n) and glucose (Cs^2/KI) concentrations, as well as the influence of glucose consumption for cell maintenance (km*Cs) on bioethanol production, were investigated (Figure 3).

The impact of maintenance kinetics (km*Cs) was also explored. The simulated results incorporating both ethanol and maintenance terms (Monod EM) were compared with results excluding the maintenance term (Monod E). In all four samples, a slight improvement in the fit between the Monod model and experimental data was observed. For example, the R-square value for G-3 increased from 0.9874 to 0.996 when the maintenance term was included. This supports the notion that a small amount of substrate is utilized solely for maintenance metabolism, as suggested by Fogler (2004).

Interestingly, no effect of glucose inhibition was detected for any of the four samples—G-0, G-0.75, G-1.5, and G-3. The term Cs^2/KI, accounting for substrate inhibition (Villdsen et al., 2011), did not yield observable effects. Substrate inhibition typically occurs when there is an excess of substrate competing for limited active sites, thereby reducing the overall efficiency of the process. For substrate inhibition term to

be effective, substrate concentration must be high compared to KI values. However, in this study, the conditions did not favour substrate inhibition, as indicated by the KI values provided in Table 2.

Based on the biokinetics analysis in this study, the best model describing glucose consumption is given by Equation (9Based on the biokinetics analysis in this study, the best

Table 2: Determined kinetics and diffusion constants

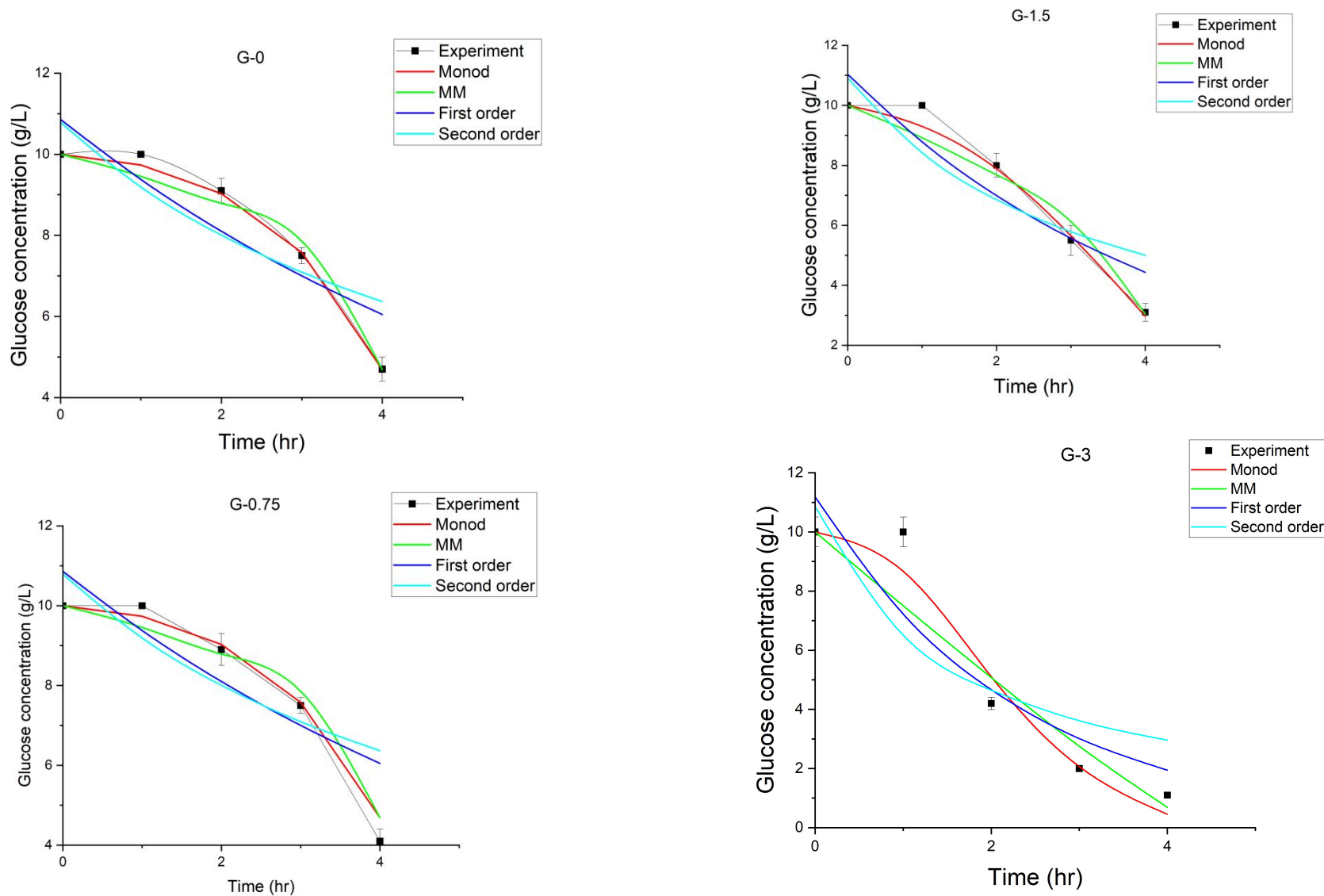| Factor	G-0	G-0.75	G-1.5	G-3
Ys/c	20.663	17.933	15.8994	12.222
CP	86.9495	89.035	91.9608	95.19101
N	4.2723	2.22	1.56367	1.460827
Umax	1.9212	1.6343	1.7221	1.98935
Ks	1.180592	1.347455	1.48836	1.2739
KI	81.5097	85.6860	50.6339	339.9482
Km	0.0328	0.0155	0.0611	0.2568
D (mm^2/hr)	0.0065	0.0092	0.0153	0.0297

Figure 2: Kinetic modelling (Monod, Michaelis-Menten, First and Second Order) of glucose consumption at 30 ºC, 150 rpm, pH 5, 30 capsules and 10 g/L glucose.
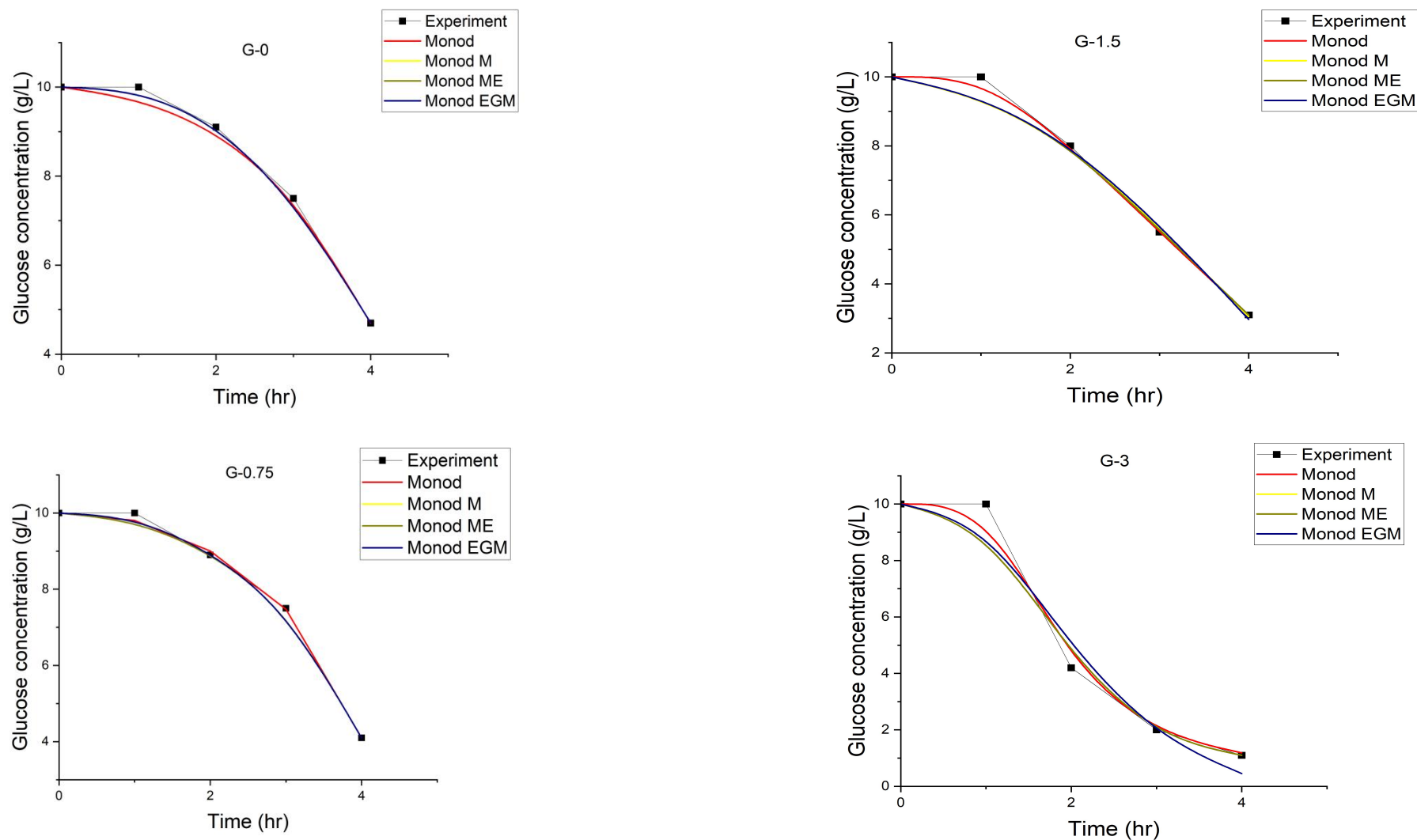
Figure 3: Kinetic modelling (Monod E, Monod EM, Monod EGM) of glucose consumption at 30 ºC, 150 rpm, pH 5, 30 capsules and 10 g/L glucose

4.0 CONCLUSION

The culmination of this study identified the Monod EM model, as the best descriptor of bioreactions in porous silica-alginate during glucose consumption. Additionally, under the given process conditions, bioethanol production was significantly affected by product inhibition and substrate usage for cell maintenance, while glucose inhibition had no significant impact. These findings are promising for the optimization of heterogeneous bioprocesses.

REFERENCES

Birol, G., Doruker, P., Kirdar, B., İlsen Önsan, Z., & Ülgen, K. (1998). Mathematical description of ethanol fermentation by immobilized Saccharomyces cerevisiae. *Process Biochemistry*, 33(7): 763–771. https://doi.org/10.1016/S0032-9592(98)00047-8

Ching, S. H., Bansal, N., & Bhandari, B. (2017). Alginate gel particles—a review of production techniques and physical properties. *Critical Reviews in Food Science and Nutrition*, 57(6): 1133–1152. https://doi.org/10.1080/10408398.2014.965773

Fogler, H. S. (2004). Elements of chemical reaction engineering (3rd ed.). Prentice Hall.

Lee, J. M. (1992). Biochemical engineering. Prentice Hall Englewood Cliffs, NJ.

Nosrati-Ghods, N., Harrison, S. T. L., Isafiade, A. J., & Tai, S. L. (2020). Mathematical modelling of bioethanol fermentation from glucose, xylose or their combination—a review. *Chemical Engineering & Technology*, 43(8): 1574-1587. https://doi.org/10.1002/cben.201900024

Rathore, S., Desai, P. M., Liew, C. V., Chan, L. W., & Heng, P. W. S. (2013). Microencapsulation of microbial cells. *Journal of Food Engineering*, 116(2): 369–381. https://doi.org/10.1016/j.jfoodeng.2012.12.022

Singh, A. and Singh, A., (2015). A comparative overview of Bioethanol production from Organic Residues of Agro waste Materials. *European Journal of Biotechnology and Bioscience*, *3*(3): 11-14.

Tse, T. J., Wiens, D. J., & Reaney, M. J. T. (2021). Production of bioethanol—a review of factors affecting ethanol yield. Fermentation, 7(4), Article 268. https://doi.org/10.3390/fermentation7040268

Villadsen, J., Nielsen, J., & Liden, G. (2011). Bioreaction engineering principles (3rd ed.). Springer.

Ylitervo, P., Franzén, C. J., & Taherzadeh, M. J. (2013). Mechanically robust polysiloxane–ACA capsules for prolonged ethanol production. *Journal of Chemical Technology & Biotechnology*, 88(6): 1080–1088.

Qian, H., Zhu, X. and Huang, S. (2023). Greenhouse gas emissions and mitigation in rice agriculture. *Nat Rev Earth Environ* **4**, 716–732 https://doi.org/10.1038/s43017-023-00482-1

Rafał Ł., Iwona H., Karolina K., Marta G., Piotr R., Andrzej P. and Marian K. (2018). Hydrogen production from biomass using dark fermentation, Renewable and Sustainable Energy Reviews, Volume 91, Pages 665-694, ISSN 1364-0321, https://doi.org/10.1016/j.rser.2018.04.043.

Roeb M, Agrafiotis C and Sattler C. (2015.) Compendium of hydrogen energy. New York: Longman.

Sandro N., Müslüm A. and Anh T. H. (2023). Smart and Sustainable Technologies in energy transition, Journal of Cleaner Production, Volume 389, 135944,ISSN 0959-6526, https://doi.org/10.1016/j.jclepro.2023.135944.

Zhao, Y., Niu, Z. and Zhao, J (2023). Recent Advancements in Photoelectrochemical Water Splitting for Hydrogen Production. *Electrochem. Energy Rev.* **6**, 14 https://doi.org/10.1007/s41918-022-00153-7

MOLECULAR SIMULATION OF IBUPROFEN ADSORPTION ON PRISTINE GRAPHENE MEMBRANES FOR ENHANCED INDUSTRIAL EFFLUENT TREATMENT

[1,2]Abbas, A. A., **[1,2]Oyegoke, T. and [1,2]Suleiman, S. O.

[1]*Green Science Promoters Forum – Modeling and Simulation, Pencil Team, ABU Zaria, Nigeria.*
[2]*Chemical Engineering Department, Ahmadu Bello University Zaria, Nigeria.*
**Corresponding Author: OyegokeToyese@gmail.com

ABSTRACT

The presence of high concentrations of pharmaceuticals like ibuprofen in water bodies poses significant environmental challenges, mainly from pharmaceutical industry discharges. This study investigates the potential of pristine graphene membranes to reduce ibuprofen contamination in effluents using molecular simulations with the Merck Molecular Force Field (MMFF) method. Graphene was evaluated as the adsorbent, while ibuprofen served as the adsorbate. Various adsorption modes were simulated by assessing different sites on ibuprofen (oxygen site, carbon sites at the acid group (C2), and non-acid group (C1)) and graphene (top, bridge, hollow) under vacuum and aqueous conditions. Results indicate that ibuprofen has a strong affinity for graphene, particularly at the C1 and C2 sites in the hollow configuration, with adsorption energies of -25.91 eV for C2 and -27.88 eV for C1 in aqueous conditions. These findings highlight graphene's potential for effective ibuprofen removal in effluent treatment.
Keywords*: Ibuprofen; Graphene Membranes; Industrial Effluent; Adsorption; Molecular Mechanics.*

1 INTRODUCTION

The increasing presence of pharmaceutical waste in water has become a significant environmental concern affecting both human and aquatic life (Khan & Barros, 2023; Kayode-Afolayan et al. 2022). Ibuprofen, widely used for its excellent anti-inflammatory effects in daily life, poses considerable environmental risks upon discharge into water bodies. Numerous studies documented in the literature (Jan-Roblero & Cruz-Maya, 2023) have highlighted the adverse effects of ibuprofen on aquatic habitats, including reproductive abnormalities in fish and other aquatic organisms, thereby underscoring its toxic effects on ecosystems and potential implications for human health.

Efforts to mitigate these risks include various methods for removing ibuprofen from effluent during wastewater treatment. Chemical oxidation, biodegradation, liquid extraction, and membrane techniques are commonly explored alongside adsorption. Adsorption, particularly through advanced materials like graphene and carbon nanotubes, has emerged as a promising approach (Badran et al., 2023, Oyegoke et al., 2024; Osman et al., 2024). Its simplicity in design, ability to be modeled using simulations, cost-effectiveness, and high efficiency make it an attractive method for removing pharmaceutical pollutants from wastewater. Moreover, adsorption technologies hold significant potential for addressing broader challenges posed by pharmaceutical waste in industrial effluents.

This study aims to contribute to this field by investigating the efficacy of pristine graphene membranes in adsorbing ibuprofen from industrial effluent. Using the Merck Molecular Force Field (MMFF) (Halgren, 1996a, 1996b) for simulation, we analyze the interaction between graphene and water molecules, focusing on different adsorption sites and modes. By enhancing our understanding of graphene's adsorption capabilities, this research seeks to propose improvements in the treatment of pharmaceutical industrial effluents and mitigate the environmental impact of ibuprofen contamination in water bodies.

2 MATERIALS & METHODS

In this study, we provide details on the method, which include the material resources, method of computation, and the design/strategy used.

2.1 Material Resources

The computing devices used for this study include the HP EliteBook 840 G3 with core i5 processor, 2.40 GHz speed, and Dell precision mobile workstation. Other resources used include Spartan V9 and Spartan 24 application software used in the modeling and simulation of the adsorption mechanism and process.

2.2 Computational Methods and Study Strategy

In this study, Molecular Mechanics (MMFF, Merck Molecular Force Field) (Halgren, 1996a, 1996b)

calculations were employed to determine the adsorption energy. The Merck Molecular Force Field (MMFF) was chosen for its ability to handle simulations involving a large number of atoms, enabling an in-depth analysis of how graphene interacts with water molecules.
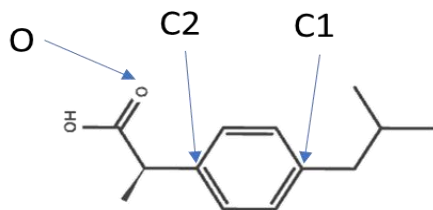

Figure 1. 2-D molecular structure of ibuprofen showing the more active sites (O, C1, and C2) on its geometry.

The stable geometry and adsorption energy of the models were obtained using the Spartan molecular modeling application software (Zakharian & Coon, 2001; Alden et al., 2014). Each molecule used in the study was built and minimized, and their structural geometry was determined using inherent molecular mechanics (MMFF) calculations with an SCF convergence of 1e-9 geometrical cycles of 9000. Energy calculations were performed automatically in electron volts (eV). Different sites of the pollutant were used to interact with varying modes of adsorption on the graphene surface in Figure 1. These sites included carbon (C1) close to the alkyl branch of the benzene ring, carbon (C2) at the benzene ring close to the acid branch of the benzene ring, and the oxygen site with a double bond (O-site) as shown in Figure 1. The modes of adsorption on the graphene surface were classified as Hollow (H), Top (T), Bridge double (BD), and Bridge single (BS) at both the Edge and Center sides of the graphene. The adsorption energy (E_{ads}) was calculated using the formula (Oyegoke et al., 2024):

$$Eads = Eab \quad - Ea \quad - Eb \qquad (1)$$

where Eads is the adsorption energy, Eab is the energy of the bonded form of the pollutant-adsorbent structure, Ea is the energy of the pollutant, and Eb is the energy of the adsorbent. A highly negative adsorption energy indicates a more stable adsorption (Bahamon et al., 2021; Wang et al., 2024).

3   RESULTS AND DISCUSSIONS

3.1   Exploration of Molecular Interaction Adsorption Studies Using MMFF

Here we explore how a species interacts with the other, the behavior of a species on the other, and also understand the different modes of adsorption in which molecules or materials are adsorbed.

3.1.1   The Interactive Adsorption Energy for Ibuprofen (IBU)-Graphene (GRA)

Here, different sites of ibuprofen—specifically C1, C2, and the O-site—are used to analyze various modes of adsorption on the graphene sheet. These modes include Hollow (H), Top (T), Bridge Double (BD), and Bridge Single (BS), which can occur on either the Edge or Centre side of the graphene.

The results presented in Table 1 show the analysis of interactions via the C1, C2, and O-sites on ibuprofen (IBU) with graphene (GRA) in a vacuum, demonstrating that the C1 and C2 sites of ibuprofen exhibit stronger interactions with graphene at the hollow (H) site, with an adsorption energy of -25.91 eV, which is more negative compared to other sites and modes.

Table 1. Analysis of Interaction via C1, C2, and O -site on IBU with the GRA in a vacuum (or gas) system.

Eads(eV)	C1	C2	O-site	Most Stable
H	-25.91	-25.91	-24.99	C1C2/H (-25.91)
BS	6.95	6.79	1.91	O/BS
BD	11.01	11.69	3.53	O/BD
T	2.42	3.12	3.35	C1/T
Most Stable	H/C1(-25.91)	H/C2(-25.91)	H/O(-24.91)	C1C2/H

Table 2. Analysis of Interaction via C1, C2, and O -site on IBU with the GRA in aqueous phase (water).

Eads(eV)	C1	C2	O-site	Most Stable
H	-27.88	-23.71	-24.82	C1/H (-27.88)
BS	7.01	6.86	2.09	O/BS
BD	11.05	11.75	3.72	O/BD
T	2.47	5.22	5.54	C1/T
Most Stable	H/C1 (-27.88)	H/C2	H/O	C1/H

The Hollow site of C1/C2 shows significant adsorption strength, whereas the O-site exhibits the least adsorption at the Hollow site, but performs better at the Bridge Single (BS) and Bridge Double (BD) modes of adsorption.

Additionally, the C1 site demonstrates the strongest adsorption strength at the Top (T) mode. This study confirms that the C1/C2 Hollow (-25.91 eV) site exhibits stronger adsorption energy compared to the O-site,

following the highest negative adsorption energy obtained in agreement with the literature (Oyegoke et al., 2024; Wang et al., 2024), which say the more negative the value of adsorption energy, the stronger the strength.

C1-site in an aqueous system

C1-site in a vacuum system

C2-site in an aqueous system
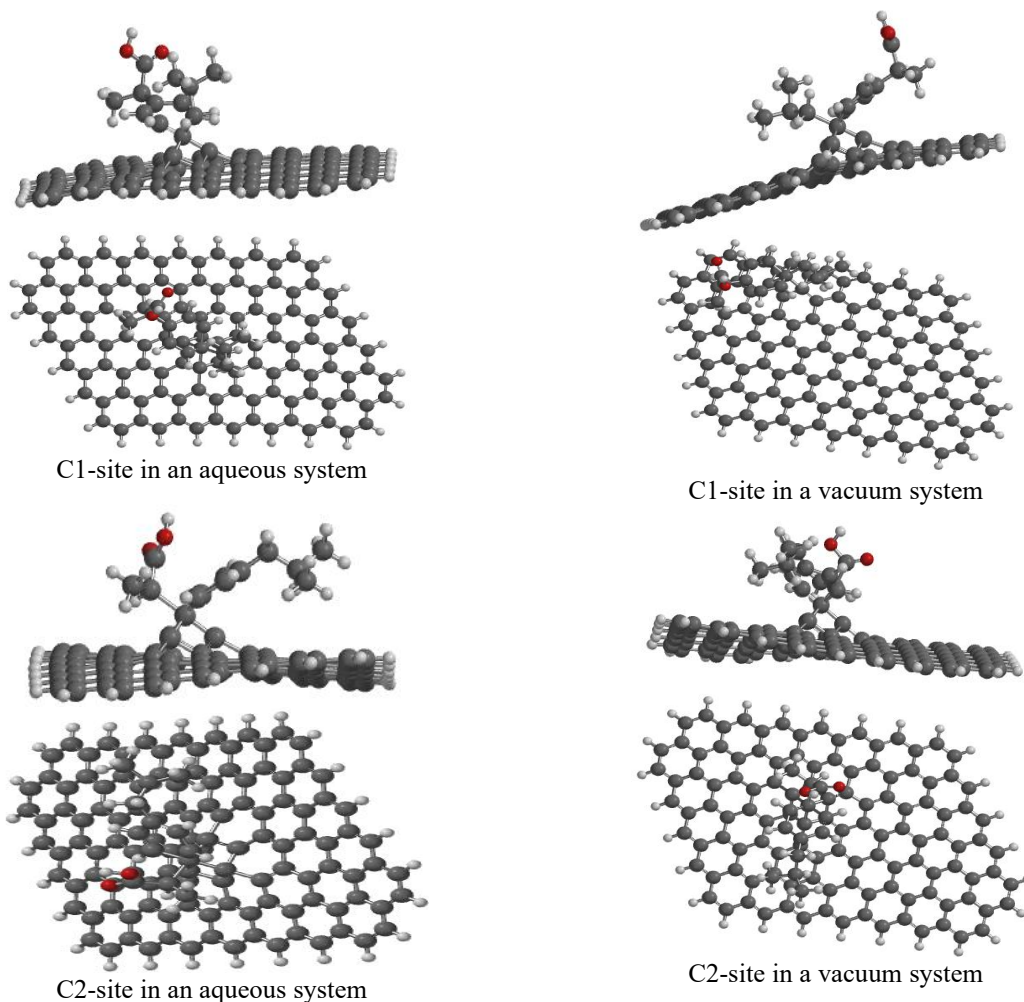
C2-site in a vacuum system

Figure 1a. Geometries for GRA adsorptions at O-site, where GRA adsorbed in water or aqueous (on the left side) and vacuum or Gas (on the right side).
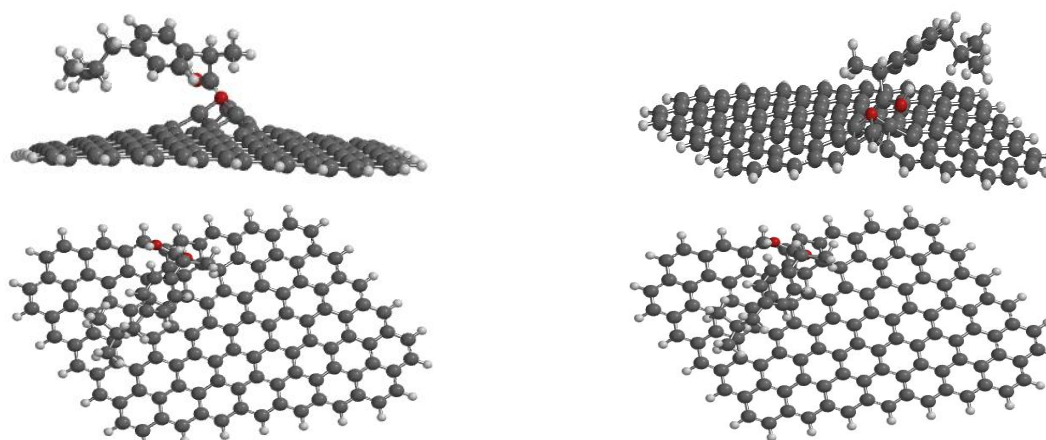
Figure 1b. Geometries for GRA adsorptions at O-site, where GRA adsorbed in water or aqueous (on the left side) and vacuum or Gas (on the right side).

Table 2 presents the analysis of interactions via C1, C2, and O-site of IBU with GRA in aqueous solution, showing similar trends to those computed in vacuum (Table 1). Specifically, ibuprofen at the C1 site exhibits the most stable adsorption energy of -27.88 eV, surpassing both C2 and the O-site, following the literature (Uzochukwu et al., 2023) that confirms it to be stronger when it is more negative. Conversely, at the Bridge Double (BD) and Bridge Single (BS) modes, the O-site demonstrates the most stable adsorption. This study reaffirms that ibuprofen adsorbs more effectively at the Hollow (H) site, particularly at the C1 site.

Figures 1a and 1b show the optimized and most stable geometrical structures of ibuprofen adsorbed on the graphene surface, providing top and side views of the C1, C2, and O-sites in various adsorption modes. These figures highlight the superior adsorption strengths of these sites in both vacuum and aqueous conditions, as observed in this study.

3.1.2 The Interactive Adsorption Energy for Water (H2O)-Graphene (GRA)

In this study, we analyze the interaction of the oxygen site of water with different modes of graphene, observing significant variations between edge and center sites in both vacuum and aqueous conditions. This provides deeper insights into water-graphene adsorption dynamics, demonstrating graphene's suitability for designing and applying technologies that rely on its adsorption properties. Table 3a provides a detailed analysis of how the oxygen site (O-site) of water interacts with graphene in a vacuum environment, across various adsorption modes on the graphene surface. The O-site of water exhibits different levels of adsorption strength depending on whether it interacts at the edge or centre of the graphene sheet. Specifically, in vacuum conditions, the O-site shows the most favourable adsorption at the edge hollow (H) mode, where it achieves notable negative adsorption energy of -24.83 eV. This contrasts with the centre hollow (H) mode, indicating a preference for the edge configuration.

Further analysis reveals that the bridge single (BS) mode demonstrates stronger adsorption at the edge (2.80 eV) compared to the centre (4.14 eV). Similarly, the bridge double (BD) and top (T) modes also show enhanced adsorption at the edge (3.84 eV and 3.09 eV respectively), compared to their centre counterparts (BD centre 4.54 eV, T centre 3.35 eV). Overall, these findings show the O-site's significant affinity for the edge hollow mode (-24.83 eV) on the graphene surface in a vacuum.

Table 3a. Analysis of Interaction via O-site on H₂O with the GRA in a vacuum (or gas) via MMFF

Eads(eV)	Edge	Center
H	-24.83	11.54
BS	2.80	4.14
BD	3.84	4.54
T	3.09	3.35

Table 3b. Analysis of Interaction via O-site on H₂O with the GRA in water (aqueous phase) via MMFF

Eads(eV)	Edge	Center
H	-22.56	11.87
BS	3.08	4.42
BD	4.09	4.79
T	5.37	5.64

Table 3b provides a detailed analysis of how the oxygen site (O-site) of water interacts with graphene in an aqueous environment, yielding results consistent with those in Table 3a. It demonstrates that the O-site of water exhibits stronger adsorption with graphene at the edge hollow (H) mode, showing significant negative adsorption energy of -22.56 eV. In contrast, the hollow (H) centre mode exhibits the least adsorption strength at 11.87 eV on the graphene surface. These findings reaffirm that the O-site of water consistently shows robust adsorption at the edge hollow mode (-22.56 eV) on the graphene surface in water.
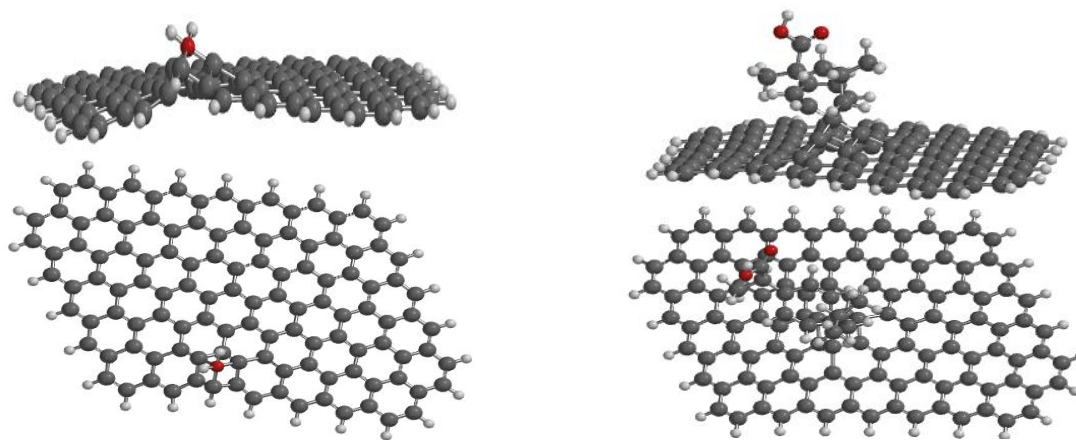
Figure 2. The stronger adsorption process geometrical structure of H₂O-GRA (Eads = -24.83 eV, i.e., on the LEFT) and IBU-GRA (Eads = -27.88 eV, i.e., on the RIGHT) interactions obtained for the use of MMFF simulation method.

3.2 Summary of Adsorption Study Results

The interaction of Ibuprofen with graphene varies significantly between the H BS BD and T, with the C1 carbon on the hollow (-27.88 eV) site showing exceptionally strong adsorption strength. Also, the interaction of water with graphene varies significantly between the edge and center. The O-site of water better interacts with the graphene at the edge having an adsorption energy of -22.56 eV compared to other modes of adsorption (BS, BD, T). Figure 2 summarizes the geometrical structure for the stronger adsorption processes evaluated using the MMFF simulation method. The H₂O-GRA interaction has an adsorption energy of -24.83 eV, indicating a highly favorable interaction between water molecules and graphene. The side and top geometries describe the orientation of the adsorption. Additionally, the IBU-GRA interaction shows an adsorption energy of -27.88 eV, highlighting a strong interaction between Ibuprofen and graphene, with side and top geometries describing the adsorption orientation.

4 CONCLUSIONS AND RECOMMENDATIONS

This study investigates the potential of pristine graphene membranes for removing ibuprofen from industrial effluents, addressing environmental concerns associated with this common pain and inflammation medication. Ibuprofen poses environmental risks when discharged into water bodies, making its removal crucial.

The results of this study provide valuable insights into the adsorption behavior of ibuprofen (IBU) and water (H₂O) on pristine graphene (GRA) surfaces, utilizing the MMFF simulation method. The analysis reveals that ibuprofen exhibits significantly stronger adsorption on graphene, particularly at the C1 and C2 sites in the hollow (H) mode, with adsorption energies of -25.91 eV in a vacuum and -27.88 eV at the C1 site in an aqueous phase. These findings indicate that the C1 site of ibuprofen forms a more stable interaction with the graphene surface compared to other sites and modes, consistent with the trend observed in both vacuum and aqueous conditions.

In contrast, water molecules show weaker but still notable adsorption on graphene, with the most favorable

interaction occurring at the edge hollow (H) mode, with adsorption energies of -24.83 eV in a vacuum and -22.56 eV in an aqueous phase. The preference of water for the edge hollow mode suggests a specific interaction pattern that could influence the design of graphene-based materials for applications requiring selective adsorption.

Overall, the study confirms that graphene exhibits a stronger affinity for ibuprofen than water, particularly at the hollow site on graphene with ibuprofen at the C1 site. The optimized geometrical structures provided insights into the orientation of the adsorbed molecules. The findings suggest that graphene could be effective in reducing the concentration of ibuprofen in potential pharmaceutical effluent discharges. Moreover, we recommend expanding research efforts to explore how graphene membranes interact with other pharmaceutical compounds commonly found in wastewater. This could enhance the versatility and applicability of graphene in comprehensive wastewater treatment solutions.

5 ACKNOWLEDGEMENTS

6 AUTHORS' CONTRIBUTIONS

Abbas, A. A.: Formal analysis, Investigation, Formal analysis, Software, Resources, Visualization, Validation, Writing – original draft, Writing – review & editing. **Oyegoke, T.:** Conceptualization, Software, Methodology, Resources, Writing – original draft, Writing – review & editing, Project administration, Supervision. **Suleiman, S. O.:** Validation, Visualization, Writing – review & editing.

7 REFERENCES

Alden, K., Read, M., Andrews, P. S., Timmis, J., & Coles, M. (2014). Applying spartan to Understand Parameter Uncertainty in Simulations. *R Journal*, *6*(2), 63 - 80.

Badran, A. M., Utra, U., Yussof, N. S., & Bashir, M. J. (2023). Advancements in Adsorption Techniques for Sustainable Water Purification: A Focus on Lead Removal. *Separations*, *10*(11), 565.

Bahamon, D., Khalil, M., Belabbes, A., Alwahedi, Y., Vega, L. F., & Polychronopoulou, K. (2021). A DFT study of the adsorption energy and electronic interactions of the SO 2 molecule on a CoP hydrotreating catalyst. *RSC advances*, 11(5), 2947-2957.

Halgren, T. A. (1996a). Merck molecular force field. I. Basis, form, scope, parameterization, and performance of MMFF94. *Journal of Computational Chemistry*, *17*(5-6), 490-519.

Halgren, T. A. (1996b). Merck molecular force field. II. MMFF94 van der Waals and electrostatic parameters for intermolecular interactions. *Journal of Computational Chemistry*, 17(5-6), 520-552.

Jan-Roblero, J., & Cruz-Maya, J. A. (2023). Ibuprofen: toxicology and biodegradation of an emerging contaminant. *Molecules*, 28(5), 2097.

Kayode-Afolayan, S. D., Ahuekwe, E. F., & Nwinyi, O. C. (2022). Impacts of pharmaceutical effluents on aquatic ecosystems. *Scientific African*, *17*, e01288.

Khan, A.H.A.; Barros, R. Pharmaceuticals in Water: Risks to Aquatic Life and Remediation Strategies. *Hydrobiology* 2023, *2*, 395-409.

Osman, A. I., Ayati, A., Farghali, M., Krivoshapkin, P., Tanhaei, B., Karimi-Maleh, H., & Sillanpää, M. (2024). Advanced adsorbents for ibuprofen removal from aquatic environments: a review. *Environmental Chemistry Letters*, 22(1), 373-418.

Oyegoke, T., Aliyu, A., Uzochuwu, M. I., & Hassan, Y. (2024). Enhancing hydrogen sulphide removal efficiency: A DFT study on selected functionalized graphene-based materials. *Carbon Trends*, *15*, 100362.

Oyegoke, T., Igwebuike, C. M., & Oyegoke, A. (2024). Unraveling the influence of biomaterial's functional groups in Cd biosorption: a density functional theory calculation. *Pure and Applied Chemistry*, 96(3), 399-412.

Uzochukwu, M. I., Oyegoke, T., Momoh, R. O., Isa, M. T., Shuwa, S. M., & Jibril, B. Y. (2023). Computational insights into deep eutectic solvent design: Modeling interactions and thermodynamic feasibility using choline chloride & glycerol. *Chemical Engineering Journal Advances*, 16, 100564.

Wang, K., Zhao, Z., Wu, G., Jiang, D., & Lan, Y. (2024). Investigating the Influence of Impurity Defects on the Adsorption Behavior of Hydrated Sc3+ on the Kaolinite (001) Surface Using Density Functional Theory. *Materials*, *17*(3), 610.

Zakharian, T. Y., & Coon, S. R. (2001). Evaluation of Spartan semi-empirical molecular modeling software for calculations of molecules on surfaces: CO adsorption on Ni (111). *Computers & Chemistry*, *25*(2), 135-144.

BIOELECTRICITY GENERATION THROUGH DUAL MFC CHAMBER WITH METHYLENE BLUE AS AN ELECTRON MEDIATOR

*Akinwumi, O. D. [1], Ajao, J. O. [1], Aremu, M. O. [1], Agarry, S. E. [1], Sulayman, A. A. [2], Olowonyo, I. A. [4] and Popoola, A. O. [3]

[1]*Biochemical Engineering Unit,* [2]*Process, Modelling and Control Unit,* [3]*Environmental Engineering Unit, Department of Chemical Engineering, Ladoke Akintola University of Technology, Ogbomoso, Oyo State*
[4] *Biochemical Engineering , Department of Chemical Engineering, Adeleke University, Ede, Osun State.*
*Corresponding Author: odakinwumi@lautech.edu.ng

ABSTRACT

Microbial Fuel Cells (MFCs) utilize the biochemical activity of microorganisms to convert substrates into electricity through metabolic processes. This study investigates the role of Methylene Blue (MB) as an electron mediator in enhancing the efficiency of bioelectricity generation from Brewery Wastewater (BW) used as a substrate. An improvised two-chambered, salt bridge (membrane-less) MFC was used, consisting of an anode chamber with a plain graphite electrode and a cathode chamber containing 50 mM potassium ferricyanide $[K_3Fe(CN)_6]$ in a phosphate buffer (pH 7.5) in the presence of mediators. The maximum power density (Pmax) and current density (ID) of the MFC with MB as a mediator reached 10,765 mW/m² and 12.45 mA/m², respectively, significantly higher than the MFC without MB (620.69 mW/m² and 2.76 mA/m²). This study demonstrated the potential of electricity generation from BW with MB as an electron mediator, serving as a new method to increase the performance of MFCs.
Keywords: Bioelectricity, Brewery wastewater (BW), Microbial fuel cells (MFCs), Methylene Blue (MB),)

1. INTRODUCTION

The use of dual-chamber Microbial Fuel Cells (MFCs) for bioelectricity generation has gained significant attention due to their ability to treat industrial wastewater efficiently while producing renewable energy. Dual-chamber MFCs typically consists of an anodic and a cathodic chamber separated by a membrane, which facilitates the transfer of protons from the anode to the cathode while electrons flow through an external circuit. This setup allows for optimized conditions for microbial activity and enhanced electron transfer, resulting in stable power outputs and effective wastewater treatment (Tan et al, 2020). The integration of MB as a bio-catalyst in the anodic chamber can further enhance the performance of these systems by providing a readily available and cost-effective substrate for microbial metabolism (Naik and Jujjavarappu, 2019). In MFC, methylene blue acts as an effective electron mediator, facilitating the transfer of electrons from the microbial cells to the anode. This mediator is crucial in enhancing the efficiency of electron transfer, thereby increasing the power output of the MFC. The role of methylene blue in electron transfer has been extensively studied, showing significant improvements in the bioelectricity generation capacity of MFCs when used in conjunction with appropriate substrates (Rossi and Setti, 2016). In dual-chamber systems, the use of methylene blue has been shown to significantly improve the overall performance, making it a vital component in the optimization of MFCs for energy production (Khaksar et al, 2017). The degradation of complex organic compounds present in organic compounds facilitates the continuous supply of electrons, thereby supporting sustained bioelectricity generation over extended periods. The performance of dual-chamber MFCs using MB as an electron mediator can be significantly influenced by various operational parameters. Factors such as pH, temperature, and substrate concentration need to be optimized to maintain high microbial activity and efficient electron transfer. For instance, maintaining a neutral to slightly alkaline pH and optimal temperature conditions can enhance the metabolic activities of the microbial consortia, thereby improving the overall efficiency of the system (Bose et al, 2018). Additionally, the continuous supply of MB as an electron ensures a steady generation of electrons, contributing to the stability and scalability of the MFCs. The integration of methylene blue in the anodic chamber of dual-chamber MFCs with BW as a substrate has shown promising results in terms of bioelectricity generation and wastewater treatment. The mediator enhances the electron transfer process, leading to higher power densities and improved system efficiency. Moreover, the use of mediator not only provides a sustainable and cost-effective substrate but also aids in the effective treatment of organic waste. This dual approach not only addresses the need for renewable energy sources but also contributes to environmental sustainability by reducing waste and generating clean energy (Fernando et al, 2016).

2. MATERIALS AND METHODS

2.1 Wastewater sample Collection

Brewery wastewater from the combined wastewater stream of a brewery in southwest Nigeria was collected in a container and transported to the reaction laboratory at 4°C for analysis. Physicochemical analyses were conducted within 48 h of sample collection, with necessary preservation techniques adapted from standard methods (APHA 1999).

2.2 Physicochemical Characteristics of BW

The characteristics of the brewery wastewater samples, including temperature, pH, total dissolved solids (TDS), conductivity, chemical oxygen demand (COD), volatile compounds, odour, and colour, were determined following the standard procedures described by the American Public Health Association (APHA 2022). The results have been reported in our previous study (Akinwumi *et al*, 2020). The BW had a temperature of 31°C, a pH of 5.4, TDS of 1170 mg/L, conductivity of 2340 μS/cm, COD of 865.23 mg/L, volatile compounds at 80°C, a pungent odour, and a brownish colour (Akinwumi *et al*, 2020).)

2. 3 MFC setup and operation

A dual-chamber MFC was improvised in the laboratory using identical plastic containers as described by Akinwumi et al, (2022) and Samsudeen et al, (2017). The anode and cathode chambers had working volumes of 5000 mL each, out of a total volume of 10,000 mL. A salt bridge served as the separator between the anode and cathode chambers. The anode chamber was loaded with 5000 mL of BW as a substrate, with an initial COD of 865.23 mg/L, while the cathode chamber contained a buffer solution. The process was carried out at an initial pH of 5.4 and a temperature of 31°C and mediator range (100-500 mL). The cathode chamber consisted buffer solution was maintained at pH of 7.5. MFC chamber consisted of a graphite rod electrode, which was suspended using a copper wire to transfer electrons produced at the anode to the cathode. A polyvinyl chloride (PVC) pipe filled with agar-agar and sodium hydroxide solution was employed as a salt bridge to facilitate proton transfer. The electrode was set at 5 cm from either side of the salt bridge, as discussed in our previous study (Akinwumi et al, 2022). An external load of 100 Ω was applied in all experiments, except when different resistors (33 Ω to 30 kΩ) were used to determine the power generation capacity of the MFCs as a function of load. The MFC was incubated for 166 days, with samples taken at three-day intervals for COD reduction analysis. COD was determined using the closed reflux method with potassium dichromate and a spectrophotometer (Merck Spectroquant instrument). Voltage, current, and power generated were measured by connecting various external resistors ranging from 33 Ω to 100 Ω while ensuring a stable cell voltage under steady-state conditions. Additionally, parameters such as power density (mW/m²) and current density (mA/m²) were computed based on the surface area of the anode electrode. The study also examined how different mediators quantities (100-500 mL) impacted bioelectricity generation from BW biotreatment and simultaneously generating electricity.

2.4 Measurement and Analyses

Cell voltage (mV) was measured using an auto range digital multimeter, while current (mA) and power (mW) were calculated using Ohm's law equation. The polarization and power density behaviour were obtained by connecting various external resistors ranging from 33 k Ω to 100 Ω when the cell voltage was stable under steady-state conditions. Current density (mA/m^2) and power density (mW/m^2) were calculated based on the anode electrode surface area. The wastewater chemical oxygen demand (COD) was calculated as reported by Akinwumi et al*., 2022*

3. RESULTS AND DISCUSSION

3.1 Effect of Methylene Blue (MB) on BW on bioelectricity generation

Mediators aid in the transfer of electrons to the anodic electrode. For bioelectricity generation to be more effective, mediators must be able to penetrate the membrane (salt bridge). Zuo et al, (2007) reported that MB has been used as an electron mediator to increase power production in MFCs. Figure 1 shows the effect of MB on bioelectricity generation. The voltage generated by the addition of MB through the transfer of electrons into the anode compartment of BW in the range of 100 mL to 500 mL. Without fruit waste, the highest voltage generated was 702 mV, while with the addition of MB, the highest voltage generated was 865 mV with 500 mL of mediator at 152 days.

Enhanced electricity generation using MFCs has long been attempted by introducing various synthetic exogenous mediators, such as methylene blue (Zuo et al., 2007, and Adebule *et al,* 2018). The effect of exogenous compounds (mediators), particularly methylene blue (MB), on power generation in the MFC was evaluated using BW as the substrate compared to control BW without a mediator.
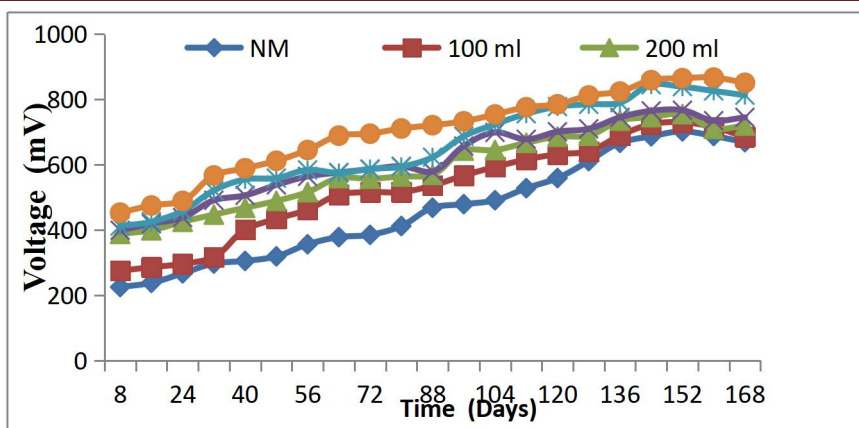
Figure: 1 Variation of Voltage generation with MFC operating time using mediator of 100 mL-500 mL and without mediator

Figures 2 and 3 present the electrical output in a dual-chambered MFC influenced by the presence of mediators over 168 days. The power density recorded for the mediated MFC reached 10,765 mW/m². The amount of current and voltage generated in an MFC at zero hour when enhanced with methylene blue (MB) was 0.401 mA and 453 mV, respectively, compared to 0.24 mA and 225 mV without MB (control). According to the report by (Babanova et al, 2011) on the efficiency of mediators in enhanced bioelectricity generation, the relatively high current and voltage recorded for the MFC with exogenous mediators may be attributed to the combined effect of the mediators, high carbohydrate, and high organic content.
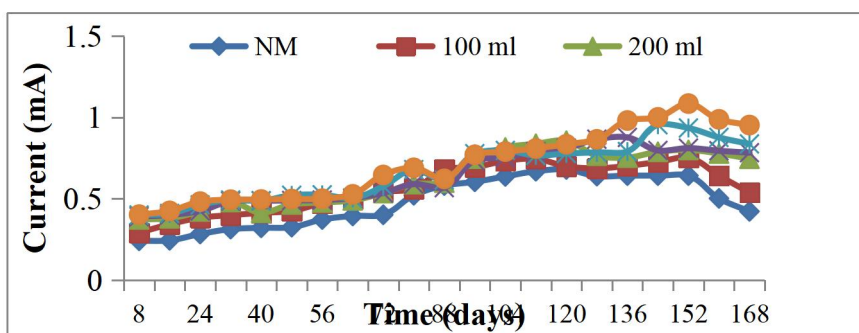
Figure 2: Current generated with and without exogenous mediators in MFC using BW waste as substrate.
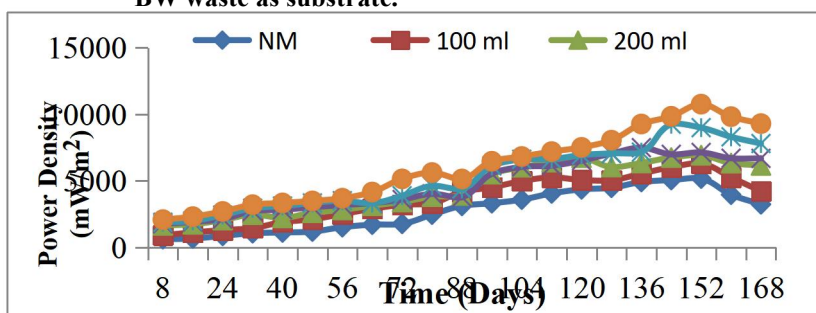
Figure 3: Power Density generated with and without exogenous mediators in MFC using BW waste as substrate.

4.0 CONCLUSION

In conclusion, the addition of mediators such as methylene blue significantly enhances the bioelectricity generation in MFCs using brewery wastewater as a substrate. The presence of these mediators facilitates electron transfer, leading to higher power and current densities. However, the long-term use of mediators may adversely affect the survival of electrogens and the overall longevity of the MFC. Further research is needed to optimize mediator usage to balance enhanced electricity generation with the sustainability of the MFC system.

5.0 REFERENCES

Adebule, A.P., Aderiye, B.I. and Adebayo, A.A. (2018). Improving Bioelectricity Generation of Microbial Fuel Cell (MFC) With Mediators Using Kitchen Waste as Substrate. Annals of *Applied Microbiology and Biotechnology Journal,* DOI:10.36876/aamb.1008

Akinwumi, O.D., Aremu, M.O. and Agarry, S.E (2020) Characterization of brewery and pharmaceutical industrial wastewater as potential for bioelectricity generatio*n. Research Journal of Engineering and Environmental Sciences.* **5** (2): 950-962.

Akinwumi, O.D., Aremu., M.O. and Agarry, S.E. (2022). Enhanced microbial fuel cell- bioelectricity generation and pollutant removal from brewery wastewater and modeling the kinetics. *Biomass Conversion Refinery.* https://doi.org/10.1007/s13399-022-03675-8

APHA-AWWA-WPCF.Standard methods for the examinations of water and wastewater (1999). 220th edition. Washington, DC, USA. American Public Health Association/ American Waterworks

Babanova, S., Hubenova, Y. and Mitov M. (2011). Influence of artificial mediators on yeast-based fuel cell performance. *J Biosci. Bioeng.* 2011; 112: 379-*387*

.Bose, D., Gopinath, M. and Vijay, P. (2018). Sustainable power generation from wastewater sources using Microbial Fuel Cell. Biofuels, 12, 1892. https://doi.org/10.1002/bbb.1892

Fernando, E.Y., Keshavarz, T., Kyazze, G and Fonseka, K. (2016). Treatment of colour industry wastewaters with concomitant bioelectricity production in a sequential stacked mono-chamber microbial fuel cells–aerobic system. Environmental Technology, 37, 255-264. https://doi.org/10.1080/09593330.2015.1068378

Naik, S. H, and Jujjavarappu, S. E. (2019). Simultaneous bioelectricity generation from cost-effective MFC and water treatment using various wastewater samples. Environmental Science and Pollution Research, 27, 27383-27393. https://doi.org/10.1007/s11356-019-06221-8

Rossi, R, and Setti. L. (2016). Effect of methylene blue on electron mediated microbial fuel cell by Saccharomyces cerevisiae. Environmental Engineering and Management Journal, 15, 2011-2018. https://doi.org/10.30638/EEMJ.2016.217

Samsudeen, N.M., Radhakrishnan, T.K. Matheswaran, M. (2017). Enhancement of bioelectricity generation from treatment of distillery wastewater using microbial fuel cell. *Environmental Progress and Sustainable energy.* 37(2). DOI: 10.1002/ep.12734

Tan, S., Ong, S., Ho, L., Wong, Y., Thung, W. and Teoh, T. (2020). The reaction of wastewater treatment and power generation of single chamber microbial fuel cell against substrate concentration and anode distributions. *Journal of Environmental Health Science and Engineering*, 18, 793 - 807. https://doi.org/10.1007/s40201-020-00504-w.

Zou, Y.J., Sun, L.X, Xu. F. and Yang L.N. (2007). Escherichia coli Microbial Fuel Cell Using New Methylene Blue as Electron Mediator. Chemical Journal of Chinese Universities. 2007; 2: 510-513.

BIODIESEL PRODUCTION FROM EXTRACTED *GMELINA ARBOREA* SEED OIL VIA DIRECT TRANSESTERIFICATION PROCESS: EFFECT OF METHANOL-TO-OIL RATIO ON YIELD

*Mohammed H.ª; Olanrewaju A. Olalekanª, Sabi'u B.ª, Bello B. Zª.; Muhammad. J. A.ª; Aliyu A.ª

ªDepartment of Chemical Engineering, Ahmadu Bello University, Zaria, Nigeria
*Email of the Corresponding author: deejer07@yahoo.com

ABSTRACT

This study examines the extraction and characterization of gmelina arborea seeds oil and investigated the effect of methanol to oil molar ratios of 3:1, 4:1 and 6:1 on biodiesel yield. The findings suggest that gmelina arborea is a high oil yielding seed (48.922 ± 0.057 wt./wt.%). The physiochemical characterization, GCMS and FTIR studies of the oil confirms that the oil contains predominantly saturated fatty acids (65.50 wt%) suitable for biodiesel production. The findings also shows that increase in methanol to oil molar ratio increases the biodiesel yield to a maximum of 95.76 ± 0.02%, indicating that the oil has great potential for utilization in biodiesel production considering its high oil content.
Keywords: Gmelina Arborea; Nonedible oil; Extraction; transesterification; Biodiesel

1. INTRODUCTION

The consideration of the argument of food versus fuel and or energy as well as the advocacy for renewable source of energy and low cost of production to mitigate concerns about greenhouse gas (GHG) emission on climate change, has led to the focus on nonedible feedstock for biofuels production globally. Biofuels production has risen globally from around 18 billion liters in 2000 to over 160 billion liters in 2021 (Demirbas *et al*., 2016; IEA, 2022). The main liquid biofuels are bioethanol, biodiesel and biolubricant which constitute one of the fastest growing fuels types. Biodiesel is produced from animal fats, waste cooking oils and vegetable oils such as soyabean, rapeseed, sunflower, coconut and palm oils been the most common feedstock (Demirbas, 2015; Demirbas *et al*., 2016; Ferrero *et al*., 2020).

However, economics considerations and the competition of edible oils for fuel production with the demand for food has led to the focus on the utilization of nonedible oils, which are oils that are not suitable and edible for human consumption due to the presence of some toxic constituents (Demirbas *et al*., 2016). Some of the prominent nonedible oils used in biodiesel production are jatropha, castor, neem, rubber, kapok and karanja seeds oil (Chuah *et al*., 2016; Demirbas *et al*., 2016; Ferrero *et al*., 2020). Several other nonedible seed oils such as *Calophyllum inophyllum*, mahua, rice bran, tobacco and yellow oleander seed among others, as well as under-utilised non-edible seed oil like *cassia tora* and *gmelina arborea* seed with high oil content (53 – 54.6 wt.%) are also available and widely grown in several countries (Demirbas *et al*., 2016; Abhishek and Ajay, 2018; Yami *et al*., 2020).

The utilisation of non-edible seed oils for biodiesel production is greatly dependent on its availability and lower cost of cultivation. To this end, availability of non-edible seed oils is a major advantage of its potential for biodiesel production. *Gmelina arborea* seed plantation are widely available in tropical moist forest from India, Burma and Sri Lanka to Southern China and has been widely introduced in Brazil, Gambia, Honduras, Malaysia and several African countries such as Ivory Coast, Malawi, Sierra Leone, Ghana and Nigeria due to the occurrence of desirable climatic features (Ademiluyi and Okeke, 1973; Duke, 2002; Umana *et al*., 2015).

In Nigeria, gmelina arborea seed plantations are widely spread across all the geopolitical regions and is widely available in several states which includes; Abia, Adamawa, Akwa Ibom, Anambra, Benue, Cross River, Delta, Edo, Imo, Kaduna, Katsina, Kogi, Kwara, Lagos, Niger, Ogun, Ondo, Osun, Oyo and Plateau states (Aturamu *et al*., 2021). Several other nonedible seeds oil is also widely spread across the country and their application in different areas have been examined. However, there is scarce study reported on the utilization of oil from *gmelina arborea* seeds, despite wider area of potential applications of these nonedible oils. This study therefore, examine extraction and characterization of *gmelina arborea* seeds oil and its potential as feedstocks for biodiesel production

2. MATERIALS AND METHODS

The major materials used in the course of the study are Gmelina arborea seed, distilled water, n-hexane, potassium hydroxide (KOH), ethanol, methanol and sulphuric acid (H_2SO_4). All chemical used were of analytical grade. Also, gmelina arborea seeds were collected around Kaduna Polytechnic main campus, Tudun Wada, Kaduna State and processed; washed and sun dried, after which it was deshelled and further dried to a constant weight. The dried seeds were mechanically crushed to obtain a particle size of 1 – 2 mm and then stored in a polythene container for further use.

2.1 Oil Extraction

Solvent extraction method was used for the oil extraction process using n-hexane and Soxhlet extractor according to the setup in Figure 1. 40 g of dried and grounded *gmelina arborea* seeds sample (1000 μm) was measured and placed in a porous material, and inserted into the thimble and placed in the inner tube of the Soxhlet apparatus. The apparatus was fitted with a round bottom flask of appropriate size containing 160 mL n-hexane solvent to give a solid-solvent ratio of 0.25 g/mL. The setup was then placed on a heating mantle with reflux condenser which was used to condense the solvent vapour, thus recycling it continuously for 2 hr extraction time. The extracted *gmelina arborea* seeds oil was isolated from the solvent by evaporation using the same Soxhlet extractor but with the leachate removed. The same procedure was repeated severally to obtained sufficient quantity of oil for biodiesel production.
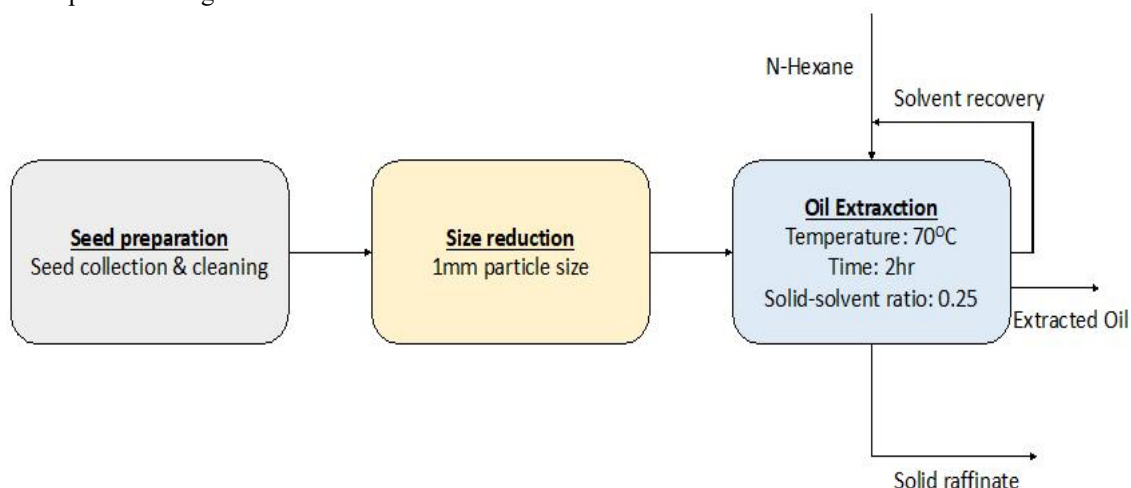
Figure 1 Oil extraction procedure

The extracted oil was placed over water bath at 90 °C for complete evaporation of remnant solvent for about 2 hours. The weights and volume of the oil was recorded and expressed as oil yield in (%) according to Equation 1.

$$Percentage\ Yield = \frac{W}{W_0}\ x\ 100 \qquad (1)$$

where; W = weight of extracted oil per batch (g) and W_o = Weight of sample per batch (g)

2.2 Physico-chemical Characterization of Extracted Oil

The extracted oil was characterized to determine its density, specific gravity etc. as well as chemical properties like saponification value, acid value, free fatty acid, etc.

2.2.1 Density and specific gravity

5 cm^3 of the extracted oil was measured in a pre-weighed measuring cylinder. The weight of the cylinder and oil was measured, and the weight of the oil was obtained by subtracting the weight of the cylinder from the weight of the extracted oil and cylinder. The density and specific gravity of the oil was obtained using the standard by AOCS (2005) as represented in Equations 2 – 4.

$$\rho_{water} = \frac{W_1 - W_0}{V_0} \qquad (2)$$

$$\rho_{oil} = \frac{W_1 - W_0}{V_0} \qquad (3)$$

where; W_1 = weight of empty measuring cylinder + sample (g); W_0 = weight of measuring cylinder (g); V_0 = volume of sample used (mL)

$$Specific\ gravity = \frac{\rho_{oil}}{\rho_{water}} \qquad (4)$$

where; ρ_{water} = density of water (g/mL) and ρ_{oil} = density of oil (g/mL)

2.2.2 Determination of saponification value

2 g of the extracted oil was added to a flask with 30 mL of 4 % ethanolic KOH solution and was then attached to a condenser for 30 minutes to ensure the sample was fully dissolved. After sample has cooled, 1 cm³ of phenolphthalein was added and titrated with 0.5 M HCl until a pink colour disappeared, this is tagged as sample (S). The same procedure was repeated for blank sample test (B). Saponification value was calculated from Equation 5 by AOCS (2005).

$$\text{Saponification value} = \frac{(B-S) \times M \times 56.1}{W} \times 100 \qquad (5)$$

where; S = sample titre value (mL); B = blank titre value (mL); M = molarity of the HCl (mol/dm³) and 56.1 g/mol = molecular weight of KOH, W = weight of oil sample (g)

2.2.3 Determination of acid value

25 cm³ of 99 % ethanol was boiled in a water bath at 90 °C (the heating is to ensure the removal of dissolved gases). 2.5 g of extracted oil was added to 25 cm³ of hot ethanol and the mixture heated again to boil. Few drops of 1 % phenolphthalein indicator were then added and titrated against 0.1 M KOH with constant shaking until a permanent pink colour is obtained. The procedure was repeated again after which the acid value was determined using the expression in Equation 6 by AOCS (2005).

$$\text{Acid value} = \frac{561 \times M \times V}{W(g)} \qquad (6)$$

where; M = Concentration of KOH (mol/dm³); V = Titre value (mL); 56.1 = Molecular weight of KOH
W = weight of oil sample (g)

2.2.4 Determination of free fatty acid

2.0 g of the extracted oil was measured into 250 cm³ Erlenmeyer flask, 100 cm³ of ethanol was added followed by 2 cm³ of phenolphthalein indicator. The mixture was shaken and titrated against 0.1 M NaOH with continuous shaking until a slight pink colour that persisted for 30 seconds was observed. The free fatty acid value was then determined using the expression in Equation 7 by AOCS (2005).

$$\text{Free Fatty Acid} = 0.503 \times \text{Acid Value} \qquad (7)$$

2.2.5 Determination of iodine value

1 g of the extracted oil sample was weighed into a conical flask and 20 cm³ of carbon tetrachloride was added to dissolve the oil. Then 25 cm³ of Wij's reagent was added to the flask using a safety pipette in fume chamber. Stopper was then inserted and the content of the flask was vigorously swirled. The flask was then placed in the dark for 30 min. At the end of this period, 20 cm³ of 10 % aqueous potassium iodide and 125 mL of water were added using a measuring cylinder. The content was titrated with 0.1 M sodium-thiosulphate ($Na_2S_2O_3$) solutions until the yellow colour almost disappeared. Few drops of 1% starch indicator were added and the titration continued by adding thiosulphate in drop wise until the blue colouration disappeared after vigorous shaking (V_S). The same procedure was repeated for blank test (VB). The iodine value is determined using Equation 8 (AOCS, 2005).

$$\text{Iodine value} = \frac{12.69 \times C \times (V_B - V_S)}{W(g)} \qquad (8)$$

where; C = Concentration of sodium-thiosulphate (mol/dm³); V_B = Volume of sodium thiosulphate used for blank (mL); V_S = Volume of sodium thiosulphate used for determination (mL) and W = Weight of the sample (g), 12.69 = conversion factor.

2.2.6 Determination of peroxide value

2.0 g of the extracted oil was added to 22 cm³ of a solution mixture of 12 cm³ chloroform and 10 cm³ acetic acid. 0.5 cm³ of saturated potassium iodide was added to the flask. The flask was corked and allowed to stay with occasional shaking for 1 minute. 30 cm³ of distilled water was then added to the mixture and titrated against 0.1 M of $Na_2S_2O_3$ until yellow colour is almost gone. 0.5 cm³ of starch indicator was quickly added and titration continued until blue colour disappeared. The peroxide value is determined by the expression given in Equation 9 to AOCS standard procedure (AOCS, 2005).

$$\text{Peroxide value} = \frac{S \times N \times 1000}{W(g)} \qquad (9)$$

where; Peroxide value = Meq peroxide per kg of sample; S = volume of titrant sample (cm³); N = molarity of $Na_2S_2O_3$ solution (mol/cm³); 1000 = conversion of units (g/kg) and W = Weight of oil sample (g).

2.3 Transesterification Process for Biodiesel Production

Direct transesterification without the need for esterification was carried out because the FFA value of the extracted *gmelina arborea* seed oil was found to be < 2. 200 g of *gmelina arborea* seeds oil was poured into a conical flask, and 1 wt% oil equivalent of potassium hydroxide (KOH) catalyst alongside the corresponding amount of methanol to oil ratio of 6:1 was mixed in a separate conical flask until the KOH dissolved completely in the methanol. The methanol-KOH solution was then added to the oil (already heated to 60 °C) and the resulting mixture stirred continuously. The mixture was heated at the desired temperature using a hot plate and stirred continuously with temperature maintained at 60 °C for a reaction time of 1 hr. At the end of the reaction time, the methyl ester phase was

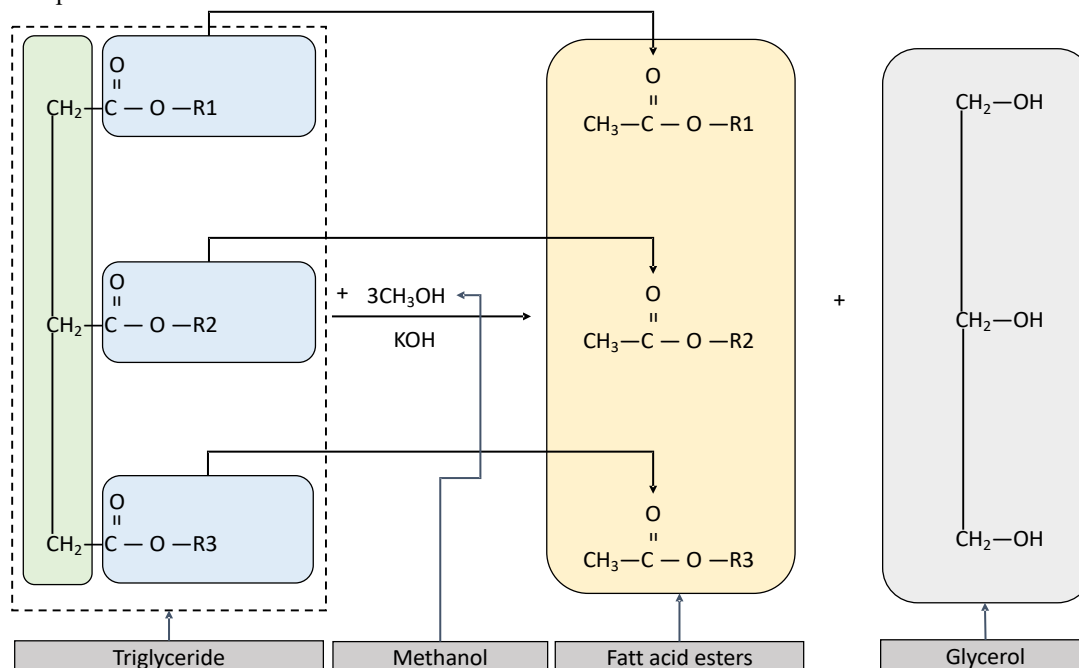separated in a separation funnel until phase separation took place.

Figure 2 Transesterification reaction.

This resulted in the formation of an upper phase consisting of methyl esters and a lower phase containing glycerol. After the separation of the layers by gravity using a separating funnel, the methyl ester phase was further purified by washing with warm water several times until the biodiesel is clear. The washed methyl ester was dried at a temperature of 100 – 120 ℃ for 60 min, and the purified methyl ester was stored for subsequent analysis. The reaction mechanism of the biodiesel production is as shown in Figure 2. The yield of biodiesel produced was determined according to Equation 10.

$$Biodiesel\ Yield\ (\%) = \frac{W}{W_0}\ x\ 100 \qquad (10)$$

where; W = weight of biodiesel produced per batch (g) and W_o = Weight of oil sample per batch (g).

3. RESULTS AND DISCUSSION
The results of oil extraction from gmelina seed and the characteristics of the extracted oil as well as biodiesel yield are presented in this section. Extraction of oil from *gmelina arborea* seed was carried out using n-hexane at a particle size of 1 mm and constant extraction time of 2 hr. The extraction runs were carried out in triplicate and the results of the oil yield presented in Table 1. The oil yield obtained from the extraction process is 48.922 ± 0.057 wt./wt.% at constant extraction time of 2 hr, particle size of 1 mm and solid to solvent ratio of 0.25 using n-hexane solvent. The high oil yield obtained at 1 mm particle size could be attributed to the high surface area of exposure at smaller particle size which increases the number of ruptured cells, resulting in high oil concentration at the particle surface which resulted in high oil yield (Ochi *et al.*, 2019).

The oil yield of 48.922 ± 0.057 wt./wt.% obtained in this study is higher than 35.1 % obtained by Agu *et al.* (2022) at 0.5 mm particle size, 55 ℃ extraction temperature and 150 min extraction time. However, the obtained oil yield in this study is slightly less than 52.09 % and 52.60 % optimum oil yield reported in the literatures at a particle size of 0.15 mm, extraction time of 2 hr and extraction temperature of 60 ℃ respectively (Ogbeide *et al.*, 2018; Ochi *et al.*, 2019). Hence, the high oil yield obtained from Gmelina arborea seed suggested that the seed could be classified as high oil yield seed which signifies great economic value for industrial applications.

3.1 Characterization of Extracted Oil
The extracted oil was characterized to determine it physico-chemical properties (acid value, free fatty acid, iodine value, peroxide value, viscosity, saponification value, moisture content, refractive index and specific gravity) for its utilization. The physico-chemical properties of the extracted *gmelina arborea* seed oil are presented in Table 1. The density and specific gravity of the extracted gmelina seed oil was determined as 0.892 g/ml and 0.896 respectively. The density (0.892 g/ml) obtained for the extracted oil compared favourably with

0.8920 g/cm^3 and 0.8977 g/cm^3 reported by Uzoh *et al.* (2014) and Sanjay *et al.* (2014) for *gmelina arborea* seed oil. However, the specific gravity of 0.938 reported by Agu *et al.* (2022) is slightly higher than 0.896 specific gravity obtained for the extracted oil in this study but comparable to 0.89 reported by (Ochi *et al.*, 2019). The specific gravity obtained is in the range of other common oils and also within the range of 0.860 – 0.900 specified by EN 14214 for oils used for biodiesel production (Ejikeme *et al.*, 2010; Ochi *et al.*, 2019).

Also, the acid and free fatty acid (FFA) value obtained for the extracted gmelina arborea seed oil were 2.805 mgKOH/g and 1.411 mgKOH/g respectively which is lower compared to 5.04 mmKOH/g and 2.52 mgKOH/g (Ochi *et al.*, 2019), and 18.23 mgKOH/g and 9.12 mgKOH/g acid value and FFA value respectively reported by Agu *et al.* (2022). However, the acid and FFA values obtained from this study is slightly higher compared to 1.082 mgKOH/g and 0.541 mgKOH/g acid value and FFA value respectively reported by Sanjay *et al.* (2014) and 0.0336 mgKOH/g and 0.0168 mgKOH/g acid value and FFA value respectively reported by Uzoh *et al.* (2014) for gmelina arborea seed oil. The low acid and FFA value of the extracted oil also suggests low levels of hydrolytic and lipolytic activities in the oils, indicating its good storage quality (Uzoh *et al.*, 2014). This showed that the extracted gmelina arborea seed oil have good storage quality when compared to those of other oil with higher acid values, because, the quantity of FFA in oil is an indicator of its overall quality.

Table 1 Physiochemical properties of extracted gmelina arborea seed oil

Properties	Presen Work	Ochi *et al.* (2019)
Saponification value, mgKOH/g	105.188	108.99
Acid Value, mgKOH/g	2.805	5.04
Free Fatty Acid (FFA), mgKOH/g	1.411	2.52
Iodine value, gI$_2$/100g	30.71	41.05
Peroxide Value, mg/100g	10.00	9.75
Density, 28 °C, g/ml	0.892	–
Specific gravity, 28 °C	0.896	0.89

Equally, the saponification value of the extracted oil was determined as 105.188 mgKOH/g. The saponification value obtained is higher than 32.258 mgKOH/g and 33.00 mgKOH/g reported in the literature (Uzoh *et al.*, 2014; Orakwue, 2017) but slightly lower than 108.99 mgKOH/g reported by Ochi *et al.* (2019) and 190.18 mgKOH/g reported by Agu *et al.* (2022). The saponification value is lower than those of other oil like castor oil (184.6 mgKOH/g), neem oil (198.28 mgKOH/g) and jatropha oil (203.36 ± 0.36 mgKOH/g) (Abdullah *et al.*, 2013; Idongesit, 2018). The low saponification value is an indication of the abundant long chain fatty acids found in the oil, which have a relatively fewer number of carboxylic functional groups per unit mass of the oil as compared to short chain fatty acids. This indicated that the oil is relatively not suitable for use in soap making since its saponification value is lower.

The peroxide value, which is a measure of the deterioration of the oil from oxidation and an indication of the amount of hydroperoxides present in an oil was also determined for the extracted oil. Table 1 shows the peroxide value obtained for gmelina arborea seed oil is 10.00 mg/100g which compared favourably with 9 mg/100g reported by Uzoh *et al.* (2014) and 9.75 mg/100g reported by Ochi *et al.* (2019). The peroxide value of 10.00 mg/100g obtained for the extracted oil is higher than those of common oil like castor oil (5.5 mg/100g) and neem oil (8.7 mg/100g) (Idongesit, 2018). Since oil with peroxide values > 10 mg/100g are regarded unstable while peroxides values < 10 mg/100g indicate that the products are stable against oxidation (Szuhaj, 2016; Duduzile-Buthelezi *et al.*, 2019). The obtained peroxide value of 10.00 mg/100g suggests that gmelina seed oil is relatively stable to oxidative degradation caused by over exposure to oxygen, heating and improper storage, can be kept for a long period of time (Ochi *et al.*, 2019).

Similarly, iodine value which is a measure of the proportion of unsaturated acids present in the extracted oil was determined for the extracted oil. Table 1 show that the iodine value of the extracted oil is 30.71 gI$_2$/100g, which compared favorably with 31.09 gI$_2$/100g reported by Uzoh *et al.* (2014) while the iodine value of 42.72 gI$_2$/100g reported by Agu *et al.* (2022) is higher than that obtained in this study. Also, the value of 30.71 gI$_2$/100g obtained for the extracted oil is lower than those of common oil like castor oil (87.94 gI$_2$/100g), neem oil (65.80 gI$_2$/100g) and jatropha oil (104.9 ± 0.025 gI$_2$/100g) (Abdullah *et al.*, 2013; Idongesit, 2018). Oils with iodine value above 135 are classified as drying oil, those with

iodine value 110 – 130 gI$_2$/100g are classified as semi-drying oil and those with iodine value below 90 are non-drying oils (Aremu *et al.*, 2015; Maliki et al., 2020). The iodine value suggests the oil contained prominently saturated fatty acids; which is not suitable as alkyd resin for paint formulation or use as varnishes; but may find uses in conjunction with amino resins as finishes for certain appliances and as plasticizers.

Overall, the result of the physico-chemical characterization of the extracted gmelina seed oil suggest that the oil is none edible, has good storage quality, relatively not suitable for soap production but suitable for biodiesel production, therefore, it's utilization for biodiesel production will not compete with human need for edible oil as the gmelina seed oil is found to be nonedible

3.1.1 Gas chromatography and mass spectrometry characterization of extracted oil

The GCMS analysis of the extracted gmelina seed oil was carried to determine the component of the extracted oil. The GCMS analysis was used to separate the extracted oil mixtures into individual components and to identify the various components from their mass spectra. Table 2 presents the identified compound in the extracted gmelina seed oil using GCMS analysis. Table 2 shows the compounds identified and their percentage area compared to the total area of chromatogram, which gives an estimate for their relative concentration in the extracted gmelina seed oil. The extracted gmelina seed oil is a complex mixture comprising of 15 identified compounds which contain mainly carboxylic acid.

The fatty acid profile of the extracted oil was compiled along with the retention time obtained from the gas chromatograph of the extracted gmelina seed oil. It was observed from Table 2 that the extracted gmelina seed oil contains fatty acids with chain length distribution ranging from $C_{12} - C_{20}$ which comprises mainly of Saturated Fatty Acids (SFAs) and Unsaturated Fatty Acids (UFAs).

Table 2 GCMS analysis of the extracted gmelina seed oil

Common Name	Chemical Formula	Composition (wt.%)
Myristic Acid	$CH_3(CH_2)_{12}COOH$	10.7081
Palmitic Acid	$CH_3(CH_2)_{14}COOH$	12.3072
Palmitoleic Acid	$C_{15}H_{29}COOH$	0.9684
Oleic Acid	$C_{17}H_{33}COOH$	18.9458
Margaric Acid	$CH_3(CH_2)_{15}COOH$	4.0027
Linoliec Acid	$C_{17}H_{31}COOH$	1.5883

Common Name	Chemical Formula	Composition (wt.%)
Magarolic Acid	$C_{16}H_{31}COOH$	5.1960
Lauric Acid	$CH_3(CH_2)_{10}COOH$	4.9707
Arachidonic Acid	$CH_3(CH_2)_{18}COOH$	4.6644
Tridecanoic acid	$CH_3(CH_2)_{11}COOH$	13.6886
Stearic Acid	$CH_3(CH_2)_{16}COOH$	10.3021
n-hexane	C_6H_{14}	0.3342
α-Linolenic Acid	$C_{17}H_{29}COOH$	4.4128
Gondoic Acid	$C_{19}H_{37}COOH$	3.0594
Pentadecylic Acid	$CH_3(CH_2)_{13}COOH$	4.8513

The GCMS analysis shows that the extracted gmelina seed oil indicates the presence of 6 unsaturated Fatty acids (UFAs) and 8 Saturated Fatty Acids (SFAs) compounds with a single alkane compound (n-hexane). The total distribution of the UFAs constitute 34.17% of the fatty acid content, with palmitoleic acid accounting for 0.97%, 18.95% oleic acid, 1.59% linoliec acid, 5.20% magarolic acid, 4.41% α-linolenic acid and 3.06% gondoic acid while the SFAs distribution constitute 65.50%, comprising of 10.71% myristic acid, 12.31% palmitic acid, 4.00% margaric acid, 4.97% lauric acid, 4.66% arachidonic acid, 13.69% tridecanoic acid, 10.30% stearic acid and 4.85% pentadecylic acid while n-hexane accounted for the remaining distribution of 0.33%. This corroborates the assertion from the results of the iodine value obtained that the extracted oil shows quite a low degree of unsaturated fatty acid and consisting majorly of saturated fatty acids.

It can be seen from Table 2 that oleic acid which is 18.95 % constitutes the highest percentage while palmitoleic acid (0.97%) accounted for the least UFAs whereas, palmitic acid (12.31%) makeup the highest and margaric acid (4%) makeup the least part of the SFAs in the extracted gmelina seed oil. The result obtained from the GCMS analysis corroborated that of the physico-chemical characterization.

3.1.2 Fourier transforms infra-red spectroscopy analysis of the extracted oil

Fourier Transforms Infra-Red (FTIR) spectrophotometer which is a measure of the quantitative and qualitative analysis of the functional group of organic and inorganic samples. The FTIR spectrum for the extracted gmelina seed oil is as shown in Figure 3. From the result of the FTIR obtained, the constituent functional groups of the extracted gmelina seed oil are mainly, carboxylic, carbonyl, aliphatic and hydroxyl functional groups of ester and carboxylic acids.

The prominent absorption peaks identified from Figure 3 are correlated with their respective functional groups vibration modes correlating the absorption bands in the FTIR spectra of the extracted oil. The absorption peaks in the region of 3688.37 cm^{-1} is attributed to O–H bond, 2910.85 – 2847.5 cm^{-1} to C–O–H, 1625.58 – 1137.21 cm^{-1} correspond to C=O and 1073.64 – 992.25 cm^{-1} correspond to C=C bond which are indicative of the distinctive feature of the carboxylate groups (COOH) that are characteristic functional group of fatty acids. Similar band were identified by Uzoh *et al.* (2014) and Ochi *et al.*, (2019) for carboxylate groups.
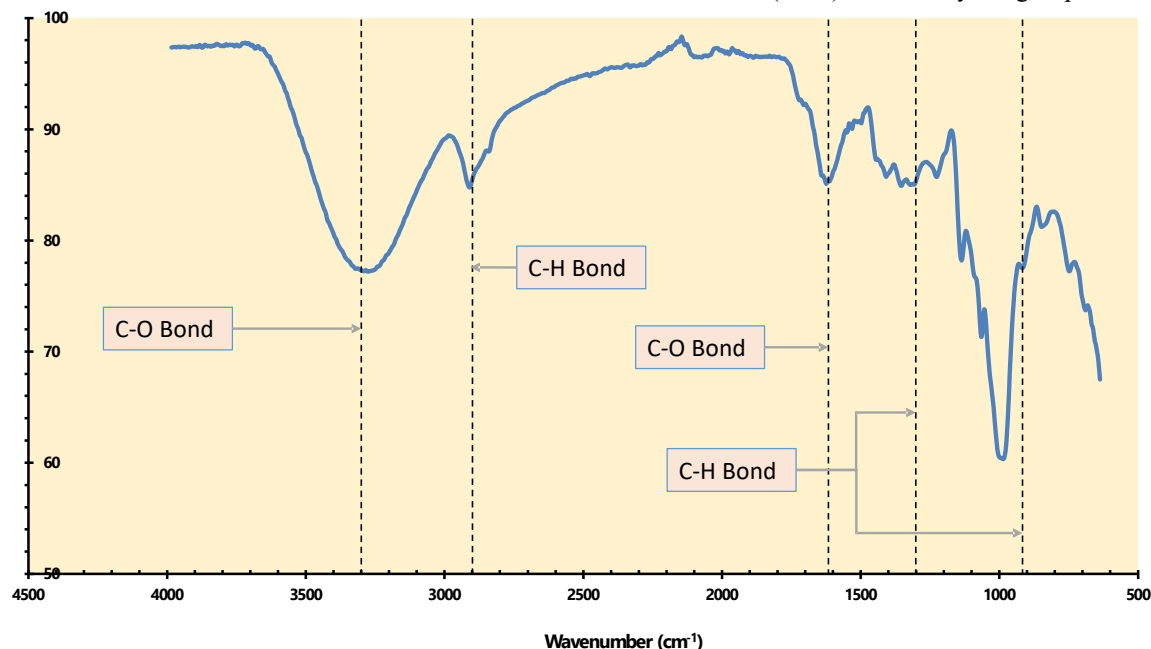

Figure 3 FTIR spectrum of the extracted gmelina seed oil

The absorption peaks in the regions of 1308.54 cm^{-1} and 837.98 – 748.01 cm^{-1} are assigned to the C–H bond which is a characteristic feature of all alkyl group, while that in the region of 2096.12 cm^{-1} is assigned to the C=C bonds which points to the presences of unsaturation within the alkyl chains. The band observed in the region of 3281.39 cm^{-1} and 1625.58 – 1137.21 cm^{-1} are assigned to C = O bonds which also indicates mainly the presence of carbonyl functional group in carboxylic acid and esters in the extracted *gmelina* seed oil (Smith, 2018). It was concluded that the presence of the different functional group of compounds and also the O-H broad peaks are attributed to the interaction of O-H bonding with hydrocarbon contents, indicating the presence of carboxylic acid and ester in the extracted *gmelina* seed oil. The result obtained from the GCMS analysis corroborate the FTIR analysis which further confirms that the constituent functional groups of the extracted *gmelina* seed oil are mainly, aliphatic, carboxylic, carbonyl and hydroxyl functional groups of carboxylic acids and alkanes.

The oil shows quite a low degree of unsaturated fatty acid thus corroborate the physioc-chemical analysis and also confirms that the oil is non-drying oil. Overall, the result of the GCMS and FTIR characterization of the extracted *gmelina* seed oil suggest that the oil contains prominently saturated fatty acids with quite a low degree of unsaturated fatty acids which makes it nonedible but suitable for biodiesel and bio-lubricant production.

3.2 Biodiesel Production

Considering the high oil yield obtained from *gmelina arborea* seed and the established physico-chemical characterization of the oil, biodiesel was produced from the extracted oil at varying methanol to oil ratio and at constant catalyst concentration (1 wt.% oil) and reaction time of 1 hr. Figure 4 presents the biodiesel yield obtained at various methanol-to-oil ratios.
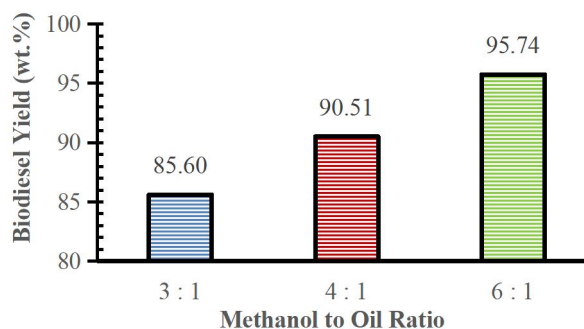

Figure 4 Effect of Methanol to oil molar ration on biodiesel production yield

The effect of alcohol-to-oil molar ratio has been reported to be one of the most important parameters that affect the conversion of vegetable oils to biodiesel, irrespective of the production route and configuration (Rahimi *et al.*, 2014; Tsaoulidis *et al.*, 2023). As can be seen in Figure 4, at constant catalyst concentration (1 wt.% oil) and reaction time (1 hr), biodiesel yield increases from 85.60% to 95.795 with increase in methanol to oil from 3:1 to 6:1 molar ratio.

The highest biodiesel yield of 95.76 ± 0.02 % was obtained at 6:1 methanol to oil ratio in this study, which corroborate with the report of maximum and/or optimum biodiesel yield at 6:1 alcohol- oil molar ratio for different oil feedstock reported in other studies (Louhasakul *et al.*, 2018; Baydir and Aras, 2022). It was reported in these studies that increase in alcohol to oil ratio beyond 6:1 does not have significant effect on biodiesel yield. However, this may or may not be the case in this work, as further studies need to be carried out in the production of biodiesel at higher methanol-to-oil ratio to ascertain this claim. The results showed that increasing methanol to oil molar ratio increases biodiesel yield via transesterification process. Hence, the biodiesel yield obtained from gmelina arborea seed oil is 95.76 ± 0.02 %, indicating that the oil has great potential for utilization in biodiesel production with respect to its high oil content and biodiesel yield.

4. CONCLUSIONS

The study investigated extraction, characterization and biodiesel production from *gmelina arborea* seed oil at methanol *to oil molar ratios of 3:1, 4:1 and 6:1.* The findings suggested that *gmelina arborea* seed is a high oil yielding seed (48.922 ± 0.057 wt./wt.%). The physico-chemical characterization, GCMS and FTIR studies of the oil suggested that the oil contains mainly saturated fatty acids suitable for biodiesel production. The biodiesel production process also shows that increase in methanol to oil molar ratio increases the biodiesel yield to a maximum of 95.76 ± 0.02%, indicating that the oil has great potential for utilization in biodiesel production considering its high oil content

5. REFERENCES

Abdullah, B. M., Yusop, R. M., Salimon, J., Yousif, E. and Salih, N. (2013). Physicochemical Properties Analysis of Jatropha curcas Seed Oil for Industrial Applications. World Academy of Science, Engineering and Technology, 84., 475 – 478.

Abhishek, M. and Ajay, K. S. (2018). Karanja Oil as an Alternative Fuel of Non-Edible oil Blends with Diesel for Four Stroke Single Cylinder Diesel Engine - A Review. *International Journal of Scientific Research in Science, Engineering and Technology (IJSRSET)*, Vol. 4, Issue 4: 239 – 243.

Agu, C. M., Orakwue, C. C., Ani, K. A., Agulanna, A. C. and Dzarma, G. W. (2022). Process Thermodynamic, Kinetics and Statistical Analysis of *Gmelina Arborea* Seed Oil Extraction as Clean Environmentally Friendly Industrial Base-Oil. *Case Studies in Chemical and Environmental Engineering*, 6, 100216.: 1 – 10.

Aremu, M. O., Ibrahim, H. and Bamidele, T. O. (2015). Physicochemical Characteristics of the Oils Extracted from Some Nigerian Plant Foods – A Review. *Chemical and Process Engineering Research*, 32: 36 – 52. www.iiste.org ISSN 2224-7467.

Aturamu, O. A., Alo, A. A. and Ige, P. O. (2021). Development of Silvicultural Management Models for Gmelina arborea Roxb. Stands in Area J4, Omo Forest Reserve, Nigeria, *Forests and Forest Products Jounal*, 21: 1 – 15.

Baydir, E., and Aras, O. (2022). Increasing biodiesel production yield in narrow channel tubular reactors. *Chemical Engineering and Processing: Process Intensification*, 170, 108719.

Chuah, L. F., Yusup, S. and Aziz, A. R. A. (2016). Influence of Fatty Acids Content in Non-Edible Oil for Biodiesel Properties. *Clean Technology and Environmental Policy*, 18: 473–482.

Demirbas, A., Bafail, A., Ahmad, W. and Sheikh, M. (2016). Biodiesel Production from Non-Edible Plant Oils, *Energy Exploration & Exploitation*, Vol. 34(2): 290 – 318.

Demirbas, M. F. (2015). Global Renewable Energy Policy. *Energy Education Science and Technology*, Part D. Vol. 7: 15 – 40.

Duduzile-Buthelezi, N. M., Tesfay, S. Z., Ncama, K. and Magwaza, L. S. (2019). Destructive and non-destructive techniques used for quality evaluation of nuts: A review. *Scientia Horticulturae*, 247, 138–146.

Ferrero, G. O., Faba, E. M. S., Rickert, Adriana, A. and Eimer, G. A. (2020). Alternatives To Rethink Tomorrow: Biodiesel Production from Residual and Non-Edible Oils Using Biocatalyst Technology. *Renewable Energy*, 150 (2020): 128 – 135.

Idongesit, E. S. (2018). Physico-Chemical Properties of Neem Seed Kernel Extract. *International Journal of Advanced Academic Research*, Vol. 4, Issue 10 (October), p. 100 – 109.

IEA (2022). Biofuels Production by Country/Region and Fuel Types, 2016 – 2022. International Energy Agency (IEA), Paris. Retrieved from, www.iea.org/data-and-statistics/charts/biofuel-production-by-country-region-and-fuel-type-2016-2022, accessed 26 March 2022.

Louhasakul, Y., Cheirsilp, B., Maneerat, S., and Prasertsan, P. (2018). Direct transesterification of oleaginous yeast lipids into biodiesel: Development of vigorously stirred tank reactor and process optimization. *Biochemical Engineering Journal*. 137: 232 – 238. doi:10.1016/j.bej.2018.06.009

Maliki, M., Ikhuoria, E. U. and Ifijen, I. H. (2020). Extraction and Physiochemical Characterization of Oils Obtained from Selected Under-Utilized Oil-Bearing Seeds in Nigeria. *ChemSearch Journal*, 11(1): 110 – 117. http://www.ajol.info/index.php/csj

Ochi, D. O., Mahmud, H., Nworie, C. E. and Aliu, S. O. (2019). Extraction, Characterization and Transesterification of Gmelina Arborea Seed Oil Using Clinker as Catalyst. *Nigerian Research Journal of Chemical Sciences*, Vol. 7: 357 – 370.

Ogbeide, S. E., Aniekwe, E. U. and Nwanno, C. E. (2018). Optimization of the Extraction Process of Gmelina Seed Oil using Response Surface Methodology. *Chemistry Research Journal*, 3(5): 94 – 102. www.chemrj.org.

Orakwue, F. C. (2017). Gmelina arborea Seed Oil Characterization, Proximate and Heavy Metal Analyses. *Chemistry Research Journal*, 2(2): 19 – 22

Rahimi, M., Aghel, B., Alitabar, M., Sepahvand, A., and Ghasempour, H. R. (2014). Optimization of biodiesel production from soybean oil in a microreactor. *Energy Conversion and Management*, 79: 599 – 605.

Smith, B. C. (2018). The C=O Bond, Part VIII: Review. *Spectroscopy*, Vol. 33, Issue 11: 24 – 29. https://www.spectroscopyonline.com/view/co-bond-part-viii-review

Szuhaj, B. F. (2016). Phospholipids: Properties and Occurrence. *Encyclopedia of Food and Health*, 360–364.

Tsaoulidis, D., Garciadiego-Ortega, E. and Angeli, P. (2023), Intensified biodiesel production from waste cooking oil and flow pattern evolution in smallscale reactors. *Frontiers in Chemical Engineering*. 5:1144009: 1 – 10. doi: 10.3389/fceng.2023.1144009.Uzoh and Onukwuli, 2014

Uzoh, C. F., Onukwuli, O. D. and Nwabanne, J. T. (2014). Characterization, kinetics and statistical screening analysis of gmelina seed oil extraction process. *Materials, Renewable and Sustainable Energy*, 3(38): 1 – 12. DOI 10.1007/s40243-014-0038-1

AOCS. (2005). Official methods and Recommended Practices of the American Oil Chemists' Society (Version 5th Edition) [Standard]. American Oil Chemists Society.

Yami, A. M., Ibrahim, M. E. and Raji, A. (2020). Utilisation Of Non-Edible Seed Oils as Potential Feedstocks for Biodiesel Production: A Review. *Nigeria Journal of Engineering Science and Technology Research*, Vol. 6, No. 2: 34 – 44.

I-OPTIMAL OPTIMISATION OF ALUMINA LEACHING FROM TERMITE MOUND USING HYDROCHLORIC ACID

Ajani, A. O.[1,2,3], Bello, W. O.[1,2,3], Afolabi, T. J.[1,2,3], Osuolale, F. N.[1], Aworanti, O. A.[1], Oladunni, S. O.[1,2,3], Ojo I. A.[1,2,3], Aremu, M. O.[1], Tijani, I, O.[1,2,3], Adeyi, V. A.[1,2,3], Amole, A.R.[1,2,3], and Alade, A. O.[1,2,3,4]*

[1] *Department of Chemical Engineering, Faculty of Engineering, Ladoke Akintola University of Technology, (LAUTECH), Ogbomoso, Nigeria*
[2] *Bioenvironmental, Water and Engineering Research Group (BWERG), LAUTECH, Ogbomoso, Nigeria*
[3] *LAUTECH SDG 6 Research Cluster (LSDGRC-6), Ladoke Akintola University of Technology, P.M.B. 4000, Ogbomoso, Nigeria*
[4] *Science and Engineering Research Group (SAERG), (LAUTECH), Ogbomoso, Nigeria*
* aoalade@lautech.edu.ng

ABSTRACT

The feasibility of synthesizing metal oxide from abandoned termite mould was investigated in this study. Ededimeji termite mound was pulverized, beneficiated and oven dried at 150 ℃ for 2 h. The optimization of Al_2O_3 leaching from termite clay was carried out using Hydrochloric acid. Some process parameters such as calcination temperature (550-900 ℃) and time (60-240 min), acid concentration (1-3 M), and stirring speed (500-1000 rpm) were considered for alumina leaching based on the I-optimal Design under the Response Surface Methodology of the Design Expert software (12.0.1). X-ray fluorescence was used to determine the chemical composition of the beneficiated clay. Maximum alumina concentration of 28.685 ppm was achieved at 550 ℃, 240 min, 3 M acid concentration and at 1000 rpm. X-ray fluorescence analysis shows that the sample contains 15.84 % alumina. Thus, abandoned termite mould can be used extensively in engineering projects to produce alumina.
Keywords: Alumina, I-optimal, Leaching, Optimization, Termite mound

1. INTRODUCTION

Aluminum (Al) is the third most abundant element on Earth after Oxygen and Silicon. It is also the second most-used metal in the universe after Iron (Nnanwube et al, 2022). Al is a valuable material due to its good physicochemical qualities and ability to make lightweight alloys with various elements, resulting in increased strength and useful properties. Its characteristics allow it to be cast and thermomechanical processed for commercial goods. Metallic aluminum does not exist in nature; it is found in the form of hydrated oxides or silicates (clays). There is increased interest in investigating alternative processes for producing alumina from low-grade ores due to the expanding global demand for this material. It has been determined that a few inexpensive minerals are viable and economically feasible sources of aluminum, which qualifies them for the synthesis of alumina (Al_2O_3). This group includes kaolin, mica, bauxite, sillimanite, fly ash, alunite, and kyanite, among other minerals (Mgbemere and Oluigbo, 2024).

Al_2O_3 is widely employed in advanced technological applications, such as the production of ceramics, refractories, high-strength materials, fireproof polymers, high-quality insulators, semiconductors, microelectronics, and high-grain materials (Lee et al, 2013; Andrews et al, 2014). Bauxite has been the primary raw material utilized in the Bayer process to produce alumina. However, kaolinitic clay has been processed to produce alumina as a substitute for bauxite because bauxite has not been found in Nigeria in commercial amounts (Al-Zahrani and Abdul-Majid, 2009). Alternatively, Al is obtainable in termite mound because of the presence of silicate (SiO_3) and Al_2O_3 (Alemu et al, 2021) through acid leaching which retains silicate but removes alumina for future use (Baba et al, 2020).

The leaching process is widely employed in extractive metallurgy because it is an environmentally acceptable, low-cost method that uses little energy and can handle low-grade ore (Ajemba and Onukwuli, 2012). Acid leaching with sulfuric acid, hydrochloric acid, or nitric acid to extract Al_2O_3 from calcined clay is one of the three methods that are frequently used to extract from clays (Olaremu, 2015; Toama et al, 2018). The process of sulfatization, which involves sintering clay with ammonium sulfate and then leaching the clay with hot water to extract Al_2O_3 is the second and the third is alkali roasting, which involves sintering clay with soda or lime and then leaching the clay with hot water to recover silica and Al_2O_3 (Guo et al, 2014; Zhang et al, 2015). It has been shown that acids are more efficient than bases for extracting Al (Olaremu, 2015). Several studies have been conducted to obtain alumina from various sources, but none has yet been reported on termite mound. Therefore, this work was aimed at optimizing the leaching of Al_2O_3 from termite mound under varied conditions such as calcination time and temperature as well as leachate concentration and stirring speed.

2. MATERIALS AND METHODS

2.1 Materials

The termite mound used for this research work was procured from Ededimeji in Ede, Osun state. Distilled water was used to prepare all aqueous solutions and for beneficiation. The concentrated Hydrochloric acid ($\geq$ 98 %) used as a leachant was of analytical (BDH) grade.

2.2 Methods

2.2.1 Grinding and Beneficiation

The procured raw termite mound was crushed, sieved and taken through beneficiation process to obtain highly pure clay free from organic matter and other micro impurities. The beneficiated termite mound was sun-dried for 5 days and oven-dried at 150℃ for 2 h. It was thereafter milled and sieved through a 425 μm sieve.

2.2.2 Characterization

The basic oxide composition of the Ededimeji termite mound was determined using X-ray Fluorescence (XRF, Shimadzu EDXRF-702HS) at a 1.54 nm wavelength of KαCu anode, X-ray tube voltage of 40 kV and 18 mA.

2.2.3 Optimization process

Optimization was done to know the best calcination temperature and time that will give optimal aluminum leaching using the following process

2.2.3.1 Experimental Design

Calcination temperature and time, leaching acid concentration and stirring rate with minimum and maximum values of 550-900℃, 60-240 mins, 1-3 M and 500-1000 rpm respectively were fed into the Design Expert software. These values were run under the I-optimal Design of the Response Surface Methodology (RSM) in the Design Expert (DOE 12.0.1) software to generate twenty-five experimental runs. The selected response was the Al concentration retained (ppm).

2.2.3.2 Calcination

The beneficiated sample (30 g) was measured into crucibles and charged into the muffle furnace (English Labscience SX-4-10 Model) at various temperatures and times generated by I- Optimal Design of the Design Expert (DOE 12.0.1) and left to cool. The calcination process was done to convert the clay to "*metaclay*" to obtain a more reactive phase of the clay (Tantawy and Alomari, 2019).

2.2.3.3 Leaching studies

Preliminary studies were conducted on calcined clay samples to determine the optimal calcination temperature and time. For every leaching experiment, 5 g of the metaclay from each run was separately mixed with 50 ml of Hydrochloric acid of varied concentrations (1, 2 and 3M) in 100 ml conical flask, as generated by the Optimal Design of the DOE. The mixtures were constantly stirred with a magnetic stirrer at varied speeds (500-1000 rpm) and allowed to react for 1 h at a constant temperature of 80℃. The filtrate was decanted and centrifuged at 1500 rpm for 30 mins. The filtrate was collected for Al analysis using atomic absorption spectroscopy (AAS) "AAS Buck Scientific 211 VGP" and the concentration of Al_2O_3 leached was recorded. (Okwuzu et al, 2022)

3. RESULTS AND DISCUSSION

3.1 Analysis of the Ededimeji termite mound (ETM) composition.

The chemical (basic oxide) composition of the mound as determined by X-ray fluorescence spectroscopy (XRF) is displayed in Table 1. SiO_2, Al_2O_3, MgO, CaO, Fe_2O_3, K_2O, Na_2O, P_2O_5, TiO_2, MnO, NiO, ZnO, CuO, SO_3 are the basic oxide present in the ETM. According to the result, ETM has an extractable content of 15.84%, suggesting that the Al_2O_3 leaching process is feasible. Numerous researches have been done on the chemical composition of termite clay from various geographical locations.

Table 1: Chemical composition of Ededimeji termite mound

Oxide	SiO_2	Al_2O_3	MgO	CaO	Fe_2O_3	K_2O	Na_2O	P_2O_5	TiO_2	MnO	NiO	ZnO	CuO	SO_3	LOI*
%	35.73	**15.84**	3.11	5.08	9.94	4.21	2.70	1.48	1.01	0.51	0.02	0.01	0.03	0.02	20.31

*LOI Loss on Ignition

Table 2 provides a comparison of this study with various literature reports. The XRF reports from various geographical locations showed different Al_2O_3 present in the termite clay. The Al_2O_3 content of Jawaj termite mound soils (JTMSs), Sene termite mound soils (STMSs), Ogbadibo, Otukpo, as reported by (Alemu et al, 2021) and (Idoko and Okieimen, 2020) were greater than 17 % which is better than that obtained from this study. However, the termite mound sample from Ethiopia has Al_2O_3 content of 10.26 % which is less than that obtained in this study (I5.84 %). This might be because of the kind of feed the termites feed on or the geographical locations and the minerals present in the soil.

Table 2: Comparison of the present study with various literature on termite clay

Properties	% Composition								
	SiO_2	Al_2O_3	Fe_2O_3	CaO	MgO	K_2O	Na_2O	MnO	P_2O_5
JTMSs*	63.00	**17.59**	5.34	0.60	1.00	1.14	2.10	0.02	0.04
STMSs*	61.38	**18.48**	5.90	0.66	1.14	1.84	1.14	0.06	0.05
TMS Ethiopia*	60.36	**10.26**	6.18	ND	1.06	2.74	1.68	0.12	0.33
Ogbadibo***	48.04	**17.15**	25.74	0.98	0.81	0.63	0.43	ND	1.00

Otukpo***	44.43	**19.04**	27.12	1.75	0.96	2.45	0.54	ND	0.48
This study	35.73	**15.84**	9.94	5.08	3.11	4.21	2.70	0.51	1.48

* (Alemu et al, 2021), ** (Idoko and Okieimen, 2020) **ND**- Not determined

Additionally, many researchers have also characterized clay with XRF and the alumina contents compared with this study are shown in Table 3. The Al_2O_3 content in
.

clays is very high compared to those in the termite mounds

Table 3: Comparison of the chemical composition of clays with this study

	SiO_2	Al_2O_3	Fe_2O_3
Adamu et al, 2022	55.76	**32.02**	0.03
Bagani et al, 2021	71.18	**20.20**	0.09
Eze et al, 2019	48.57	**27.83**	3.125
Eze et al, 2019	45.64	**29.93**	3.166
Nnanwube and Onukwuli, 2023	55.64	**22.66**	12.65
This study	35.73	**15.84**	9.94

3.2 Model summary for the aluminum leaching from termite mound

The study category used for the experimental design in the leaching of Aluminum from termite clay was I-optimal Design, under Response Surface Methodology (RSM). The factors considered were temperature (A), time (B), acid concentration (C) and stirring rate (D) while the response was Al conc. The first two factors were for calcination while the other two were for leaching. Twenty-five (25) experimental runs were generated. The cubic model showed the least standard deviation of 0.2687 as well as the highest R^2 of 0.9967 and Adjusted R^2 of 0.9209, however, no value was generated for its Predicted R^2. The model with the next lowest standard deviation, highest R^2, Adjusted R^2 and Predicted R^2 was considered. The quadratic model was therefore selected for the response.

3.2.1 Response from Experimental Data

The response at different temperature, time, acid concentration and stirring rate conditions as generated by the software (DOE 12.0.1) is represented in Table 4. The highest Al concentration of 28.685 ppm was obtained at Run 12 (550°C, 240 min, 3 M and 1000 rpm) while the lowest Al concentration of 25.16 ppm was obtained at Run 5 (900°C, 60 min, 1 M and 700 rpm). From the result, the optimal leaching condition of aluminum occurs at Run 12.

Table 4: Results of Response from Experimental Data

	Calcination		Leaching		Response
Runs	**Temperature (°C)**	**Time (min)**	**Acid conc (M)**	**Stirring rate (rpm)**	**Conc of Al (ppm)**
1	900	180	3	1000	26.78
2	700	180	2	1000	26.85
3	900	150	2	600	25.55
4	550	60	1	800	25.73
5	900	60	1	700	25.16
6	550	240	3	500	28.06
7	900	120	2	600	26.12
8	550	120	1	500	25.77
9	900	240	3	900	26.32
10	550	240	1	800	26.24
11	700	120	1	600	26.62
12	550	240	3	1000	28.69
13	900	60	3	500	27.56
14	700	60	1	1000	26.24
15	650	120	2	700	27.77
16	700	150	2	700	27.78
17	800	240	1	800	25.50
18	550	180	1	1000	26.46
19	750	60	2	800	27.39

	Calcination		Leaching		Response
Runs	Temperature (°C)	Time (min)	Acid conc (M)	Stirring rate (rpm)	Conc of Al (ppm)
20	800	240	3	500	26.72
21	550	60	3	800	27.32
22	750	60	2	800	27.01
23	650	240	3	600	27.99
24	800	120	1	700	25.35
25	550	120	2	1000	27.54

Analysis of variance (ANOVA)

The model equation developed is significant with an F-value of 9.38, which suggests a 0.06 % chance of occurrence due to noise as represented in Table 5. In this case, A, C, AB, and A² are significant model terms at P-values less than 0.05. The Lack of Fit F-value of 2.27 implies the Lack of Fit is not significant relative to the pure error. There is a 47.61% chance that a Lack of Fit F-value this large could occur due to noise. The standard deviation, mean, coefficient of variation (C.V), R^2, Adjusted (Adj) R^2, and predicted (pred) R^2 obtained from the analysis were 0.4076, 26.74, 1.52, 0.9242, 0.8180 and 0.2301 respectively. Adequate Precision of 10.918 which is greater than 4 was found to be desirable to navigate the design space. It is also observed from the table that the higher the F-value, the lower the P-value.

Table 5: Analysis of Variance (ANOVA) for the Al Conc

Source	Sum of Squares	Df	Mean Square	F-value	p-value
Model	20.25	14	1.45	8.70	0.0008*
A	6.03	1	6.03	36.27	0.0001*
B	0.3315	1	0.3315	1.99	0.1882
C	8.48	1	8.48	51.05	< 0.0001*
D	0.1092	1	0.1092	0.6569	0.4365
AB	1.01	1	1.01	6.09	0.0333*
AC	0.0315	1	0.0315	0.1893	0.6727
AD	0.0003	1	0.0003	0.0016	0.9684
BC	0.0342	1	0.0342	0.2058	0.6598
BD	0.1526	1	0.1526	0.9182	0.3605
CD	0.0206	1	0.0206	0.1242	0.7319
A²	1.88	1	1.88	11.30	0.0072*
B²	0.0696	1	0.0696	0.4192	0.5319
C²	0.0582	1	0.0582	0.3503	0.5671
D²	0.0217	1	0.0217	0.1308	0.7251
Residual	1.66	10	0.1662		
Lack of Fit	1.59	9	0.1766	2.45	0.4615+
Pure Error	0.0722	1	0.0722		
Cor Total	21.91	24			

*-significant for p<0.05, +- not significant, A= temperature, B=Time, C=Acid Conc, D=Stirring rate

Model Equations Generated

The model equation in terms of the coded factors for the response is given in Eqn 1. The positive factors indicate the favorability of the response while the negative signs show opposition to the increased response (Alade et al, 2012). The coefficients of C, D, AC, AD and BC are positive which means they have a positive influence on the concentration of Aluminum leached. High Acid concentration and stirring rate have a positive impact on the concentration of Aluminum leached. The combined influence of temperature-acid conc, temperature-stirring rate, time-acid concentration and time-stirring rate of 0.0732, 0.0084, 0.0714 and 0.3192 respectively have positive effects on the concentration of Al leached.

$$Al\ conc = +\ 27.37 - 0.7402A - 0.1772B + 1.04C + 0.1174D - 0.4803AB + 0.0732AC + 0.0084AD + 0.0714BC + 0.31BD - 0.0950CD - 0.7430A^2 - 0.1823B^2 - 0.1600C^2 - 0.1033D^2 \quad (1)$$

Diagnostic Case Studies

The stacking and distribution frequencies of the result obtained for the selected response are represented in the diagnostic plots in Fig 1a. The points distribution exists between 2 and 98% which indicates that the results

obtained are well spread within the design space and not lopsided. The diagnostic case studies for the Al concentration show the residuals obtained from the difference between the actual (experiment) value and the predicted (software-generated) value. The positive residual values suggest that the actual value is greater than the predicted value while the negative residual values generated mean that the predicted value is greater than the actual value (Salman, 2014) . The predicted versus actual plots for Al concentration (Fig 1b) show that the closer the points to the normal line the higher the R^2 and vice versa. The plot shows the highest R^2 value of 0.9242 indicating that the experimental and predicted values have a good agreement with just 0.0758 error (Salman, 2014). The relationship between the positive and the negative residuals is presented in Fig 1c. It shows the runs that are outliers and can be removed.
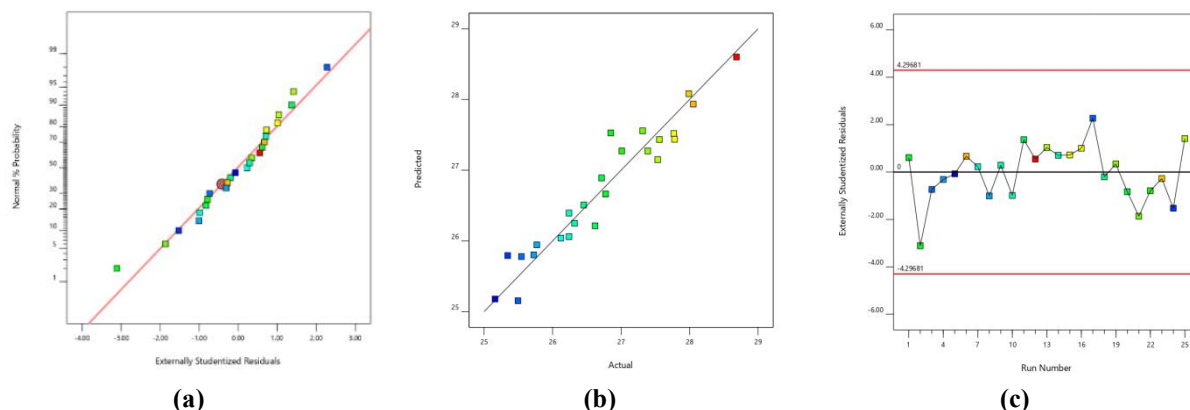

(a)   **(b)**   **(c)**
Figure 1: (a)Normal Plot of Residuals (b) Predicted vs Actual (c) Residuals vs Run

Model Graphs for Al concentration

The model graph shows the relationship existing between the selected factors and the response as illustrated in Figures 2a–c. The curves observed in these figures indicated that the model equations are quadratic although a very nearly linear relationship is shown in the three figures (Alade et al, 2012). A corresponding increase in acid concentration (Table 5) results in an increase in the concentration of Al leached (Fig 2a). Consequently, the positive interaction between the
.

calcinated temperature and the acid concentration indicates that an increase in the two increases the aluminum concentration as shown in Figure 2b. The calcination temperature was eminent at around 800 °C and the acid concentration that gives the optimal result is 3 M. The interaction between the stirring rate and the acid concentration has a positive impact on the leaching of Al. An increase in the acid concentration and the stirring rate increases the Al concentration leached as shown in Figure 2c
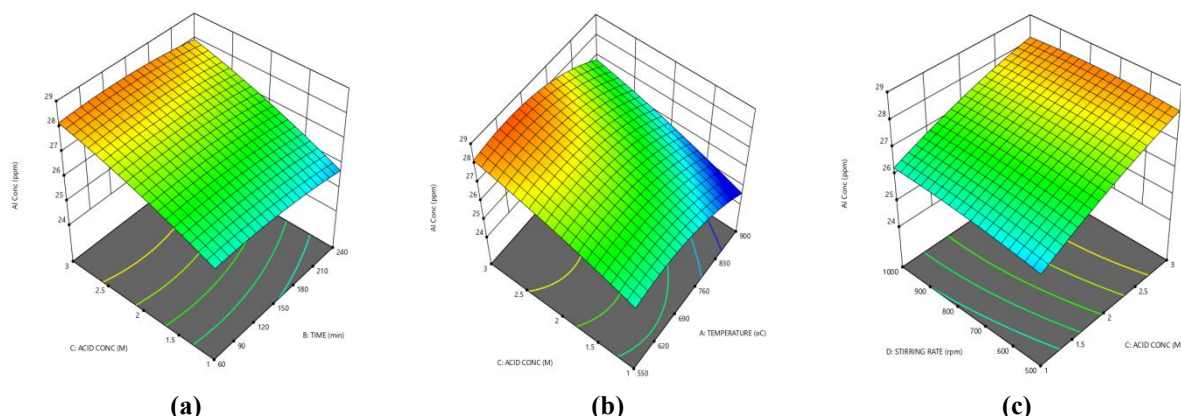

(a)   **(b)**   **(c)**
Fig 3: 3D-plot relating acid concentration and (a) time (b) temperature (c) stirring rate

Process Optimization

The maximum values obtained experimentally were optimized by the software to generate values for the response at the highest possible desirability. The goals for temperature, time and acid concentration and stirring rate were 550, 240, 3 and 1000 respectively, set as 'target', while the response was set as 'maximise'. The optimised value for Al conc was 550 °C, 240 mins, 3M and 1000 rpm at 0.995 desirability.

4. CONCLUSION

Data provided by this study on the thermal treatment of termite mound leachability confirms that termite mound can be a good source of alumina production via an acidic route. The availability of termite mound and the mild conditions needed in the leaching step for the total

dissolution of Al content are sellable advantages. The optimal conditions for the alumina to dissolve in HCl include calcination temperature of 550°C at 240 min with a leaching temperature of 80°C, HCl of 3M concentration and a stirring speed of 1000 rpm. This research establishes that Ededimeji termite mound can be used as the main raw material for Alumina production.

5. ACKNOWLEDGEMENTS

REFERENCES

Adamu, E. K., Nurelegne, T. S., and Belachew, Z. T. (2022). Characterization and Optimization of Calcination Process Parameters for Extraction of Aluminum from Ethiopian Kaolinite. *International Journal of Chemical Engineering, 2022*: 1-18.

Ajemba, R. O., and Onukwuli, O. D. (2012). Determination of the optimum dissolution conditions of Uukpor clay in hydrochloric acid using response surface methodology. *International Journal of Engineering Research Application, 2*(5): 732-742.

Alade, A. O., Amuda, O. S., Ogunleye, O. O., and A, O. A. (2012). Evaluation of interaction of carconization temperatures and concentrations on the adsorption capacities and removal efficiencies of activated carbons using Response Surface Methodology (RSM). *Journal of Bioremediation and Biodegradation, 3*: 1-4.

Alemu, M. L., Tesfaye, G. K., and Fekadu, F. F. (2021). Termite Mound Soils for Sustainable Production of Bricks. *Studia Geotechnica et Mechanica, 43*(2): 142–154. doi:doi:https://doi.org/10.2478/sgem-2021-0006

Al-Zahrani, A. A., and Abdul-Majid, M. H. (2009). Extraction of alumina from local clays by Hydrochloric acid process. *JKAU: Engineering Science, 20*(2): 29-41.

Andrews, A., ElsieNsiah-Baafi, S., Gawu, Y., and Olubambi, P. A. (2014). Synthesis of high alumina refractories from lithomargic clay. *Ceramics International, 40*: 6071-6075.

Baba, A. A., Olowo, V. Y., Raji, M. A., and Akinribido, J. P. (2020). Preparation of Industrial α- Alumina Powder from Ijero Ekiti (Nigeria) Kaolin ore by Acid Leaching Process. *Chemistry Africa*, 1-6. doi:https://doi.org/10.1007/s42250-020-00159-y

Bagani, M., Balomenos, E., and Panias, D. (2021). Exploitation of Kaolin as an Alternative Source in Alumina Production. *materials proceedings, 5*(24): 1-8.

Eze, J. U., Anyakwo, C. S., Osoka, E. C., Nnodum, A. N., Onuoha, C., and Anusi, M. O. (2019). Extraction of Alumina from Local Clays Using Hydrochloric Acid. *International Journal of Scientific Research and Engineering Development, 2*(4): 642-653.

Guo, Y., Yan, K., Cui, L., Cheng, F., and Lou, H. H. (2014). Effect of Na2CO3 additive on the activation of coal gangue for alumina extraction. *International Journal of Mineral Process, 131*: 51-57.

Idoko, O. A., and Okieimen, F. E. (2020). Mineralogy and Geochemical Composition of Termite Mound Soils from Idoma Area of Benue State, Nigeria. *J. Chem Soc. Nigeria, 45*(2): 365 - 377.

Kong, D., Zhou, Z., Song, S., and Jiang, R. (2023). Acid Leaching Extraction Mechanism of Aluminum and Iron Ions from Coal Gangue Based on CaF2 Assistance and Process Optimization. *Materials, 16*(499): 1-14.

Lee, S. J., Kim, H. S., Park, N., Lee, T. J., and Kang, M. (2013). Low-temperature synthesis of alpha alumina from aluminum hydroxide hydrothermally synthesized using [Al(C2O4)x(OH)y] complexes. *Chemical Engineering Journal, 230*: 351-360.

Mgbemere, H. E., and Oluigbo, C. V. (2024). Synthesis of Alumina From Kaolin Found in Ajebo, Ogun State. Nigeria. *ESKİŞEHİR Technical University Journal of Science And Technology A- Applied Sciences and Engineering, 25*(1): 115-122.

Nnanwube, I. A., and Onukwuli, O. D. (2023). Characterization and kinetics of alumina leaching from calcined Akpugo kaolinite for potential aluminum recovery. *South African Journal of Chemical Engineering, 43*: 24-37.

Nnanwube, I. A., Keke, M., and Onukwuli, O. D. (2022). Assessment of Owhe kaolinite potential aluminium source in hydrochloric acid and hydrogen peroxide solutions: kinetics modeling and optimization. *Cleaner Chemical Engineering, 2*(2022): 1-23. doi:https://doi.org/

Okwuzu, F. T., Igwegbe, C. A., Okafor, V. N., Ugwu, J. I., and Obi, C. V. (2022). Kinetics Study of Alumina Leaching from Ogbunike Clay Using Hydrochloric Acid. *European Journal of Sustainable Development Research, 6*(4). doi:https://doi.org/10.21601/ejosdr/12395

Olaremu, A. G. (2015). Sequential leaching for the production of alumina from a Nigerian clay. *International Journal of Engineering Technology Management and Applied Sciences, 3*(7): 2349-2356.

Salman, J. M. (2014). Optimization of preparation conditions for activated carbon from palm oil fronds using response surface methodology on removal of pesticides from aqueous solution. *Arabian Journal of Research, 5*(21): 2939-2944.

Tantawy, M. A., and Alomari, A. A. (2019). Extraction of Alumina from Nawan Kaolin by Acid Leaching. *Oriental Journal of Chemistry, 35*(3): 1013-1021.

Toama, H. Z., Al-Ajeel, A. A., and Jumaah, A. H. (2018). Studying the efficiency of lime-soda sinter process to extract alumina from colored kaolinite ores using factorial technique of design of experiments. *Engineering Technology Journal, 36*(A No 5): 500-508.

Zhang, D., Pan, X., Yu, H., and Zhai, Y. (2015). Mineral transition of calcium aluminate clinker during high-temperature sintering with low-lime dosage. *Journal of Materials Science and Technology, 31*(12): 1244-1250.

PRODUCTION OF BIOPLASTICS FROM CASSAVA AND POTATO PEEL WASTES USING GLYCEROL AND SORBITOL AS PLASTICIZERS WITH CACO3 AS FILLER

*Dawaka A.[1], Nasir. A.S.[2], Mahmud A.[3], Bello B. Z.[4], Muhammad. J. A.[5] and Aliyu A.[6]

Department of Chemical Engineering, Ahmadu Bello University, Zaria, Nigeria
*Email of the Corresponding author: annedawakag@gmail.com

ABSTRACT

This study investigates bioplastic production from agricultural waste, specifically potato (Solanum tuberosum) and cassava (Manihot esculenta) peel starches. Using glycerol and sorbitol as plasticizers and calcium carbonate ($CaCO_3$) as a filler, bioplastic films were produced via solution casting. Various ratios of potato and cassava peel starches were tested for density, water absorption, and tensile strength. Films with 50% cassava and 50% potato starch and sorbitol exhibited the highest density (1.4 ± 0.04 g/cm³), while glycerol-based films had lower density (0.75 ± 0.02 g/cm³). Water absorption tests showed that higher cassava starch content increased water uptake, due to its hydrophilic nature. Tensile strength analysis revealed superior strength in films with high cassava starch content, with 100% cassava and sorbitol films showing 3.8 ± 1.02 MPa. Sorbitol proved more effective than glycerol in enhancing mechanical properties.

 Keywords: Ecofriendly Plastics; Renewable plastics; Waste-to-wealth; Potato Peel; Plasticizer; Filler.

1. INTRODUCTION

Recently, environmental problems caused by petroleum-based plastics have been increasing. Therefore, researchers have begun to investigate new materials that may be alternatives to plastics. Bioplastics are considered as green materials alternatives to plastics and they are produced from renewable resources such as corn and potatoes, or microorganisms under certain conditions (Maulida et al., 2016; Siah et al., 2015). Unlike conventional plastics, which are non-biodegradable and contribute significantly to pollution, bioplastics are designed to degrade naturally, reducing the environmental footprint (Balaseragam, 2018).

Plastic is widely used in daily human activities, especially as food packaging materials, due to its light, flexible, transparent, and durable properties (Joye, 2018). However, the inability of traditional plastics to be recycled or biodegraded naturally has resulted in massive accumulation, causing contamination and degradation of the environment (Maulida et al., 2016; Darni & Utami, 2009). With the production of plastics reaching 270 million tons globally, and an estimated 10-100,000 tons floating on ocean surfaces, the impact on ecosystems and living organisms, including humans, plants, and animals, is profound (Roser, 2018; Balaseragam, 2018).

In response to these challenges, scientists have been developing biodegradable polymers, or bioplastics, as an alternative (Maulida et al., 2016; Avella, 2009). Bioplastics, derived from natural sources like starch, cellulose, chitin, and lignin, are more sustainable and environmentally friendly (Krithika & Ratnamala, 2019). Starch has shown great potential due to its abundance, biodegradability, and suitability for various industrial applications (Ma et al., 2009; Yang et al., 2019). It is a

promising base material for bioplastics, offering the advantage of reducing reliance on non-renewable resources (Joye, 2018).

One of the significant sources of starch is cassava (Manihot esculenta Crantz), a perennial shrub grown throughout the lowland tropics. Nigeria, as the largest

producer of cassava in the world, generates substantial amounts of cassava peel waste (FAO, 2012). Similarly, the food industry generates considerable quantities of potato peel waste (Aro et al., 2010). Traditionally, these wastes have been discarded, leading to environmental pollution and the loss of valuable resources (Ofuya & Obilor, 1993; Olabinduiwu & Odunfa, 2012). By converting cassava and potato peels into bioplastics, not only can we reduce waste, but we can also create value-added products, contributing to a waste-to-wealth initiative (ILRI, 2016).

Potato (Solanum tuberosum) and cassava (Manihot esculenta) starches were selected for this study due to their abundant availability, cost-effectiveness, and beneficial film-forming properties. These starches are derived from agricultural waste (peels), which aligns with the sustainability goals of reducing waste and utilizing renewable resources for bioplastic production.

Potato starch is highly valued for its high amylopectin content, contributing to the flexibility and mechanical strength of bioplastic films. This makes it a strong candidate for low-cost, biodegradable plastics (Patel et al., 2023) . Cassava starch, with its high amylose content, enhances the tensile strength and water absorption capacity of bioplastic films. Its availability in tropical regions and effective biodegradability further support its use (Kaseem et al., 2023).
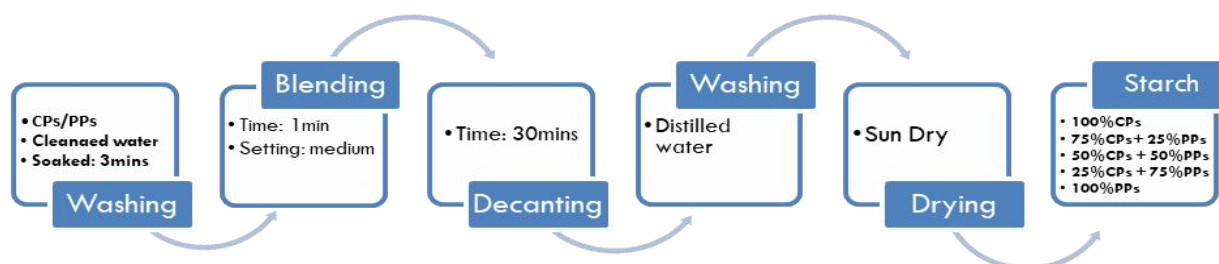
Figure 1 Preparation of starch from cassava and potato peel wastes

This study focuses on the production of bioplastics from cassava and potato peel wastes starch mixtures, using glycerol as a plasticizer and considered how calcium carbonate and hydrochloric acid as fillers affect the tensile strength, density and water absorptivity of bioplastic products. The utilization of these agricultural wastes for bioplastic production aligns with global efforts to find sustainable and eco-friendly materials (Adewuji, 2020).

2. MATERIALS AND METHODS

The major materials used in this study were cassava peels, potato peels, distilled water, glycerol and sorbitol. All chemicals used were of analytical grade. The cassava and potato peels were collected from local farms in Zaria community. The collected cassava and potato peels were washed thoroughly with distilled water to remove any dirt and impurities.

2.1 Isolation of Starch

In this study, starches were extracted from potato peel (Solanum Tuberosum) and cassava (peel wastes after blending for about 1 minute on the medium setting using a kitchen blender (Kenwood BLP15), the liquid was decanted using a sieve cloth, and the starch was allowed to settle to the bottom of the beaker for 30 minutes which a fine powder was produced by removing the starch from the slurry, washing it with distilled water, and then dried under sun which forms a white and brown powdery, flour-like consistency. The powdered peels were stored in airtight polythene containers to prevent moisture absorption and contamination before further processing.

Starch samples extracted from potato peels (PPs) and cassava peels (CPs) were combined in various proportions to produce bioplastic films.

The starch blends were prepared labelled with the following compositions 100%CPs, 75%CPs + 25%PPs, 50%CPs + 50%PPs, 25%CPs + 75%PPs, and 100%PPs.

2.2 Preparation of Starch-Based Films

Two different bioplastic films were produced using the solution casting method, with each formulation mixed with either glycerol or sorbitol as the plasticizer.

Sorbitol-Based Bioplastics:

5g of each starch blend was mixed with 1.6 mL of sorbitol and 1.6 mL of $CaCO_3$ as fillers. The mixture was thoroughly stirred and heated on a heating mantle at 90°C for 15 minutes. The resulting mixture was then poured into petri dishes and spread evenly. The petri dishes were placed in an oven and dried at 60°C for 24 hours. After drying as shown in Fig. 2, the films were allowed to cool to room temperature and were carefully peeled off from the petri dishes.

Glycerol-Based Bioplastics:

In a similar process, 5g of each starch blend was mixed with 1.6 mL of glycerol and 1.6 mL of $CaCO_3$ as fillers. The mixture was heated and stirred under the same conditions as the sorbitol-based films. The mixture was then poured into petri dishes, dried in an oven at 60°C for 24 hours, cooled to room temperature, and carefully peeled off.

2.3 Characterization of Starch-Based Films

The starch-based film was characterized to determine the physical properties of the films such as density, water absorption and tensile strength.

2.3.1 Density

The density of the bioplastic film samples was determined following ASTM D792-91 standards. Samples with approximate dimensions of 1x1 cm² were weighed using a standard chemical digital weighing scale accurate to 0.1 g. The volume of each sample was calculated using the water displacement method, where the sample weight was divided by the calculated volume to obtain the density.

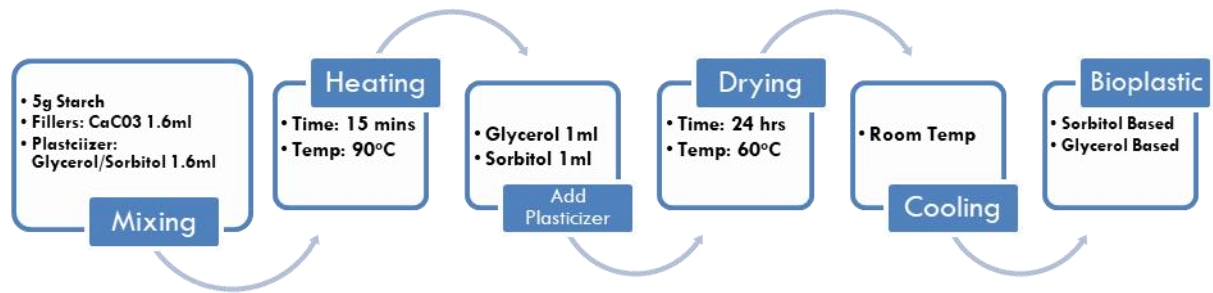$$Density_\rho = \frac{mass\,(g)}{Volume\,(cm3)} \times 100 \qquad Eqn\ 1$$

Figure 2 Preparation of Starch-Based Films

2.3.2 Water Absorption

Water absorption of the bioplastic film samples was evaluated to assess their hydrophilic properties. Samples with an area of approximately 1x1 cm² were initially weighed (M_1). They were then dried at 70°C for 3 hours, cooled to room temperature, and immediately re-weighed to obtain the initial dry weight.

Subsequently, the samples were submerged in distilled water for 3 hours without agitation. After removing from water, the samples were weighed again to determine the final weight (M_2).

The percentage water absorption was calculated using the following formula:

$$W\ abs_w = \frac{Wet\ weight\ t_{w1} - Dry\ weight\ t_{wo}}{Dry\ weight\ t_{wo}}\ X\ 100 \qquad \text{Eqn 2}$$

2.3.3 Tensile Strength

The tensile strength of the bioplastic film samples was measured to evaluate their mechanical properties. Tensile strength is defined as the stress required to break a sample divided by its cross-sectional area (A). It is expressed in MPa (megapascals).

$$Tensile\ Strength\ t_{\partial} = \frac{F}{A}\ (Mpa) \qquad \text{Eqn 3}$$

F = force required to break the sample
A = cross-sectional area of the sample

3. RESULTS AND DISCUSSION

This section presents the outcomes of bioplastic production from potato and cassava peels, focusing on the mechanical properties and water absorption characteristics of the produced bioplastics. The production process involved varying ratios of potato and cassava peels, different plasticizers (sorbitol and glycerol), and CaCO3 filler as detailed in the Materials and Methods section.
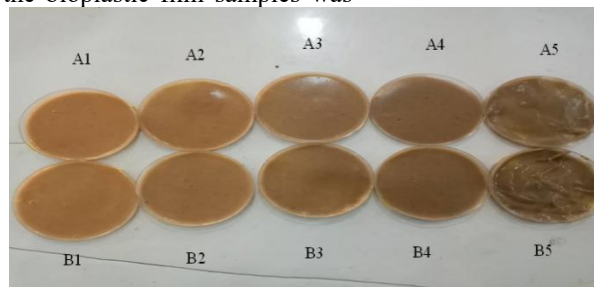

Figure 3 Bioplastic samples from glycerol based and sorbitol based

Samples labeled A1 through A5 consist of 100% CPs, 75% CPs + 25% PPs, 50% CPs + 50% PPs, 25% CPs + 75% PPs, and 100% PPs, respectively, with sorbitol as the plasticizer. Also, samples B1 through B5 are composed of 100% CPs, 75% CPs + 25% PPs, 50% CPs + 50% PPs, 25% CPs + 75% PPs, and 100% PPs, respectively, with glycerol as the plasticizer.

3.1 Density measurement

The effect of potato to cassava peel starch ratio and glycerol and sorbitol as plasticizer on density is shown in Fig.2 below. The highest density was recorded for and 50%CPs + 50%PPs in sorbitol plasticizer, while the film 50%CPs + 50%PPs with glycerol plasticizer was recorded with lowest density. This difference is likely attributed to the swelling of the polymer network due to the plasticizer, which reduces the overall density of the film (Wypych, 2017). Similar observations were reported by Edhirej et al. (2017), who investigated the use of various plasticizers, including glycerol and other compounds, on different starch-based films. Also, Oluwasina et al. (2019) noted an increase in density of cassava starch bioplastic films when oxidized starch was added, which contributed to a denser film structure.
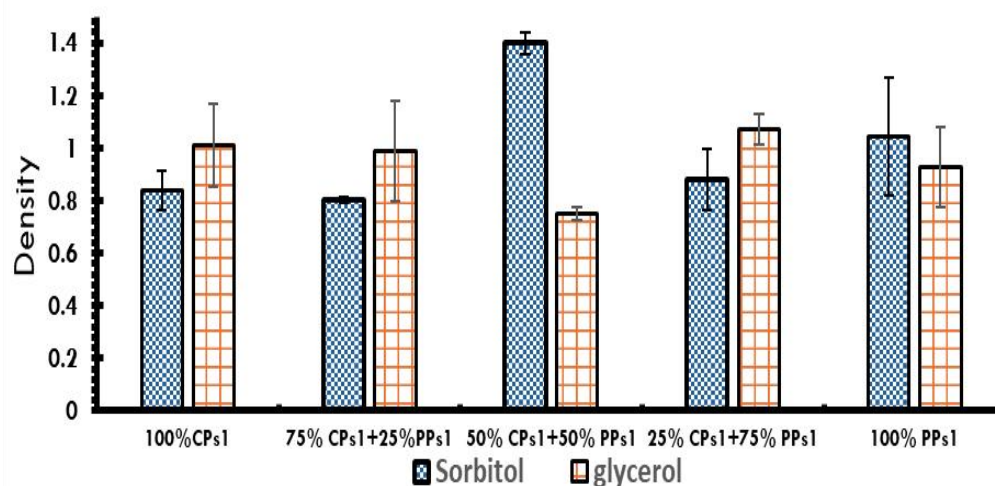
Figure 4 Density of bioplastics formed using variable ratios of potato to cassava peels with sorbitol or glycerol as plasticizer

3.2 Water absorption measurement

The bioplastics (biofilms) produced in this study were immersed in water to verify the effect of filler type and potato to cassava peel starch ratio on the hydrophilic nature of the starch-based films. Water diffuses into the network chains of the films, thus, causing the film to swell. This phenomenon may be due to the abundant active hydroxyl groups of films which were vacant at the initial stage of absorption process. However, the active sites were gradually saturated until they could no longer accommodate any water molecules. This point is referred to as equilibrium state (Sanyang et al., 2015). The water uptake of bioplastic films obtained is shown in Fig. 4. It can be observed that the rate of water absorption increased when the concentration of cassava starch in the bioplastic increased. This is due to the hydrophilic

properties of both glycerol and cassava starch. These properties increased the affinity between glycerol and water, hence increased the water absorption (Suryanto, 2017). The fact that cassava starch contains a hydroxyl (OH), carbonyl (CO), and ester (COOH) shows that the concentration of hydrophilic properties in the bioplastics is higher in films with higher ratio of cassava peel starch than potato peel starch. Moreover, the properties of the CaCO3 that is hydrophobic, causing the sample to repel the water that is why the biofilms made with CaCO3 as a filler absorbed less amount of water than films produced using HCl as filler, similar trend was reported by Maulida et al., (2016) with an improved result. Therefore, the presence of the CaCO3 tends to increase the strength of the bioplastic film.
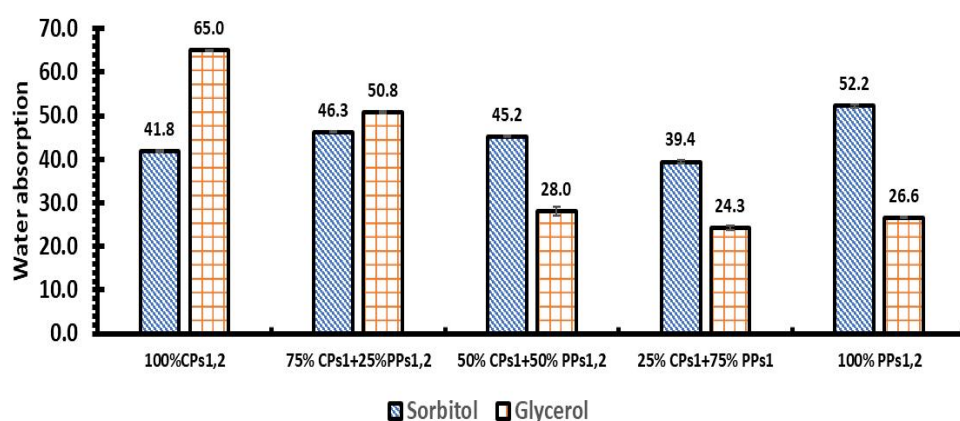

Figure 5: Water absorption of bioplastics formed using variable ratios of potato to cassava peels with sorbitol or glycerol as plasticizer

3.3 Tensile strength

Knowledge of the mechanical properties of films is necessary for their potential use in future applications, for example, in the food packaging industry. Plasticizers significantly affected the tensile strength of the bioplastic samples. The results obtained for maximum tensile strength of the films as presented in Fig. 6, reveals that the starches with high amylose content 100%CPS + 0%PPS for sorbitol plasticizer and 50%CPS + 50%PPS for glycerol plasticizer, lead to more resistant films (higher tensile strength). Crystallinity of the film is also related to its mechanical behavior. 100%CPS + 0%PPS

for sorbitol plasticizer and 50%CPS + 50%PPS for glycerol plasticizer and CaCO3 filler led to more resistant films with tensile strength of 3.8MPa which is an improvement from films reported in literature. Earlier studies on biofilms plasticized with glycerol and sorbitol have revealed comparable results in tensile testing (Ooi et al., 2012; Tapia-Blácido et al., 2013). Glycerol's superior plasticizing effect compared to sorbitol is largely due to its lower molecular mass, which is approximately half that of sorbitol. This smaller molecular size facilitates more effective interactions between glycerol and starch molecules (Shafqat et al., 2021).
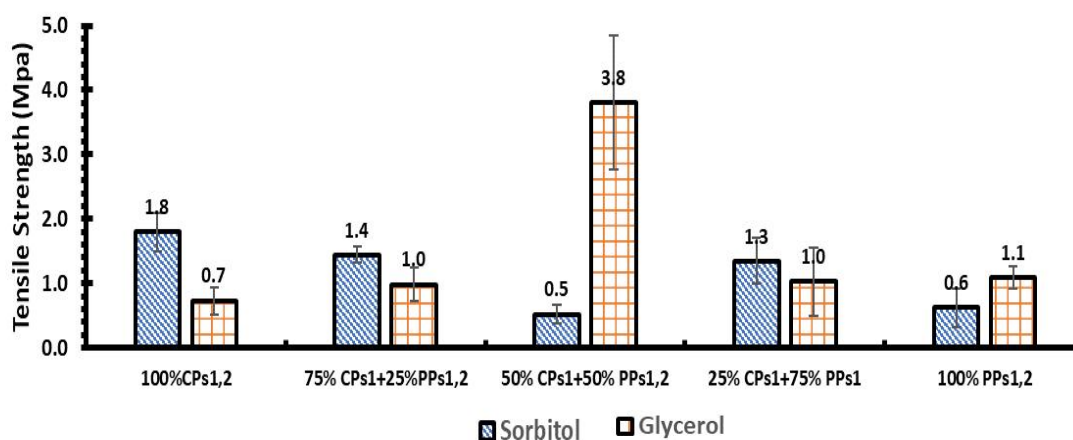

Figure 6 Tensile strength of bioplastics formed using variable ratios of potato to cassava peels with sorbitol or glycerol as plasticizer

Discrepancies observed in the result, such as variations in tensile strength and water absorption rates, can be attributed to multiple factors including the inherent differences in the chemical compositions and properties of cassava and potato starches, as well as the precision in experimental conditions. Additionally, slight deviations in processing conditions, such as temperature and drying times, can also impact the reproducibility of bioplastic properties (Sanyang et al., 2015). Variability in the purity of extracted starch and potential contamination during handling may further contribute to these discrepancies (Yang et al., 2019).

4. CONCLUSIONS

This study investigated the production of bioplastics from potato and cassava peel wastes, focusing on the mechanical properties and water absorption characteristics of the resulting bioplastics. The production process involved varying the ratios of potato peel starch (PPS) to cassava peel starch (CPS), utilizing different plasticizers (sorbitol and glycerol), and incorporating CaCO3 as a filler. The following conclusions were drawn from the results.

- The density measurements indicated that highest density of 1.4 ± 0.04 g/cm^3 was recorded for and 50%CPs + 50%PPs with sorbitol as plasticizer, while the film 50%CPs + 50%PPs with glycerol plasticizer was recorded with lowest density of 0.75 ± 0.02 g/cm^3. This is attributed to the swelling of the polymer network due to the plasticizer.
- Water absorption tests showed that bioplastics with higher CPS content exhibited greater water uptake, due to the hydrophilic properties of cassava starch and glycerol. The equilibrium state of water absorption revealed that bioplastics with CPS had a higher affinity for water.
- Tensile strength analysis demonstrated that bioplastics with 100% CPS + 0% PPS (sorbitol) and 50% CPS + 50% PPS (glycerol), exhibited higher tensile strength 1.8 ± 0.07 Mpa and 3.8 ± 1.02 MPa respectively. Glycerol was found to be a more effective plasticizer than sorbitol due to its lower molecular mass, which enhances interaction with starch molecules. The results align with previous studies, confirming glycerol's superior plasticizing effect.

To fully understand the influence of starch properties on bioplastic films, future research should focus on a comprehensive characterization of the starch obtained from potato and cassava peels. Techniques such as amylose content determination, X-ray diffraction (XRD), X-ray fluorescence (XRF), and Scanning Electron Microscopy (SEM) could provide valuable insights into the crystalline structure, elemental composition, and surface morphology of the starches, which in turn affect the film properties.

5. REFERENCES

Adewuji, A. A. (2020). Sustainable development of biodegradable plastics from agricultural wastes. *Journal of Applied Sciences and Environmental Management*, 24(4), pp. 523-529.

Aro, S. O., Aletor, V. A., Tewe, O. O., & Agunbiade, J. A. (2010). Evaluation of the nutritive value of brewers' dried grains supplemented with or without enzyme and cassava peel meals. *African Journal of Biotechnology*, 9(24), pp. 3574-3577.

Avella, M. & Errico, M. E. (2009). Biodegradable starch/clay nanocomposite films for food packaging applications. *Food Chemistry*, 93(3), pp. 467-474.

Balaseragam, S. (2018). Biodegradable polymers. In T. R. Gardner (Ed.), *Encyclopedia of Polymers and Composites* (pp. 1-16). CRC Press.

Cano, A., Jiménez, A., Cháfer, M., Gónzalez, C., & Chiralt, A. (2014). Effect of amylose: amylopectin ratio and rice bran addition on starch films properties. *Carbohydrate Polymers*, 111, pp. 543-555.

Darni, Y. & Utami, R. (2009). Properties of bioplastic based on cassava starch. *Makara Journal of Technology*, 13(1), pp. 19-24.

Edhirej, A. M., Zaidan, U. H., & Ahmed, S. (2017). Study on the effect of plasticizers on the properties of starch-based films. *Journal of Polymers and the Environment*, 25(4), pp. 1182-1191.

FAO. (2012). *FAOSTAT*. Food and Agriculture Organization of the United Nations. Retrieved from http://www.fao.org/faostat/en/#data/QC

Gin, W. A., Jimoh, A., Abdulkareem, A. S., & Giwa, A. (2014). Utilization of cassava peel waste as a raw material for activated carbon production: Approach to environmental protection in Nigeria. *International Journal of Engineering Research & Technology (ISSN: 2278-0181)*, 3(1), pp. 35-42.

Gin, W. A., Jimoh, A., Abdulkareem, A. S., & Giwa, A. (2014). Kinetics and isotherm study of heavy metals removal from electroplating wastewater using cassava peel activated carbon. *International Journal of Engineering Research & Technology (ISSN: 2278-0181)*, 3(1), pp. 25-34.

ILRI. (2016). *Cassava peel utilization*. International Livestock Research Institute. Retrieved from https://www.ilri.org/research/cassava-peel-utilization

Joye, S. R. (2018). Food packaging permeability behavior: A report. *Critical Reviews in Food Science and Nutrition*, 58(6), pp. 1015-1026.

Kaseem, M., Khedher, N. B., & Khelifa, N. (2023). Cassava starch for sustainable bioplastic production: Properties and environmental benefits. *International Journal of Biopolymer Science*, 45(4), pp. 567-580. https://doi.org/10.1016/j.biopel.2023.56789

Krithika, R. & Ratnamala, S. K. (2019). Recent advances in biodegradable polymers: A review. *Polymers for Advanced Technologies*, 30(9), pp. 2431-2446.

Maulida, S., Hasnunidah, N., & Fajri, R. (2016). The influence of filler on mechanical properties of cassava peel starch bio-plastic. *AIP Conference Proceedings*, 1744(1), pp. 030011.

Ma, X., Chang, P. R., & Yu, J. (2009). Properties of biodegradable thermoplastic pea starch/carboxymethyl cellulose and pea starch/microcrystalline cellulose composites. *Carbohydrate Polymers*, 75(3), pp. 472-478.

Olabinduiwu, I. O., & Odunfa, S. A. (2012). Utilization of cassava flour in baked products. *Journal of Food Processing and Preservation*, 6(2), pp. 121-126.

Oluwasina, O. O., Akinmoladun, T. I., & Akinmoladun, A. S. (2019). Effect of oxidized starch on the density of cassava starch bioplastic films. *International Journal of Biopolymer and Biocomposite*, 21(2), pp. 145-155.

Ooi, C. S., Lim, H. N., & Chai, S. T. (2012). Mechanical properties of biofilms plasticized with glycerol and sorbitol. *Journal of Applied Polymer Science*, 125(2), pp. 1027-1036. https://doi.org/10.1002/app.35578

Patel, M., Sharma, N., & Patel, R. (2023). Potato starch-based bioplastics: Characteristics and applications. *Journal of Renewable Materials*, 11(2), pp. 123-135. https://doi.org/10.1080/21663831.2023.1234567

Roser, M. (2018). *Our World in Data*. Retrieved from https://ourworldindata.org/plastic-pollution

Sanyang, M. L., Sapuan, S. M., Jawaid, M., Ishak, M. R., & Sahari, J. (2015). Effect of plasticizers on the tensile properties of biodegradable films from sugar palm starch. *Polymers*, 7(6), pp. 1106-1124. https://doi.org/10.3390/polym7061106

Shafqat, N., Rehman, S., & Ali, M. (2021). Plasticizing effects of glycerol and sorbitol on starch-based films: A comparative study. *Materials Science and Engineering*, 80(5), pp. 567-576. https://doi.org/10.1016/j.msea.2021.139101

Tapia-Blácido, D. R., Gómez-Guillén, M. C., & Montero, M. P. (2013). Biofilms from starch: Influence of glycerol and sorbitol on mechanical properties. *Carbohydrate Polymers*, 97(1), pp. 155-162. https://doi.org/10.1016/j.carbpol.2013.03.012

Talja, R. A., Peura, M., Serimaa, R., & Jouppila, K. (2008). Effect of amylose content on physical and mechanical properties of potato-starch-based edible films. *Biomacromolecules*, 9(2), pp. 658-663.

Wypych, G. (2017). *Handbook of Plasticizers* (3rd ed.). ChemTec Publishing.

Yang, Y., Xie, H., Zhang, Y., & Liu, E. (2019). Extraction and characterization of starch from potato peel waste. *Food Chemistry*, 297, p. 124963. https://doi.org/10.1016/j.foodchem.2019.12496

CHARACTERIZATION OF CELLULOSE FROM WASTE BAOBAB POD FOR FUTURE UTILIZATION IN WASTEWATER TREATMENTS

Adeyi, V. A.[1,2,3], Agarry, S. E,[1,2,3], Popoola, A.O.[1], Akinwunmi O. D.[1], Afolabi, T. J.[1,2,3], Alagbe, S. O.[1], Olugbodi, H. O.[4], Akinjobi, T. A.[5], Agboola, T.T.[6], Salaudeen, S.[7], Adetoro, R. O.[8], Kehinde, T O.[9] and Alade, A. O.[1,2,3,10*]

[1] Department of Chemical Engineering, Ladoke Akintola University of Technology, P.M.B. 4000, Ogbomoso, Nigeria

[2] Bioenvironmental, Water, and Engineering Research Group (BWERG), Ladoke Akintola University of Technology, P.M.B. 4000, Ogbomoso, Nigeria

[3] LAUTECH SDG 6 Research Cluster (LSDGRC-6), Ladoke Akintola University of Technology, P.M.B. 4000, Ogbomoso, Nigeria

[4] Department of Food Engineering, Faculty of Engineering, Ladoke Akintola University of Technology, (LAUTECH), Ogbomoso, Nigeria

[5] Native Environmental Science Department, Northwest Indian College, 2522 Kwina Road, Bellingham, Washinton, 98226, USA

[6] Department of Agriculture and Bioenvironmental Engineering, Faculty of Engineering and Technology, Oyo State College of Agriculture and Technology, Igboora, Nigeria

[7] Department of Civil Engineering, The Oke-Ogun Polytechnic, Saki, Nigeria

[8] Analytical/Environmental Chemistry Unit Department of Pure and Applied Chemistry, Osun State University, P.M.B. 4494, Osogbo, Nigeria

[9] Department of Civil Engineering, Ladoke Akintola University of Technology, P.M.B. 4000, Ogbomoso, Nigeria

[10] Science and Engineering Research Group (SAERG), Ladoke Akintola University of Technology, Ogbomoso, Nigeria

* Corresponding Author: aoalade@lautech.edu.ng +234 7037885961

ABSTRACT

This study involved the development and the characterization of cellulose from Waste Baobab Pod (WBP) The WBP were collected, washed, air-dried, crushed, milled and screened to a uniform size (40 μm). Cellulose was developed successfully through chemical extraction (alkalization, bleaching and acid hydrolysis). Characterization was done through proximate analysis, ultimate analysis and analytical characterization. The moisture content, ash content and crude fibre were 6%, 8.51% and 24.23% respectively while the carbon-hydrogen, Nitrogen, Sulphur and Oxygen contents were 45.13%, 18.39%, 7.74%, 0.14% and 28.60% respectively. The values obtained from the proximate and ultimate analysis compared favourably with other studies on cellulose. The presence of hydroxyl groups, alkenes, amines, carboxylic groups, alkanes, amides, nitro compounds, ethers, and amines as depicted by FTIR shows that the product produced was cellulose. The production of cellulose from WBP was feasible and portends the WBP as a resourceful agromaterial with potential industrial applications.
Keywords: Baobab, Cellulose, Wastewater.

1. Introduction

Cellulose is a polysaccharide consisting of β (1→4) linked D glucose units which is a natural, nontoxic biodegradable polymer that is of high tensile and compressive strength (Wang *et al*, 2021; Rani *et al*, 2019). It is widely used in pharmaceutical industries, paper industries, food industries, textile industries, cosmetics, and nanotechnology amongst others. It has been used in drug- delivery systems in the treatment of cancer and other diseases (Rani *et al*, 2019). Cellulose is hydrophilic, and non-soluble in many solvents due to its hydrogen bonds and crystallinity. It is also made up of glucose units bound together by various glycosidic linkages and contains hydroxyl (OH) groups (Rahman *et al*, 2018). It is also biocompatible, highly porous, and has a high specific surface area and low density (Nur *et al*

al, 2021). It is obtained from plants, animals, algae, fungi and minerals but is most abundant in plant fibers. Natural plant fibers consist of cellulose, hemicellulose, lignin, extractives and inorganics (Rahman *et al*, 2018). Agricultural wastes, also known as agro waste, such as husks, bagasse, shells, straws, barks, leaves, and pods amongst others have high cellulose contents (Rani *et al*, 2019). It has been observed from the literature that various methods such as chemical, mechanical and chemo-mechanical methods have been used in producing cellulose from different agricultural wastes (Nur *et al*, 2021). (Wang *et al*,2021) used sweet sorghum (whole plant) in the production of bacterial cellulose. It was deduced that the bacterial cellulose produced gave a yield higher than that of the commercial D- glucose. Cellulose was also extracted from khat (*Catha dulis*) waste by (Gabriel *et*

al, 2021). Characterization of the cellulose produced by (Gabriel *et al*, 2021) was done and it was concluded that cellulose can be derived from abundant agricultural sources which can be useful in industrial applications.

The Baobab tree belongs to the Malvacae family. It is a large tree that is as high as 25 m and can be found in the same spot for as long as 100 years. It can produce up to about 673,000 tonnes of fruit in a year (Nedjai *et al*, 2021). The Baobab tree has been found over the years to be very useful ranging from its leaves being used as soaps to its bark which is being used in making ropes. It is also a source of daily economy for many households. The waste generated from the baobab tree while being harvested is its fruit pod (Youssif and Taiseer, 2018). The harvest of the fruits is being done indiscriminately which leads to the indiscriminate discard of its pods basically wherever they are harvested. This means that the pods are discarded anyhow thereby littering the environment nearer to where harvest was or is being done (Nedjai *et al*, 2020). The need for the reuse of the pods into useful products is therefore necessary. This study therefore aims at producing cellulose from baobab and characterization of the cellulose produced.

2. MATERIALS AND METHODS

2.1 Materials

The main material used in this study was Waste Baobab Pod (WBP) while the reagents used were Hydrogen Peroxide, Sodium Hydroxide (NaOH), Glacial Acetic Acid (CH$_3$COOH), Sodium Chlorite (NaClO$_2$), Hydrochloric acid (HCl) and Distilled water. All reagents used were of analytical grade and were used without further purification. Waste Baobab Fruit Pod used was sourced from the Sahara region of the country, specifically, Biliri and Kaltungo Local Governments of Gombe, Gombe State, Nigeria which was transported to and stored at Bioenvironmental, Water and Engineering Research Group (BWERG), L.A. Gbadamosi Chemical Engineering Laboratory, LAUTECH, Ogbomoso.

2.2 Methods

2.2.1 Pre-treatment of WBP

The baobab fruit pod was washed with a brush, distilled water and detergent to remove any external impurities and sun-dried for 72 h. It was then crushed with a milling machine and sieved to get a specific particle size (40 µm) based on the method used by (Kabbashi *et al*, 2017) with slight modifications where necessary. The pre-treated material was then stored in labelled airtight containers to prevent gaining dirt.

2.2.2 Development of Waste Baobab Pod Cellulose

The pretreated WBP was utilized in the production of cellulose. It was soaked in 4% wt. of NaOH in the ratio 1 g: 25 mL for 24 h after which the mixture was agitated with a magnetic stirrer for 2 h at a temperature of 80 °c. The mixture was then washed with distilled water and neutralized using HCl. The neutralized mixture was then soaked in a mixture of acetic acid and sodium chlorite of ratio 1 g:10 mL for another 24 h after which the mixture

was washed with distilled water to a neutral phase and then dried to a constant weight at 50°c. A 30% H$_2$O$_2$ (Hydrogen Peroxide) solution was then prepared and added to the dried material at a ratio of 1 g: 15 mL of the solution. The mixture was left for another 24 h after which it was filtered and washed to a neutral phase. The developed cellulose termed Waste Baobab Pod cellulose (WBPC) was dried in the oven at a temperature of 50°c until constant weight was achieved (González-Delgado *et al*, 2022).

2.2.3 Characterization of WBPC

Proximate analysis, ultimate analysis and analytical characterization were done on the WBPC. This includes moisture content, ash content, Carbon content and oxygen-containing functional groups.

2.2.3.1 Proximate Analysis

2.2.3.1.1 Moisture content procedure

Moisture content was determined using the method adopted by (Remison, *et al*, 2022) with slight modifications. The Petri dish used was washed and oven-dried at 105°C for 30 mins to allow for total dryness of the Petri dishes. The empty petri dish was transferred to a desiccator to cool for about 30 mins to avoid moisture from the air. The dried and cooled petri dish was weighed on an analytical weighing balance and recorded as W$_1$ while 5 g of WBPC was weighed into the cooled petri dish (W$_2$). This was oven-dried at 105 °C for 1 h and transferred into the desiccator to cool down for 30 mins which thereafter was weighed (W$_3$) until constant weight. Moisture content value was calculated according to Equations 1

$$Moisture\ content = \frac{W_2 - W_3}{W_2 - W_1} \times 100 \qquad 1$$

where W_1 (g) is the initial weight of the petri dish, (W_2 g) is the weight of WBPC and petri dish and W_3 (g) is the weight after drying.

2.2.3.1.2 Ash content procedure

Crucibles used were washed and dried in the oven for 30 mins to ensure total dryness which were cooled in the desiccator for another 20 mins. The cooled crucibles were weighed and recorded as W$_1$ on an analytical weighing balance after which 2 g of WBPC was weighed into the cooled crucible (W$_2$). A muffle furnace was heated up before placing W$_2$ into it. The sample (W$_2$) was placed in the muffle furnace at a temperature of 600 °C for 3 hrs. When completely ashed it was put in a desiccator to cool down for 1 h. The sample was weighed until constant weight and recorded as W$_3$ (Remison, *et al*, 2022). The ash content was calculated as Equation 2

$$Ash\ content\ (\%) = \frac{W_3 - W_1}{W_2 - W_1} \times 100 \qquad 2$$

where W_1 (g) is the weight of an empty crucible W_2 (g) is the weight of WBPC and empty crucible and W_3 (g) is the weight after the ash process.

2.2.3.1.3 Crude fiber determination

The crude fibre was determined by adopting the method used by Oguche and Musa, (2022). 3g of WBPC was

mixed with 100 mL of 1.25% sulphuric acid (H_2SO_4) in a clean beaker to be boiled between 30-40 mins while adding water intermittently to achieve constant volume. In the case of excess foaming, 2mL of antifoam solution was added and boiled for another 30 mins while adding water intermittently to maintain a constant volume. It was filtered and washed with hot water to attain a neutral state. The residue was washed into a beaker, and 200 mL of 1.25% Sodium Hydroxide (NaOH) was added to the residue and boiled for 30 mins as done for the acidic process. However, the mixture was then allowed to stay for 5 mins, filtered and washed to maintain a neutral state, the residue was then transferred into an already-weighed crucible. The crucible was transferred into an oven at 100 °C to get dried and cooled in a desiccator. The crucible and content were placed in an already heated furnace to get its fibre content at a temperature of 450 °C for 1 h. The remaining residue (fibre) was weighed after cooling in a desiccator to determine the crude fibre value. Crude fibre content was calculated using Eqn 3

$$Crude\ fibre\ (\%) = \frac{weight\ of\ fibre}{weight\ of\ sample} \times 100 \qquad 3$$

2.2.3.2 Ultimate analysis
This was determined according to American Society for Testing and Materials (ASTM) standards D 3174-76 for agrowaste. The percentage of Carbon, Nitrogen, Hydrogen, Oxygen and Sulphur in the WBPC was reported.

2.2.3.2.1 Determination of Carbon and Hydrogen
The wet Raw Sample WBPC were dried of oxygen in the oven for 1 minute thereby converting the carbon and hydrogen into carbon (IV) oxide (CO2) and water (H2O) respectively. The products of this combustion were passed over weighed tubes of anhydrous calcium chloride ($CaCl_2$) and potassium hydroxide (KOH) which absorb H2O and CO_2 respectively. The increase in weight of the $CaCl_2$ tube represents the weight of water (H_2O) formed while the increase in the weight of KOH in the tube represents the weight of carbon (IV) oxide (CO_2) formed. % of Hydrogen (H) and Carbon (C) in the sample can be calculated as expressed in equations 4 and 5 respectively.

$$\% \ of\ Carbon\ in\ the\ Sample = \frac{12Z}{44X} \times 100 \qquad 4$$

$$\%Hydrogen = \frac{2Y}{18X} \times 100 \qquad 5$$

where X is the weight of the sample taken, Y is the increase in the weight of the $CaCl_2$ tube and Z is the increase in the weight of the KOH tube.

The percentage of carbon in the sample = % of hyd

2.2.3.2.2 Determination of Nitrogen
The Nitrogen estimation in the sample was done by Kjeldahal's method. 1.00g of the prepared Raw Sample WBPC was measured and recorded as W (g). The samples were heated with concentrated H_2SO_4 (tetraoxosulphate (VI) acid) in the presence of K_2SO_4 (Potassium tetraoxosulphate (VI) salt) and $CuSO_4$ (Copper (II) tetraoxosulphate (VI) salt) in a long-necked flask called Kjeldahal's flask thereby converting the nitrogen in the sample into ammonium sulphate. When a clear solution is obtained that is when all the nitrogen present is converted to ammonium sulphate, the solution was treated with 50% NaOH (Sodium hydroxide) solution. The ammonia formed was distilled over and absorbed in a known quantity of standard H_2SO_4 solution. The volume of an unused acid was then determined by titration against a standard solution of NaOH. The amount of acid neutralized by liberated NH_3 from the sample was then evaluated using Equation 6.

$$Titre\ Value\ (V_t)\ cm^3 = V_1 - V_2 \qquad 6$$

where V_1 is the volume of H_2SO_4 neutralized (cm^3) and V_2 the volume of H_2SO_4 neutralized in determination (cm^3). The % Nitrogen was then determined using Equations 7 and 8

$$\% \ of\ Nitrogen\ in\ the\ WBPC = \frac{0.0014 \times 5 \times v_t}{W_{(g)}} \qquad 7$$

where $W_{(g)}$ is the weight of the sample, v_t is the titre value

$$\% \ of\ Nitrogen\ in\ the\ sample = \frac{Volume\ of\ acid\ used \ \times Normality}{Weight\ of\ sample\ taken} \times 1.4 \qquad 8$$

2.2.3.2.3 Determination of Sulphur
Raw Sample WBPC (25 mL) was dissolved and pipette into 50 mL standard flasks followed by 20 mL gelatine $BaCl_2$ solution and made up to 50 mL mark. The solutions were allowed to stand for 30 minutes. The absorbance of the standard solution and the samples were read from the spectrophotometer at 420 nm. The graphs of absorbance against concentration of standards were plotted and sample concentration was evaluated from the graph. The procedure was repeated twice for all samples and the mean values were obtained. Sulphur in the samples was determined using Equation 9

$$\% \ of\ Sulphur\ in\ WBPC = \frac{R \times V \times D_f}{Weight\ of\ sample\ used} \qquad 9$$

where R is the absorbance from the Graph reading, V is the total volume (25 mL) and D_f is the Dilution factor.

2.2.3.2.4 Determination of Hydrogen and Oxygen in the sample
The percentage of hydrogen and oxygen in the sample was obtained indirectly by adding the percentage of total carbon, nitrogen and sulphur together and subtracting from 100 as indicated in Equation 10

$$\% \ Hydrogen\ + \%Oxygen = 100 - (\% \ C + \%N + \%S) \qquad 10$$

where C. N and S were values obtained from Carbon, Nitrogen and S respectively.

2.2.3.3 Analytical characterization
This was done by employing the use of FTIR for deducing the surface chemistry. This was done to further ascertain if the product produced is cellulose.

2.2.3.3.1 Determination of the Surface Chemistry

Fourier Transform Infrared Spectrometer (FTIR) was employed to identify and determine the major chemical functional groups of the surface of WBPC before and after the adsorption process. The method used by (Pinto *et al*, 2022) was used. Sample tablets were prepared by mixing potassium bromide (KBr) with the WBPC at a ratio of 100:1 (by weight). The frequency range used was at a range of 4000 to 400 cm⁻¹ with a resolution of 4 cm⁻¹ for 64 (or 32) scans depending on the type of machine used.

3. RESULTS AND DISCUSSION
3.1 Characterization of cellulose from WBP
This involves proximate (moisture content, ash content, crude fibre), ultimate analysis (Oxygen, Nitrogen, sulphur) and analytical characterization (FTIR).
3.1.1 Moisture content
The moisture content analysis done on WBPC was derived as 6.00 %. This compared favourably with that presented by Youssif and Taiseer, (2018) as 5.35-9.58 % for the CarboxyMethylCellulose (CMC) and 2.66 % for the cellulose of baobab respectively and also with cellulose derived from other agricultural wastes. (Khan

et al, 2020) presented the moisture content of wheat straw and wheat husk cellulose as 10.98 and 10.19 respectively while (Samsalee *et al*, 2023) derived the moisture content from his study on rice straw cellulose as 5.53 % (Table 1). The high moisture content in this study could be due to the increased surface area from the production of the cellulose and also the presence of hydrophilic functional groups (O-H groups) (Samsalee *et al*, 2023). The moisture content derived from this study fell between the range of 5-7 % as required for celluloses (Vora and Shah, 2015).

3.1.2 Ash Content
Ash content obtained from this study was 8.51 %. Ibrahim *et al*, (2013) reported the ash content from rice straw and banana plant waste cellulose as 11.3 % and 6.38 % respectively while (Youssif and Taiseer, 2018) presented the ash content from the baobab cellulose as 0.17%. (Romruen *et al*, (2022) reported the ash content for the cellulose obtained from rice straw, corn corb, phulae pineapple leaves and phulae pineapple peels as 9.96 %, 3.17%, 6.35% and 4.79% respectively. The ash contents derived from WPBC compared relatively with other celluloses as presented in Table 1.

Table 1: Comparison of Proximate analysis

Material	Moisture Content (%)	Ash Content (%)	Crude Fibre (%)	References
Rice straw cellulose	ND	11.3	ND	(Ibrahim *et al*, 2013)
Banana plant waste cellulose	ND	6.38	ND	(Ibrahim *et al*, 2013)
Baobab CMC	5.35-9.58	ND	ND	(Youssif and Taiseer, 2018)
Baobab Cellulose	2.66	0.17	ND	(Youssif and Taiseer, 2018)
Wheat straw	10.98	ND	43.90 %	(Khan *et al*, 2020)
Wheat husk	10.19	ND	25.00 %	(Khan *et al*, 2020)
Rice straw,	ND	9.96	ND	(Romruen *et al*, 2022)
Corn corb,	ND	3.17	ND	(Romruen *et al*, 2022)
Phulae pineapple leaves	ND	6.35	ND	(Romruen *et al*, 2022)
Phulae pineapple peels	ND	4.79	ND	(Romruen *et al*, 2022)
Rice husk	5.53	ND	ND	(Samsalee *et al*, 2023)
WBPC	6.00	8.51	24.23	This study

CMC- Carboxymethyl Cellulose, ND- Not Determined

3.1.3 Crude Fibre
The value obtained from this study was 24.23 % for crude fibre. (Khan *et al*, 2020) deduced that 43.90 % and 25.00 % of crude fibre was present in the wheat straw and wheat husk cellulose respectively. The value obtained from the WBPC was in the same range as that presented by (Khan *et al*, 2020) (Table 1).
3.1.4 Ultimate analysis

The ultimate analysis done on the WBPC to determine the Carbon, Hydrogen Nitrogen, Sulphur and oxygen content were derived as 45.13 %, 18.39 %, 7.74 %, 0.14% and 28.60 % respectively. (Vora and Shah, 2015) deduced that carbon and Hydrogen were present in powdered corn husk cellulose at 42.63 % and 6.59 % (Table 2)

Table 2: Comparison of Ultimate Analysis

Material	Carbon %	Hydrogen %	Nitrogen %	Sulphur %	Oxygen %	References
Corn cob powdered cellulose	42.36	6.59	ND	NI	NI	(Vora and Shah, 2015)
WBPC	45.13	18.39	7.74	0.14	28.60	This study

ND: Not Detected, NI: Not Included

3.1.5 Determination of Surface Chemistry
This involves the use of FTIR for the determination of the functional groups present in the WBPC. The determination of surface chemistry which is the functional groups of the WPBC was done using FTIR.

The spectra obtained from the FTIR for WBPC are presented in Figure 1. The cellulose contains hydroxyl groups, alkenes, amines, carboxylic groups, alkanes, amides, nitro compounds, ethers, and amines (Table 3) which are typical of cellulose (Ibrahim *et al*, 2013). The

peak wavelengths of 3500.46 cm⁻¹ were attained for the hydroxyl group with a transmittance of 36.73 % for the O-H stretching vibration of phenolic hydroxyl, 2998.95 cm⁻¹ was the wavelength of the alkanes functional group at a transmittance of 52.80 % with a C-H stretching vibration, 1901.74 cm⁻¹ peak wavelength with 64.12 % transmittance was received for the C=N stretching vibrations of the amines group while the carboxylic group had a C=O stretching vibration at 48.15% transmittance at a peak wavelength of 1700.65 cm⁻¹. Alkenes functional group for run 5 had a wavelength of 1582.90 cm⁻¹ at 56.34 % transmittance with a C=C stretching vibration, and the amide functional group had a wavelength of 1521.67 cm⁻¹ at a transmittance of 56.34 % with a N=H stretching vibration, the peak value of run 7 was 1446.38 cm⁻¹ which was a hydroxyl group at a transmittance of 56.41 % having In-plane O-H bending and C-O stretch of dimmers, the peak value of run 8 was 1350 cm⁻¹ for alkanes at a transmittance of 48.20 % having CH₃ deformation vibrations while the Nitro compounds group had their peak wavelength at 1248.95 cm⁻¹ at a transmittance of 48.23 % for –NO₂ stretching vibrations of aromatic nitro compounds. The peak value of run 10 was 1127.34 cm⁻¹ for ethers at a transmittance of 40.17 % for C-O stretching vibrations, 992.49 cm⁻¹ peak value was obtained for Amines at a transmittance of 75.02 % for –C-NH₃ stretching vibration of primary aliphatic amines while the peak value of 800.62 cm⁻¹ was attained for alkanes in run 12 at a transmittance of 76.13 % for CH out of plane deformation vibrations. The peak values obtained from the Spectra of Figure 1 were like those obtained by (Youssif and Taiseer, 2018) and (Isah *et al*, 2023).
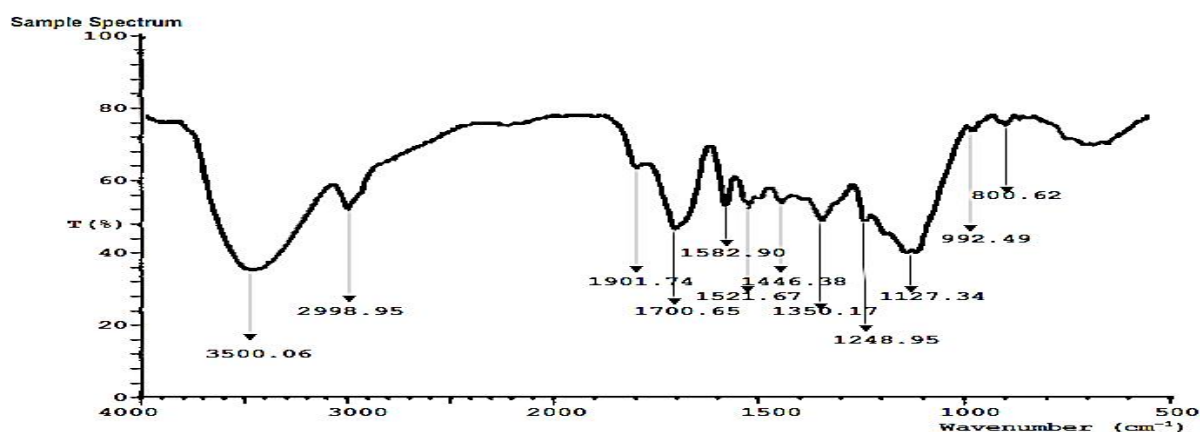

Figure 1: FTIR of WBPC

Table 3 WBPC functional groups

Peak Wavelength (cm⁻¹)	Transmittance (%)	Assignment	Functional group
3500.46	36.73	O–H stretching vibration of phenolic hydroxyl	Hydroxyl group
2998.95	52.80	C–H stretching vibration	Alkanes
1901.74	64.12	C=N stretching vibration	Amines
1700.65	48.15	C=O stretching vibration	Carboxylic
1582.90	56.34	C=C Stretching vibration	Alkenes
1521.67	56,38	N-H stretching vibration	Amide
1446.38	56.41	In-plane OH bending and C–O stretch of dimmers	Hydroxyl
1350.17	48.20	CH₃ deformation vibrations	Alkanes
1248.95	48.23	-NO₂-stretching vibrations of aromatic nitro compounds	Nitro compounds
1127.34	40.17	C–O stretching vibration	Ethers
992.49	75.02	- C- NH₃stretching vibration of primary aliphatic amines	Amines
800.62	76.13	CH out- of- plane deformation vibrations	Alkanes

4. CONCLUSION

The characterization of the WBPC was achieved and it can be concluded based on the results and comparison with other related studies that the product obtained from this study was cellulose.

5. ACKNOWLEDGEMENT

REFERENCES

Gabriel, T., Wondu, K. and Dilebo, J. (2021). Valorization of Khat (Catha Edulis) Waste for the Production of Cellulose Fibers and Nanocrystals. *PLOS ONE, 16*(2): 1-20.

González-Delgado, A.D., Villabona-Ortíz, A. and Tejada-Tovar, C. (2022). Evaluation of Three Biomaterials from Coconut Mesocarp for Use in Water Treatments Polluted with an Anionic Dye. *Water, 14*(408): 1-15.

Ibrahim, M.M., El-Zawawy, W.K., Juttke, Y., Koschella, A and Heinze, T. (2013). Cellulose and Microcrystalline Cellulose from Rice Straw and Banana Plant Waste: Preparation and Characterization. *Cellulose, 20*: 2403-2416.

Isah, I.A., Sani, A.M. and Kusfa, A.A. (2023). Isolation and Characterization of Cellulose Nanocrystals from Baobab Pod Fibres using Acid Hydrolysis. *Nigerian Journal of Science and Engineering Infrastructure, 1*(1): 134-143.

Kabbashi, N.A., Mirghani, M.E.S., Alam Md. Z, Qudsieh, S.Y and Bello, I.A. (2017). Characterization of the Baobab fruit shells as adsorption material. *International Food Research Journal, 24*(Suppl), S472-S474.

Khan, J., Asad, M.J., Mahmood, R.T., Wattoo, F.H., Zainab, T., Nazir, S., Shah, M.B. and Ahmed, D. (2020). Proximate Analysis of Lignocellulosic Biomass and its Utilization for Production, Purification and Characterization of Ligninolytic Enzymes by Aspergillus flavus. *Archives of Environmental Protection, 46*(1): 3–13.

Nedjai, R., Kabbashi, N.A., Alkhatib, M.F.R. and Alam, M.Z. (2020). Removal of Phenol from Aqueous Solution by Adsorption onto Baobab Fruit Shell Activated Carbon: Equilibrium and Kinetics Studies. *Journal of Environmental Treatment Techniques, 9*(3): 686-697.

Nedjai, R., Kabbashi, N.A., Alam, M.Z. and Al-Khatib, M.F.R. (2021). Statistical Optimization of Adsorption Processes for the Removal of Phenol by Activated Carbon Derived from Baobab Fruit Shell. *IOP Conference Series: Materials Science and Engineering. 1192*, pp. 1-7. Bristol: IOP Publishing.

Nur, A.A., Mohd, S.A.R., Masita, M., Muhammad, H.S., Nilofar, A., Zahira, Y., Halim R. and Zeynab, E. (2021). Nanocellulose from Agricultural Waste as an Emerging Nanotechnology Material for Nanotechnology Applications – An Overview. *POLIMERY, 66*(3): 157-168.

Oguche, S.O. and Musa, P.J. (2022). Comparative Proximate Analysis of Three Species of Tiger Nut (Cyperus esculentus) in Idah, Kogi State, Nigeria. *International Journal of Scientific Research in Multidisciplinary Studies, 8*(7): 31-35.

Pinto, L. A., Dotto, G. L., & Piccin, J. S. (2011). Adsorption Isotherms and Thermochemical Data of FD & C Red N° 40 Binding by Chitosan. *Brazilian Journal of Chemical Engineering, 28*(2): 295-304.

Rahman, N.S.A., Yhaya, M.F., Azahari, B. and Ismail, W.R. (2018). Utilisation of Natural Cellulose Fibres in Wastewater Treatment. *Cellulose, 25*(9): 4887-4903.

Rani, R., Singh, A. and Ahmad, W. (2019). Synthesis of Agro Waste Nano Composites Using Coconut and Rice Husk for Adsorption of Chromium Ions. *International Journal of Health and Clinical Research, 2*(11): 1-4.

Remison, A., Odion-Owase, O. A. and Egielewa, S. (2022). Proximate Analysis of Yeast Fermented Oil Palm SAP. *Direct Research Journal of Biology and Biotechnology, 8*(1): 7-12.

Romruen, O., Karbowiak, T., Tongdeesoontorn, W., Shiekh, K.A. and Rawdkuen, S. (2022). Extraction and Characterization of Cellulose from Agricultural By-Products of Chiang Rai Province, Thailand. *Polymers, 14*(9): 1-13.

Samsalee, N., Meerasri, J and Sothornvit, R. (2023). Rice Husk Nanocellulose: Extraction by High-Pressure Homogenization, Chemical Treatments and Characterization. *Carbohydrate Polymer Technologies and Applications, 6*: 1-10.

Vora, R.S. and Shah, Y.D. (2015). Production of Micro Crystalline Cellulose from Corn Husk and Its Evaluation as Pharmaceutical Excipient. *International Journal of Research and Scientific Innovation, 2*(11): 69-74.

Wang, Q., Nnanna, P.C., Shen, F., Huang, M., Tian, D., Hu, J., Zeng, Y., Yang, G. and Deng, S. (2021). Full utilization of Sweet Sorghum for Bacterial Cellulose Production: A Concept of Material Crop. *Industrial Crops and Products, 162*: 1-8.

Youssif, A.A.A and Taiseer, H.M. (2018). Synthesis and Characteristic of Carboxymethyl Cellulose from Baobab (Adansonia Digitata L.) Fruit Shell. *International Journal of Engineering and Applied Sciences (IJEAS), 5*(12): 1-10.

CIRCULAR ECONOMY IN FAECAL SLUDGE MANAGEMENT (FSM); CASE STUDIES OF SPECIFIC LOW-INCOME AREAS

Yusuf Oladimeji Majolagbe (PMP)[1], Ismail Olawale Saheed[1], Ibrahim Kolawole Muritala[2], Samson Kolawole Fasogbon[1].

[1]*Mechanical Engineering Department, University of Ibadan, Ibadan, Nigeria.*
[2]*Research & Innovation Department, Afridat Research and Innovation GmbH, Duisburg, Germany*
*Correspondence E-mail: yusufmab@yahoo.com

ABSTRACT

Faecal sludge (FS) is the semi-solid waste from onsite sanitation systems like pit latrines and septic tanks, composed of feces, urine, and household wastewater. Effective Faecal Sludge Management (FSM) is critical in low-income areas to prevent environmental and health hazards. This review assesses FSM in selected low-income areas, focusing on stages of the sanitation service chain, with the goal of proposing policy improvements and optimizations for a circular economy. Through a comprehensive literature review and case studies, global best practices in FSM were examined, particularly in emptying and transport stages, alongside institutional and social challenges. The findings highlight the need for FSM to receive equal attention as collective sanitation, and that no one-size-fits-all solution exists for all cities. Adopting a circular economy can transform FSM from a waste disposal issue into an opportunity for resource recovery, improving both environmental sustainability and public health outcomes.

KEYWORDS:
Faecal Sludge Management; Onsite Sanitation; Circular conomy; Septage Treatment; Low-income Areas.

1.0 INTRODUCTION

1.1 Faecal Sludge Management

Faecal sludge (FS) is defined as "the solid or semi-solid mixture of human excreta and water that is generated through the use of on-site sanitation facilities, such as pit latrines and septic tanks, which has not been transported through a sewer system" (World Health Organization, 2022). "Faecal sludge is the heterogeneous mixture of human excreta, water, and solids generated from on-site sanitation systems, including pit latrines, septic tanks, and dry toilets, and can range in consistency from a liquid slurry to a semi-solid or solid material."Strande et al. (2020). It is excreta (faeces and urine) as well as anything else that goes into the on-site containment technology, which could include anything from flush water, and cleansing materials, to menstrual hygiene products.

1.2 Faecal Sludge Management Practices

The circular economy is a holistic system approach that looks to create a closed loop of material flows, where waste is minimized, and products and materials are kept in use as long as possible (Elegbede et al 2023). Hence, the global best practice in FS is to ensure resource recovery for environmental and financial sustainability. On-site sanitation systems (OSS) are used in many communities in developing countries in place of a sewerage system due to their cost.

2.0 Faecal Sludge Management Scenario and Sanitation in Low-Income Areas

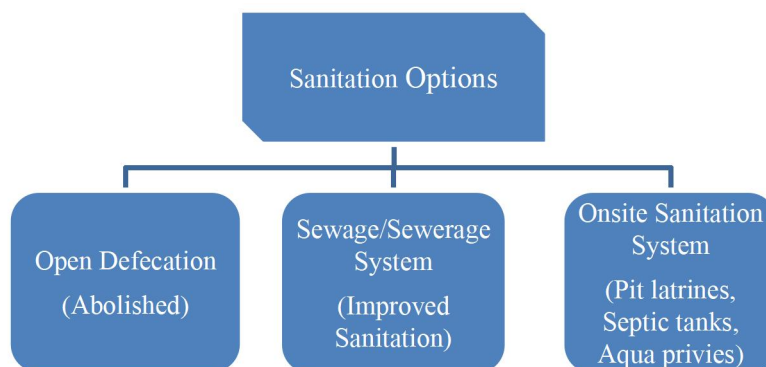The low-income areas to be used in this review work are listed in the table below.

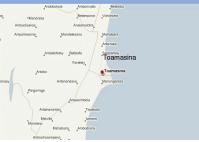**Figure 1: Sanitation Options**

Table 1: Comparison of different details with respect to sanitation, septage, sewerage and their treatment methods.

AREAS	NIGERIA Lagos	INDIA Devanhalli	BURKINA FASO Ouagadougou	MADAGASCAR Taomasina	GHANA Kumasi	INDONESIA Jambi
Population (2024)	229.6m	1.44b	24.3m	31.4m	34.2m	280m
Urban Population	111.5m	493.2m	6.72m	11.15m	18.40m	158.32m
% Access to on-site sanitation	85%	70%	88%	97%	30%	88%
% Septage Treatment	20%	20%	5.6%	38%	10%	7.3%
% Sewerage Treatment	10%	30%	2%	3%	4%	2%
% Access to Improved Sanitation	26.5%	14%	12%	34%	14%	59%
Treatment method	Chemical Stabilization modular type Septage Pre-treatment Unit.	Solid-liquid separation, stabilization, dewatering of sludge, and pathogen removal.	Faecal sludge treatment plants are equipped with drying beds to separate liquids and solids and ponds to treat liquids.	humification beds (sludge handling).	Anaerobic Digestion followed by drying and composting	Solid Separation unit, Waste Pond Stabilisation.

2.1 Faecal Sludge Management (FSM) scenario in Lagos, Nigeria

Lagos over the years has witnessed geometric growth in its population; this ever-increasing population has posed a greater challenge to infrastructural development. The non-availability of the required infrastructure has turned the supposed megacity into a slum. This infrastructural deficiency in Wastewater Management has led to the indiscriminate discharge of raw Septage (Septic Liquor) into the drain, water body, and the environment at large. According to the Inaugural Speech for a second term by His Excellency Governor, Babatunde Raji Fashola "... the expansion of access to potable water supply, and wastewater and sewage treatment will be at the forefront of our development and budgeting initiatives". In Lagos State, there is no doubt that the wastewater sector has been growing very quickly over the past Fifteen years. Lagos currently has Five Septage handling stations (SHS), **Namely: Abesan SHS, Odo Iya Alaro SHS, Oregun SHS, Tolu SHS and Lekki SHS. Amuwo Odofin SHS and Iddo SHS** are currently not in use.

2.2 Faecal Sludge Management (FSM) scenario in India

If sanitation is to be managed safely, it is important to go beyond the toilet and examine containment, emptying, transport, treatment, and reuse or disposal of Faecal waste. FSM is central to achieving the vision of an 'Open Defecation Free' India. Developing solutions to challenges of FSM, therefore, has an important place in the sanitation story of the country

2.3 Faecal Sludge Management (FSM) scenario in Ouagadougou, Burkina Faso

Ouagadougou is the capital city of Burkina Faso and is situated in the sahelo-Soudanese region of Africa. Most of the the country's population (88%) utilize on-site sanitation systems that produce large amounts of FS, making the population vulnerable to water-borne diseases (Bassan et al., 2013).

2.4 Faecal Sludge Management (FSM) scenario in

Taomasina, Madagascar

Toamasina is the second largest city in Madagascar with an estimated population of 300,000. Sanitation without a sewer system is predominant: 97% of households use latrines (38% septic tanks, 62% single pits). 97% of the sludge was manually and unhygienically drained by informal operators to be buried in the yards

2.5 Faecal Sludge Management (FSM) scenario in Kumasi, Ghana

Kumasi is the fastest developing city in Ghana and is the second largest city in the country, with an estimated population of 2.4 million (WaterAid, 2016). Faecal Sludge Management (FSM) in Kumasi, Ghana, faces significant challenges due to inadequate sanitation infrastructure, limited treatment and disposal, insufficient funding, and lack of regulations and enforcement, resulting in environmental and health risks

(World Bank, 2020).

2.6 Faecal Sludge Management (FSM) scenario in Jambi, Indonesia

Most premises in Jambi (89%) have an on-site sanitation system the inhabitants consider a septic tank, which means that 11% of the households in the survey area still have no toilets.

2.7 Generic or Adapted Low-Income Area Sanitation Value Chain

57% of the global population uses safely managed sanitation services, which includes sewer connections and improved on-site sanitation systems. However, only **39%** of people are connected to sewers, which remains consistent with previous estimates.
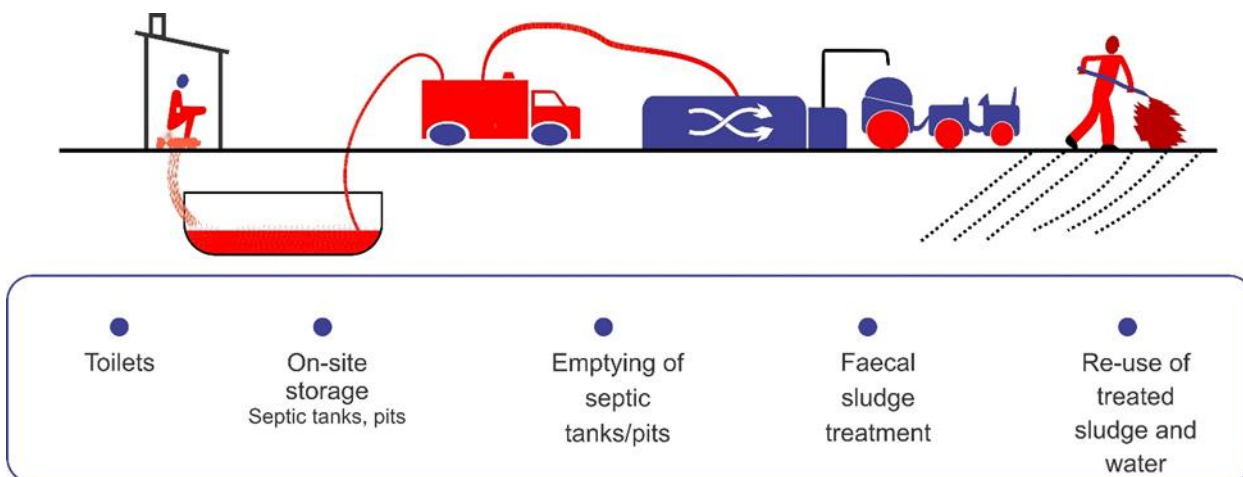

Figure 2 - Value Chain for Faecal Sludge Management India is based on the work of the Ministry of Drinking Water and Sanitation in New Delhi, India.

3.0 GOOD PRACTICES IN FAECAL SLUDGE MANAGEMENT

3.1 Case Studies

3.1.1 Case study of LAGOS, NIGERIA

The abolition of the pail system in Lagos State led to the adoption of septic tank-soak away systems for on-site treatment of septage (septic liquor) to manage liquid domestic wastes (Lagos State Government, 2020). This approach aims to reduce heavy organic and toxic pollutants by over 80% before discharge into the environment, improving parameters such as Suspended Solids (TSS), Turbidity, and Colour (Adelekan & Olukanni, 2016).

3.1.2 Case study of DEVANAHALLI, INDIA

The indicator for measuring progress against Sustainable Development Goal 6.2 (SDG 6.2), which aims to achieve universal access to sanitation by 2030, is the percentage of the population using safely managed sanitation services (United Nations, 2020).

3.1.3 Case study of OUAGADOUGOU, BURKINA FASO

Ouagadougou, the capital city of Burkina Faso, has a population of approximately 2.5 million inhabitants, accounting for about 14% of the nation's population (Institute National de la Statistique et de la Démographie (INSD), 2013; Water & Sanitation for the Urban Poor [WSUP], 2014).

3.1.4 Case study of JAMBI, INDONESIA

As a first step, it was proposed to produce a Septage Management Plan for the City of Jambi as a decision support tool, which could then serve as a model for the rest of the Metropolitan Sanitation Management Investment Project (MSMIP) target cities and elsewhere in Indonesia.

3.2 TREATMENT OPTIONS

Many wastewater treatment plants in low-income areas have failed, and improper co-treatment with septage has even been the cause of some failures through lack of

source control and the poor ratio of co-mixing. WWTPs are typically not designed for septage loadings, which leads to process disruptions and failures.

3.2.1 TREATMENT OPTIONS IN LAGOS

A Modular Septage Treatment plant has been put in place as a stopgap to the indiscriminate discharge of Faecal sludge into the water bodies, this highly mechanized system has not been easy to use for the current operators at the Septage Handling Stations. This review also revealed that about 85% of our domestic wastewater ends in the septic tank, 5% in the public secondary and tertiary drains and about 10% in government and private treatment plants as sewage for treatment. This act has been the constant practice in the metropolis using some designated Septage Handling Stations (SHS), namely: Abesan SHS, Odo-iyalaro SHS, Oregun SHS, Lekki SHS and Tolu SHS as points of disposal while relying 100% on the receiving water bodies to do the treatment.

Figure 3 – Abesan Modular Septage Pre-Treatment Plant, 201

WEAKNESSES:
➢**Incomplete Coverage:** Limited-service coverage, especially in underserved areas, poses a challenge to achieving universal sanitation access.
➢**Ageing Infrastructure:** Some existing infrastructure may be outdated, requiring significant investment in rehabilitation and maintenance.
➢**Capacity Gaps:** LSWMO may face challenges in terms of workforce capacity and expertise, hindering efficient service delivery.
➢**Limited Public Awareness:** Despite efforts, public awareness about LSWMO and LASWARCO (the regulator) remains insufficient, given the vast population of over 23 million residents.

ATS:
➢**Population Growth:** Rapid urbanization and population growth may strain existing infrastructure and worsen sanitation challenges.
➢**Environmental Impact:** Inadequate wastewater management poses risks to water bodies, ecosystems, and public health.
➢**Economic Constraints:** Budget constraints limit financial resources available for wastewater management initiatives.

STRENGTHS:
➢**Foundational Infrastructure:** Lagos State has a legacy of wastewater treatment plants and sewer networks, forming the foundation for effective management.
➢**Emerging Regulatory Framework:** Ongoing efforts towards developing a robust regulatory framework, including the presence of LASWARCO and LUWASH, demonstrate progress in shaping the regulatory landscape.
➢**Historical Financial Capacity:** The potential for revenue generation through innovative solutions, partnerships, and efficient financial management indicates a historical financial capacity for LSWMO.

OPPORTUNITIES:
➢**Technological Advancements:** Embracing smart technologies and innovations in wastewater treatment can enhance efficiency and service delivery.
➢**Public-Private Partnerships (PPPs):** Collaborating with private entities can bring external expertise, funding, and innovative solutions to the sector.
➢**Circular Economy Practices:** Exploring circular economy principles can lead to sustainable resource usage and potentially create marketable by-products.
➢**WASH Sector Policy:** The newly developed WASH Policy presents an opportunity to elevate public awareness about the entire Water, Sanitation, and Hygiene (WASH) sector, including wastewater management.

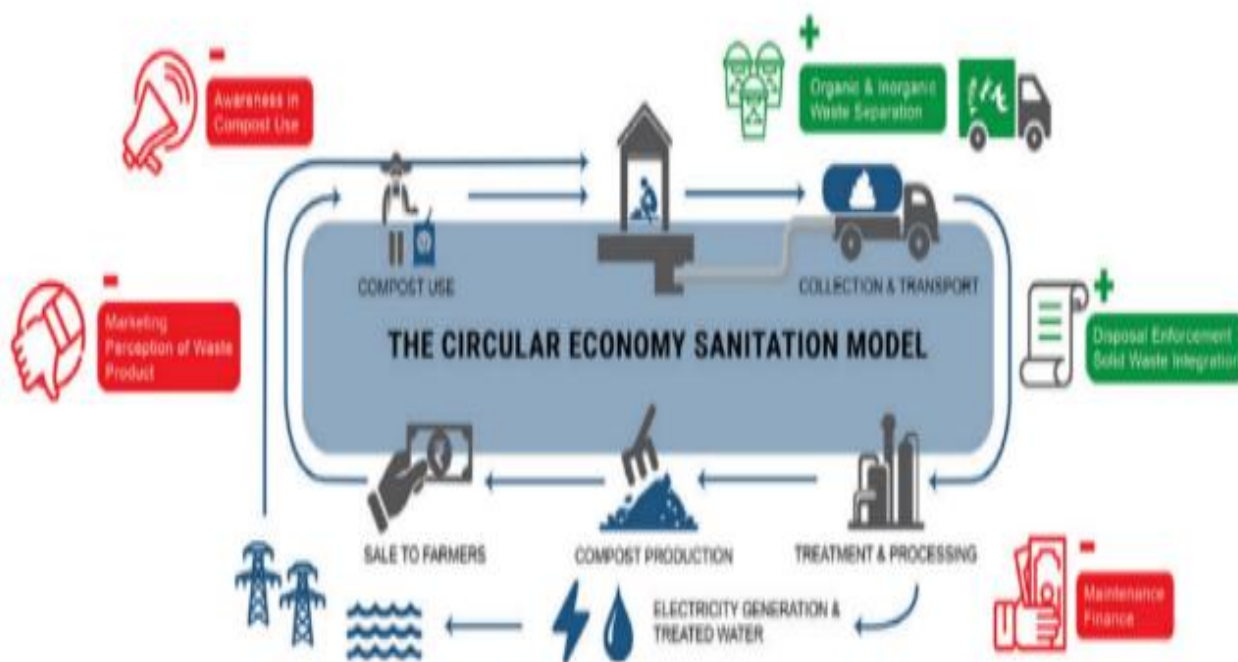**Figure 4 - Lagos State Wastewater Management Office (LSWMO) SWOT Analysis**

Figure 5 – The Circular Economy Sanitation Model (Adapted from Evaluating the Circular Economy for Sanitation: Findings from A Multi-Case Approach)

Lagos Sanitation Economy faces challenges in managing wastewater due to its large population. A circular sanitation economy offers a solution by focusing on resource recovery and minimizing waste generation.
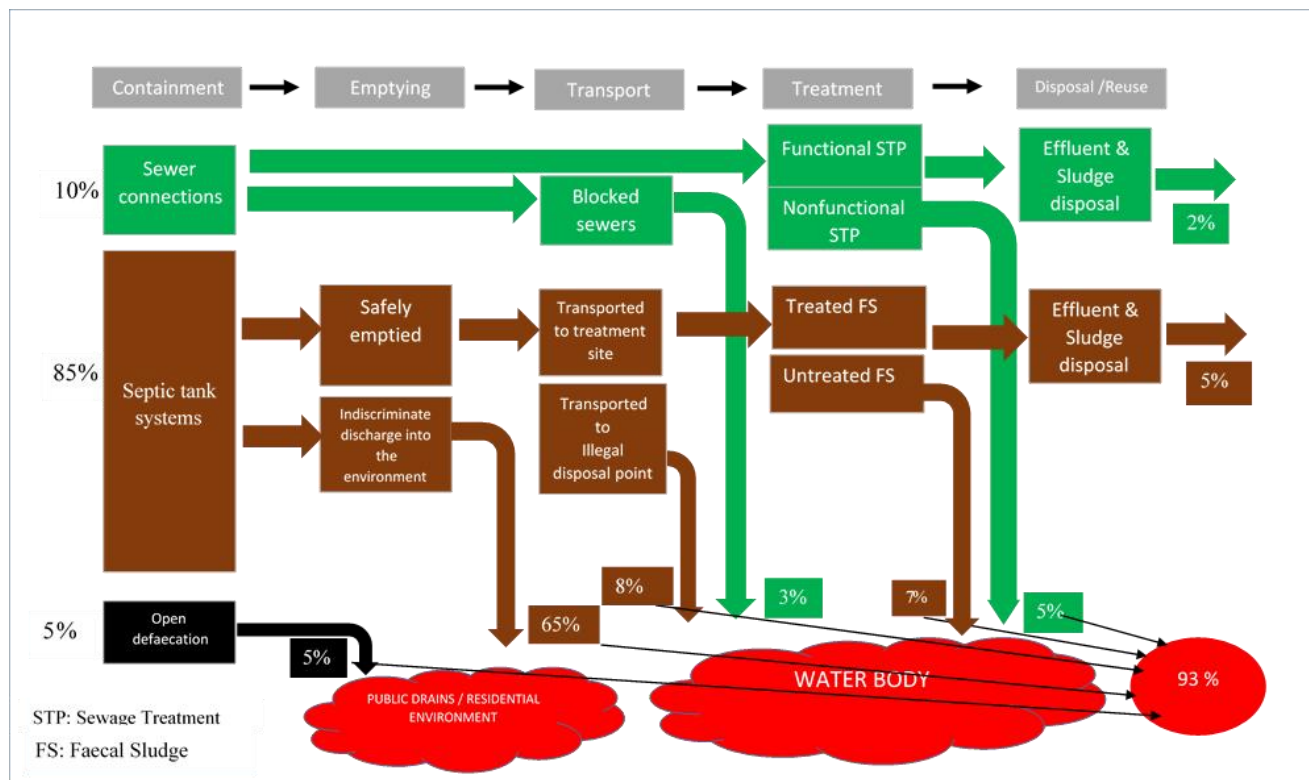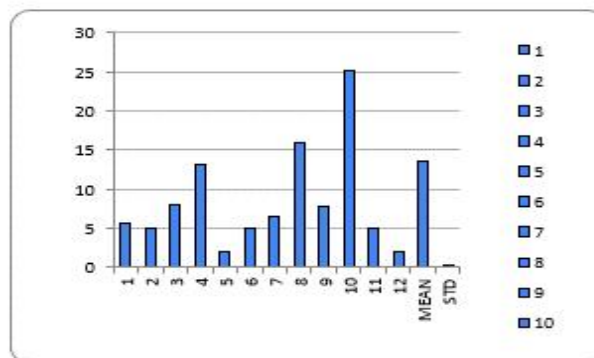

**Figure 7 - Wastewater Shit Flow Diagram for Lagos State**

BIOLOGICAL OXYGEN DEMAND ANALYSES OF SEPTAGE SAMPLED IN LAGOS STATE														
LOCATION	1	2	3	4	5	6	7	8	9	10	11	12	MEAN	STD
BOD5 ×100	5.6	5.05	7.95	13.2	2.13	5.07	6.58	16	7.8	25.2	4.93	2.05	13.6	0.3

NUMBERS	LOCATIONS
1	IKORODU/MILE12
2	IKEJA/OGBA/AGEGE
3	KETU/OJOTA
4	MARYLAND/BARIGA
5	ORILE/APAPA/AJEGUNLE
6	MILE2/ISOLO/BADAGRY
7	EGBEDA/ISHERI
8	ABULE-EGBA/PLEASURE
9	LAGOS ISLAND
10	APAPA/ORILE
11	MAINLAND/SURULERE
12	LEKKI/V.I./IKOYI

CHEMICAL OXYGEN DEMAND ANALYSES OF SEPTAGE SAMPLED IN LAGOS STATE														
LOCATION	1	2	3	4	5	6	7	8	9	10	11	12	MEAN	STD
COD ×100	63.7	86.4	95.5	168	35.5	66.4	109	202	121	284	60	41	163	0.8

NUMBERS	LOCATIONS
1	IKORODU/MILE12
2	IKEJA/OGBA/AGEGE
3	KETU/OJOTA
4	MARYLAND/BARIGA
5	ORILE/APAPA/AJEGUNLE
6	MILE2/ISOLO/BADAGRY
7	EGBEDA/ISHERI
8	ABULE-EGBA/PLEASURE
9	LAGOS ISLAND
10	APAPA/ORILE
11	MAINLAND/SURULERE
12	LEKKI/V.I./IKOYI
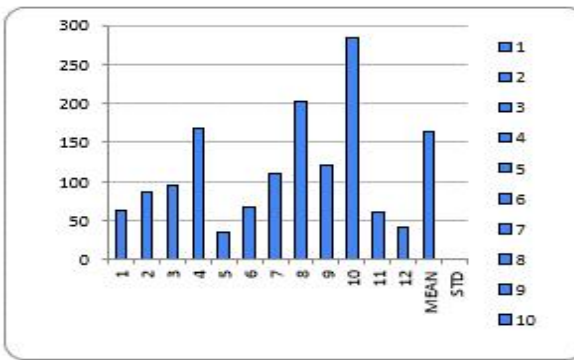
The ab... around ... then M... ... ally not same t... ... gement evacuated as at when due. More focus on these areas to achieve circular economy through scheduled evacuation towards a safely managed sanitation.

... ystems. Some technologies, such as twin leach pits, provide on-site treatment, and if correctly built and operated, these can be securely emptied and reused at the household level.
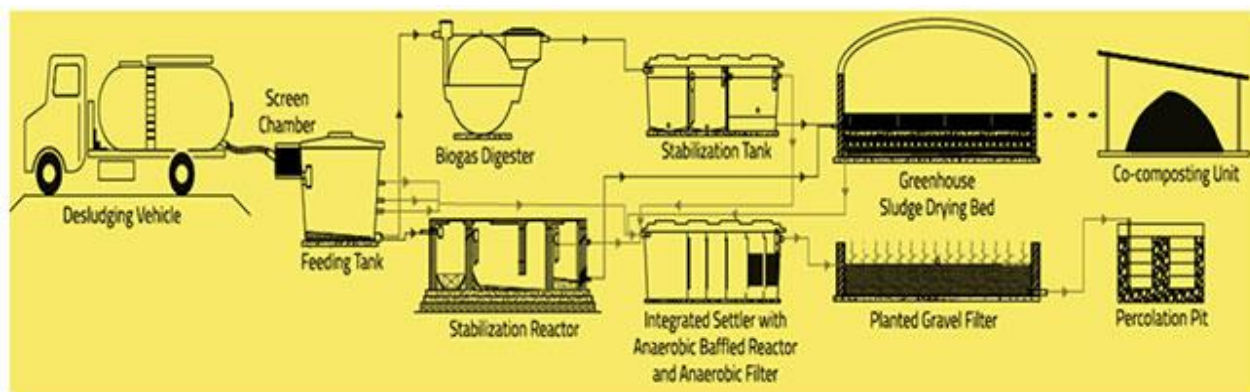
Figure 9 - Faecal Septage Treatment Plant

3.2.3 Treatment Options in Ouagadougou, Burkina Faso

Market-driven business: In the city of Ouagadougou,

should be promoted. The demand for mechanical emptying is very high. This model could be applied only in the town of Ouagadougou.

thirty-nine enterprises are delivering the service in faecal sludge emptying and transportation. Big enterprises that own 3 to 5 trucks with high management skills levels

3.2.4 Treatment Options in Taomasina, Madagascar

Only 34 % of the Madagascar population has access to

improved sanitation facilities for human excreta disposal. The aim of the Madagascar Action Plan (MAP) is to increase this percentage for the rural population to 68% in 2012, following the Sustainable Development Goals. The treatment plant in Toamasina is situated 12 km from the city centre on land provided and owned by the city council.

3.2.5 Treatment Options in Kumasi, Ghana

As reported by Murray and Drechsel (2011), a study on the cost of operations, maintenance and monitoring of five treatment plants in Ghana showed they do not have the necessary equipment to ensure effective treatment of the faecal sludge or leachate they receive. Plant operation, performance and effluent content are, in many cases, not monitored. Over time, there has been considerable improvement with Septage Collection by private operators and the kumasi Metropolitan Assembly (KMA) as well as Treatment at the Kumasi Wastewater Treatment Plant.

3.2.6 Treatment Options in Jambi, Indonesia

The Talang Bakung IPLT, located just outside the city's boundary to the east of the kelurahan of TalangBakung (in the Desaor village of Tangkit, kecamatan of Sungai Gelam, kabupatenMuaro Jambi), some 14 km away from the city center, consists of a waste pond stabilization (WSP) system preceded by a solids separation unit.

4.0 CONCLUSION

This review investigated six different low-income cities sanitation value chain to identify barrier and opportunities to advancing sustainable systems towards circular economy. Overall, across the six cases, all of them faced major similarities in either scalability or financial viability, selling and marketing of product, inability to collect septage and using models that do not fully treat the sludge.

Achieving Circular Economy for sanitation that fully treats, and re-uses FS would require the development of a City-Wide Inclusive Sanitation, FS Quantification prior sizing of FSTP, WASH policy and FSM Plan. These documents would provide the need for mechanical support in upgrading the Septage Handling Stations to a Faecal Sludge Management Treatment Plant (FSTP) across local Government Areas and Council Development Areas by retrofitting with innovative technologies to help in introducing a profitable public-private partnership approach to achieve Circular Economy for Sanitation in Low-income areas like Lagos. In Lagos, there are existing Septage Handling Stations which are legal discharge locations, adapting technology like weighing bridge, vehicle trackers, dewatering plants and sludge valorization plants would facilitate data collection and improved resource recovery. The Lagos State Government also approved the Water Sanitation and Hygiene Policy in February 2024 to achieve the Lagos Sanitation Economy.

It is important to note, however, that merely transplanting elements and lessons to these areas with inadequate FSM and hoping for a quick fix will not work (key informant 1, 2019). FSM requires a comprehensive overview of the current practices of the community or state to develop a sustainable approach that will ensure that the health and safety of the population is maximized through resource recovery using circular economy approach as an end-to-end approach.

6.0 REFERENCES

Andres, L. et al., 2019. Circular Economy in Faecal Sludge Management: A Systemic Review. *Journal of Cleaner Production*, 235, pp.1220-1230.

Central Public Health and Environmental Engineering Organisation (CPHEEO), 2019. *Faecal Sludge Management: A Guidance Manual*. New Delhi: CPHEEO.

Chandana, N. & Rao, B., 2021. Assessing inter and intra-variation in the characteristics of faecal sludge from Vadgaon Maval, Maharashtra: for better faecal sludge management in India. *Journal of Environmental Management*, 300, p.113634. doi: 10.1016/j.jenvman.2021.113634.

Dirix, D., Rossi, F. & van der Hoek, H., 2021. Faecal sludge management in Toamasina, Madagascar: Emptying – Transport - Treatment. *Journal of Environmental Management*, 281, p.111808. doi:10.1016/j.jenvman.2021.111808.

Elegede, I., Muritala, I., Afeez, Y. & Majolagbe, Y., 2023. BS8001 Circular Economy Standards. In: *Springer Nature Switzerland AG*. doi:10.1007/978-3-030-02006-4_39-1.

Ganesan, P., n.d. *Review of Household use of Septic Tanks and Faecal Management in Rural India*.

International Water Association (IWA), 2019. *Fecal Sludge Management: A Guide for Low-Income Countries*.

Kengne, C.W.E.S., Djumyom, G.V. et al., 2021. Quantification and Characterisation of faecal sludge from on-site sanitation systems prior to the design of a treatment plant in Bangangte, West Region of Cameroon. *Environmental Challenges*, 5, p.100236.

Lagos State Government, 2020. *Faecal Sludge Management in Lagos State: A Case Study*. Lagos: Lagos State Government.

Lagos State Government, 2024. *Memorandum of Understanding between Lagos State Government and Jospong Group of Companies (Zoom lion Limited) for Faecal Sludge Treatment and Utilization*. Lagos: Lagos State Government.

Lagos State Waste Water Management Office, 2019. *Strategic Action Plan 2023 – 2027*.

Mallory, A., Akrofi, D., Dizon, J. et al., 2020. Evaluating the circular economy for sanitation: Findings from a multi-case approach. *Science of the Total Environment*, 744, p.140871.

Ministry of Housing and Urban Affairs, 2024. *Faecal Sludge Management (FSM) in India: Strategies and approaches*.

Ministry of Housing and Urban Affairs, Government of India, 2019. *Faecal Sludge Management (FSM) Policy*.

OECD iLibrary, 2024. *Achieving strong and balanced regional development in India*. Retrieved August 2024.

Strande, L., Ronteltap, M. & Brdjanovic, D., 2020. Faecal sludge management: A review of the current status, challenges, and future directions. *Journal of Environmental Management*, 261, p.110081. doi: 10.1016/j.jenvman.2020.110081.

Tanoh, R.K., Oteng, A.B., Mensah, P.Y. & Amoah, I.D., 2020. Septage management in Kumasi, Ghana: Challenges and opportunities. *Journal of Environmental Management*, 261, p.110012. doi:10.1016/j.jenvman.2020.110012.

UNDESA, 2024. *World Urbanization Prospects: The 2024 Revision*. United Nations Department of Economic and Social Affairs, Population Division. Retrieved August 2024.

United States Agency for International Development (USAID), 2024. *Lagos Urban Water Sanitation and Hygiene (LUWASH) report*.

WaterAid India, 2017. *Quality and sustainability of toilets: A rapid assessment of technologies under Swachh Bharat Mission – Gramin*.

WHO/UNICEF Joint Monitoring Programme (JMP) for Water Supply, Sanitation and Hygiene, 2021. *Progress on Drinking Water, Sanitation and Hygiene 2000-2020*. Geneva: World Health Organisation.

World Population Review, 2024. *Nigeria Population 2024*. Retrieved August 2024.

AN INNOVATIVE SMART PILOT SOLAR DRYING SYSTEM FOR SUSTAINABLE AGRICULTURE IN SOKOTO STATE

*Kafayat A. Ibrahim[1]., Kamilu O. Lawal[2], Ibrahim K. Muritala[3],Abdulsalam, N.[4]
[1]Department of Electrical & Electronics Technology, Federal College of Education, Gidan Madi, Sokoto, Nigeria.
[2]Department of Electrical & Electronics Engineering, Abubakar Tafawa Balewa University, Bauchi, Nigeria.
[3]Department of Technology Development, Research & Innovation, Afridat Research and Innovation, GmbH, Duisburg, Germany.
[4]Nascomsoft Embedded Hub, Bauchi State
*Email: ibrahimkafayatsubomi@gmail.com.

ABSTRACT

Agricultural product drying systems preserve quality and extend the shelf life of harvested crops. Solar drying reduces reliance on traditional methods, often contributing to deforestation and environmental degradation. This work presents a sustainable process for preserving agricultural produce, helping to improve food security and reduce post-harvest losses. Emerging trends include renewable energy sources, automation and monitoring systems. Data shows many farmers lack drying structures and equipment (80%), relying on direct sun drying with disadvantages. The designed system allows for three different modes and input of drying parameters. The collector has a dimension of 1516 by 344mm, with a tilt angle of the collector being 15°. The drying chamber has a dimension of 480mm by 500mm. The chimney has a height of 200m and a diameter of 46mm. Research aligns with Sustainable Development Goals (SDGs) for agriculture. The results showed the importance of deploying smart drying systems in the state.
Keywords: *Agricultural Produce; Drying Technology; Food Quality; Smart System; Solar Radiation; Solar Thermal Process; Sustainable Solutions*

1. INTRODUCTION

Food security is vital for Nigeria, Africa's most populous nation, ensuring safe, nutritious food for all citizens. (FAO-UN, 2015). Achieving this, is challenging due to a growing population (United Nations Population Fund, 2021) and climate-related disruptions to agriculture (Intergovernmental Panel on Climate Change, 2022) and placing a growing strain on food production resources (United Nations Population Fund, 2021). Sokoto State in Nigeria has abundant solar energy potential, but faces challenges in agriculture and energy access (Sokoto State Government, 2021). Post-harvest losses are a major issue in Sokoto State, affecting food availability and economic losses. Solar dryers offer a sustainable solution by dehydrating crops with renewable energy. (Ozturk et al.2009 & Koua et al,.2009). Traditional drying methods in Nigeria have limitations, making

solar dryer a promising alternative. (Aregbesola et al., 2021). Studies show that solar dryer can reduce post-harvest losses and improve food preservation and quality. (Oladejo et al., 2016). Solar drying technologies have been found to be cost-effective and beneficial for smallholder farmers. (Alibassi and Madani, 2012). Solar dryers can also contribute to economic development by preserving crop quality and promoting value addition. (Ogundele, 2022 & (Okonkwo and Ertekin, 2022)). (Bala and Debnath, 2012) examined the performance of solar dryers in tropical climates and found that these systems can significantly reduce drying time and improve the quality of dried products. Integration of desiccant materials in solar dryer can enhance drying efficiency. Figure 1 and 2 shows the Direct and Indirect solar dryer:
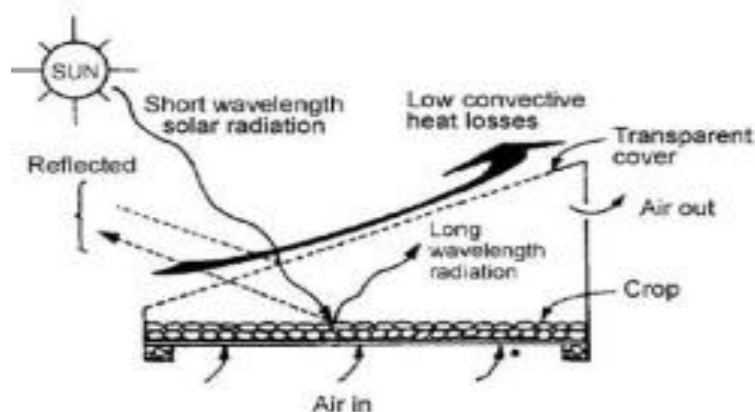

Figure 1: Direct Solar Dryer (Shittu et. al., 2018)

With the recent advancement in technology, smart solar drying systems present significant progress in food preservation technology. It uses sensors and controls to automatically manage airflow, heating, and ventilation for optimal food preservation. This innovative system can be used for any farm produce. With the addition of a renewable energy source in the form of solar panels, the system has the option of ensuring its operation continues when there is a power outage. Figure 2 is the diagram of an indirect solar dryer.
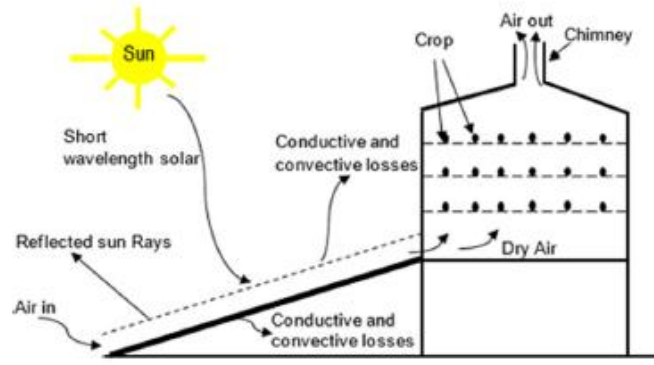

Figure 2: Indirect Solar Dryer (Princewill et al, 2023*).*

2.   METHODOLOGY

The methodology for the development of the Solar drying system for farmers in Sokoto State, Nigeria involves two key stages: literature review, needs assessment, and the design and development of the innovative solar-based drying system. Research was based on needs assessment of region's agricultural products and drying challenges, emphasizing engagement with local stakeholders. Customized solar-based drying system was designed based on finding from needs assessment, incorporating solar collectors, drying trays, ventilation mechanisms, and monitoring/control devices.

2.1 MATERIALS

Some of the materials used in the construction of the solar-based system for agricultural products drying for Sokoto State Nigeria are presented below:

❖ MBF Wood**:** Two sheets of MBF wood were used for the drying chamber construction

❖ Malena Wood: The solar collector is made of Malena wood, to prevent outdoor weather conditions, especially the action of solar radiation. The collector will face south to receive maximum direct sunlight throughout the day. The tilt angle of 15^0 was used in the design should be seasonally adjustable to optimize sun exposure based on location and time of year. In the collector is also a fiber material for proper insulation and to minimize heat loss to the surroundings. The design ensures proper airflow without excessive heat loss.

❖ Metal Sheet: Dark metal sheet with selective coating for efficient solar energy absorption.

❖ Transparent Glass: 5mm thick glass for trapping heat and allowing sunlight inside the collector.

❖ ARDUINO ATMEGA 328: Controls system intelligence and sensor readings.

❖ DHT-22 Sensor**:**   Monitors temperature and humidity levels in the drying chamber.

❖ Heater: It provides another option for drying if there is no solar radiation. It can also be used with the conventional dryer to reduce the drying time of some farm produce.

❖ DC Fan (12V): This is used for heat circulation in the drying chamber.

The design includes adjustable vents and airflow channels to enhance air circulation, preventing moisture buildup and ensuring uniform drying. Insulating materials minimize heat loss, maintaining higher temperatures within the chamber for efficient drying. This mode capitalizes on the abundant sunshine in Sokoto State but remains susceptible to weather variability, necessitating the inclusion of other operational modes for comprehensive functionality.

2.2 OPERATION

The system offers three (3) modes:

(i)   Indirect Solar Drying Mode,

(ii)   Smart Drying Mode, and

(iii)   Combination of (i) ad (ii) above

In first mode, solar radiation is the sole energy source for drying agricultural produce in a UV-resistant chamber. Smart drying mode uses technology for faster drying, with solar PV and DC battery system for energy storage. Smart sensors regulate humidity and temperature, stopping the system when the desired humidity level is reached. A micro-controller adjusts operation based on sensor data. Combined mode relies on battery backup and smart sensors for consistent drying in minimal solar radiation or cloudy days.
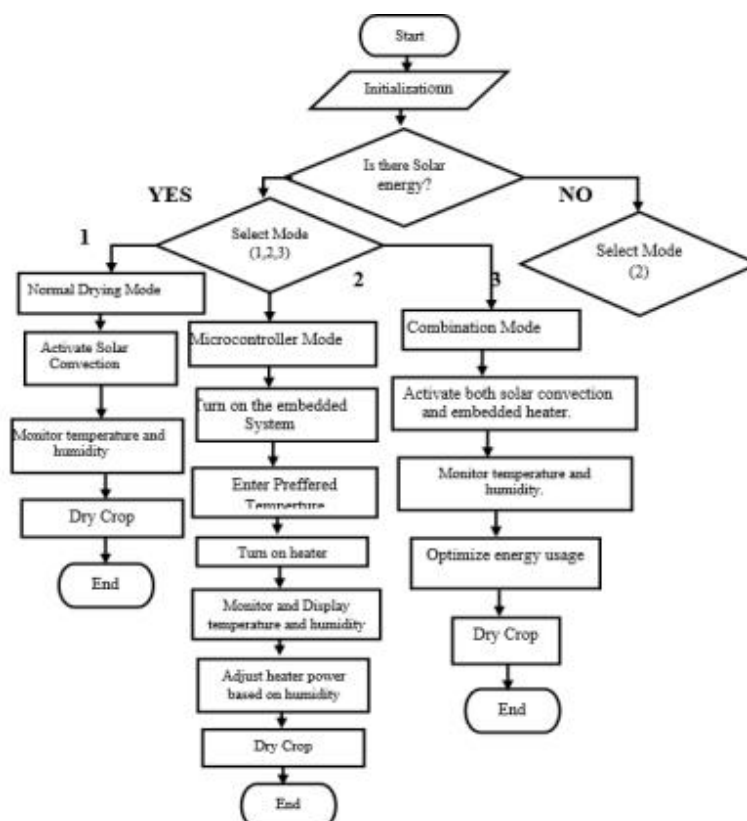
Figure 3: Flow Chart of the Solar-based Dryer

3. RESULTS AND DISCUSSION

This section discusses designing a smart pilot solar drying system for agricultural products in Sokoto State. Farmers need reliable, affordable and efficient drying methods. Most farmers in the state lack modern drying techniques. About 80% have no drying structure and 60% never used drying equipment. Over 80% of farmers use direct sun drying, which has disadvantages like pests and weather damage. Onions take days to dry using direct solar drying, but with an improved system, it will only take hours once the correct conditions are known. Most farmers (59%) do not use specific drying equipment, relying on traditional methods. 83% use direct sun drying due to simplicity and abundant sunlight in Sokoto state. Direct solar drying can be inefficient and inconsistent, leading to spoilage. This is evident in figures 6 and 7.
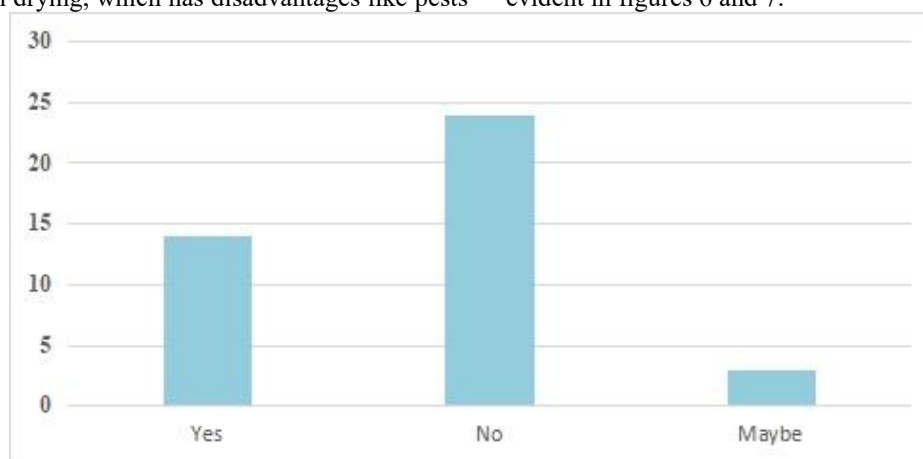

Figure 4: Farmers that use Drying Equipment or Technology in the State.
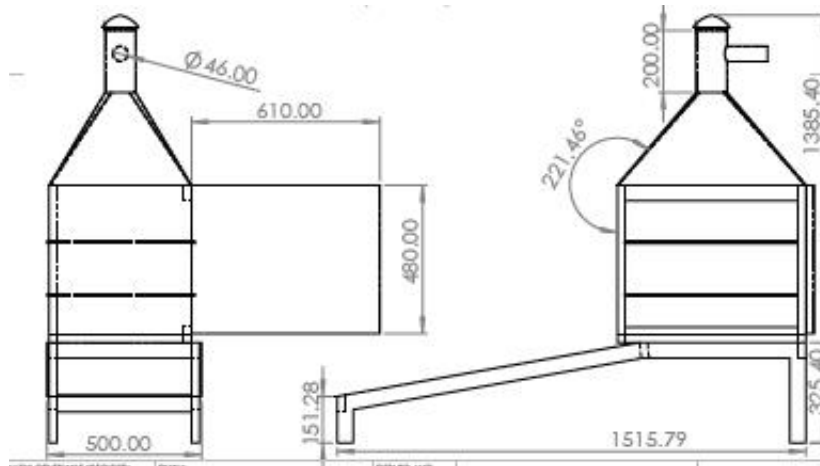
Figure 5: Methods of Solar drying in Sokoto State

Figure 6: Front and Side View of the Pilot Smart Solar Dryer with Dimensions

Table 1: Smart Solar Dimensions in mm

S/N	Solar Dryer Part	Dimension
1.	Chimney Chamber (mm)	580 by 500
2.	Chimney Height (mm)	200
3.	Chimney Diameter (mm)	46
4.	Glass Thickness (mm)	5
5.	Glass Tilt Angle (°)	15
6.	Solar Collector(mm)	1516 by 343.22
7.	Drying Chamber (mm)	500 by 480
8.	Dryer Length (mm)	1515.79
9.	Dryer Breadth (mm)	500
10.	Dryer height (mm)	1385.40

Figure 7: Designed and Constructed Solar-based Dryer Demonstration (Prototype).

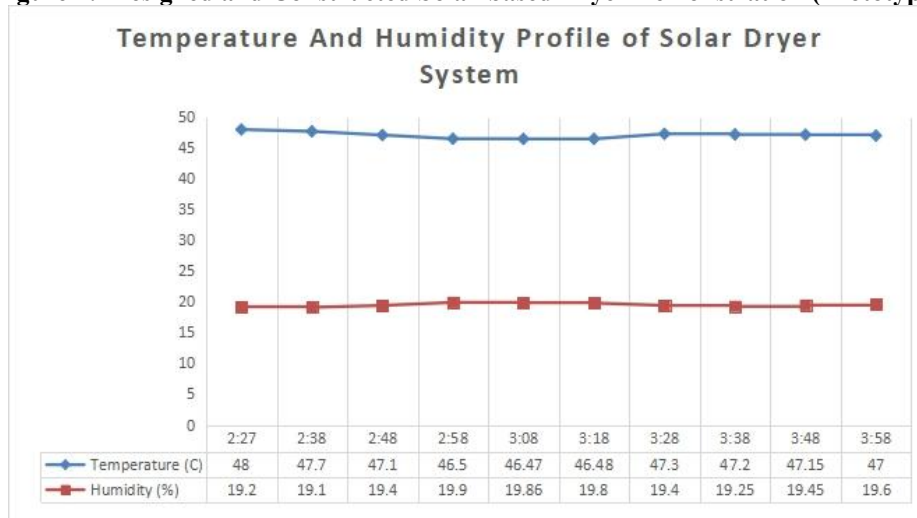|	2:27	2:38	2:48	2:58	3:08	3:18	3:28	3:38	3:48	3:58
Temperature (C)	48	47.7	47.1	46.5	46.47	46.48	47.3	47.2	47.15	47
Humidity (%)	19.2	19.1	19.4	19.9	19.86	19.8	19.4	19.25	19.45	19.6

Figure 8: Result of demonstration of figure 7 based on temp. And humidity profile of solar dryer system.

During the testing Solar Dryer in Figures 8, data in Table 2 show drying from 2:27 pm until 3:58 pm. System maintains 46.47-48°C 19.1-19.9% humidity, ideal for drying produce like onions, tomatoes, garlic, maize, soybeans, cowpeas, moringa leaves and rice. Fish may need lower temp. drying time varies based on moisture content. Regular monitoring and adjustment needed for optimal result.

4. CONCLUSIONS

The research achieved objectives, developing an innovative solar drying system for farmers in Sokoto State. The system incorporates advanced functionalities to optimize the drying process for quality farm produce. A needs assessment identified challenges in local agricultural drying processes, ensuring the system effectively addresses the critical issues like prolonged drying times and post-harvest losses. By integrating solar energy with smart technology, the proposed system offers a versatile, efficient, and sustainable solution for post-harvest preservation in Sokoto State. Further development of this solution addresses post-harvest challenges, promoting better food preservation and reducing losses. The solar drying system extends the shelf life of agricultural products, enhancing food security and economic stability in the region.

6. REFERENCES

Alibassi, H. A. & Madani, M. H. (2012). The Influence of Drying Methods on the Physicochemical Propertiesof Carrot Slices. International Journal of Food Science & Technology, 47(1), 172-178

Aregbesola, O.A., Ogundipe, O.O., & Abegunde, K.O. (2021), Post-harvest Losses in the Nigerian Food Supply Chain: Causes and Solutions. Food Reviews ,55,542-553: https://doi.org/10/1016/j.ser.2021.11.077

Bala, B.K. and Debnath, N. (2012) Solar Drying Technology: Potentials and Developments. Journal of Fundamentals of Renewable Energy and Applications, 2, R120302. https://doi.org/10.4303/jfrea/R120302

Food and Agriculture Organization of the United Nations. (2015). The State of Food Insecurity in the

World 2015. Strengthening the Enabling Environment for Food Security and Nutrition: https://www.fao.org/3/a-i4030e.pdf

Intergovernmental Panel on Climate Change (2022) Climate Change 2022: Impacts, Adaptation, and Vulnerability.

International, 37:5,2062–2080. https://www.tandfonline.com/journals/timp20.

Koua, E., Finkenstadt, A., Muller, B., Sanders, S. & Lucas, D. B. (2009) Low-cost Solar Dryers for Developing Countries. Drying Technology, 27(6), 797-802. DOI: 10.1080/07373930802642321

Ogundele Femi (2022), Post Harvest Losses and Food Security in Nigeria: An Empirical Review. African Journal of Agriculture and Food Science 5(3), 77-89. DOI: 10.52589/AJAFSC0442Z7J

Okonkwo HO and Ertekin C (2022). Review on Solar Drying in Nigeria. Turkish Journal of Agricultural Engineering Research (TURKAGER), 3(2), 397-429. https://doi.org/10.46592/turkager.1060019

Oladejo, E. I., Abegunde, O. A., Ogundipe, O. O. & Akinlabi, A. A. (2016) Performance Evaluation of a Mixed-mode Solar Dryer for Drying Pepper Fruits. Journal of Stored Products Research, 66, 129-135. DOI: 10.1016/j.jspr.2016.03.006

Ozturk, S., Colak, H. & Dincer, A. (2009) Performance Analysis of a Solar Dryer for Drying of Apricots. Energy Conversion and Management, 50(4), 1057-1063. https://doi.org/10.1016/j.enconman.2008.10.012

Shitu Abubakar, Samaila Umaru, Fatai O. Anafi, Aminu S. Abubakar & Dangana M. Kulla (2018), Design And Performance Evaluation Of A Mixed-Mode Solar Crop Dryer. FUOYE Journal of Engineering and Technology,V(3),Issue1,ISSN: 2579-0625, 2579-0617.https://doi.org/10.46792/fuoyejet.v3i1.133

Sokoto State Government. (2021), Sokoto State. Retrieved from **http://www.sokotostate.gov.ng/**

Princewill, Nwadinobi Chibundo l, Nwaiwu Uchechukwu, Awani Victor Toju, & Ogbu Kosiso Michelangelo (2023), Development of an Improved Smart Solar Post-harvest Dryer. Int.J.Adv.Sci.Eng.Vol.9, No.3, 2998-3005, E-ISSN: 2349 5359; P-ISSN: 2454-9967. https://doi.org/10.29294/IJASE.9.3.2023.2998-3005

United Nations Population Fund. (2021). World Population Prospects 2021.

JOURNAL OF THE NIGERIAN SOCIETY OF CHEMICAL ENGINEERS INSTRUCTION TO AUTHORS

6. TYPES OF PUBLICATION

The Journal of the Nigerian Society of Chemical Engineers will publish articles on the original research on the science and technology of Chemical Engineering. Preference will be given to articles on new processes or innovative adaptation of existing processes. Critical reviews on current topics of Chemical Engineering are encouraged and may be solicited by the Editorial Board. The following types of articles will be considered for publication:

a. Full length **articles or review papers**.
b. **Communication** – a preliminary report on research findings.
c. **Note** – a short paper describing a research finding not sufficiently completed to warrant a full article.
d. **Letter to the Editor** – comments or remarks by readers and/or authors on previously published materials.

The authors are entirely responsible for the accuracy of data and statements. It is also the responsibility of authors to seek ethical clearance and written permission from persons or agencies concerned, whenever copyrighted material is used.

For now the journal is published twice in a year, March/April and September/October.

7. MANUSCRIPT REQUIREMENTS

a. The **Manuscript** should be written in clear and concise English and typed (single column) in Microsoft Word using double spacing on A4-size paper, Times New Romans font and 12 point. A full length article or review should not exceed 15 pages. Margin should be Normal (i.e. 2.54cm for Top, Bottom, Left & Right margins).
b. The **Manuscript** should be prepared in the following format: Abstract, Introduction, Materials and Methods, Results, Discussion, Conclusion, Acknowledgements, and References.
c. The **Manuscript** must contain the full names, address and emails of the authors. In the case of multiple authorship, the person to whom correspondence should be addressed must be indicated with functional email address. As an examples, authors' names should be in this format:
Momoh, S. O., Adisa, A. A. and **Abubakar, A. S.**
If the addresses of authors are different, use the following format:
*Momoh, S. O.[1], Adisa, A. A.[2] and **Abubakar, A. S.[3]**

Use star * to indicate the corresponding author.

d. **Symbols** should conform to America Standard Association. An abridged set of acceptable symbols is available in the fourth edition of Perry's Chemical Engineering Handbook. Greek letters, subscripts and superscripts should be carefully typed. A list of all symbols used in the paper should be included after the main text as **Nomenclature**.
e. All **Units** must be in the SI units (kg, m, s, N, etc).
f. The **Abstract** should be in English and should not be more than 200 words. The Abstract should state briefly the purpose of the research, methodology, results, major findings and major conclusions. Abstracts are not required for Communications, Notes or Letters.
g. **Citation** must be in the Harvard Format i.e. (Author, Date). Examples are (Smith, 1990) or (Jones et al, 2011). (Kemp, 2000) demonstrated that …..; (Mbuk, 1985; Boma, 1999; Sani, 2000) if more than two authors. (Telma, 2001a), (Telma, 2001b); etc if the citation have the same author and year of publication.
For more information on Harvard Referencing: Guide visit http://www.citethisforme.com/harvard-referencing
h. **References** must also be in the Harvard Format i.e. (Author, Date, Title, Publication Information). References are listed in alphabetical order. Examples are shown below:
Haghi, A. K. and Ghanadzadeh, H. (2005). A Study of Thermal Drying Process. *Indian Journal of Chemical Technology*, Vol. 12, November 2005, pp. 654-663
Kemp, I.C., Fyhr, C. B., Laurent, S., Roques, M. A., Groenewold, C. E., Tsotsas, E., Sereno, A. A., Bonazzi, C. B., Bimbernet, J. J. and Kind M.(2001). Methods for Processing Experimental Drying Kinetic Data. *Drying Technology,* 19: 15-34.
i. **Tables** should contain a minimum of descriptive materials. Tables should be numbered serially throughout the manuscript in Arabic numerals (1, 2, 3, etc), and should be placed at the referenced point with captions (centralised) placed at the top of the table.
j. **Figures**, charts, graphs and all illustrations should be placed at the referenced point, numbered serially throughout the manuscript in Arabic numerals (1, 2, 3, etc) and incorporated in the text. Caption for Figures should be placed at the bottom of the Figure (centralised). Lettering set or symbols should be used for all labels on the figures, graphs, charts, photographs even when drawn in colours. (Note that

figures drawn in colours may be unreadable if printed in black and white).

k. **Equations** should be typed using MS Word Equation Editor and should be centred and numbered serially throughout the manuscript (in Arabic numeral) at the right margin.

l. Wherever possible, **Fractions** should be shown using the oblique slash. E.g. x/y

m. **Footnotes** should not be incorporated in the text.

n. **Acknowledgements** should appear at the end of the paper, before the list of references.

8. SUBMISSION OF MANUSCRIPTS

Manuscripts should be submitted by sending a Microsoft Word document (taking into account the Manuscript Requirements described in section 2 above) to the following email address: nschejournal@yahoo.com and copy stevmomoh@yahoo.com.

All correspondences are directed to the Editor-in-Chief using the submission emails addresses: nschejournal@yahoo.com and copy stevmomoh@yahoo.com. Meanwhile the online submission of articles on the journal website will soon be ready.

Authors should note that:

a. All authors listed in the manuscript have significantly contributed to the research.

b. All authors are obliged to provide retractions or corrections of mistakes.

c. All references cited are listed and financial support acknowledged.

d. It is forbidden to publish same research in more than one journal.

The fee charged for paper review and publication will be borne by the authors as follows:

a. Manuscript Review charges = N6,500 payable by both Members and Non-Member. Overseas is $30.00.

b. Publication Charges = N10,000 payable by Non-Members and Members who are not financially up-to-date. Overseas is $40.00.

c. Members would only get one (1) Journal free and buy the other if they so wish.

d. Corresponding Author whose paper is published on a particular edition would get one (1) free copy on behalf of all the co-authors. Other co-authors will buy if they so wish.

All fees are paid after the paper had been accepted for publication. These charges may be reviewed from time to time by the Governing Board of Directors of the Society.

9. ACCEPTED PAPERS

On acceptance, authors will be required to submit a copy of their manuscripts using Microsoft Word by emails to nschejournal@yahoo.com and copy stevmomoh@yahoo.com.

The following additional information should be observed for accepted papers: (i) Typed in Microsoft Word using 1.15 spacing on A4-size paper, Times New Romans font and 10 point; (ii) Margin should be 2.54cm for Top & Bottom; 2.20cm for Left & Right margins; (iii) The abstract should be one column document while the body of the manuscript should be double columns with 0.5cm gutter spacing except some tables and figures that may have to go in for one column document.

10. PUBLICATION

Full NSChE Journal edition in hard copy will be published twice annually – March/April Edition and September/October Edition.

11. REPRINT

Reprints are available on request at a moderate fee per page. Orders must be placed before the paper appears in Print.

12. READER'S INFORMATION

The papers are wholly the view of their author(s) and therefore the publisher and the editors bear no responsibility for such views.

13. SUBSCRIPTION INFORMATION

The subscription price per volume is as follows:

a. Individual Reader - N3,000.00
b. Institutions, Libraries, etc.- N5,000.00
c. Overseas Subscription - $100.00

Request for information or subscription should be sent to the Editor-in-Chief through the following emails addresses: nschejournal@yahoo.com and copy stevmomoh@yahoo.com.

14. COPYRIGHT NOTICE

By submitting your manuscript to the Journal, you have agreed that the copyright of the published material belongs to the journal.

15. PRIVACY STATEMENT

The names and email addresses entered in this journal site will be used exclusively for the stated purposes of this journal and will not be made available for any other purpose or to any other party.